

SHALLOW SUBSURFACE GEOPHYSICAL APPLICATIONS IN ENVIRONMENTAL GEOLOGY Field Guide and Conference Proceedings

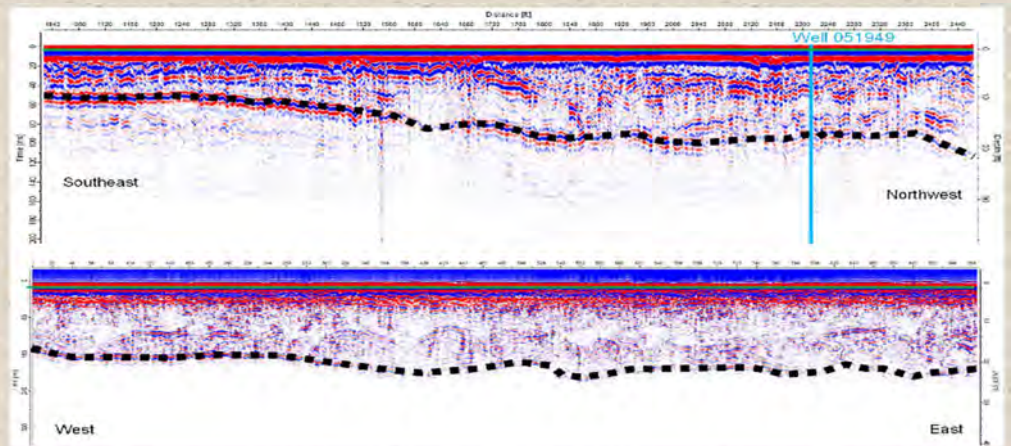
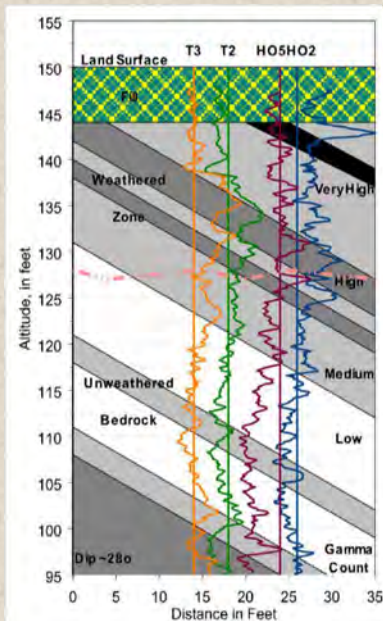
EDITED BY

Michael P. Gagliano

New Jersey Geological and Water Survey
and

Suzanne Macaoay Ferguson

PennJersey Environmental Consulting

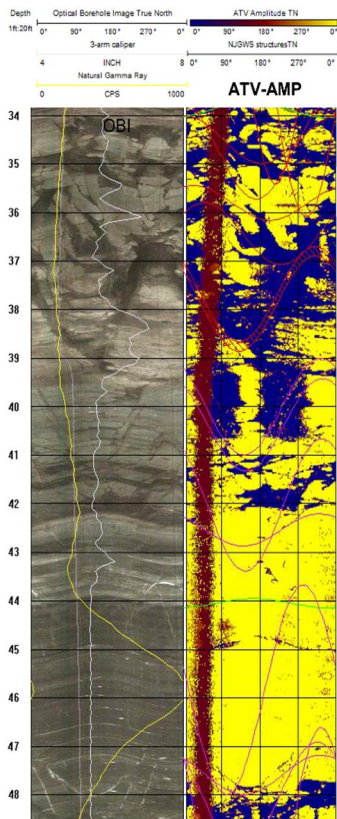


THIRTY-THIRD ANNUAL MEETING OF THE GEOLOGICAL ASSOCIATION OF NEW JERSEY

OCTOBER 14-15, 2016

THE NEW JERSEY STATE MUSEUM
TRENTON, NEW JERSEY





SHALLOW SUBSURFACE GEOPHYSICAL APPLICATIONS IN ENVIRONMENTAL GEOLOGY

Field Guide and Conference Proceedings

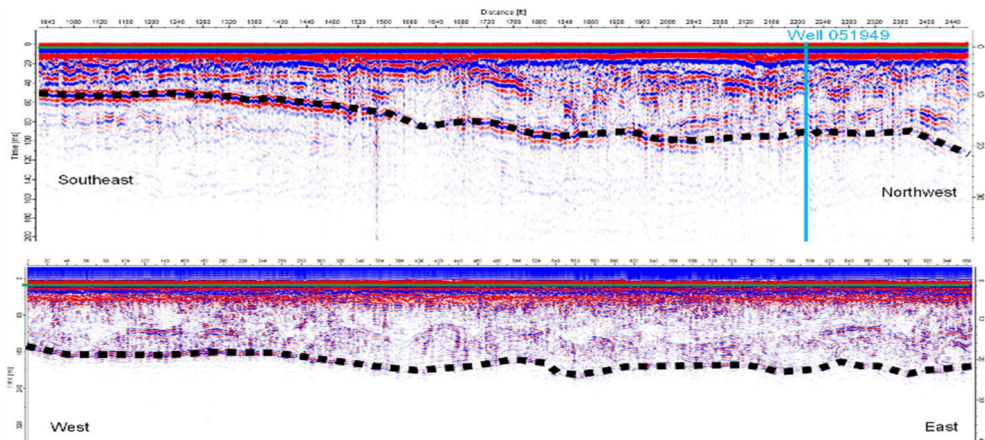
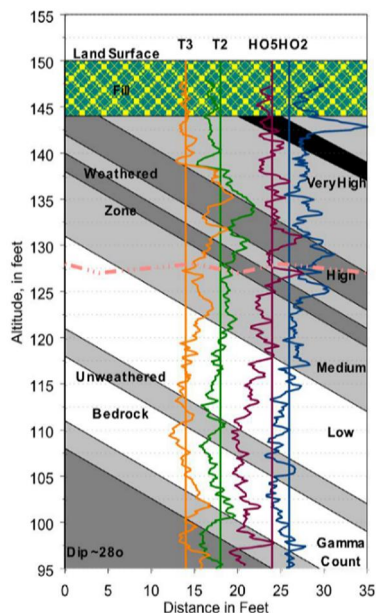
EDITED BY

Michael P. Gagliano

New Jersey Geological and Water Survey
and

Suzanne Macaoay Ferguson

PennJersey Environmental Consulting



THIRTY-THIRD ANNUAL MEETING OF THE GEOLOGICAL ASSOCIATION OF NEW JERSEY



OCTOBER 14-15, 2016

THE NEW JERSEY STATE MUSEUM
TRENTON, NEW JERSEY

A WORD FROM OUR SPONSORS

PennJersey Environmental Consulting

PEC

PEC's Licensed Site Remediation Professionals have an average of 35 years experience assessing and remediating properties, allowing us to provide each of our clients with creative solutions to best fit their needs.

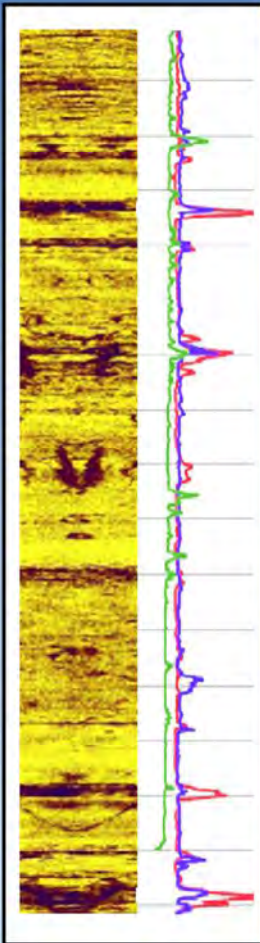
744 Milford Warren Glen Road
Milford, NJ 08848-1647
(888) 679-7462 or (908) 329-6060
www.pennjerseyenv.com

Clients depend on PEC for:

- Due Diligence
- ISRA Compliance
- Brownfields
- Cost Recovery
- Expert Testimony
- Underground Tanks

Have a Difficult Subsurface Issue at Your Site? We can assist!

Our **tools, analytical techniques & unique approaches** reveal new lines of evidence to help answer critical questions like these:



- Have offsite sources contributed to the impact at a site?
- How can an existing bedrock well network be used in a new way, to identify offsite locations most likely contributing to commingled plume impact?
- How can a long-running site investigation be completed with a minimum of drilling and well installation expense?
- How can a groundwater investigation & remediation be streamlined to focus on zones and pathways of greatest importance?
- Do the Conceptual Site Model and Classification Exception Area in use at a site reasonably reflect site conditions? Is the remedy protective?
- What location and depth is appropriate for a new sentinel well needed at a bedrock site?



PRINCETON GEOSCIENCE, INC.
15 Vandeventer Ave. • Princeton, NJ 08542
tel: 609.279.0008 • fax: 609.252.9238
www.princetongeoscience.com

FIELD GUIDES & PROCEEDINGS OF PRIOR MEETINGS

GANJ I: Puffer, John H., ed., 1984, *Igneous Rocks of the Newark Basin: Petrology, Mineralogy, and Ore Deposits, and Guide to Field Trip*.

GANJ II: Talkington, Raymond W., and Epstein, Claude M., eds., 1985, *Geological Investigations of the Coastal Plain of Southern New Jersey: Part 1 - Field Guide; Part 2A - Hydrology and Coastal Plain; Part 2B - Paleontologic Investigations*.

GANJ III: Husch, Jonathan, M., and Goldstein, Fredric R., eds., 1986, *Geology of the New Jersey Highlands and Radon in New Jersey*.

GANJ IV: Gallagher, William B., ed., 1987, *Paleontology and Stratigraphy of the Lower Paleozoic Deposits of the Delaware Water Gap Area*.

GANJ V: Husch, Jonathan, M., and Hozik, Michael J., eds., 1988, *Geology of the Central Newark Basin*

GANJ VI: Grossman, I. G., ed., 1989, *Paleozoic Geology of the Kittatinny Valley and Southwest Highlands N. J.*

GANJ VII: Brown, James O., and Kroll, Richard L., eds., 1990, *Aspects of Groundwater in New Jersey*.

GANJ VIII: Crawford, Maria L., and Crawford, William A., eds., 1991, *Evolution and Assembly of the Pennsylvania - Delaware Piedmont*.

GANJ IX: Ashley, Gail M., and Halsey, Susan D., eds., 1992, *Environmental Geology of the Raritan River Basin*.

GANJ X: Puffer, John H., ed., 1993, *Geologic Traverse Across the Precambrian Rocks of the New Jersey Highlands*.

GANJ XI: Benimoff, Alan I., ed., 1994, *Geology of Staten Island, New York*.

GANJ XII: Baker, John E. B., ed., 1995, *Contributions of the Paleontology of New Jersey*.

GANJ XIII: Dalton, Richard F., and Brown, James O., eds., 1996, *Karst Geology of New Jersey and Vicinity*.

GANJ XIV: Benimoff, Alan I., and Puffer, John H., 1997, *The Economic Geology of Northern New Jersey*.

GANJ XV: Puffer, John H., ed., 1998, *The Economic Geology of Central New Jersey*.

GANJ XVI: Puffer, John H., ed., 1999, *New Jersey Beaches and Coastal Processes from a Geologic and Environmental Perspective*.

GANJ XVII: Harper, David P. and, Goldstein, Fredric L., eds., 2000, *Glacial Geology of New Jersey*.

GANJ XVIII: Lacombe, Pierre, and Herman, Gregory, eds., 2001, *Geology in Service to Public Health*.

GANJ XIX: D'Amato, Dana, ed., 2002, *Geology of the Delaware Water Gap Area*.

GANJ XX: Hozik, Michael J., and Mihalasky, Mark J., eds., 2003, *Periglacial Features of Southern New Jersey*.

GANJ XXI: Puffer, John H., and Volkert, Richard A., eds., 2004, *Neoproterozoic, Paleozoic, and Mesozoic Intrusive Rocks of Northern New Jersey and Southeastern New York*.

GANJ XXII: Gates, Alexander E., ed., 2005, *Geology of the Central Newark Basin - The View from the 21st Century*.

GANJ XXIII: Macaoay, Suzanne, and Montgomery, William, eds., *Environmental Geology of the Highlands*.

GANJ XXIV: Rainforth, Emma C., ed., 2007, *Contributions to the Paleontology of New Jersey (II)*.

GANJ XXV: Gorrington, Matthew L., ed., 2008, *Environmental and Engineering Geology of Northeastern New Jersey*.

GANJ XXVI: Freile, Deborah, ed., 2009, *New Jersey Coastal Plain Stratigraphy and Coastal Processes*.

GANJ XXVII: Lacombe, Pierre, ed., 2010, *Geology of the Greater Trenton Area and Its Impact on the Capitol City*.

GANJ XXVIII: Rainforth, Emma C., and Uminski, Alan, eds., 2011, *Environmental Geology of Central New Jersey*.

GANJ XXIX: Alexander, Jane, ed., 2012, *Geology and Public Lands*.

GANJ XXX: Benimoff, Alan I., ed., 2013, *Igneous Processes During the Assembly and Breakup of Pangaea: Northern New Jersey and New York City*.

GANJ XXXI: Duzgoren-Aydin, Nurdan S., ed. 2014, *Global Environmental Issues and Local Consequences: Earth Surface Processes and Urban Environmental Quality*.

GANJ XXXII: Herman, Gregory C., and Macaoay Ferguson, Suzanne, eds., 2015, *Neotectonics of the New York Recess*.

GEOLOGICAL ASSOCIATION OF NEW JERSEY 2015/2016 EXECUTIVE BOARD

President.....Mr. Michael P. Gagliano, NJ Geological and Water Survey
Past President..... Dr. Gregory C. Herman, NJ Geological and Water Survey (Retired)
President ElectDr. Michael Hozik, The Richard Stockton College of New Jersey
Recording Secretary.....Mr. Stephen J. Urbanik, NJ Department of Environmental Protection
Membership Secretary..... Ms. Suzanne Macaoay Ferguson, Pennjersey Environmental Consulting
TreasurerDr. Emma Rainforth, Ramapo College of New Jersey
Councilor at LargeDr. William Montgomery, New Jersey City University
Councilor at LargePierre Lacombe, United States Geological Survey
Councilor at LargeMr. Alan Uminski, Environmental Restoration, LLC
Conference Committee..... Dr. Alan I. Benimoff, College of Staten Island/CUNY
Conference Committee.....Dr. Jane Alexander, College of Staten Island/CUNY



CONFERENCE SCHEDULE

Friday, October 14, 2016 - Oral Presentations
The New Jersey State Museum Auditorium

- 10:30 - 12:00 Teachers' Workshop – USGS Trenton
2D and 3D Fractured-bedrock characterization methods using oriented borehole imagery, Gregory C. Herman, Fern Beetle-Moorcroft, Michael P. Gagliano, Michelle E. Kuhn, and Mark A. French, NJ Geological & Water Survey, Trenton, NJ
- 12:00 - 1:00 Registration
- 1:00 - 1:30 Opening Remarks, State of the GANJ Organization & Business Meeting
Michael P. Gagliano, New Jersey Geological and Water Survey and GANJ President
- 1:30 - 2:00 NJGWS Calibration and Flow Studies Using a Heat-Pulse Flow Meter Model HFP-2293
Gregory C. Herman, Ph.D., New Jersey Geological and Water Survey (Retired)
- 2:00 - 2:30 Assessment of Electrical Resistivity Method to Map Groundwater Seepage Zones in Heterogeneous Sediments Michael P. Gagliano, New Jersey Geological and Water Survey
- 2:30 - 3:00 Break
- 3:00 - 3:30 Aquifer Heterogeneity and the Importance of Calibrating Ground-Penetrating Radar Data in Environmental Investigations Alex R. Fiore, U.S. Geological Survey
- 3:30 - 4:15 Borehole Televiwer Synoptic and Hydrogeologic Framework of Adjacent RACER and NAWC Industrial Sites, West Trenton, Mercer County, New Jersey Gregory C. Herman, Ph.D., New Jersey Geological and Water Survey (Retired)
- 4:15 - 5:30 Mapping Bedrock Fractures and Other Subsurface Conditions in Urbanized Environments Using the Multi-Channel Analysis of Surface Waves (MASW) Geophysical Method Richard Lee, P.G., R.GP, President and Principal Geophysicist, Quantum Geophysics
- 6:30 Dinner

Saturday, October 15, 2016 - Field Trip
New Jersey Geological and Water Survey, 25 Arctic Parkway, Ewing, NJ

- 8:00 - 9:00 Field Trip Starts at Stop 1: New Jersey Geological & Water Survey Geophysics garage
- 9:00 - 9:45 Travel to Stop 2
- 9:45 - 10:45 Stop 2: Prallsville Mills
- 10:45 - 11:15 Travel to Stop 3
- 11:15 - 12:15 Lunch
- 12:15 - 1:15 Stop 3: Villa Victoria Brook
- 1:15 - 1:30 Travel to Stop 4
- 1:30 - 3:45 Stop 4: NAWC
- 3:45 - 4:00 Return to New Jersey Geological and Water Survey

TABLE OF CONTENTS

TEACHERS WORKSHOP

2D and 3D Fractured-bedrock characterization methods using oriented borehole imagery, Fern Beetle-Moorcroft, Gregory C. Herman, Michael P. Gagliano, Michelle E. Kuhn, and Mark A. French, NJ Geological & Water Survey, Trenton, NJ..... 1

PRESENTATIONS

NJGWS Calibration and Flow Studies Using Heat-Pulse Flow Meter Model HFP-2293, Gregory C. Herman, Ph.D., New Jersey Geological and Water Survey (Retired)..... 18

Assessment of Electrical Resistivity Method to Map Groundwater Seepage Zones in Heterogeneous Sediments, Michael Gagliano, New Jersey Geological and Water Survey ..49

Aquifer heterogeneity and the importance of calibrating ground-penetrating radar data in environmental investigations, Alex R. Fiore, U.S. Geological Survey.....59

Borehole Televiewer Synoptic and Hydrogeologic Framework of Adjacent RACER and NAWC Industrial Sites, West Trenton, Mercer County, New Jersey, Gregory C. Herman, Ph.D., New Jersey Geological and Water Survey (Retired)66

KEYNOTE PRESENTATION

Mapping Bedrock Fractures and Other Subsurface Conditions in Urbanized Environments Using the Multi-Channel Analysis of Surface Waves (MASW) Geophysical Method, Richard Lee, P.G., R.GP, President and Principal Geophysicist, Quantum Geophysics 100

FIELD TRIP GUIDE

Stop 1– New Jersey Geological and Water Survey, Ewing, NJ. Fern Beetle-Moorcroft and Michael Gagliano, New Jersey Geological & Water Survey 101

Stop 2 – Stockton Formation, Prallsville Mills, Stockton, NJ. Francesca Rea and Don Monteverde, New Jersey Geological & Water Survey..... 109

Stop 3 – Lockatong Formation, Villa Victoria Brook, Ewing, NJ. Gregory C. Herman, Princeton Geoscience, Inc..... 123

Stop 4 – Naval Air Warfare Center, Ewing, NJ. Pierre Lacombe, Thomas Imbrigiotta, Dan Goode, Alex Fiore, Claire Tiedeman U.S. Geological Survey, Trenton, NJ and Menlo Park California. 128

TEACHERS WORKSHOP

2D and 3D Fractured-bedrock characterization methods using oriented borehole imagery

Fern Beetle-Moorcroft, Gregory C. Herman, Mike X. Gagliano, Michelle X. Kuhn, and Mark A. French, NJ Geological & Water Survey, Trenton, NJ

Introduction

GANJ 33 provides an appropriate venue to share the methodology used by staff at the NJ Geological & Water Survey (NJGWS) to characterize geologically complex fractured-bedrock aquifer systems in New Jersey. The NJGWS staff utilizes a combination of subsurface geophysical log data, including optical, and surficial outcrop data in order to measure and accurately portray crosscutting geological feature relationships. This allows for the identification of permeable planes, the conduits along which groundwater flows through fractured aquifers. This workshop focuses on specific personal-computing (PC) software and the methods currently used by the NJGWS to manage and visually characterize subsurface borehole televiewer (BTV) data and outcrop data in complicated geological settings. Specifically, this workshop details the key concepts used to interpret BTV and outcrop data for establishing local hydrogeological frameworks for groundwater supply and pollution work. Prospect Park Quarry, Paterson, NJ is used as a case study to exemplify this methodology.

The first portion of the workshop serves as an introduction to 'structural-feature relative-density profiling' – a profile structural-interpretation method developed by the NJGWS staff. The process involves: 1) the delineation and characterization of visible features in BTV data in WellCAD, 2) the organization of features in Microsoft (MS) Excel, 3) the analysis of features in GeOrient 9.5, and 4) the creation of a 'structural-feature density profile' (Google Earth and MS PowerPoint). The final profile portrays the most common feature orientations in their relative proportions using apparent dip. When combined with surface-borne geological constraints, this method can be used to portray plausible and constrained profile representations of complexly fractured aquifer systems as seen in Chapter 5 (Herman, 2016).

The second portion of the workshop involves using the 'Excel to KML Formatter,' a customized, online tool, to facilitate the three-dimensional (3D) visualization of subsurface data using Google Earth (GE). This tool takes 2D and 3D geological symbols, created in Trimble Navigation's SketchUp Software, and allows the user to define the locations and orientations of features. Thus, the use of the tool and GE renders BTV data into a malleable 3D well field model that can be dynamically viewed and analyzed. As GE does not allow exploration of the subsurface, subsurface features, such as well data, must be lifted above ground for viewing. This allows for the direct comparison of features in multiple wells and visualization of common planar orientations. The concluding activity involves exploring data from Park Quarry in GE.

Prospect Park Quarry: An Ideal Case Study

Prospect Park Quarry (PPQ) is located in Prospect Park, Passaic County, New Jersey and was the first Watchung basalt trap rock quarry (Figure 1). The quarry first opened in 1901 and was fully operational until a few years ago (The Mineral Industry of New Jersey, 1910). Currently, the quarry is being filled in preparation for building a new housing development. At the present time, PPQ represents an ideal case study for fractured bedrock aquifer systems because: 1) there are three monitoring wells varying in depth in close proximity to the quarry pit, 2) the formation contact between the basalt and the sedimentary unit is present in the well records, and 3) there is ample exposed bedrock (Figure 2). The presence of multiple wells in close proximity to one another allows for data from a range of depths and greater potential for correlation of features between wells. The presence of a formation contact allows for the creation of a more accurate geologic cross section. A large amount of exposed bedrock on all sides of the quarry pit allows for documentation of a large number of features and changes in stratigraphy.



Figure 1: gives geographic context for the location of Prospect Park Quarry within the Paterson Quadrangle and the state of New Jersey.

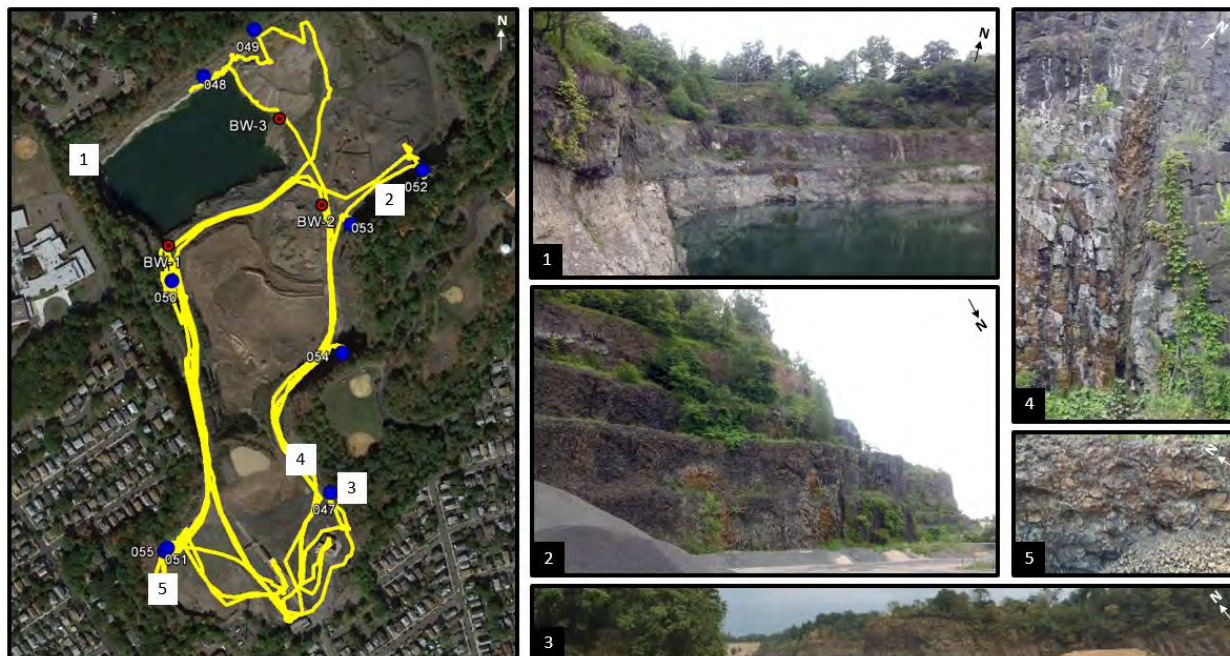


Figure 2: shows a birds-eye view of Prospect Park Quarry on the left. The yellow path is a GPS track for one site visit. The numbered boxes represent the location of each photograph taken in the quarry. 1) shows the abandoned quarry pit, which has subsequently filled in with water, 2) depicts the reddish plumose structures, 3) is a panorama along the top of the quarry, 4) shows the fault (Figure 15) from down strike, and 5) is an image of the pillow basalts.

Geological Analysis of Borehole Televier (BTV) Data

Borehole Televier Data (BTV) data provides a lens into the subsurface, as well as, access to quantifiable structural data in situ and at depth. At the NJGWS, through years of working with BTV data, we have developed a clear and concise method for transforming raw BTV data into a 'structural-feature, relative-density profile.' Each of these steps is outlined in detail below.

Raw BTV/OPTV Data

Borehole imaging began in the 1950's using rigged photographic cameras and evolved into first generation optical imaging devices by the 1980's (Lowell and others, 1999). Today, the NJGWS utilizes an optical televier (OPTV), which provides a continuous, orientated, detailed, color image of the borehole substrate (Figure 3A). The OPTV captures 360° stacked photographic rings in geographic alignment collected at 1mm depth intervals. Once captured, the 360° image is then unrolled in WellCAD to occupy a 2D surface, causing features to resemble 'V's' where the amplitude indicates the dip and the trough shows the dip direction (Figure 3B). OPTV data is incredibly powerful and informative, but can at times be an overwhelming amount of information to analyze. Thus, it is important to break down the information using a methodical, time-tested approach such as the one described below. In order to make learning the process as simple as possible, useful shortcuts and tips are included.

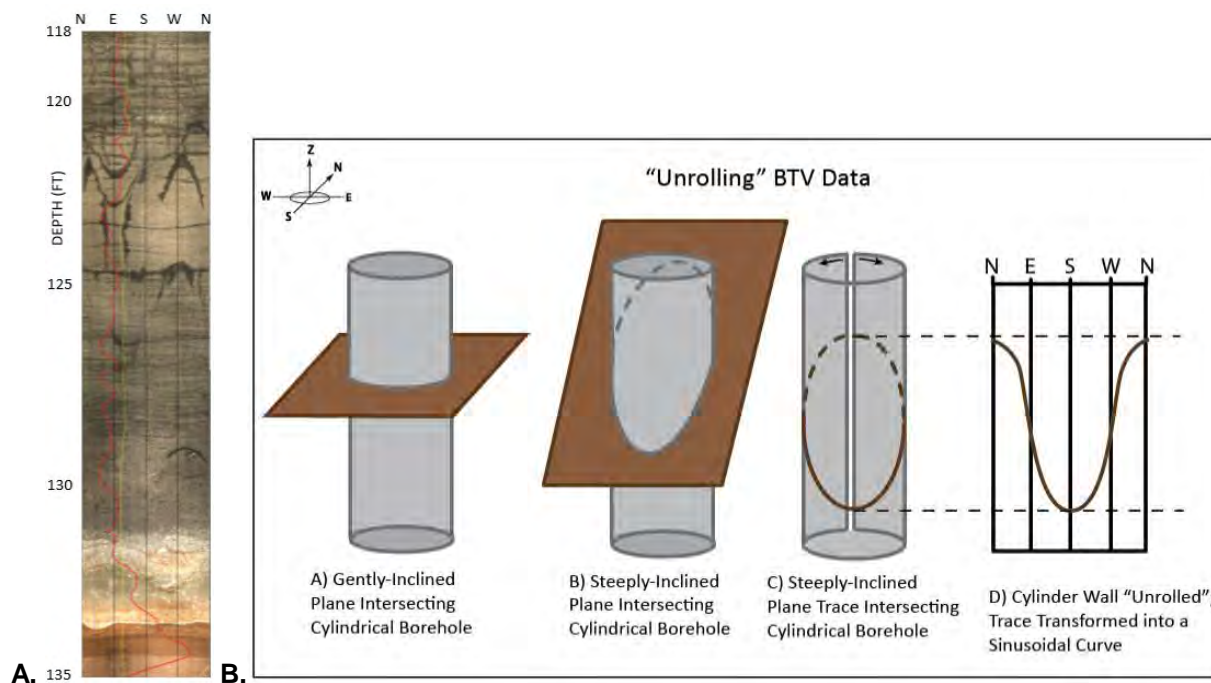


Figure 3: A) OPTV example image excerpt from Well #2 at PPQ from 118-135 ft depth. The features present resemble 'V's'. B) Schematic diagram illustrating how cylindrical BTV records are processed by 'unwrapping', flattening, and transforming borehole data. The trough of the trace (or bottom of the 'V') gives the structure dip azimuth. Higher dips correlate with sharper V's.

Pre-Analysis Corrections: Telemetry, True North, and Interpolation of Bad Traces

Prior to analyzing and quantifying features it is essential to apply a few corrections. Boreholes tend to be slightly tilted from vertical and drift more from vertical with increasing depth. Borehole telemetry is influenced by both rheological contrasts in adjacent lithologies and variations in the crustal stress regime with depth from lithostatic loading. Since feature measurements assume borehole verticality, a telemetry correction for structural measurements is needed to account for drift in boreholes generally deeper than a couple of hundred feet (Herman and Curran, 2010). The telemetry correction relies on incremental sampling of the borehole azimuth (direction) and borehole tilt (Herman et al., 2015). No example is provided here as the wells at PPQ are all less than 250 ft deep.

When captured, OPTV images are automatically oriented to magnetic north and thus, must be rotated by 12.5° counterclockwise to match true north. Additionally, 1mm increments are sometimes missing from the record and can be fixed by interpolating bad traces, which joins both sides of the image to remove small gaps.

Classification of geological structures

The creation of a detailed classification scheme is the first step in rendering BTV data into an interpretive geological cross section. At NJGWS, we categorize features in WellCAD using the geological and hydraulic variables specified in Figure 4. Features are classified first by their type (primary or secondary) and then

by a series of additional characteristics (kind, sense, permeable, and altered).

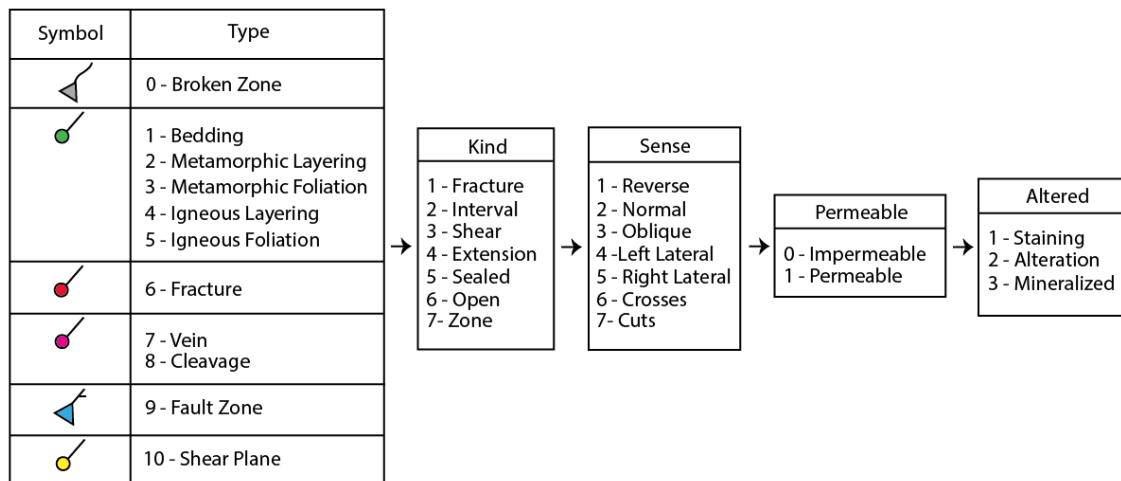


Figure 4: depicts the NJGWS Geological Classification Scheme used in WellCAD. Features are classified in the following order: type, kind, sense, permeable, and altered.

Primary features are depositional features and indicate paleohorizontal. Examples of primary features are: bedding and igneous/metamorphic layering. Secondary features are post-depositional and caused by paleo-stresses. Examples of secondary features include: 1) unhealed fractures lacking visual evidence of secondary minerals cementing fracture interstices, 2) healed fractures (i.e. veins) having cemented or partially cemented interstices, and 3) faults showing evidence of structural shear or slip (i.e. kinematic motion). Whether a fractured-bedrock aquifer behaves *isotropically*, equivalent to porous media, or with layer-controlled hydraulic anisotropy depends on the bulk heterogeneity. The identification and classification of features assists with determining the bulk heterogeneity.

Additional characteristics are organized into the categories of kind, sense, permeable, and altered (Figure 4). Kind is a descriptor for the type and mainly assists with describing secondary features. E.g. a fracture can be given kind: interval, shear, extension, or open to describe the state of stress of its formation. Similarly, a fracture in the orientation of bedding (i.e. a reactivated bedding plane) can be given type: bedding and kind: fracture. Sense relates to fault type (e.g. reverse, normal) and movement (oblique, right lateral, left lateral). Permeable provides the opportunity to note if a particular feature is permeable. Altered relates to hydrothermal alteration of the protolith (i.e. staining, mineralization).

Figure 5 provides example features present in the OPTV record from BW #1 at PPQ and shows how they were classified. The first feature in green is an example of a reactivated, impermeable, igneous layering plane. The second feature in red is an open, impermeable, fracture. Once all of the features are marked and classified, the data is exported as a comma separated values (csv) file.

The csv file is then opened in MS Excel and sorted A-Z by type. The csv file uses the number values above in Figures 4 and 5 to define the type (i.e. bedding =1; igneous layering =4; fracture=6) and additional

characteristics. At NJGWS, we change the numbered categories to descriptions (e.g. change type: 1 to type: bedding) for record keeping purposes. Once we have edited the structural data in MS Excel, we import it back into WellCAD as a comments log. This allows a reader looking at the log to see the analytical description of each feature. We also copy the feature orientation data into text files for each unit, separating primary features (i.e. bedding, igneous/metamorphic layering, and igneous/metamorphic foliations) and secondary features (e.g. fractures, veins, cleavage, fault zone, and shear plane) for ease of analysis in GEOrient 9.5.

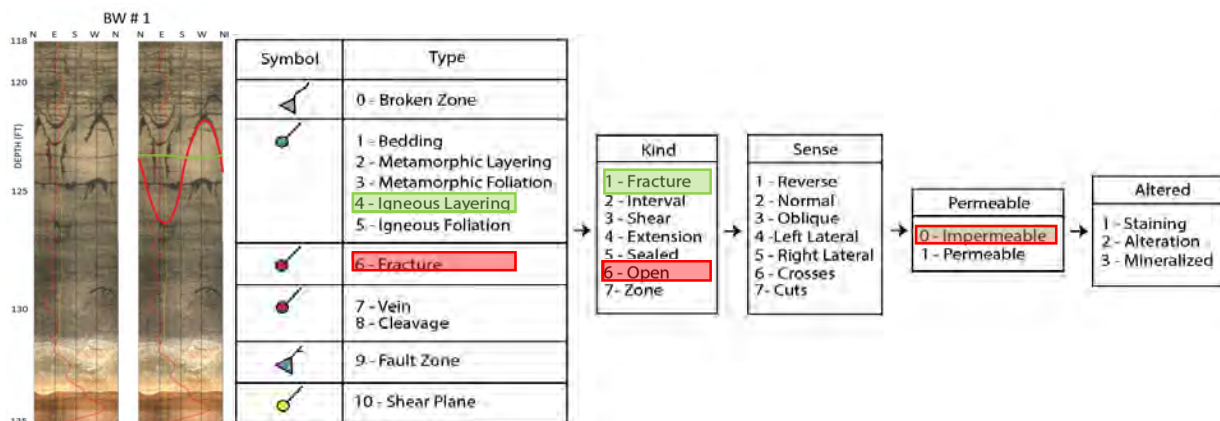


Figure 5: shows two features chosen in wellCAD along with their classifications.

Structural analysis using GEOrient 9.5 stereographic and histogram plots

Now that we have delineated and precisely characterized all of the features present in the BTV record, we begin our next level of analysis – determining the frequency of each type of feature orientation. Software that includes stereographic and histogram plots is ideal for this type of analysis. At NJGWS, we use GEOrient 9.5 to create a rose diagram (circular data frequency dip azimuth histogram) and equal-angle, lower-hemisphere stereonet projections – contour plots and cyclographic plots to analyze structural trends (Holcombe, 2011). Each plot is created separately for primary and secondary features in each rock unit (Figures 6 and 7). Specifically, these plots are used to determine the mean orientation(s) of primary features and the five most common secondary feature orientations. Rose diagrams show the relative dominance of each planar feature and provide a mean resultant direction (dip azimuth), which is particularly useful for discriminating between features having similar strike, but opposing dips (Figure 6A). This is pertinent for understanding the patterns of cross bedding seen in alluvial systems (see Chapter 5) or borehole-scale folding of the geological layers. Contour diagrams show polar lines contoured based upon the density/frequency of similar measurements and are used for determining the relative percentages of bedding and fracture orientations. These density/frequency maxima can then be manually selected to define up to five great circles – the five most representative planes (Figure 6B). Cyclographic plots depict the composite set of measurements of great circle traces (Figure 6C). The cyclographic plot is ideal for checking the other two plots. The most common planar orientations should match the maxima on the contour diagram the mean resultant direction from the rose diagram.

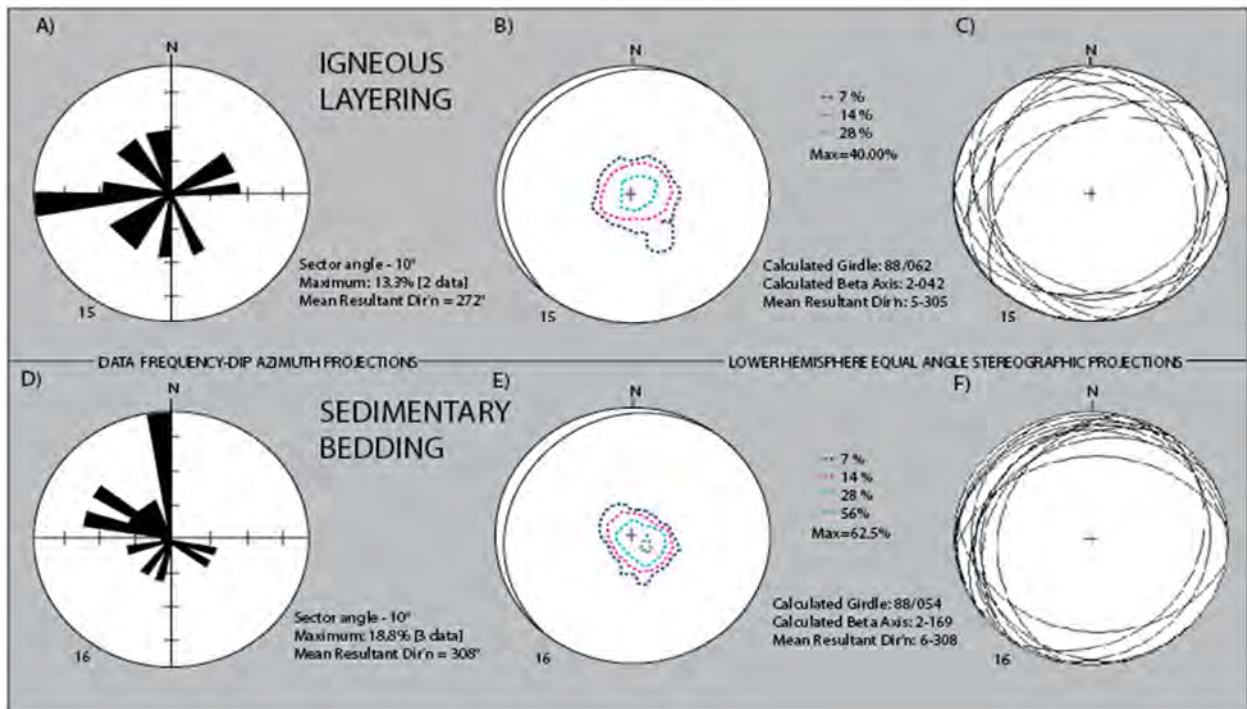


Figure 6: Stereographic and histogram plots for layering/bedding features; diagrams A, B, and C show igneous layering in the basalt unit and diagrams D, E, and F show bedding in the sedimentary unit. There is cross-bedding present in the sedimentary unit and evidence of change in the flow direction of the basalt unit. The majority of the features are shallow dipping.

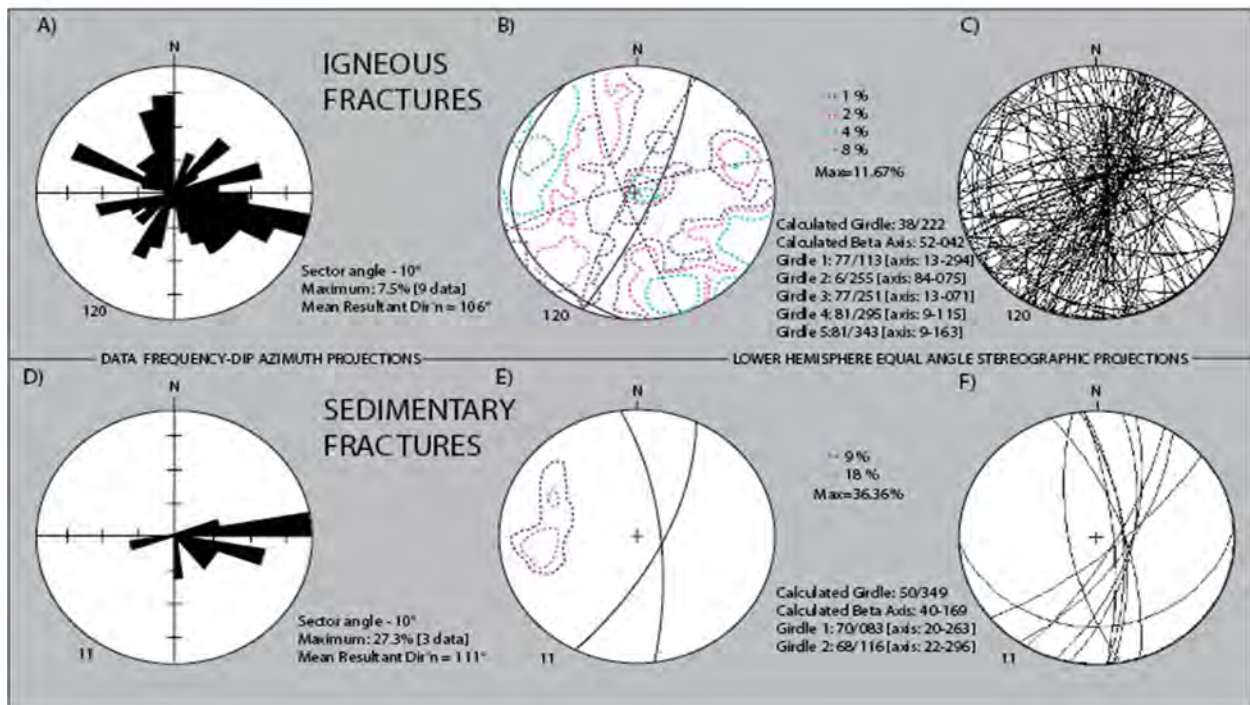


Figure 7: depicts stereographic and histogram plots for secondary features (i.e. fractures); diagrams A, B, and C show secondary features in the basalt unit and diagrams D, E, and F show secondary features in the sedimentary unit. The basalt unit is highly fractured with five main orientations present. There are fewer data points for the sedimentary unit and only two main orientations present.

Structural analysis using Prospect Park as an example

Figures 6 and 7 use data from Prospect Park Quarry to provide an example of the complexities associated with stereonet analysis and the importance of comparing multiple visual representations. Looking at the rose diagrams (Figure 6A and 6D), igneous layering has a due west maximum and sedimentary bedding has a due north maximum. This information alone suggests that the intersection of bedding/layering from the two units would be nearly orthogonal. However, the mean resultant directions of the two units are 272° and 308° respectively. This lends itself to the interpretation that there is cross-bedding present in the sedimentary unit and variance in flow direction in the basalt unit. The rose diagram provides no information about the dip of the units, whereas, the contour diagram looks at both the dominant dip and dip azimuth. Diagrams 6B and 6E have very similar dip and dip azimuths, suggesting little structural change between the deposition of the two units. The planes diagram provides the opportunity to check that the resultant planes are dominant. In this case, the mean resultant planes from the contour diagrams are dominant, but only slightly as a result of the cross-bedding.

Structural-Feature Density Profiling

Creation of the 'structural-feature density profile' is the next step in displaying subsurface structural trends. This process is used to develop geologic profiles including the orientations of the most representative structural planes. This approach can be used for outcrop and/or BTV data and utilizes the apparent dips of each representative plane determined from stereonet analysis. The first step involves choosing an ideal cross section location. The profile trace should be normal to stratigraphic layering and in close proximity to collected data points (Figure 8A). This allows stratigraphic dips to be portrayed in their true orientation and data points to be easily projected onto the cross section. Once the location of the profile trace is chosen it must be drawn in GE using the ruler tool and saved as a named feature, in this case 'Prospect Park Profile'. The elevation profile is then generated by right clicking the feature in the table of contents and selecting 'show elevation profile'. A screen shot can be taken using the 'snipping tool' and pasted into MS PowerPoint (PP). In PP, the profile is traced using the second 'curve tool' and the amount of vertical exaggeration is determined (7B). Using the example of Prospect Park, the true ground distance represented is 3,690' and the actual profile line length is 4.68". In order to remove the vertical exaggeration, the total height of the profile is divided by 9.6 in the 'size and position setting'. The 1:1 scaling created Figure 8C, the true profile.

After the profile line is scaled, wells not located directly on a profile line must be orthogonally projected onto the profile at their correct elevation, not the land surface of the profile. BW#1 lies on the cross section and thus does not need to be projected. BW#2 and BW#3 do not lie on the cross section and are orthogonally projected onto the cross section from ~ 700 ft to the NE of the cross section at their appropriate elevations (Figure 9A). From the BTV analysis (Figure 10), we know that the contact separates the igneous unit above and the sedimentary unit below and is dipping 5° NW, a much gentler dip than depicted in Figure 9A. The 'Raw Geologic Cross Section does not take into account the location of the well within the stratigraphic sequence. From the data, we know that BW#2 is down dip from the cross section. The 'Refined Geologic

SHALLOW SUBSURFACE GEOPHYSICAL APPLICATIONS IN ENVIRONMENTAL GEOLOGY
 GANJ XXXIII Annual Conference and Field Trip

Cross Section' takes this into consideration and places BW#2 at its correct place in the sequence (Figure 9B). BW#3 record is cloudy and the contact cannot be noted, so the actual location of BW#3 in the section is unknown.

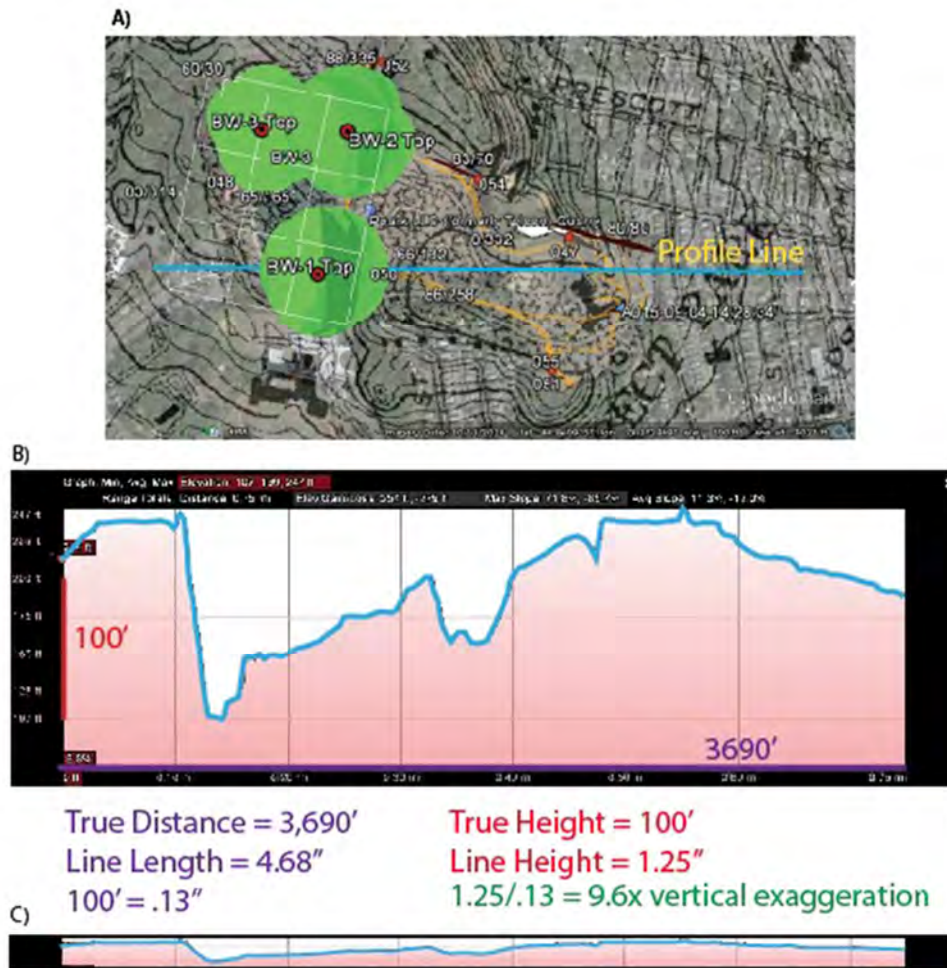


Figure 8: depicts the process of generating an elevation profile in GE and removing vertical exaggeration to create a 1-1 profile. A) shows the location of the profile line for Prospect Park, which runs through BW#1 and is located near to BW#2 and BW#3. B) depicts the cross-section generated in GE C) shows the 1-1 profile. This 1-1 profile is used later on for the geologic cross section (Figure 8) and the 'Structural-Feature Relative Density Profile' (Figure 10E).

Once the contact and wells have been placed on the cross section, the bedding and layering orientations – primary and secondary – must be added. These orientations are taken from the stereonet analysis (Figure 6) and apparent dip is calculated. We use this apparent dip calculator, www.impacttectonics.org/geoTools/appdipcalc.html - which uses the true dip and the deviation angle between a measured planes dip direction (azimuth) and the trend of the profile trace to calculate the apparent dip (Figure 11). For PPQ, the primary igneous layering has an apparent dip of 4° NW and the secondary igneous layering has a dip of -4° SE; the primary sedimentary bedding had a dip of 5° NW and the secondary sedimentary bedding has a dip of -5° SE. Both units are dominated by shallow dipping primary features and include cross-bedded features (Figure 9).

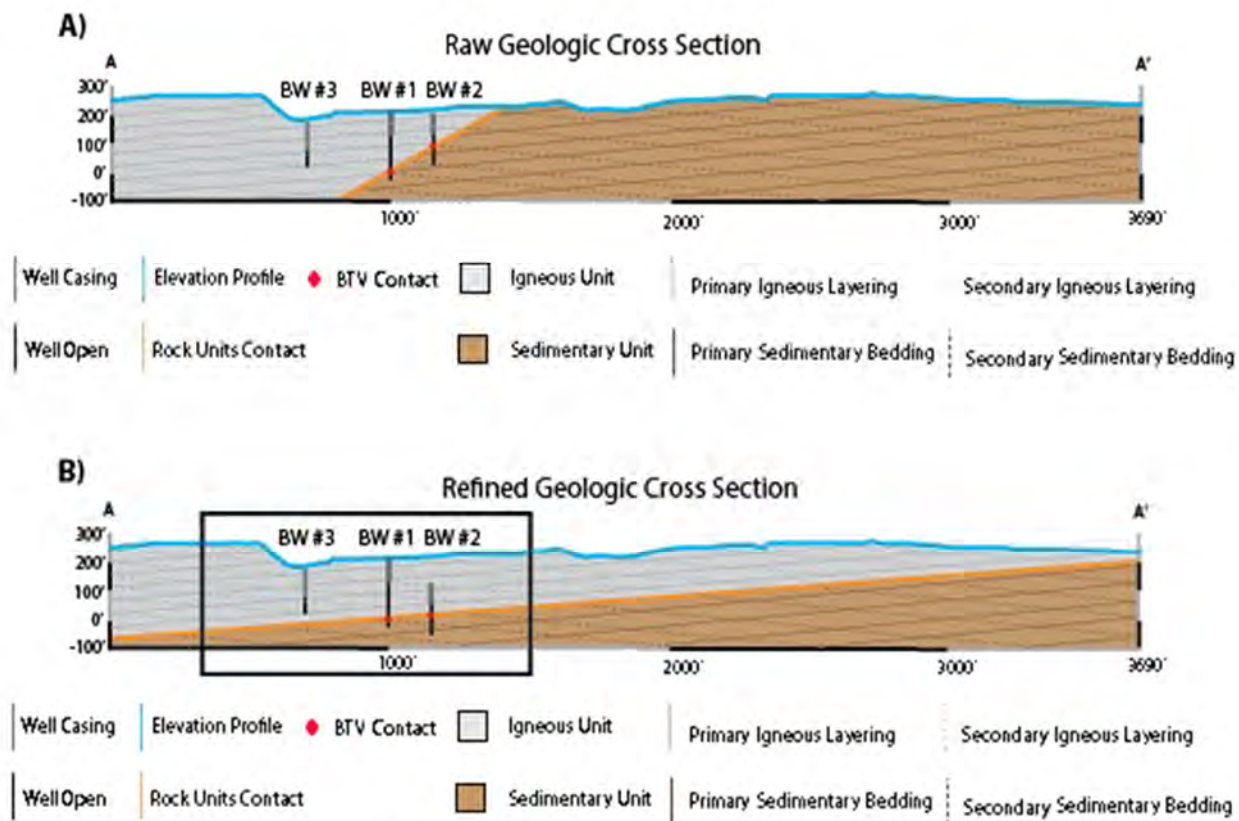


Figure 9: depicts geologic cross sections for the elevation profile shown above in Figure 7. Cross section A) is a raw geologic cross section meaning that the wells are projected onto the cross section at their approximate elevations, but structural effects are not accounted for; whereas, cross section B) is a refined cross section and accounts for the structural impact of each wells' actual location.

Once the framework of the geologic profile is complete, we generate a base unit for bedding/layering and fracture geometry. These base units include all bedding and fracture orientations in their relative abundance as determined by the stereonet and histograms. The primary and secondary bedding/layering orientations are taken from Figure 9. The fracture orientations are taken from the dominant planes determined by the contour diagrams (Figure 12A and 12B). There are effectively four dominant secondary feature orientations in the basalt unit. Three of the dominant planes each account for 8% of features and one accounts for 4% (Figure 12A). There are two dominant secondary feature planes in the sedimentary unit. Each accounts for 18% of features (Figure 12B). Figures 12C and 12D show the base units for the igneous and sedimentary units respectively. Once the base units are complete, they are transposed onto the profile and indicate relative flow pathways (Figure 12E). A higher abundance of horizontal or slightly dipping fractures indicates more bedding plane movement, whereas, a higher abundance of vertical or steeply dipping fractures indicates a greater likelihood of vertical movement and thus, greater potential contamination at depth.

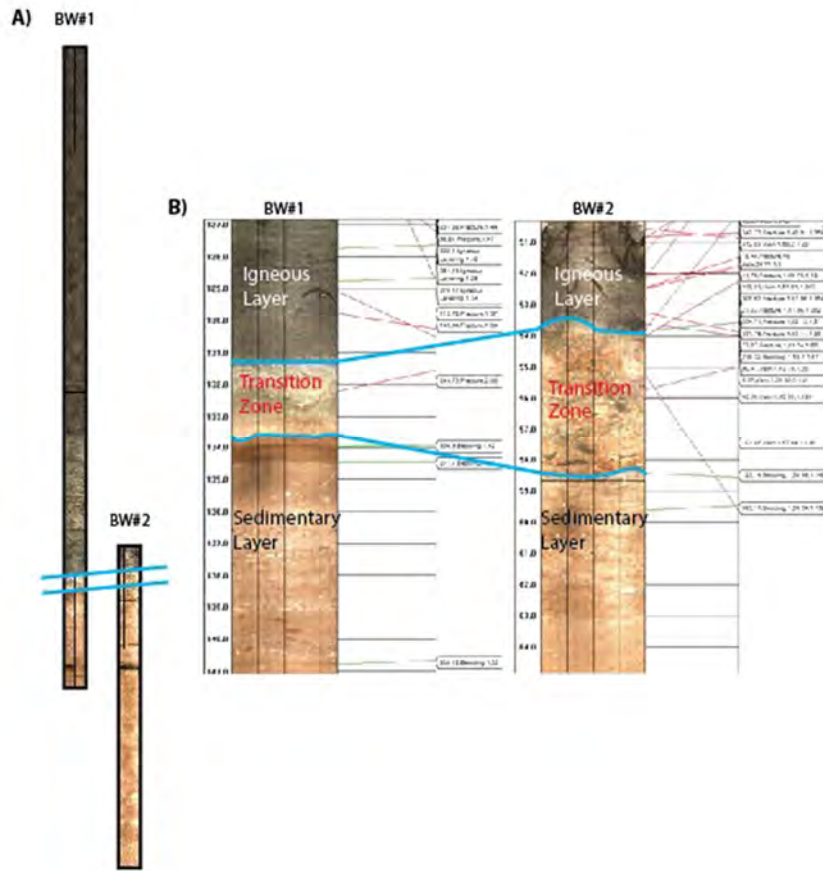


Figure 10: displays the BTV images, copied from WellCAD, for BW#1 and BW#2; BW#3 is omitted because the record is too cloudy. A) shows the full BTV record and B) shows a close up of the contact. The contact separates the dark grey igneous unit from the light orange sedimentary unit. A) shows the slope of the contact as 5°, the average apparent dip of layering and bedding in the two units. B) outlines the transition zone and shows that the same unit may not appear exactly the same.

Apparent Dip Calculator

Example Input

Take from an Excel spreadsheet and calculate apparent dip given cross section azimuth, true dip, and plane dip azimuth.
 Cut & Paste from a MS Excel Worksheet using the format found in the example input above. Do not include the headers.

You can also enter the values for the input field (true dip, cross section, plane dip azimuth) in comma separated form.

True Dip	Cross Section Azimuth	Plane Dip Azimuth	Apparent Dip(Degrees)
5°	145°	305°	4° - Igneous
6°	145°	308°	5° - Sedimentary

Figure 11: depicts the online apparent dip calculator used to calculate the apparent dips for the cross sections.

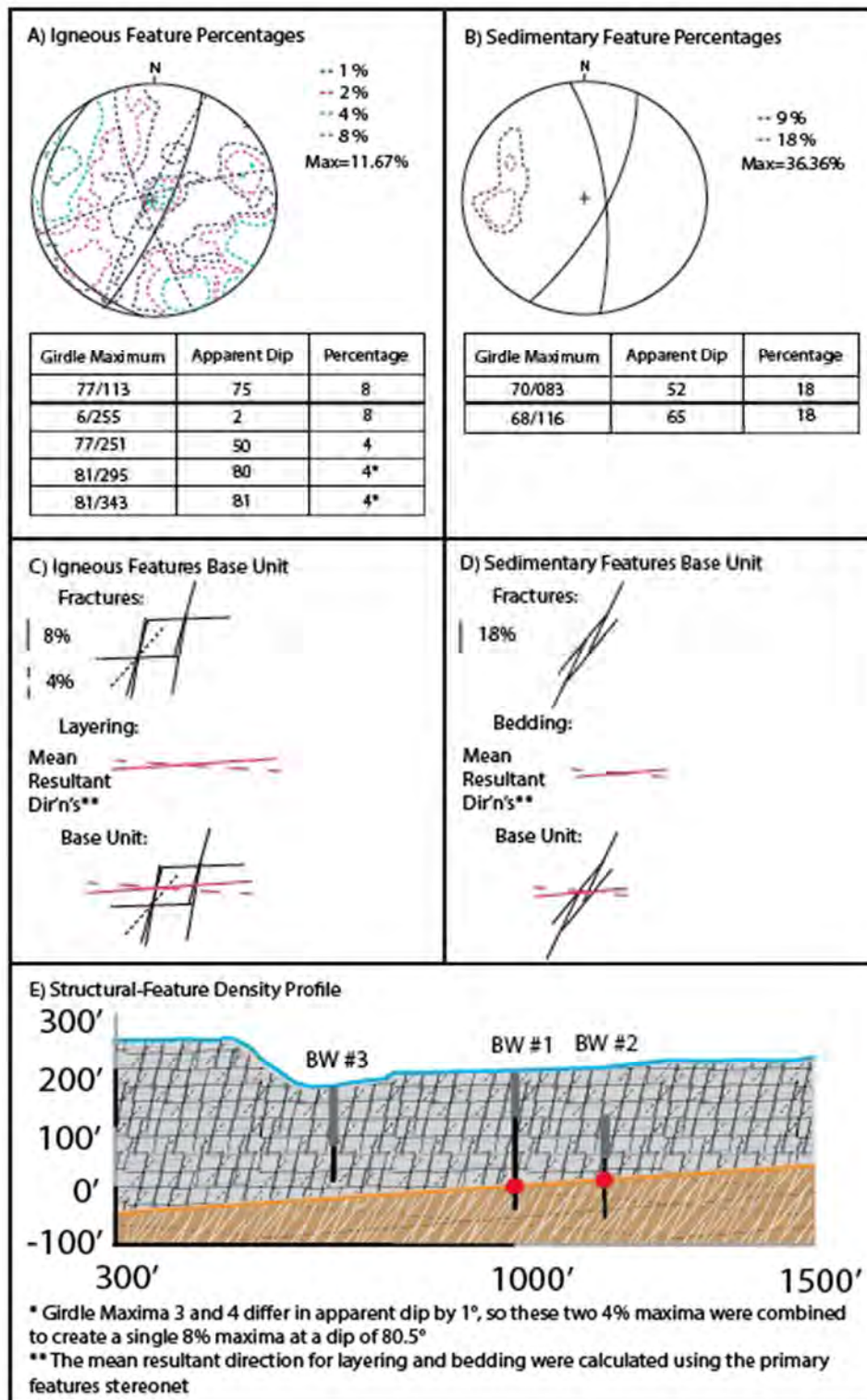


Figure 12: shows the creation of the 'Structural-Feature Relative-Density Profile'. A) and C) focus on the igneous unit and B) and D) look at the sedimentary unit. A) and B) show the stereographic contour diagrams used to determine the most common orientations. C) and D) show the base units for each rock unit. E) shows the final 'structural-feature relative-density profile'

Google Earth (GE) 2D and 3D Geological analyses

In order to aid in the understanding of geologic feature orientations and to compare features in adjacent wells or well and bedrock data, we have created 2D geologic symbols and 3D geologic models that can be placed at specified coordinates (latitude-longitude) and elevations in GE (Herman, 2013; De Paor and Whitmeyer, 2011). The 2D symbols are structural-geological symbols (i.e. strike/dip, dip/dip-azimuth, etc.) and the 3D models contain circles/ellipses with tilt that mimic the planar orientation of bedrock and/or feature data (Figure 13). The symbols are already generated in SketchUp and can be manipulated in any orientation using the online 'Excel to Kml Formatter' which can be found at <http://www.impacttectonics.org/geoTools/exceltoKML.html> (Figure 14).

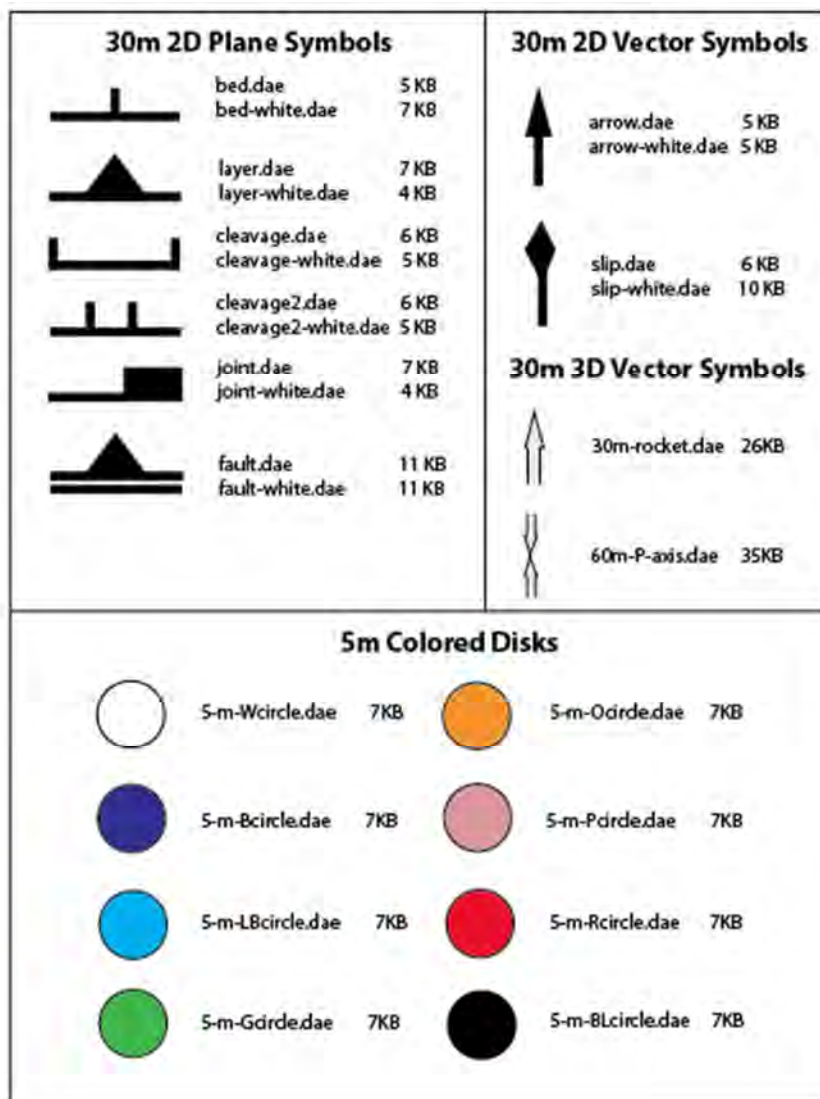


Figure 13: portrays the 2D and 3D symbols generated by the NJGWS staff in Trimble Navigation's SketchUp software for use in GE.

Excel to KML Geologic Symbols (symbol key at bottom)

Convert data from an Excel spreadsheet to geological symbols and circles in KML format.

Cut & Paste variable input from a formatted MS Excel Worskheet into the following windows, using the variables noted above the window.

Download example input here:

The symbol (*.dae) files that this tool uses must reside within the directory that you load the resulting *.KML file into Google Earth from, or by using on-line symbols using the <http://www.impacttectonics.org/GEsymbols/> prefix for each symbol. The full set of symbols in a *.zip file with explanations and related topics are available at <http://www.impacttectonics.org>

KML Name: Include Timestamp Info

Anno Spacing: Bed and layer dip line (~1.5 m): Joint, arrow, slip-line (~ 8.0 m) or 5-m 3D circle:

Station	Longitude	Latitude	Altitude	Azimuth	Dip/Plunge	Xscale	Yscale	Zscale	Symbol	Note	Orientation(2D/3D)	Date Time
BW#1	-74.1743°	40.9428°	240	260	67	10	5	1	5-m-Rcircle.dae	fracture	3D	
BW#1	-74.1743°	40.9428°	238	107	61	10	5	1	5-m-Rcircle.dae	fracture	3D	
BW#1	-74.1743°	40.9428°	233	337	75	10	5	1	5-m-Rcircle.dae	fracture	3D	

Figure 14: displays the Excel to KML tool, which converts structural data into planes in GE. The tool requires data to be input in an excel file, with each category in its own row (station, longitude, latitude, etc.) and in the proper order as shown in the diagram. The information regarding the symbol names can be downloaded from the website shown. It is important that the symbols are linked to a saved place in your directory or linked to the web using the link shown. Once all of the information is compiled it must be copied and pasted into the tool. Avoid inserting any extra spaces as this will prevent the tool from functioning properly. Finally, the “generate KML” button creates a KML file, which is automatically saved to downloads. The file is now ready for use and can be opened in GE.

Before generating the symbols, it is necessary to project the subsurface data above ground (Figure 15) and to correct for telemetry (page 4). We use the following criteria to pick an appropriate high point for the model: all wells in the well field must be entirely above ground, planar features in the well should be mostly above ground (important to account for steeply dipping features near the base of the well), and wells must be placed at their accurate relative elevation (reflecting ground elevation). Outcrop feature data must be placed at the elevation of the outcrop – this can be determined using the elevation of the site as found in GE. Once these necessary corrections have been completed, the features can be generated using the MS Excel to kml tool (Figure 14). It is easiest to enter the required information in an Excel file and then copy the data into the tool. This preserves the required spacing. We typically use different colored symbols to

SHALLOW SUBSURFACE GEOPHYSICAL APPLICATIONS IN ENVIRONMENTAL GEOLOGY
 GANJ XXXIII Annual Conference and Field Trip

differentiate between bedding and secondary feature data and use the following scale for the x, y, and z dimensions – 10, 5, and 1 respectively. Sometimes, it is helpful to add additional categories to highlight a specific plane. For Prospect Park Quarry, there are two different rock units which have been coded in different colors. When working on a pollution study, it can be helpful to highlight potential fractures responsible for transmitting contaminants. To edit already generated symbols, right click on an individual plane (make sure to select the feature and not the annotations) and select properties. This opens a window with a field called “link” which lists the color of the symbol in text. Simply edit the text in the link to change the color of the desired feature. Figure 16 shows the finished floating well field for Prospect Park Quarry as an example.

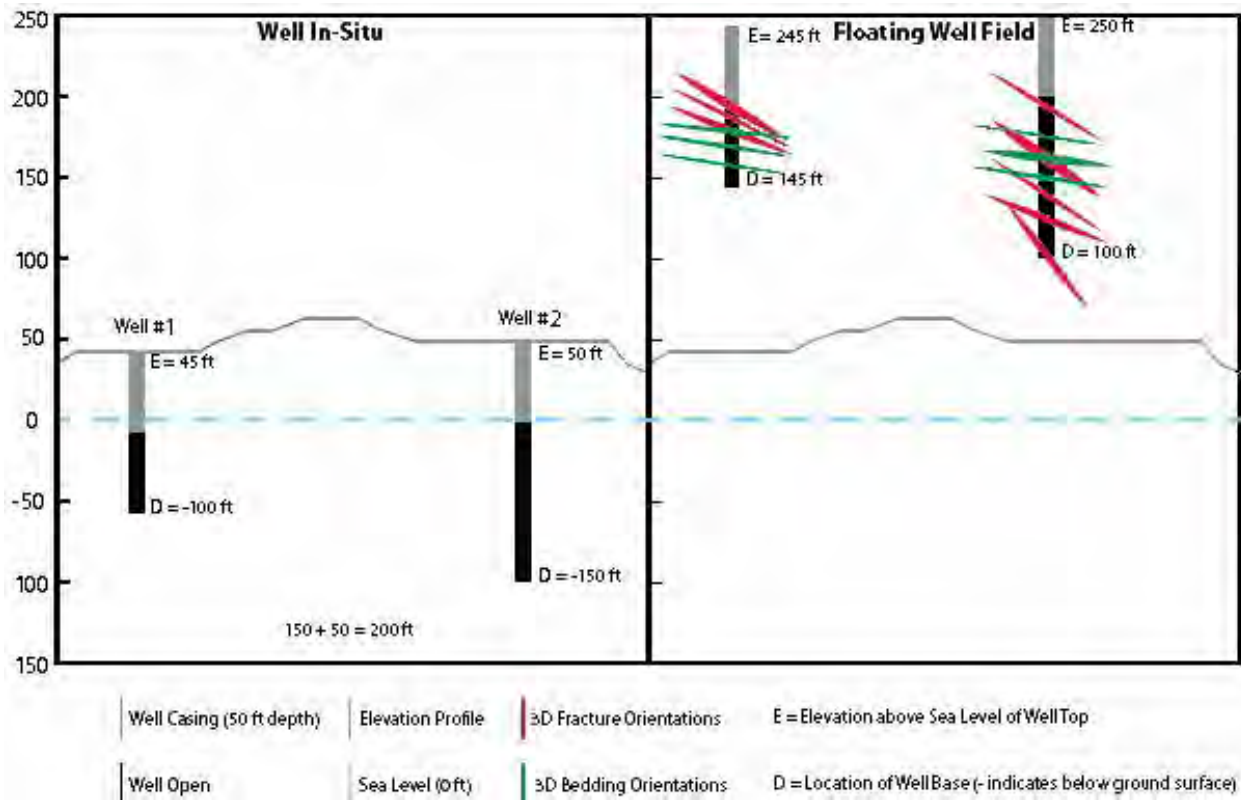


Figure 15: makes clear the translation of well data taken in situ and at depth to a floating well field model. The initial elevation and depth of well #1 are 45ft and -55ft respectively. This translated to an elevation of 245ft and a depth of 145ft for the floating well field. Well #2 had an initial elevation of 50ft and a depth of -150ft. The model for Well #2 has an elevation of 250ft and a depth of 50ft. This floating well field meets the aforementioned criteria.

Altitude Options in GE

GE Provides five options for altitude: relative to ground, relative to sea floor, absolute, clamped to ground, and clamped to sea floor. When a newly generated kml file is opened in GE; features are automatically placed relative to ground. The relative options measure from the chosen surface (meaning GE views the chosen surface as 0 ft), ground and seafloor respectively; thus, if the ground surface is 75 ft and a plane

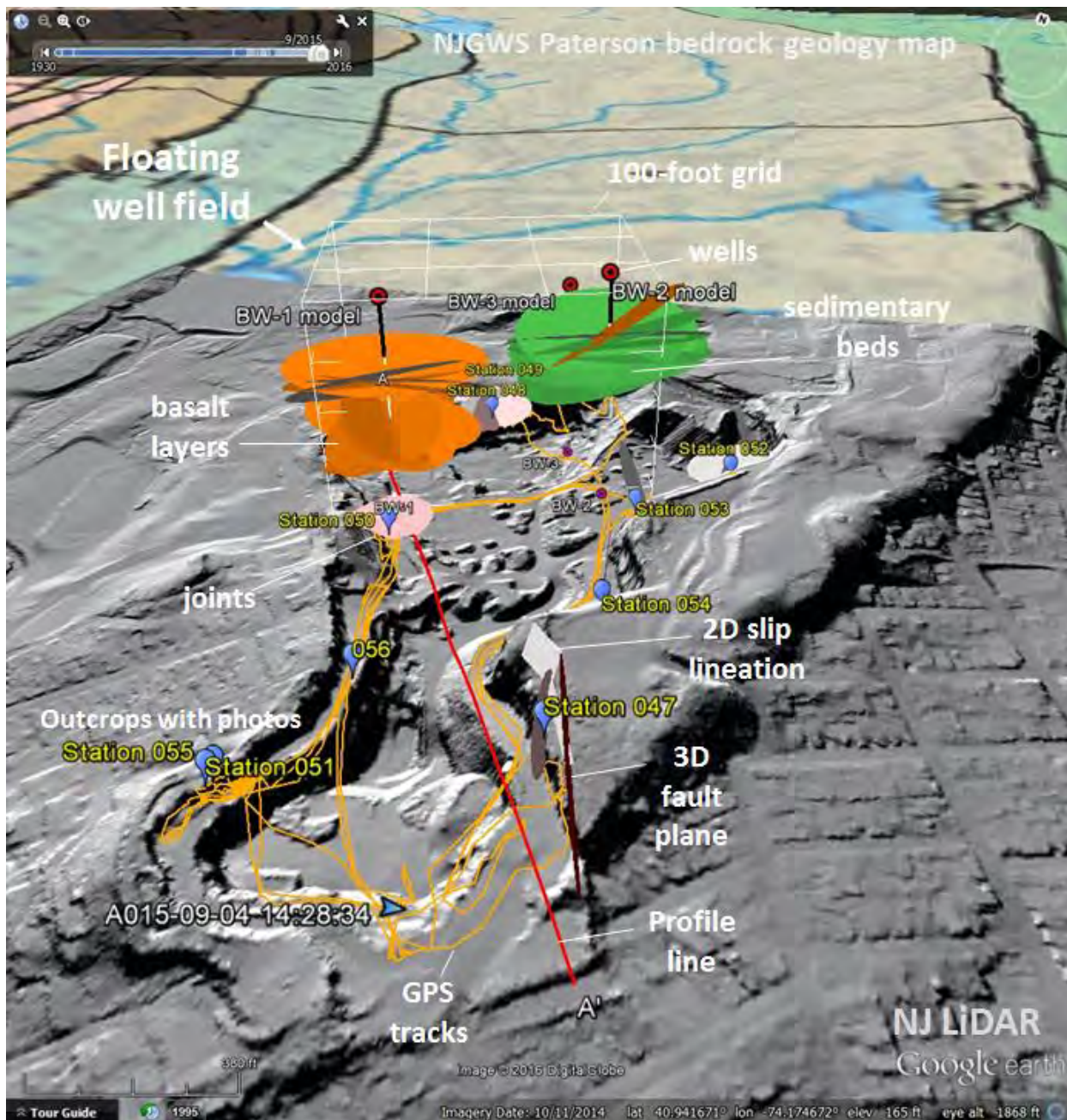


Figure 16: GE display of the NJGWS outcrop and BTV data for Prospect Park Quarry. Basalt layering is shown in orange and sedimentary bedding is in green. The cross-cutting bedding planes represents cross bedding in the sedimentary unit and multidirectional flows in the basalt. Note the offset of the bedrock ridge along the 3D fault plane, and the mismatch of layering and bedding across the projected fault zone.

is given an altitude of 25 ft, the plane will be placed at 100 total ft and 25 ft above the ground surface. The absolute option measures directly from sea level; so, if the ground elevation is 25 ft and a plane is given an altitude of 35 ft, the plane will be placed 10 ft above the ground. As our elevation profiles represent a range of ground elevations, we typically think of elevation in terms of absolute for well and/or other subsurface measurements. The clamped to ground/seafloor options place the center of the feature at ground/seafloor

SHALLOW SUBSURFACE GEOPHYSICAL APPLICATIONS IN ENVIRONMENTAL GEOLOGY

GANJ XXXIII Annual Conference and Field Trip

level. This is useful for outcrop data, where measurements are typically taken at the ground surface.

In addition to creating planes for bedding/layering and features present in well data, the Excel to Kml Tool is also useful for modeling outcrop data. Planes are generated the same way, except instead of giving the planes an absolute altitude, the planes can be clamped to the ground. Outcrop data can provide information regarding general bedding trends, unit contacts, faults, and common fracture planes. Being able to visualize this information in GE aids in quarry prospecting, in determining the extent of potential contamination, and in a more complete understanding of the area's subsurface geology.

Exercise using outcrop and BTV data to render features in Google Earth (GE)

For this conference, we have posted the outcrop and BTV data for Prospect Park Trap Rock Quarry for free download: www.ganj.org/2016/2016data.html. This data includes a GE kmz file containing: 1) a GPS track of data collection, 2) waypoints marking outcrops where structural data was collected, and 3) BTV data including Optical Borehole Imaging (OBI) for the three monitoring wells. Also included is a MS PowerPoint File, which shows the structural interpretation methods outlined above.

The goal of this exercise is to utilize MS Excel, MS PowerPoint, and GE kmz data on your laptop to practice the discussed methodology. We will present the methods used and demonstrate ways of inserting and manipulating graphics in both 2D and 3D perspectives.

References

- De Paor, D.G. and Whitmeyer, S.J. 2011. Geological and Geophysical Modeling on Virtual Globes Using KML, COLLADA, and Javascript. *Computers and Geosciences*, v. 37, p. 100-110.
- Herman, G. C. and Curran, John, 2010, Borehole geophysics and hydrogeology studies in the Newark basin, New Jersey (38 MB PDF), *in* Herman, G. C., and Serfes, M. E., eds., *Contributions to the geology and hydrogeology of the Newark basin: N.J. Geological Survey Bulletin 77*, Appendixes 1-4, 245 p
- Herman, G. C., 2013, Utilizing Google Earth for geospatial, tectonic, and hydrogeological research at the New Jersey Geological and Water Survey: *Geological Society America Abstracts with Programs*, Vol. 45, No. 17, p. 110
- Herman, G. C., French, M. A., and Curran, J., 2015. [Borehole Geophysical Logs and Geological Interpretation of Two Deep, Open Boreholes in the Passaic Formation, Elizabeth City, Union County, New Jersey](#): NJ Geological & Water Survey Geological Series Report GSR 42, 26 p., 2 appendixes, [1 zip file](#) (14.5 MB).
- Herman, G.C., 2016. Chapter 5. Borehole Televiewer Synoptic and Hydrogeological Framework of Adjacent GM-RACER and NAWC Industrial Sites, West Trenton, Mercer County, New Jersey: GANJ XXXIII Shallow Subsurface Geophysics; Applications in Environmental Geology.
- Holcombe, R., 2011. GEOrient 9.5 [Computer Software]. Retrieved from <http://www.holcombe.net.au/software/>
- Lowell, M.A., Williamson, G., & Harvey, P.K., (eds.) 1999, Borehole Imaging: applications and case histories. *Geological Society of London Special Publication 159*, 1-43.
- The Mineral Industry of New Jersey for 1926: 10.

PRESENTATIONS

NJGWS Calibration and Flow Studies Using Heat-Pulse Flow Meter Model HFP-2293

Gregory C. Herman, Mark A. French, and Rachel M. Filo, New Jersey Geological and Water Survey



Chief James T. Boyle and coauthor Mark French oversees HFM system testing in the NJGWS garage. The HFP-2293 is positioned in the clear, 7.5-inch pipe to the right and setup for upward, low-flow testing.

Introduction

A heat-pulse flow meter (HFM) is a geophysical sonde used to measure sub-vertical (axial) water-flow rates in water wells. It's ordinarily deployed in a static, non-trolling mode and works when a field operator triggers a heat-pulse to be released from a wire grid (Figure 1B) into a water column. Moving water will carry a heat pulse past one of two heat sensors (thermistors) that are housed within the sondes measurement chamber and situated at fixed distances (~ 2cm) above and below the heat source (Figures 1 and 2). The time it takes for the maximum amplitude of the heat-pulse to pass by a thermistor is the instrument-response time (IRT). An IRT is used to calculate axial flow rates (feet or meters per second or minute) using a mathematical equation that relates IRTs to flow as determined by calibration flow tests. Volumetric rates (gallons or liters per minute) are calculated by multiplying axial flow rates by the area of the borehole cross section, which is a function of borehole diameter. Ordinarily, the field technician records multiple firing-and-response cycles at various fixed depths to determine an average flow rate at each depth (Figure 2).

HFM technology was developed in the early 1980's and is in widespread use today for groundwater investigations involving open boreholes developed in fractured bedrock having discreet, permeable subsurface features (Hess, 1986; Hess and Paillet, 1990; Paillet, 1998). HFM technology is recognized in a New Jersey Department of Environmental Protection (NJDEP) procedure manual (NJDEP, 2005) and guidance document (NJDEP, 2012) as a geophysical instrument that can help identify discreet, permeable fractures and the nature of borehole cross flows in a well field. This information is helpful for characterizing and remediating groundwater pollution sites in fractured-bedrock terrain, but lingering issues have hampered quantitative use of HFM results to determine aquifer characteristics. For example, the manufacturer's design of the HFP-2293 restricts its use to low-flow measurements below ~1gpm and there has been little quality-assurance testing done on this model to see how it performs under varying hydraulic conditions resulting from changes in borehole-diameter, flow rates and directions. This report therefore summarizes a series of flow tests conducted by the NJGWS using a Mt. Sopris Model No. HFP-2293 subject to varying flow conditions and using different flow-diverter designs, two of which allow a percentage of the water column to bypass the sondes measurement chamber (Figure 1). Initial field tests in 2011 were run in cased sections of 6- and 8-inch diameter water wells while inducing upward flows at controlled flow rates ranging between 1.2 to 3.0 gallons-per-minute (gpm). A subsequent set of laboratory tests run in 2014 at the NJGWS facility used custom-built flow chamber s capable of sustaining uniform, bi-directional axial flows at rates between 0.01 and 8 gpm in vertical pipes of 5.5- to 7.5-inch diameters. This apparatus was used to test two HFP-2293 sondes and three different flow diverters, two of which allow a percentage of cross flows to bypass the measurement chamber. The test results were charted using MS Excel to derive flow-calibration curves for each diverter to use during subsequent field work in order to expand the HFP-2293 operational range and to increase its reliability. A MS Excel worksheet was also developed to aid in calculating flow rates in the field or office that factors in slight variations in borehole diameter. The test results show that instrument behavior is best represented using power functions that

test at about 80% to 90% accurate at flow rates below ~8 gpm. Recommendations on deploying and using a Model 2293 HFM are made for using the customized bypass diverters and flow calculator based on past experiences.

Background

Mount Sopris Instruments Model 2293 Heat-Pulse Flow Meter (2005 version)



Robertson Geologging, Ltd. Heat-Pulse Flow Meter (1999 version)

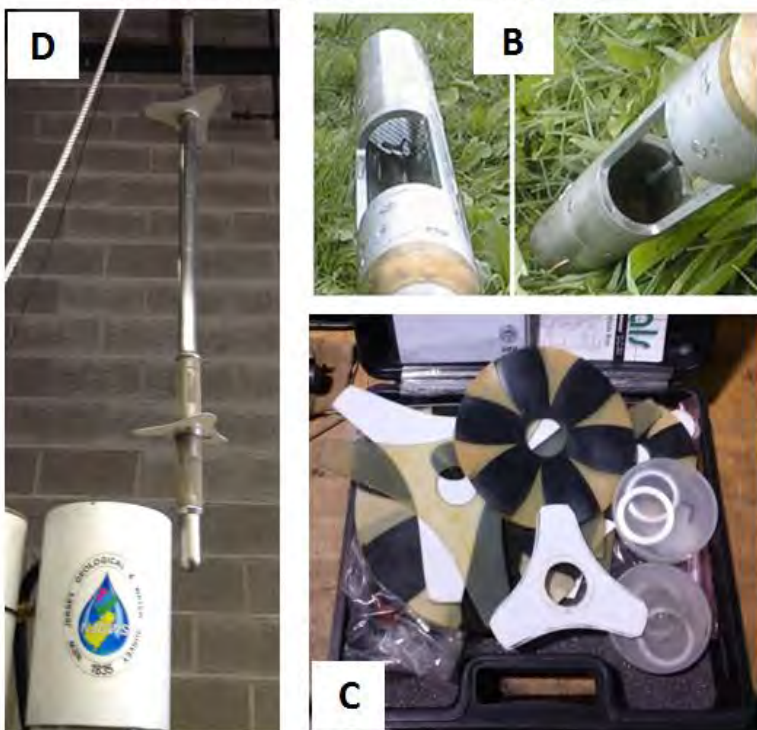


Figure 1: Photograph of the NJGWS heat-pulse flowmeter sondes and flow diverters. (A) Detailed views of the measurement chambers of two different sondes without flow diverters (C) attached. The Mt. Sopris HFP-2293 (top) includes screen guards covering two, lateral-entry ports into a closed-ended measurement chamber. The Robertson Geologging model (bottom) has one lateral port and is open-ended on its bottom (B). The HFP-2293 standard deployment scheme uses the yellow (latex) and black (neoprene) flexible petals (C) that mostly seal the borehole annular space and divert nearly all cross flows through the instrument-measurement chamber. The Robertson tool was deployed using the two centralizers pictured in (D) that were also tested on the HFP-2293 for flow-rate measurements >1 gpm, the recommended threshold of the HFP-2293. A wire-grid heat source is pictured on the left side of photo (B).

The NJ Geological and Water Survey (NJGWS) purchased a Mt. Sopris model number HFP-2293 flow meter in 2010 for use in characterizing fractured-bedrock aquifers in support of publicly funded groundwater investigations within the NJDEP. This instrument is part of a logging system that includes flow diverters to facilitate measuring in-situ groundwater-flow rates between ~0.03 to 1.0 gpm according to the manufacturer's product specifications. This is the second HFM system used by the NJGWS. The first was a Robertson Geologging, Ltd. system purchased in 1999 that was tested in the field to be about

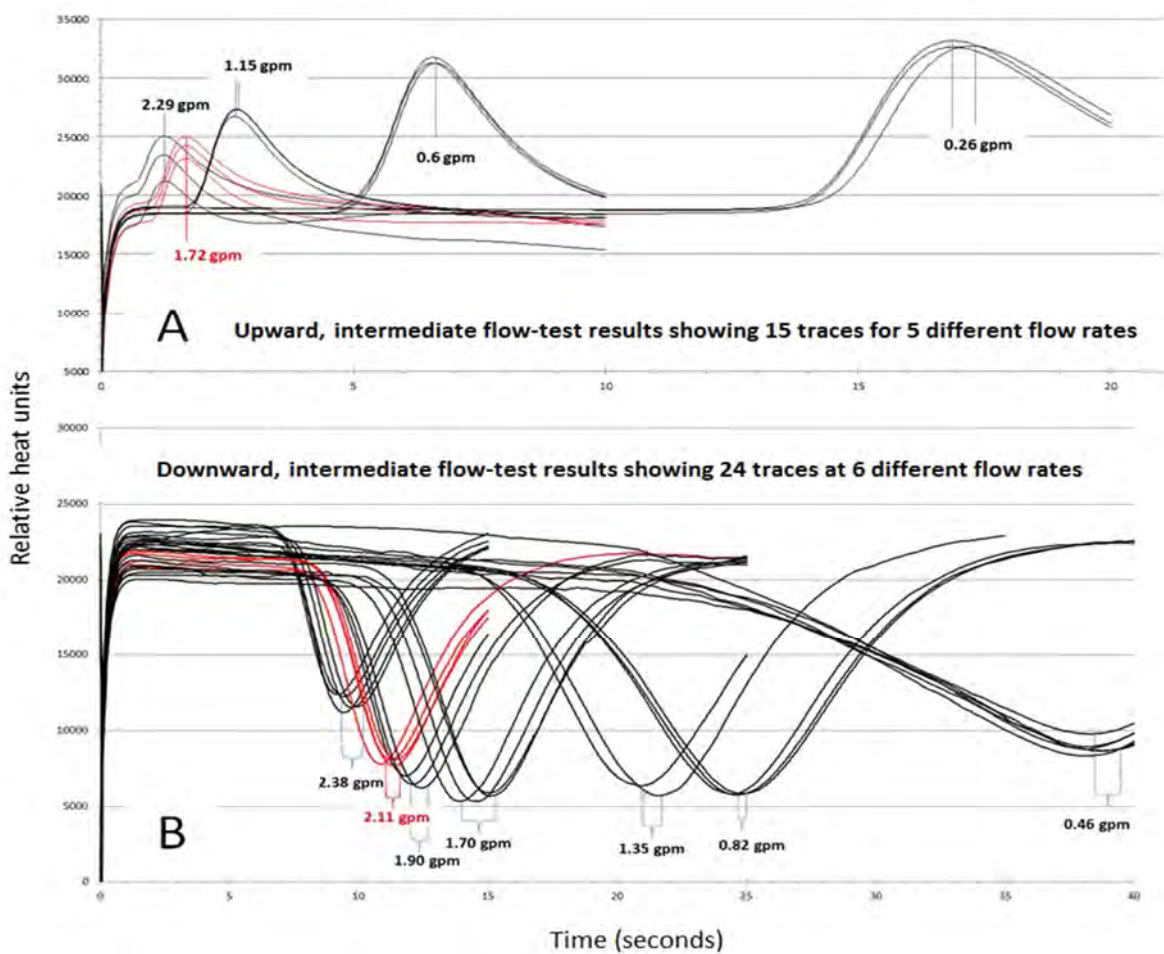


Figure 2: MS Excel scatterplots of instrument-response times (IRTs - x-axes) versus themistor responses (y-axes) using relative thermal units. Note that upward flows (A) register upward deflections and downward flows (B) register downward deflections. Multiple readings were taken at controlled flow rates to derive average response times; these were then charted versus flow rates (gpm) to derive reference curves (Figure 3). The red traces are colored for clarity.

80% accurate when measuring cross flows ranging from 0.7 to 25.0 gpm in 6- and 8-inch diameter water wells drilled to depths ranging to about 500 ft. (Herman, 2006). That sonde was operated in a stationary, non-trolling mode and deployed with centralizers (1C) that partially restricted cross flows in the borehole but not the measurement chamber. The flow-chamber design of the Mt. Sopris sonde is similar to that of the Robertson one (Figure 1A), but the HFP-2293 is supplied with a set of flow diverters made of flexible, yellow latex and black neoprene (Figure 1C) that mostly seal the annular space between the lateral entry ports and channel cross flows through the sondes measurement chamber (Figure 1AC). Use of the tool in this manner provides measurements at low-flow rates (\sim 1.0 gpm), but cross-flow rates in water wells developed in bedrock aquifers in this region are an order of magnitude higher in places (Herman, 2010; 2006). Therefore, standard deployment methods for the HFP-2293 cannot solely be relied upon to gain results from the expected range of encountered cross flows in this region.

2011 Field Tests Using Customized Diverters for Borehole Cross Flows Exceeding 1.0 GPM

Field testing of the HFP-2293 began in 2011 for upward cross flows exceeding ~1.0 gpm using customized diverters that allow different percentages of water to bypass the instrument measurement chamber during testing (Figures 1C and D). As for the previous study using the Robertson HFM (Herman, 2006), these tests were only conducted for upward, axial flows at stepped-rates (Figure 3) controlled by a throttled water pump positioned above the flow meter in the water column. The calibration of downward axial flows wasn't done owing to the inconvenient arrangement of having the pump's discharge pipe rising through the section of borehole annular space being tested and thereby compromising the borehole hydraulics. These initial tests were conducted in steel-cased sections of 6- and 8-inch diameter wells located at the Stony Brook-Millstone Watershed Association well field in Mercer County, NJ. The wells are located near a pond and have shallow static water levels (wells 93 and 97 of Herman and Curran, 2010) with near-instantaneous recovery at low-flow rates.

For each test, the sonde was outfit with two tri-wing centralizers of Mt. Sopris design (Figure 1B). The translucent –yellow, plastic centralizers of tri-wing design provided with the sonde (Figure 1D) served as templates for duplicating the design using white, thin plastic cut from the bottom of a 5-gallon bucket (Figures 1C and 1D). One centralizer was positioned on the upper part of the sonde and the other was placed between the screen guards in the middle of the instrument's measurement chamber to restrict, rather than fully divert cross flows (Figure 1D). The HFP-2293 was submerged within two feet of the bottom of casing and at least 10 feet below a small submersible pump connected to a rheostat flow-rate controller at the surface. A series of steady-state pumping tests were run using stepped rates varying from 1.0 to 3.0 gpm and measured using a stopwatch to gauge the rate and volume of pump discharge into a 5-gallon graduated bucket. During each test phase, the sonde was fired multiple times to record a set of IRTs after achieving near-steady-state flow conditions at each pumping rate (Figure 2). Each set of test data were charted on scatter graphs using MS Excel with instrument-response times plotted on the x axis and flow rates plotted on the y axis (Figure 3).

Statistical regression curves were then derived for each test plot using MS Excel statistical functionality to produce the best mathematical formulae and reference curves for subsequent field use. As seen in the results of the earlier flowmeter tests with the Robertson system, power functions provide the most accurate regression statistics for the observed non-linear system responses in comparison to other standard statistical options included in MS Excel including polynomial, exponential, and logarithmic solutions. But despite employing these power-solution reference curves, subsequent field use of the HFP-2293 under low-flow conditions sometimes resulted in significant discrepancies when compared to flow rates determined with other methods such as timing the recovery of the static water table in well casing after pumping the well. We therefore set out to further test and customize the HFP-2293 in order to expand its operating range and to better understand its limitations. To do this we designed (Figure 4) and built (Figures 5 and 6) customized flow chambers using 6 foot lengths of clear piping having 5.5- and 7.5 inch diameters.

SHALLOW SUBSURFACE GEOPHYSICAL APPLICATIONS IN ENVIRONMENTAL GEOLOGY

GANJ XXXIII Annual Conference and Field Trip

The HFP-2293 was then outfit with three different sets of flow diverters (Figure 7), two of which allow varying amounts of flowing water to bypass the sonde in order to test the new system under varying hydraulic conditions.

2014 Laboratory Tests Using a Custom-Built Flow Chamber and Flow Diverters

Prior to 2014, field calibration of both HFM systems was only done for upward axial flows in shallow water wells because of the aforementioned restrictions that compromised testing of downward-directed flows in the field. The NJGWS flow chamber therefore provides the means to more thoroughly test flow meters in pipes of varying diameters, flow rates and directions. The apparatus frame was constructed using ¾-inch plywood that is built to receive upright-standing pipes ranging between 5.5 and 8-inch diameters (Figure 4 to 6). For these tests, it was supplied with two 6-foot long, clear acrylic pipes having ¼-inch thick walls and

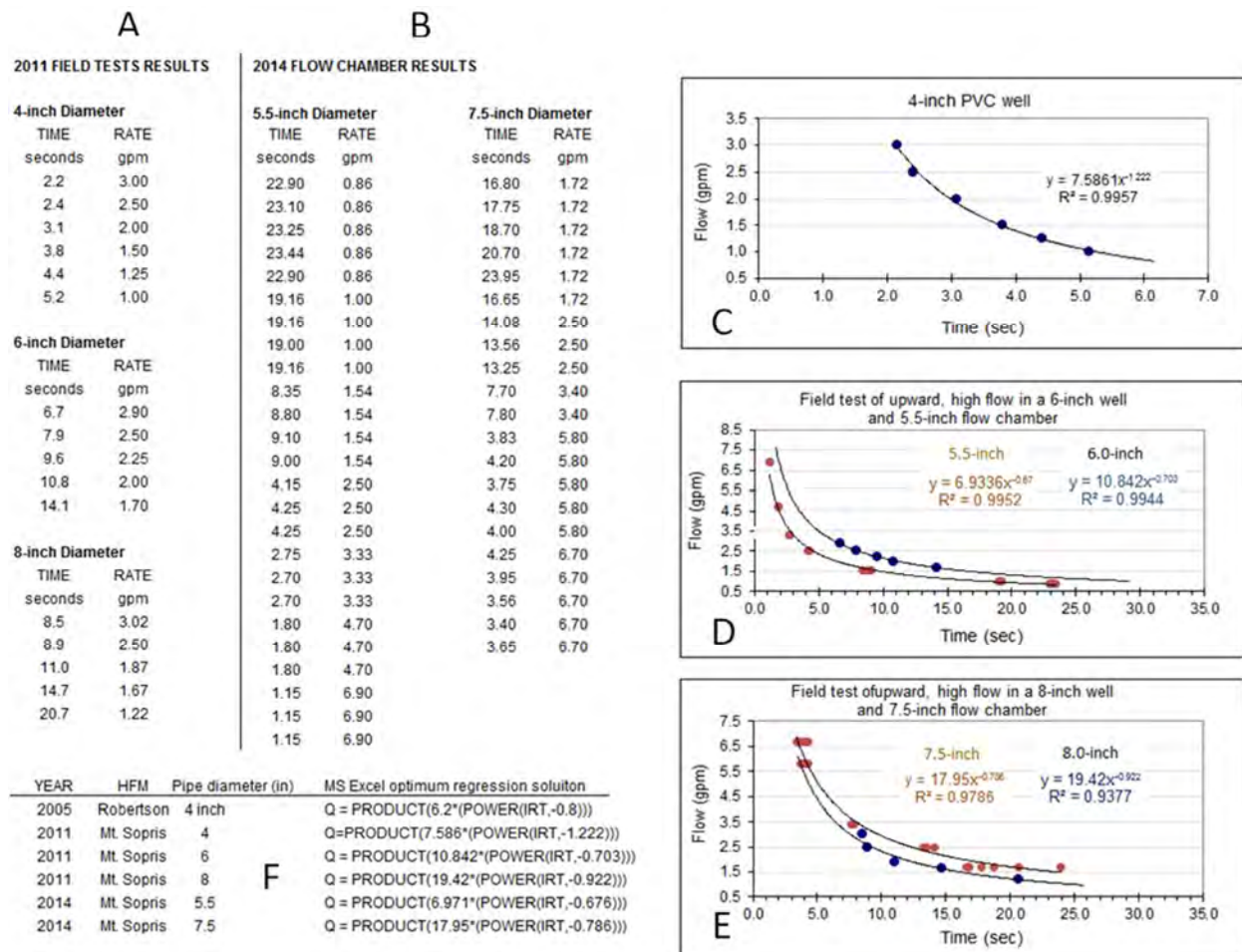
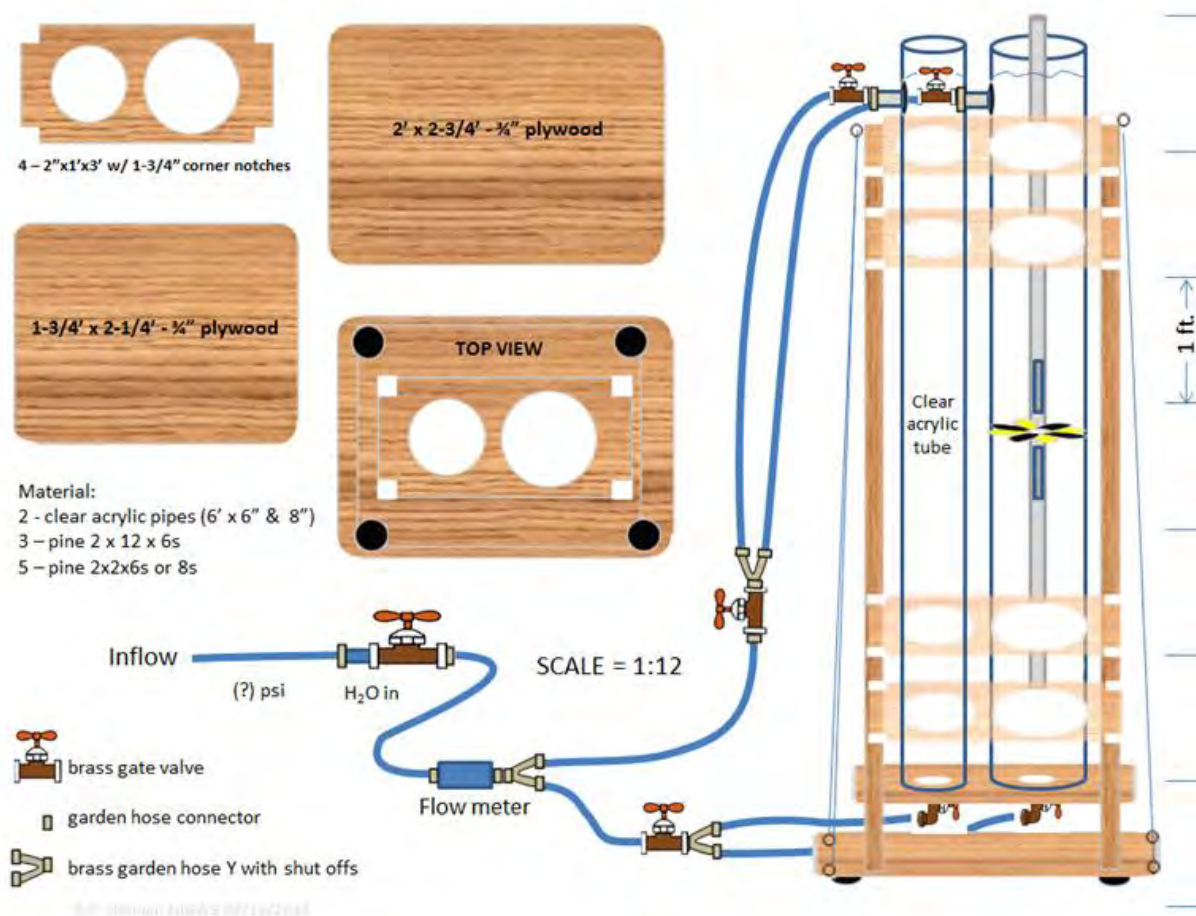


Figure 3: Results of 2011 field- and 2014-laboratory testing of the HFP-2293 at borehole flow rates of 0.5 to ~8 gpm using the customized bypass diverter pictured in Figure 1D. The 2011 initial tests were only run for upward flows. Laboratory test results run in 2014 in 5.5- and 7.5-inch diameter pipes are summarized in (B) and plot alongside the earlier results in (D) and (E) for comparison. The sequence of statistical regression curves summarized in (F) summarize the statistically optimum power functions derived from the respective tests with correlation coefficients (R^2) exceeding 0.93 and mostly above 0.97(C-E). See text for further discussion.

SHALLOW SUBSURFACE GEOPHYSICAL APPLICATIONS IN ENVIRONMENTAL GEOLOGY
 GANJ XXXIII Annual Conference and Field Trip

5.5- and 7.5-inch inside diameters (ID). The pipe outside diameters are the same as the ID of 6- and 8- inch schedule 40 PVC pipes, so the clear ones fit snugly inside cut PVC pipe segments. Each acrylic tube is set and glued inside a short segment of schedule 40 PVC pipe that was capped, drilled, and tapped to receive 1-inch galvanized pipe nipples as flow ports to connect supply lines and discharge hoses (Figure 5A). Pipe nipples with garden-hose adapters were set into the upper PVC pipe segment for inflow or outflow ports depending upon the desired flow direction (Figure 6A). Larger-diameter ports were also plumbed into the PVC pipe segments using 1¼-inch pipe nipples or threaded pipe adapters to connect larger pipes when testing higher flow rates (Figure 5C). Depending upon the rate and direction of flow desired, input flows were connected directly to a municipal supply line (Figure 5A and B) or run through a constant-head bath to establish flows in the 0.01 to 10.5 gpm range.



Volume of water in pipe (V) with water column (h)

6" V = 1.47 h, 8" V = 2.81 h	1 gallon of water = 8.342 pounds
6 in. volume = 1.47 gal/ft x 6 ft = 8.82 gal	6 in. weight = 73.57 psf at bottom (0.51 psi)
8 in. volume = 2.81 gal/ft x 6 ft = 16.86 gal	8 in. weight = 141.96 psf at bottom (0.985 psi)

Figure 4: The schematic design of an upright-standing apparatus housing pipes with standard water-well diameters that can mimic sub-vertical (axial) cross-flows in open boreholes.

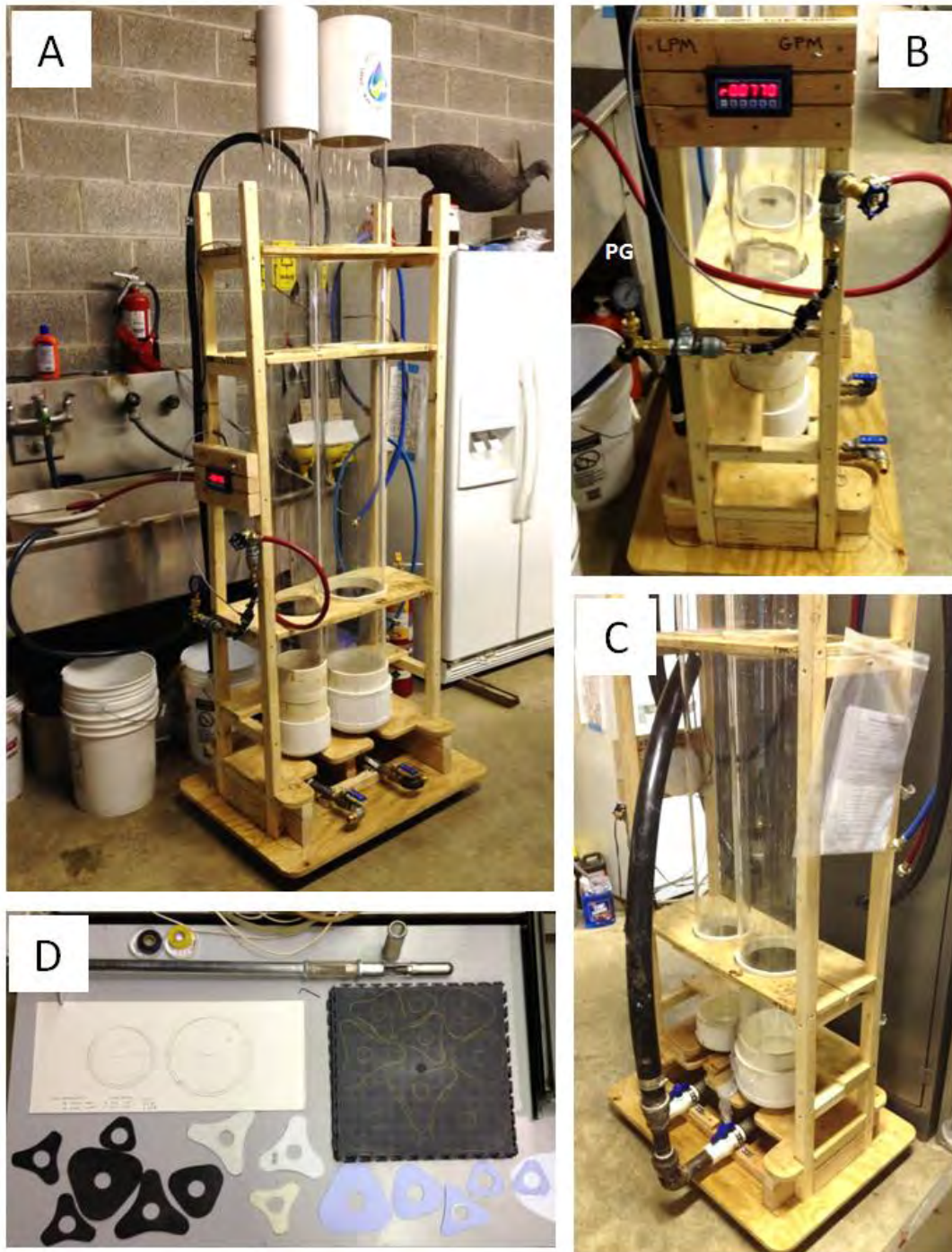


Figure 5: The HFP-2293 was tested using a custom-built flow chamber (A to C) and flow diverters of three different designs (D). The plywood frame holds the pipes upright and can be disassembled for pipe removal, modification, or substitution. As depicted when facing the front, the left side houses 5.5 to 6-inch (outside diameter or OD) pipes and the right side holds 7.5 to 8-inch OD pipes. An in-line pressure gauge (PG in photo B) and an electronic, digital flowmeter (A and B) provide monitoring points during testing. The flow diverters (5D) were cut from flexible, 1/4-inch thick, black-rubber floor matting (right side of D) using the blue-paper templates (lower right D) cut from a printed CAD design. Also note the lower screen guard is off the HFP-2293 in the upper right of photo D. The CAD file is available for free download as part of this report (www.ganj.org/2016/2016_NJGWS_HFM-2293_Flow_diverters.skp).

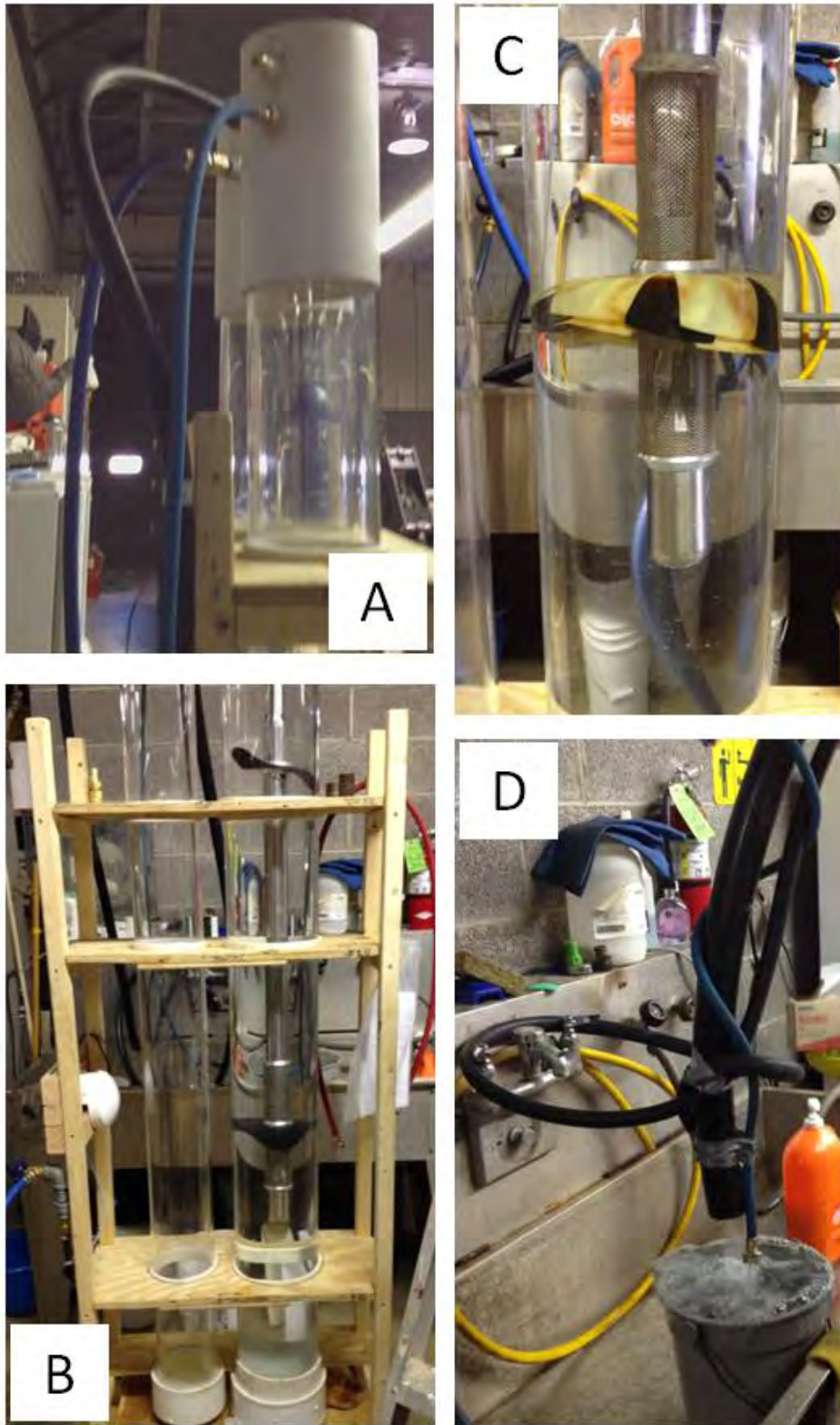


Figure 6: Photographs detailing the three deployment schemes tested in 2014 at the NJGWS lab (garage). Designs for low- (C), intermediate- (B), and high-flow (Figure 1D) rates were tested. The low-flow scheme is the default HFP-2293 deployment scheme of Mt. Sopris design. The other two are the NJGWS customized bypass diverters that allow a percentage of cross flow to bypass the sondes' measurement chamber (Figure 7).

SHALLOW SUBSURFACE GEOPHYSICAL APPLICATIONS IN ENVIRONMENTAL GEOLOGY
 GANJ XXXIII Annual Conference and Field Trip

The bath is a 250-gallon plastic water tank sitting on a table in a loft over the flow chamber (Figure 8). A standard water-pressure gauge was attached to the input line using a T-connector with a shutoff valve (Figure 5B) to monitor water-pressures that fluctuated between ~15 to 50 pounds-per-square inch when connected to the municipal water-supply line. This line was used to generate flow rates greater than 1.0 gpm. An electronic flow meter was purchased and placed into the input line to monitor flow rates. Each chamber is therefore outfit with upper and lower flow ports in a plumbing system that provides either upward or downward axial flows at controlled flow rates ranging from about 0.01 to 8 gpm (Table 1). A series of flow tests were run using the HFP-2293 sonde with flow diverters of all three designs

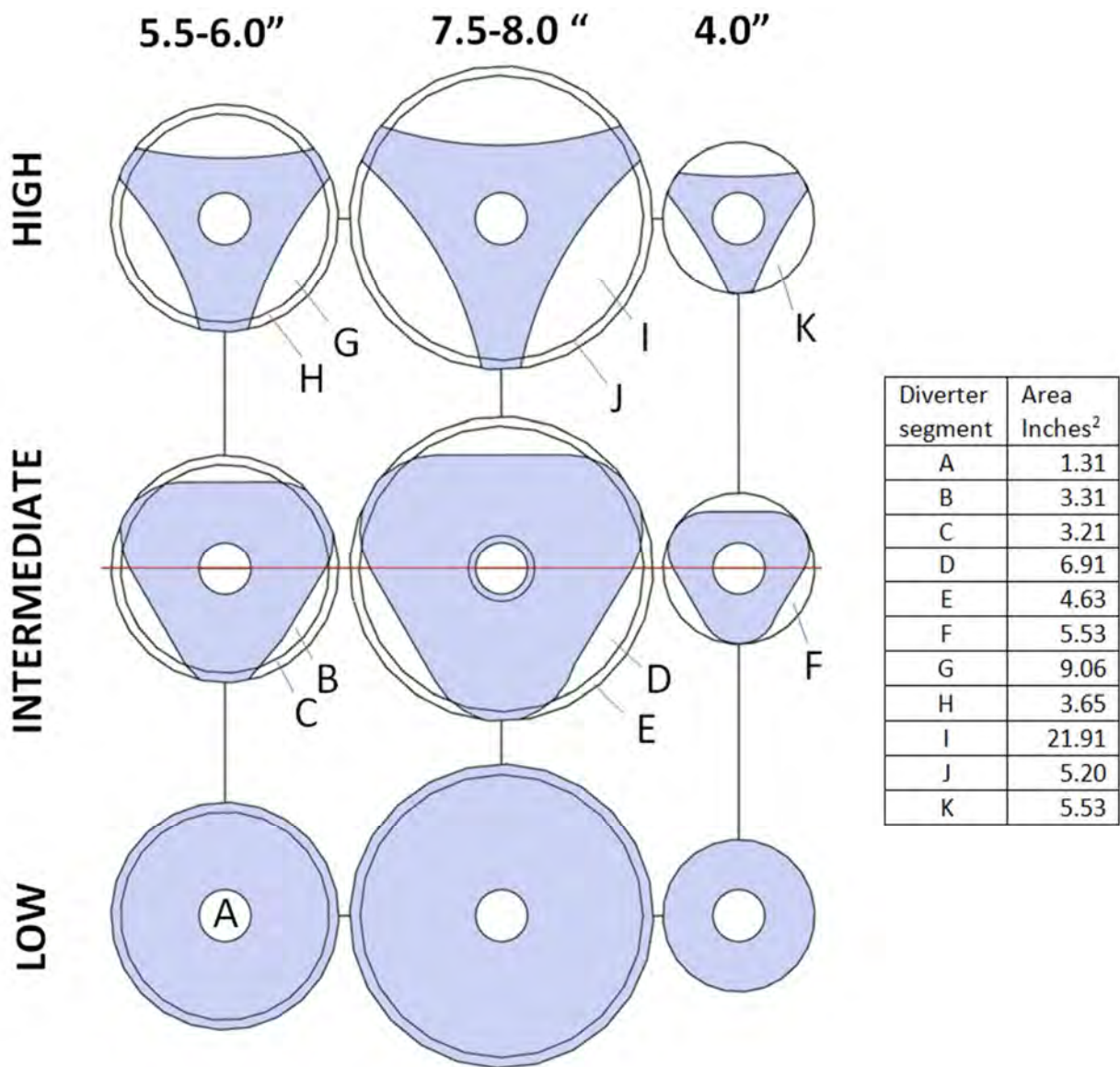


Figure 7: SketchUp Make software (Trimble, Inc.) was used to design two passing-flow diverters covering high- and intermediate-flow rates. The diagram and accompanying table detail the total area of the borehole cross section that is open to flow using each respective design (www.ganj.org/2016/2016_NJGWS_HFM-2293_Flow_diverters.skp).



Figure 8: A 250-gallon plastic tank lofted about 8-ft above the testing apparatus provided a steady water supply needed for low-flow testing. Ms. Rachel Filo attends to the flow apparatus during testing.

(Figures 5D, 7 and 9) and variable rates of upward- and downward axial flows. All test results are tabulated as Appendix A and chartered as scatter plots in Figures 10 to 12. The Mt. Sopris diverters used for the low-flow tests are constructed of soft, yellow-and-black rubber formed into overlapping petals (Figures 5D, 6C, and 9D). The Mt. Sopris translucent yellow, plastic, tri-wing centralizer was used as a template for the high-flow bypass diverter (Figures 1C, 1D, 5D, 11 and 12C). A second bypass diverter was designed that provides less bypass area (Figure 7) and therefore an ‘intermediate’ range of flow rates. The customized flow diverters were designed using Trimble Inc. SketchUp Make software and cut out of stiff, but flexible, ¼-inch-thick rubber matting marketed as trafficMASTER Utility Floor Tiles product number 615 904 (Figure 5D). The CAD file of the custom-designed bypass diverters is available for download from the GANj web site as noted in Figures 5 and 7. The two customized flow diverters were tested at high (>0.9 to <7.0 gpm) and intermediate (>0.2 to 20 gpm) flow rates (Figures 11, 12B, 12C, and 13). The 4-inch designs (Figure 11) have not been tested yet.

A second HFP-2293 was temporarily loaned to us by Princeton Geosciences, Inc. during testing at intermediate flow rates in order to provide a comparison of flow-test responses for the same model sonde. Two sets of examples gained from these tests are charted in Figure 14 to illustrate how IRTs can vary for various flow rates and directions. As found in the prior HFM calibration study (Herman, 2005) all charted test results are best represented using power functions that have regression coefficients (R^2) exceeding 0.97 (Figure 8 and Table 1).

SHALLOW SUBSURFACE GEOPHYSICAL APPLICATIONS IN ENVIRONMENTAL GEOLOGY
GANJ XXXIII Annual Conference and Field Trip

Table 1: Summary of test results and instrument-response time-to-flow rate equations derived for use with the HFP-2293 flowmeter

Equation	Power-equation derived using MS Excel scatterplots	Borehole diameter (in.) and flow scheme	R ²	Volumetric flow range		Response time
				gpm	lpm	sec.
2	$y = 00.405 x^{-1.098}$	5.5 Low down	0.99	>0.01	>0.01	>1.8
3	$y = 00.467 x^{-1.174}$	5.5 Low up	0.99	<0.40	<0.40	<32.0
4	$y = 02.278 x^{-0.724}$	5.5 Intermediate down	0.97	>0.20	>0.01	>1.5
5	$y = 02.631 x^{-0.799}$	5.5 Intermediate up	0.99	<2.00	<0.40	<42.0*
6	$y = 05.899 x^{-0.536}$	5.5 High down	0.99	>0.90	>0.01	>1.0
7	$y = 06.419 x^{-0.640}$	5.5 High up	0.99	<7.00	<0.40	<24.0
8	$y = 00.503 x^{-0.965}$	7.5 Low down	0.99	>0.02	>0.01	>0.9
9	$y = 0 1.356 x^{-1.220}$	7.5 Low up	0.93	<1.00	<0.40	<21.0
10	$y = 03.361 x^{-0.541}$	7.5 Intermediate down	0.99	>0.30	>0.01	>1.8
11	$y = 05.024 x^{-0.866}$	7.5 Intermediate up	0.99	<3.00	<0.40	<32.0
12	$y = 11.301 x^{-0.556}$	7.5 High down	0.98	>1.50	>0.01	>1.8
13	$y = 17.950 x^{-0.786}$	7.5 High up	0.98	<8.00	<0.40	<32.0

Comparison of Mt. Sopris and NJGWS Low-Flow Calculations

The power functions derived from laboratory testing at low-flow rates were next compared to flow values obtained using the Mt. Sopris MatrixHeat (ver. 3.3) software (Figure 14). The flow solution used in this software uses a 2nd-order polynomial that is modified form of the quadratic equation to approximate the observed, non-linear nature of the instrument-response time (IRT) to flow-rate responses (Figures 8-10):

$$\text{Eq. 1: Flow (Q)} = K1/DT + K2/DT^2$$

where K1 and K2 are constant values derived using tests conducted at low and high flow rates in a laboratory flow chamber at Mt. Sopris Instruments, Inc.

Each HFP-2293 is calibrated before shipping at the Mt. Sopris office in an upright-standing apparatus including a 6-inch-diameter clear-acrylic pipe. Calibration readings at both low- and high-flow rates are gathered and recorded on an 8.5x11" certificate of calibration included in the operator's manual with the most recent calibration results for the NJGWS tool included in Table 2. Fred Paillet of the US Geological Survey provided us proof of this method in a written communication date January 7, 2015. The derivation uses six steps (a. to f. below) to calculate the respective K values for upward and downward flow.

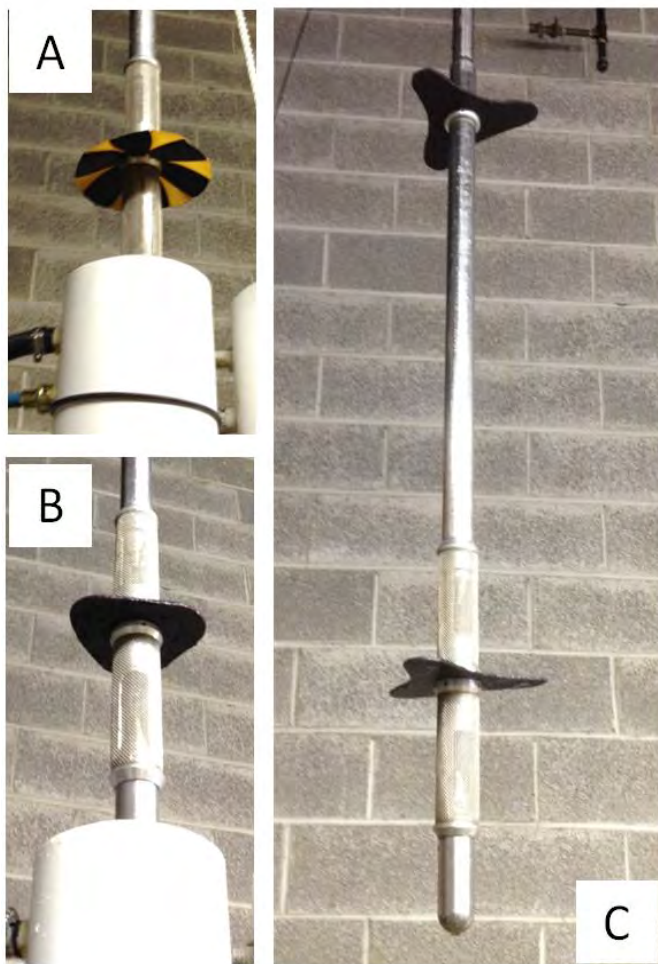


Figure 9: Photographs detailing the low (A), intermediate (B) and high flow-rate (C) deployment schemes tested for field use.

a. Assume $Q = AX^2 + Bx + C$ with $X =$ the inverse of the pulse travel time (T) or $X = 1/T$

b. The variable C can be set to 0 because $Q = 0$ for very large values of T .

c. The calibration results for low and high flows in a given direction give a coupled set of equations:

$$\text{Eq. 14} \quad Q_{LF} = A_{LF}X^2 + B_{LF}X,$$

and

$$\text{Eq. 15} \quad Q_{HF} = A_{HF}X^2 + B_{HF}X$$

d. By letting $K1 = B$ and $K2 = A$, then solving for A and B using the calibrated flow-vs.-time responses in Table 2 for UPWARD flow:

$$0.03 = 0.01A + 0.10B, \text{ and}$$

$$1.0 = 2.0408A + 1.4286B$$

Rearranging and factoring Eq. 2 gives:

$$0.01A = 0.03 - 0.10B \quad \text{or} \quad A = 3.0 - 10.0B$$

e. Substitute $A = 3.0 - 10.0B$ for A in Eq. 3, and by rearranging to solve for B :

$$1.0 = 2.0408(3.0 - 10.0B) + 1.4286B = 6.1224 - 20.4082B + 1.35B = 6.1224 - 21.7582B$$

$$\text{Therefore:} \quad \mathbf{B \text{ (or } K1) = 0.2814}$$

f. Substituting $B = 0.2814$ into Eq. 2 to solve for A :

$$0.03 = 0.01A + 0.1(0.2814) \quad \text{or} \quad 0.01A = 0.03 - 0.02814 = 0.00186/0.01$$

$$\text{Therefore:} \quad \mathbf{A \text{ (or } K2) = 0.1860}$$

This process is repeated using the downward flow parameters to derive the downward K value in the same manner (Table 2).

SHALLOW SUBSURFACE GEOPHYSICAL APPLICATIONS IN ENVIRONMENTAL GEOLOGY
GANJ XXXIII Annual Conference and Field Trip

Table 2: 08/02/2014 Mount Sopris calibration results
for the NJGWS probe, HFP-2293 SERIAL NO. 5006

DIRECTION	LOW FLOW				HIGH FLOW			
	gpm	T (seconds)	1/T	1/T ²	gpm	T (seconds)	1/T	1/T ²
UP	0.03	10.00	0.1000	0.0100	1.00	0.70	1.4286	2.0408
DOWN	0.03	9.75	0.1026	0.0105	1.00	0.70	1.4286	2.0408

Figure 14 summarizes the derived set of power functions that returned the lowest statistical errors, and shows that the manufacturer's method offers a close match to the control rates only for upward, axial flows in ~6-inch boreholes. These tests also show significant departures in ~ 8-inch diameter boreholes between upward- and downward-flow responses (Figure 14 B). This is elaborated below in the concluding section below.

MS Excel Worksheet for Calculating Flow Rates Based on HFP-2293 Response Times, Including Linear Functions for Adjusting Flow Rates Based on Borehole Diameter for Passing-Flow Measurements

A comparison of test results acquired in the field in 2011 and the laboratory in 2014 provided the basis for including a linear 'caliper' function in the flow-calculation worksheet to adjust calculated flow rates based on variations in borehole diameter (caliper) when deploying the tool at intermediate to high rates of flow in ~6- to 8-inch diameter wells (Figures 6, 9, and 14). The method uses a linear function derived from conducting tests in both 7.5- and 8-Inch wells that relates an ideal percentage of passing-flow area (PFA) versus the borehole diameter (Figure 9). Each resulting function detailed in Figure 13 is programmed into the MS Excel flow-calculator worksheet as part of the workbook accompanying this report.¹

The acquisition of HFM IRTs and calculation of flow-rates from using the custom flow diverters is thus,

- 1) Calculate flow rates based on IRTs using the appropriate regression (power) curve derived for the respective 5.5 (PWR5.5) or 7.5-inch (PWR7.5) pipes, and then
- 2) Modify the calculated flow rate using a caliper factor (CF) for each case (5.5-6.2 or 7.5-8.2), using the linear equations (Figure 11) derived from charting the percentage of PFA and the borehole diameter (CALIPER).

¹ The MS-Excel workbook for use with the NJGWS custom flow diverters is available to download at the following URL: www.ganj.org/2016/2016%20MS_HFM_2293_NJGWS-diverters.xls.

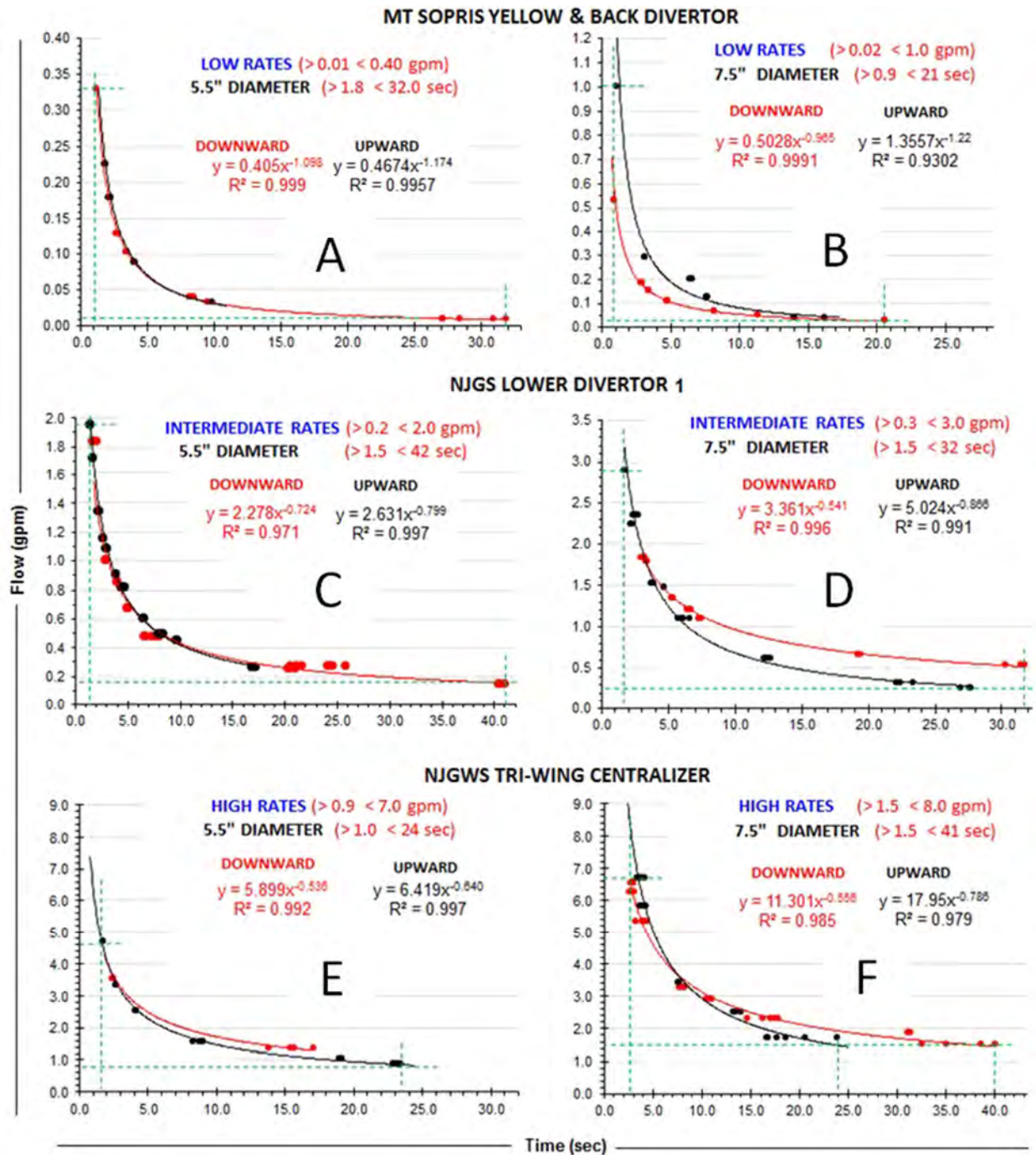


Figure 10: MS Excel charts of IRTs (seconds) versus flow rates (gpm) for the twelve different flow-test experiments needed to initially characterize upward and downward cross flows using two different pipe diameters (5.5- and 7.5-inch) and three deployment schemes covering 'low', 'intermediate', and 'high' rates. The results of downward-directed flow test are charted using red points and lines whereas upward-directed ones are colored black. The time- and flow-rate limits of each test are marked using green-dashed lines on each chart, and mathematical equation for each of the best-fit regression trends are summarized, and repeated in Table 1 and for use in the MS Excel rate calculator (Figure 15).

Table 4 summarizes typical errors that one can expect to encounter when using this customized setup and basing the error of accuracy on the difference in observed and calculated flow rates in the 6- and -inch diameter wells.

Notes and Discussion

This study set out to more thoroughly test the capabilities and limitations of a HFP-2293 system and in the course, we fabricated a solution to expand the instrument's operating range to cover borehole cross flows at rates between ~1.0 to 8 gpm. These applications are currently being field tested and await subsequent reevaluation and refinement. But for now, we now have a better understanding of some of the system limitations and pitfalls of using the standard operational method, and we provide an alternative way of deploying this system and calculating flow rates to achieve higher accuracy from using the MS

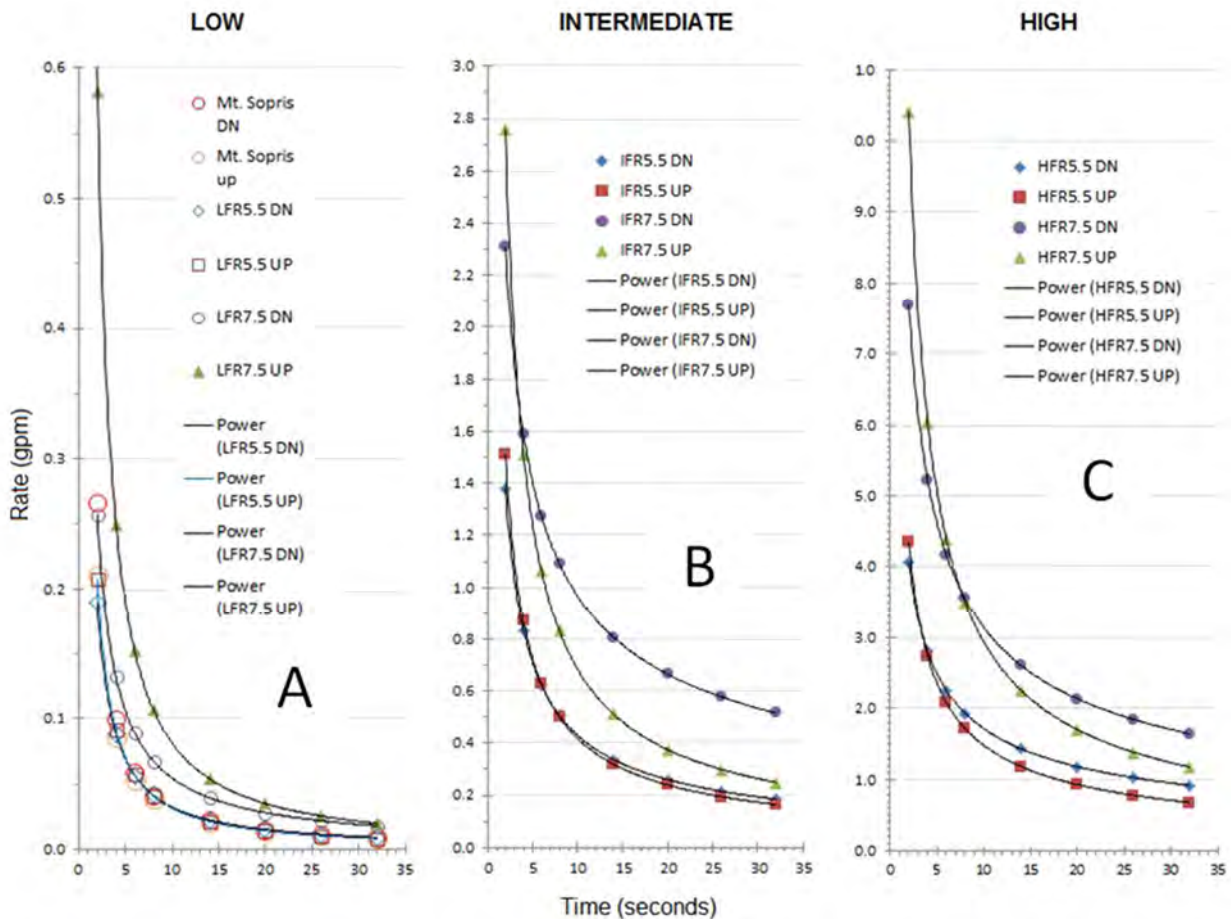


Figure 11: Charted test results from testing three diverter schemes using the flow chambers. Low-flow used the Mt. Sopris black-and-yellow full diverters whereas intermediate- and high-rates used the customized diverters that allow a percentage of flow to bypass the HFP-2293 measurement chamber. Table 2 summarizes the respective flow ranges and testing statistics.

Excel flow-calculator worksheet derived from both field and laboratory testing. But more work could attain even better results. For example, the flow chambers are capable of being outfitted with standard 4, 6, and 8-inch PVC schedule 40 pipes to compare the results obtained using the 5.5- and 7.5-inch clear-acrylic ones. The clear pipes were used first in order to help position and effectively seat the diverters and for visually inspecting the placement and seating of the instrument-measurement chamber as far from flowing ports as possible in order to obtain the best test results. More tests can be run to test axial flows in slightly larger-diameter pipes to confirm the earlier field tests and refine the methodology more. Below are some operational and test notes that may be useful when using HFM systems and discussion of some key test results.

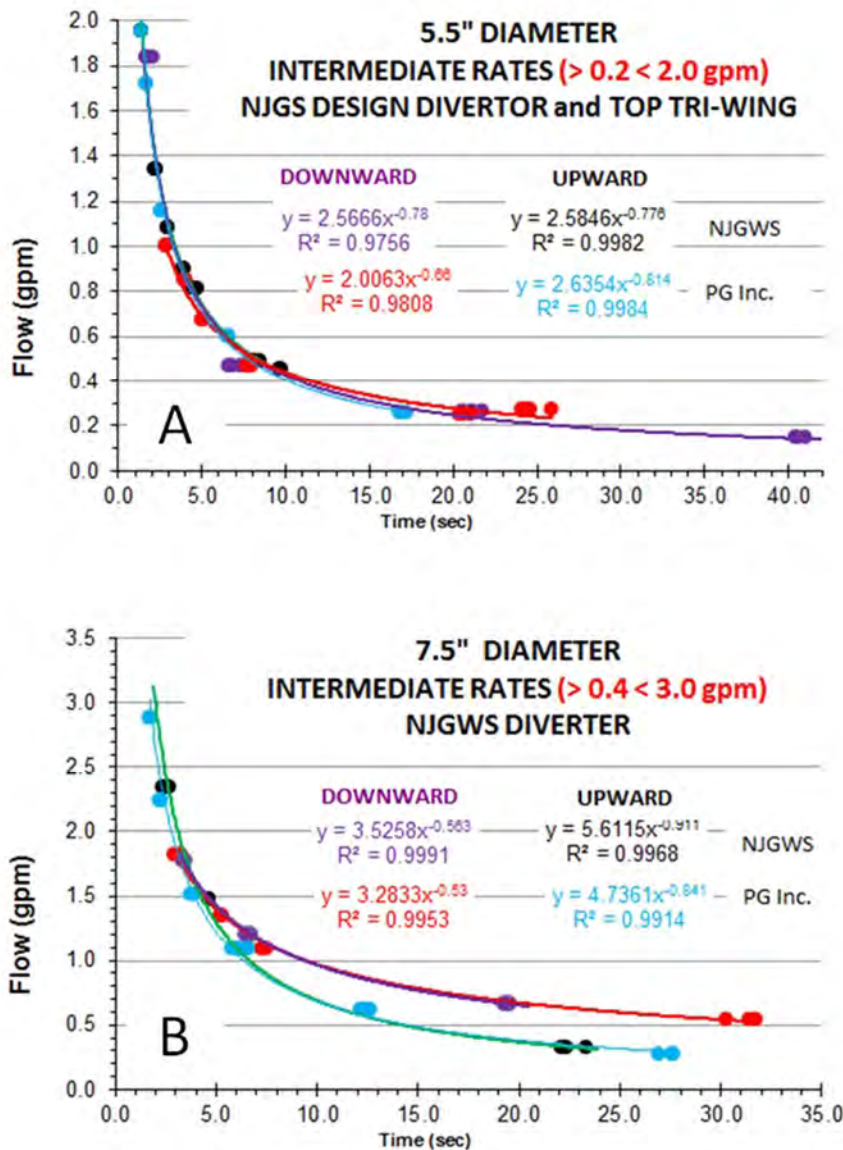


Figure 12: HFP-2293 tests results from using two different models under the same laboratory conditions. Flow responses in both upward and downward directions for the two tools for the intermediate- and high-flow schemes were nearly identical.

results. Figures 8A and 9A show that at low-flow rates below 1 gpm in 5.5 to 6-inch wells while and using the fully diverted setup, that directional flow behavior is very similar such that a single power curve could be used to attain a IRT-to-flow rate conversion that is over 95% accurate for either flow direction. Moreover, Table 3 and Figure 14 show that relying on the manufacturer's software to determine flow rates only achieves about 80 to 90% accuracy of flow determinations, especially depending upon the flow direction. At higher flow rates using the passing-flow deployment schemes, flow responses show even more separation depending upon flow direction such that two reference curves are needed to address each deployment scheme in order to achieve

SHALLOW SUBSURFACE GEOPHYSICAL APPLICATIONS IN ENVIRONMENTAL GEOLOGY
GANJ XXXIII Annual Conference and Field Trip

the most accurate results (Table 4). In general, this simply shows that a heat pulse is transmitted upward at a comparatively faster rate than a downward-directed one. This makes sense thermodynamically with regard to heat rising by convection through a fluid. However, this tendency is reversed for an unknown reason in the 5.5 to 6-inch diameter pipes when fully diverted (Figure 8B). Another notable test result is that the trend lines for intermediate- to high-flow rates tend to cross over at various points (Figures 8D, 8F, 9B and 9C). More work is needed in order to better understand these relationships. Figure 10 and Table 4 shows that the larger-diameter pipes resulted in significantly different IRTs registered in different directions for the same flow rates, and why it is therefore necessary to calibrate a HFM system for use in larger- and smaller-diameters wells other than the more common 5.5- to 6-inch. This also serves as a reminder that

Diameter	Area	% of borehole area (BHA) allowing passing flow for the three diverter schemes and borehole sizes							
		Low	% BHA	Intermediate		% BHA	High		% BHA
inches	Inches ²								
4.0	12.56	1.31	10.4	2.91	A+F	23.2	6.84	A+K	54.5
5.5	23.75	1.31	5.5	4.62	A+B	19.4	10.37	A+G	43.6
6.0	28.27	1.31	4.6	7.83	A+B+C	27.7	14.02	A+G+H	49.6
			0.9			8.3			6.0
7.5	44.17	1.31	3.0	8.22	A+D	18.6	23.22	A+I	52.6
8.0	50.26	1.31	2.6	12.85	A+D+E	25.6	28.42	A+I+J	56.5
			0.4			7.0			3.9

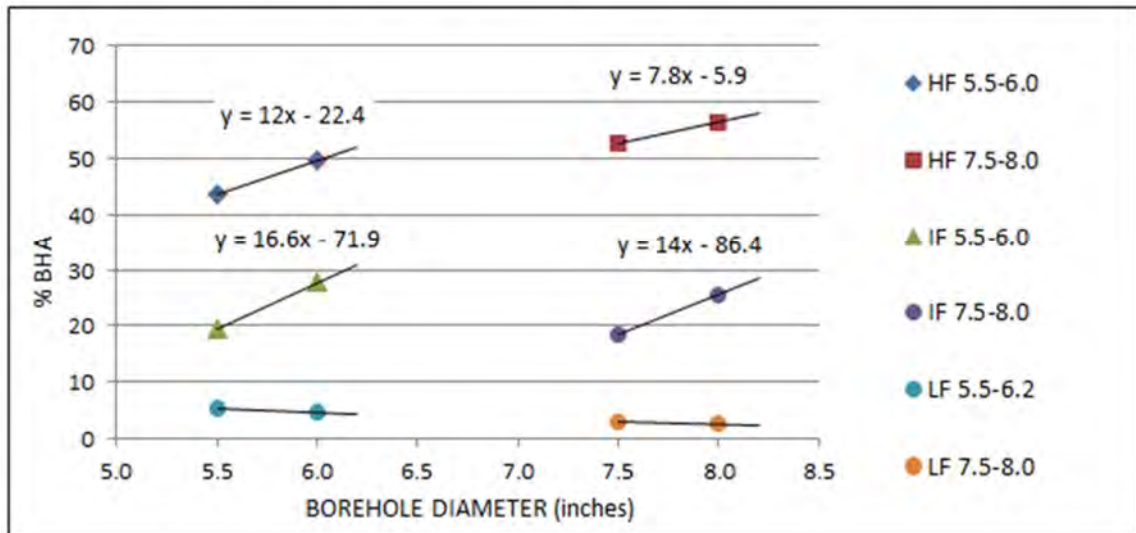


Figure 13: Table and accompanying chart detailing the relative percentages of passing flow provided by each diverter design diagrammed in Figure 11. Four (4) linear-regression equations were derived to quantify the changes in flow area accompanying small changes in borehole diameter, for example in going from a 5.5- to 6-inch diameter hole. Only those equations for the intermediate- and high-rate designs were incorporated into the MS- Excel flow calculator (Figure 14) because very small changes in area are noted in for the low-flow scheme whereas they vary up to ~8% for the passing-flow schemes.

SHALLOW SUBSURFACE GEOPHYSICAL APPLICATIONS IN ENVIRONMENTAL GEOLOGY
GANJ XXXIII Annual Conference and Field Trip

Table 3: Comparison error summary of Mt. Sopris and NJGWS flow calculations versus controlled rates in a 5.5-inch diameter pipe

LOW FLOW MT SOPRIS DIVERTER WITH UPPER TRI-WING CENTRALIZER												
	UPWARD FLOW						DOWNWARD FLOW					
	Rate	Time	NJGWS		Mt. Sopris		Rate	Time	NJGWS		Mt. Sopris	
No.	gpm	Sec.	gpm	error	gpm	error	gpm	Secs	gpm	error	gpm	error
1	0.033	9.900	0.032	4.2	0.030	8.8	0.010	31.02	0.009	8.0	0.010	4.5
2	0.088	4.100	0.089	1.3	0.080	10.4	0.010	31.93	0.009	11.5	0.010	1.6
3	0.088	4.000	0.092	4.1	0.082	7.3	0.010	27.27	0.011	6.3	0.012	16.7
4	0.088	4.000	0.092	4.1	0.082	7.3	0.010	28.52	0.010	1.6	0.011	12.6
5	0.180	2.200	0.185	2.8	0.166	8.2	0.010	27.16	0.011	6.7	0.012	17.0
6	0.180	2.150	0.190	5.4	0.171	5.2	0.033	9.550	0.034	2.5	0.038	13.5
7	0.180	2.350	0.171	5.0	0.153	17.3	0.033	9.600	0.034	1.9	0.038	13.0
8	0.180	2.300	0.176	2.4	0.158	14.3	0.040	8.600	0.038	5.3	0.043	7.2
9	0.226	1.850	0.227	0.4	0.206	9.5	0.040	8.400	0.039	2.6	0.044	9.7
10	0.226	1.880	0.223	1.5	0.202	11.7	0.040	8.150	0.040	0.7	0.046	12.8
11	0.226	1.950	0.213	5.9	0.193	17.0	0.040	8.250	0.040	0.6	0.045	11.6
12							0.102	3.450	0.104	1.7	0.135	24.3
13							0.102	3.500	0.102	0.1	0.132	22.8
14							0.102	3.550	0.101	1.5	0.130	21.4
15							0.102	3.500	0.102	0.1	0.132	22.8
16							0.130	2.700	0.136	4.3	0.188	31.0
17							0.130	2.750	0.133	2.3	0.184	29.2
18							0.130	2.750	0.133	2.3	0.184	29.2
19							0.330	1.250	0.317	4.2	0.594	44.4
20							0.330	1.200	0.331	0.4	0.634	47.9
21							0.330	1.250	0.317	4.2	0.594	44.4
			AVG	3.4		9.7			AVG	3.3		20.8

proper calibration of a HFM is necessary when using one to calculating aquifer transmissivity (Day-Lewis and others, 2011) because using inappropriate IRT-to-flow reference curves will produce unreliable results. The MatrixHeat polynomial solution is only reliable for use by returning close flow rates only in the solutions derived here versus the Mt. Sopris solution included in the current revision of the MatrixHeat software. Calculated values for the 5.5-inch pipe (A) cluster nicely along a single reference curve except in the case of downward flows where we begin see small lag effects for downward flows, perhaps from countering upward-convection as a heat-pulse tends to rise in a sub vertical fluid column. Although the derived accuracy error for the ~6-inch well is ~12% at about 2 gpm, the value for a ~8-inch-diameter well at a similar rate is about three times that (~36%). It is important to note that as currently built, the caliper factor for the ~8-inch wells is inverted with respect to the ~6-inch ones because as Figure 3 shows, the relationships for small-to-larger diameter wells with respect to the observed flow rates is reversed; that is, calculated flow rates increase with an increase in borehole diameter for the smaller wells but decreases for the larger ones. We therefore multiplied the power solutions by the caliper factor for the smaller wells, but divided the power solution by the caliper for the larger ones. This approach is considered preliminary with the hope of future refinement and improvement from more field deployment and further laboratory testing. The error analysis

SHALLOW SUBSURFACE GEOPHYSICAL APPLICATIONS IN ENVIRONMENTAL GEOLOGY
 GANJ XXXIII Annual Conference and Field Trip

summarized in Table 5 emphasizes the magnitude of errors that can arise when deploying the tool in the custom, passing-flow mode, especially for the larger-diameter wells.

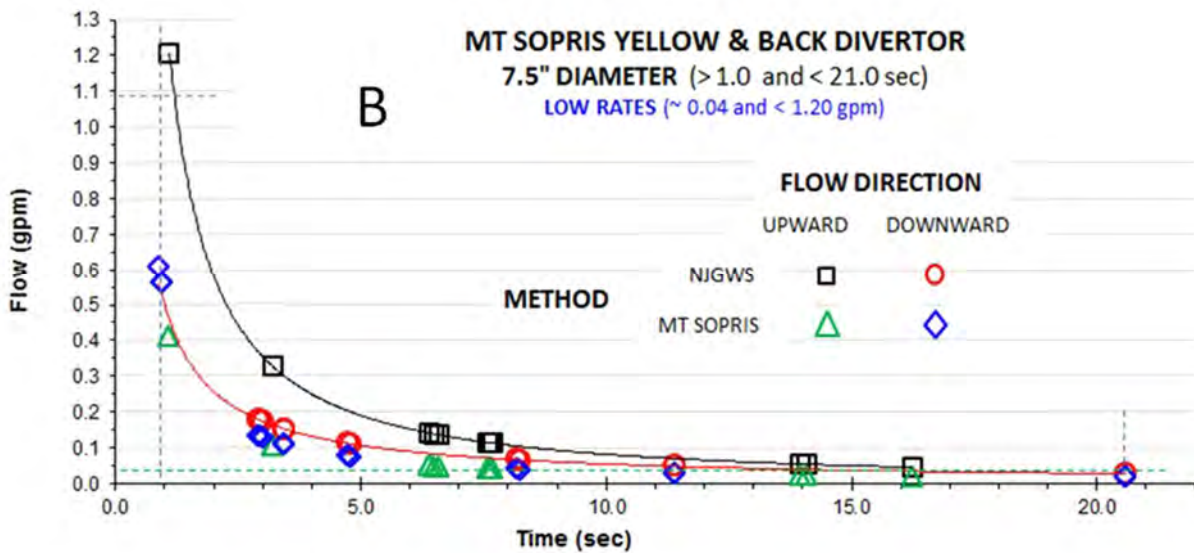
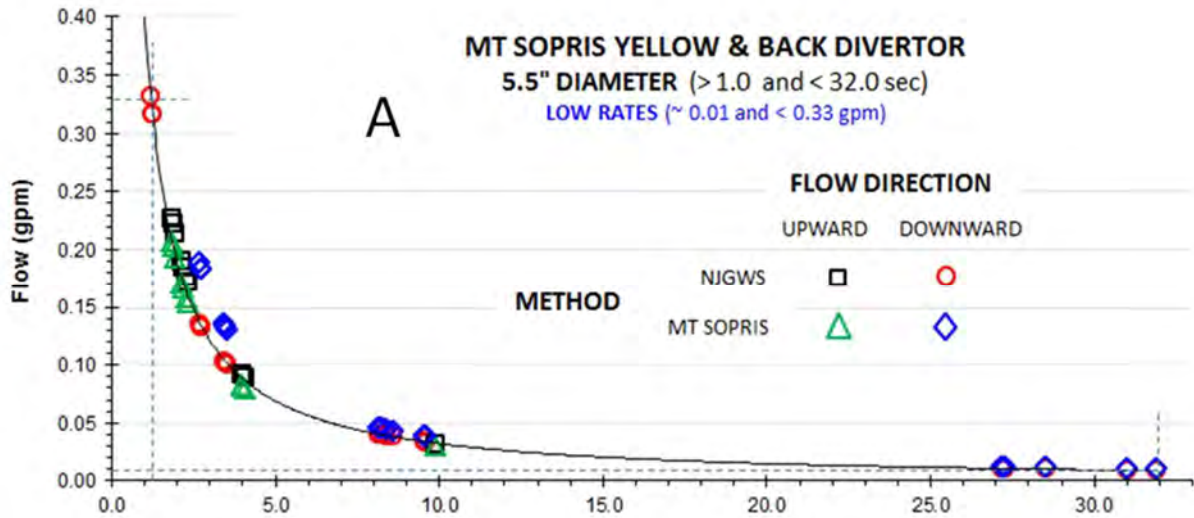


Figure 14: MS Excel charts comparing calculated flow rates in the 5.5- and 7.5inch-diameter pipes using the power solutions derived here versus the Mt. Sopris solution included in the current revision of the MatrixHeat software. Calculated values for the 5.5-inch pipe (A) cluster nicely along a single reference curve except in the case of downward flows where we begin see small lag effects for downward flows, perhaps from countering the upward-directed effects of heat-pulse that convection in a sub vertical fluid column. Chart B shows that the MatrixHeat solution that is calibrated for use in 6-inch holes consistently underestimates flow in the ~8-inch holes and by a large margin for upward cross flows.

SHALLOW SUBSURFACE GEOPHYSICAL APPLICATIONS IN ENVIRONMENTAL GEOLOGY
GANJ XXXIII Annual Conference and Field Trip

Table 4: Comparative flow rates at different IRTs with summary of percentage differences between downward and upward axial flows in the 2 to 32 second time window calculated using the derived power equations of Table 2.

HFR5.5 sec	Calculated down	up	% DIFF
2	4.068425	4.363137	-7.2
4	2.805913	2.730879	2.7
6	2.257820	2.076179	8.0
8	1.935184	1.709253	11.7
14	1.433685	1.170880	18.3
20	1.184203	0.920023	22.3
26	1.028851	0.770501	25.1
32	0.920488	0.669597	27.3
AVG =			14.3

HFR7.5 sec	Calculated down	up	% DIFF
2	7.686776	10.41010	-35.4
4	5.228433	6.037335	-15.5
6	4.173158	4.389728	-5.2
8	3.556304	3.501352	1.5
14	2.605372	2.255318	13.4
20	2.136703	1.703942	20.3
26	1.846680	1.386422	24.9
32	1.645332	1.177651	28.4
AVG =			17.4

IFR5.5 sec	Calculated down	up	% DIFF
2	1.379139	1.512160	-9.6
4	0.834953	0.869110	-4.1
6	0.622547	0.628605	-1.0
8	0.505495	0.499519	1.2
14	0.337099	0.319422	5.2
20	0.260380	0.240214	7.7
26	0.215334	0.194786	9.5
32	0.185279	0.165008	10.9
AVG =			6.2

IFR7.5 sec	Calculated down	up	% DIFF
2	2.309996	2.756498	-19.3
4	1.587647	1.512397	4.7
6	1.274937	1.064561	16.5
8	1.091181	0.829801	24.0
14	0.806145	0.511096	36.6
20	0.664678	0.375282	43.5
26	0.576724	0.299008	48.2
32	0.515445	0.249798	51.5
AVG =			28.5

LF5.5 sec	Calculated down	up	% DIFF
2	0.189201	0.206970	-9.4
4	0.088388	0.091727	-3.8
6	0.056630	0.056986	-0.6
8	0.041292	0.040653	1.5
14	0.022336	0.021075	5.6
20	0.015098	0.013865	8.2
26	0.011319	0.010189	10.0
32	0.009012	0.007985	11.4
AVG =			6.3

LF7.5 sec	Calculated down	up	% DIFF
2	2.575736	2.756498	-7.0
4	1.319494	1.512397	-14.6
6	0.892235	1.064561	-19.3
8	0.675948	0.829801	-22.8
14	0.393896	0.511096	-29.8
20	0.279191	0.375282	-34.4
26	0.216743	0.299008	-38.0
32	0.177389	0.249798	-40.8
AVG =			25.8

SHALLOW SUBSURFACE GEOPHYSICAL APPLICATIONS IN ENVIRONMENTAL GEOLOGY
GANJ XXXIII Annual Conference and Field Trip

Table 5: Example results calculated using the MS Excel flow-calculator with some field-test results from 2011 (Figure 3) taken at high rates of flow when using the high-rate bypass diverter.

High rate of upward flow in a 5.5 to 6.2-inch diameter well								
CALIPER (in)	TIME (s)	OFR _{6.0}	CFR _{5.5}	ERR1%	CAL _{5.5to6.2}	AFR	ERR2%	PFA%
6	9.6	2.25	1.52	32.3	1.14	1.73	12.1	49.6
High rate of upward flow in a 7.5 to 8.2-inch diameter well								
CALIPER (in)	TIME (s)	OFR _{8.0}	CFR _{7.5}	ERR3%	CAL _{7.5to8.2}	AFR	ERR4%	PFA%
8	11	1.87	2.73	-45.8	1.07	2.54	-35.7	56.5

OFR-Observed flow rate (gpm), CFR-calculated flow rate (either for 5.5- or 7.7-inch hole in gpm), CAL-Caliper factor, PFA-Percentage passing flow area relative to borehole cross-section area

A somewhat vexing aspect of deploying a HFM system can be the equalization process. This is the routine preceding release of a heat pulse into the water column. During this routine, the system operator monitors a visual display of a line that continuously charts the amplitude of the response curve determined from heat-sensor readings provided by the two thermistors over a period of time. The ideal equalization curve is stable and flat over a prolonged period, from over a dozen seconds to minutes if necessary, before firing a heat pulse and registering the IRT. From our experience, if there are transient pumping effects in the area of the borehole being tested, or in the case of the laboratory test, transient fluctuations in the water pressure in the supply line, equalization does not return a stabilized signal but can fluctuate and periodically spike rather than returning a stable signal indicating stabilized cross flows (Figure 2). During the laboratory tests we also sometimes observed equalization curves that rhythmically fluctuated as low-frequency sinusoidal curves that compromised acquisition of test data at certain flow rates and that probably reflect flow-regime changes at various combinations of pipe diameter and flow rate. This is an interesting aspect of these tests that merits further work in order to understand this phenomenon more thoroughly.

Following are three some operational tips that may be helpful when deploying HFM systems that we have learned from deploying out HFM systems:

- 1) Cross-flow rates can vary in direction and magnitude relative to nearby topographic and structural geological conditions (Herman, 2014). In many cases, directions of cross flows can be reasonably estimated before logging by first constructing a simple hydrogeological profile that includes the topographic grade, structural attitude of geological strata, and the well-construction information including the total depth of the well, the depth of casing, and the penetrated, open stratigraphic interval. Of course, knowing the depth of permeable geological features before HFM testing can be useful and save deployment time. Many examples of more thoroughly developed profiles are available for various fractured-bedrock aquifers in New Jersey that exemplify these concepts (Michalski? Herman, 2010; Herman and Curran, 2010).

SHALLOW SUBSURFACE GEOPHYSICAL APPLICATIONS IN ENVIRONMENTAL GEOLOGY
 GANJ XXXIII Annual Conference and Field Trip

- 2) Cross-flow rates vary drastically in different aquifer systems, with solution-prone ones like dolomite and limestone typically having the highest measured rates (Herman and Curran, 2014)
- 3) Transient pumping effects depend on standard water-use cycles that peak during the early morning, mid-day, and late afternoon times during low-flow testing.

NJ GEOLOGICAL & WATER SURVEY FLOW CALCULATOR FOR A HPFM 2293

5.5 to 6.2-inch Diameter Boreholes					
FLOW RATE & DIRECTION	FLOW RANGE GPM	TIME RANGE seconds	CALIPER inches	TIME seconds	FLOW GPM
LOW UP	> .01 < 0.4	> 1.8 < 32.0	5.3	5.3	0.066
LOW DOWN	> .01 < 0.4	> 1.8 < 32.0	20.0	20.0	0.015
INTER UP	> 0.2 < 2.0	> 1.5 < 42.0	6.0	20.0	0.34
INTER DOWN	> 0.2 < 2.0	> 1.5 < 42.0	6.0	20.0	0.37
HIGH UP	> 0.9 < 7.0	> 1.0 < 24.0	6.0	20.0	1.06
HIGH DOWN	> 0.9 < 7.0	> 1.0 < 24.0	6.0	20.0	1.35

7.5 to 8.2-inch Diameter Boreholes					
FLOW RATE & DIRECTION	FLOW RANGE GPM	TIME RANGE seconds	CALIPER inches	TIME seconds	FLOW GPM
LOW UP	> .02 < 1.0	> 0.9 < 21.0	10.0	10.0	0.082
LOW DOWN	> .02 < 1.0	> 0.9 < 21.0	10.0	10.0	0.054
INTER UP	> 0.3 < 3.0	> 1.5 < 32.0	8.0	10.0	0.94
INTER DOWN	> 0.3 < 3.0	> 1.5 < 32.0	8.0	10.0	1.33
HIGH UP	> 1.5 < 8.0	> 1.5 < 41.0	8.0	10.0	2.74
HIGH DOWN	> 1.5 < 8.0	> 1.5 < 41.0	8.0	10.0	2.92



Rev. 02/2015

Method for using a caliper function for refining calculated flow rates in variable-diameter boreholes when using the PFA diverter schemes

Figure 15: A screen-captured image of the NJGWS MS Excel flow calculator used with a HFP-2293. Two sheets provide IRT to flow-rate calculates for ~6 to 8 inch wells when using three diverter schemes covering low-, intermediate-, and high-flow ranges. Photographs summarize the respective deployment schemes.

As a final note, we set out to test our HFM system with the intent of refining its operational range and therefore its potential use. As is typical with testing of scientific instrumentation, the facilities needed for testing and the amount of time required to adequately understanding its operational thresholds and

precision is ordinarily cost prohibitive, and in this case benefits from research conducted by this government agency. This technology is relatively new and rapidly evolving, sometime in parallel, with competing technologies that may someday render HFM technology obsolete. But for now, these instruments are gaining a foothold in the industry to aid with groundwater-pollution investigations in response to regulatory oversight. These instruments are not required to be certified for use, nor are their operators. We therefore simply continue to refine our toolkit used to characterize complex, fractured-rock aquifers that benefit from knowing the rates and directions of groundwater cross flow in open boreholes.

Acknowledgments

We thank Ms. Bay Weber of the Stony Brook-Millstone Watershed Association for site access to use their well field in Hopewell Township. We thank John Curran, Steve Spayd, Gregg Steidl, Mike Gagliano, Michelle Kuhn, Ray Bousenberry, Ted Pallis and Brian Buttari of the NJGWS Geological Research and Support Section for approval, contributing advice and providing constructive feedback during this work and for contributing to a productive atmosphere of cooperation and teamwork. James T. Boyle, Chief of the NJGWS Groundwater Supply and Analysis section, and pictured on the report cover, proved valuable suggestions implemented during the tests. We thank Jim Peterson and Princeton Geosciences, Inc., for use of their HFM during testing, and providing a scientific review of this work during report editing and production. We thank Tenika Haywood for helping procure the test equipment. We also thank Jim Lococo of Mt. Sopris Instrument Company for reviewing and providing comments on this work.

References

- Herman, G. C., 2010, Hydrogeology and borehole geophysics of fractured-bedrock aquifers, Newark Basin, New Jersey (5 MB PDF), in Herman, G. C., and Serfes, M. E., eds., Contributions to the geology and hydrogeology of the Newark basin: N.J. Geological Survey Bulletin 77, Chapter F., p. F1-F45.
- Herman, G. C., 2006, Field Tests Using a Heat-Pulse Flow Meter to Determine its Accuracy for Flow Measurements in Bedrock Wells (2 MB PDF): New Jersey Geological Survey Technical Memorandum TM06-1, 8 p.
- Herman, G. C., 2006 Hydrogeological framework of the Brunswick aquifer at Heron Glen Golf Course, Hunterdon County, New Jersey Geological Survey Newsletter Vol 2., No. 1, Winter 2006, p. 8-11. Herman, 2012.
- Herman, G. C. and Curran, John, 2010, Borehole geophysics and hydrogeology studies in the Newark basin, New Jersey (38 MB PDF), in Herman, G. C., and Serfes, M. E., eds., Contributions to the geology and hydrogeology of the Newark basin: N.J. Geological Survey Bulletin 77, Appendixes 1-4, 245 p.
- Hess, A.E., 1986, identifying hydraulically-conductive fractures with a low-velocity borehole flowmeter: Canadian Geotechnical Journal, v. 23, no. 1, p. 69-78.
- Day-Lewis, F.D., Johnson, C. D., Paillet, F.L., and Halford, K.J., 2011, A computer program for flow-log analysis of single holes (FLASH): Ground Water, doi: 10.1111/j.1745-6584.2011.00798.x

SHALLOW SUBSURFACE GEOPHYSICAL APPLICATIONS IN ENVIRONMENTAL GEOLOGY
GANJ XXXIII Annual Conference and Field Trip

Hess, A.E., and Paillet, F.L., 1990, Applications of the thermal-pulse flowmeter in the hydraulic characterization of fractured rocks: American Society for Testing Materials, ASTM STP 101, p. 99-112.

Paillet, F.L., 1998, Flow modeling and permeability estimation using borehole flow logs in heterogeneous fractured formations: Water Resources Research, vol. 34, no. 5, p. 997-1010.

National Research Council Committee on Fracture Characterization and Fluid Flow, 1996, Rock Fractures and Fluid Flow: Contemporary Understanding and Applications: National Academy Press, Washington, D.C., 568 pages

New Jersey Department of Environmental Protection, 2012, Ground Water Technical Guidance: Site Investigation, Remedial Investigation, and Remedial Action Performance Monitoring.

http://www.state.nj.us/dep/srp/srra/training/sessions/gw_overview.pdf

New Jersey Department of Environmental Protection, 2005, Field sampling procedures manual, URL:

<http://www.nj.gov/dep/srp/guidance/fspm/>.

SHALLOW SUBSURFACE GEOPHYSICAL APPLICATIONS IN ENVIRONMENTAL GEOLOGY
GANJ XXXIII Annual Conference and Field Trip

Appendix A

Tables of laboratory testing of the Mt. Sopris HFP-2293 under varying flow conditions

Table A1: Low-flow test, Mt. Sopris yellow-and-black diverter in a 5.5-inch diameter pipe

ID	UPWARD		$y = 6.419x^{-0.640}$		DOWNWARD		$y = 5.899x^{-0.536}$	
	Rate gpm	Time (x) secs.	Calculated (y) gpm	Error %	Rate gpm	Time (x) secs.	Calculated (y) gpm	Error %
1	0.033	9.900	0.032	3.5	0.010	31.020	0.009	7.4
2	0.088	4.100	0.090	1.9	0.010	31.930	0.009	11.4
3	0.088	4.000	0.092	4.9	0.010	27.270	0.011	5.4
4	0.088	4.000	0.092	4.9	0.010	28.520	0.010	0.3
5	0.180	2.200	0.186	3.5	0.010	27.160	0.011	5.9
6	0.180	2.150	0.191	6.3	0.033	9.550	0.033	0.0
7	0.180	2.350	0.172	4.2	0.033	9.600	0.033	0.7
8	0.180	2.300	0.177	1.8	0.040	8.600	0.038	6.2
9	0.226	1.850	0.228	1.0	0.040	8.400	0.038	3.8
10	0.226	1.880	0.224	0.9	0.040	8.150	0.040	0.5
11	0.226	1.950	0.215	5.1	0.040	8.250	0.039	1.8
12					0.102	3.450	0.102	0.4
13					0.102	3.500	0.101	1.1
14					0.102	3.550	0.099	2.7
15					0.102	3.500	0.101	1.1
16					0.130	2.700	0.134	3.2
17					0.130	2.750	0.131	1.1
18					0.130	2.750	0.131	1.1
19					0.330	1.250	0.313	5.2
20					0.330	1.200	0.327	0.8
21					0.330	1.250	0.313	5.2
			AVERAGE	3.4				3.1

SHALLOW SUBSURFACE GEOPHYSICAL APPLICATIONS IN ENVIRONMENTAL GEOLOGY
GANJ XXXIII Annual Conference and Field Trip

Table A2: Low-flow test, Mt. Sopris yellow-and-black diverter in a 7.5-inch diameter pipe

ID	UPWARD		$y = 17.95x^{-0.786}$		DOWNWARD		$y = 11.301x^{-0.556}$	
	Rate gpm	Time (x) secs.	Calculated (y) gpm	Error %	Rate gpm	Time (x) secs.	Calculated (y) gpm	Error %
1	0.039	13.950	0.054	39.5	0.026	20.600	0.027	2.8
2	0.039	14.100	0.054	37.7	0.026	20.600	0.027	2.8
3	0.039	16.250	0.045	15.8	0.048	11.400	0.048	0.1
4	0.123	7.600	0.114	7.2	0.048	11.400	0.048	0.1
5	0.123	7.650	0.113	7.9	0.068	8.250	0.066	3.5
6	0.123	7.700	0.112	8.6	0.068	8.200	0.066	2.9
7	0.200	6.400	0.141	29.6	0.110	4.750	0.112	1.6
8	0.200	6.500	0.138	30.9	0.110	4.800	0.111	0.6
9	0.200	6.600	0.136	32.2	0.150	3.450	0.152	1.5
10	0.290	3.200	0.328	13.1	0.150	3.450	0.152	1.5
11	0.290	3.200	0.328	13.1	0.150	3.450	0.152	1.5
12	0.290	3.200	0.328	13.1	0.184	2.950	0.177	3.8
13	1.000	1.100	1.207	20.7	0.184	2.900	0.180	2.2
14					0.184	3.000	0.174	5.3
15					0.528	0.900	0.557	5.4
16					0.528	0.950	0.528	0.1
17					0.528	0.950	0.528	0.1
			AVERAGE	20.7				2.1

SHALLOW SUBSURFACE GEOPHYSICAL APPLICATIONS IN ENVIRONMENTAL GEOLOGY
GANJ XXXIII Annual Conference and Field Trip

Table A3: Intermediate flow test, NJGWS custom diverter 1 in a 5.5-inch diameter pipe

ID	UPWARD		$y = 2.631x^{-0.799}$		DOWNWARD		$y = 2.278x^{-0.724}$	
	Rate gpm	Time (x) secs.	Calculated gpm	Error %	Rate gpm	Time (x) secs.	Calculated (y) gpm	Error %
1	<i>0.26*</i>	<i>16.90</i>	0.27	7.3	<i>0.15</i>	<i>40.45</i>	0.16	7.8
2	<i>0.26</i>	<i>17.25</i>	0.27	5.6	<i>0.15</i>	<i>41.02</i>	0.15	4.6
3	<i>0.26</i>	<i>16.90</i>	0.27	7.3	<i>0.15</i>	<i>40.57</i>	0.15	5.5
4	0.45	9.65	0.43	4.4	0.25	20.60	0.25	0.3
5	0.45	9.75	0.43	5.2	0.25	21.14	0.24	2.2
6	0.45	9.65	0.43	4.4	0.25	20.60	0.25	0.3
7	0.49	8.50	0.48	2.9	0.25	20.39	0.25	0.4
8	0.49	8.20	0.49	0.0	<i>0.27</i>	<i>21.75</i>	0.24	9.6
9	0.49	8.00	0.50	1.9	<i>0.27</i>	<i>20.65</i>	0.25	6.1
10	<i>0.60</i>	<i>6.60</i>	0.58	2.9	<i>0.27</i>	<i>21.20</i>	0.24	7.9
11	<i>0.60</i>	<i>6.55</i>	0.59	2.3	<i>0.27</i>	<i>25.90</i>	0.21	21.8
12	<i>0.60</i>	<i>6.65</i>	0.58	3.5	<i>0.27</i>	<i>24.16</i>	0.22	17.7
13	0.81	4.45	0.80	1.5	0.27	24.35	0.22	18.2
14	0.81	4.55	0.78	3.2	0.27	24.68	0.22	19.0
15	0.81	4.80	0.75	7.2	<i>0.47</i>	<i>6.80</i>	0.55	17.7
16	0.90	3.95	0.88	2.5	<i>0.47</i>	<i>7.30</i>	0.53	11.9
17	0.90	3.90	0.89	1.5	<i>0.47</i>	<i>6.65</i>	0.56	19.6
18	0.90	3.90	0.89	1.5	<i>0.47</i>	<i>6.75</i>	0.56	18.4
19	1.08	3.00	1.09	1.3	0.47	8.05	0.49	4.3
20	1.08	3.05	1.08	0.1	0.47	7.85	0.50	6.2
21	1.08	3.05	1.08	0.1	0.47	7.95	0.49	5.2
22	<i>1.15</i>	<i>2.65</i>	1.21	5.0	0.47	7.75	0.50	7.2
23	<i>1.15</i>	<i>2.65</i>	1.21	5.0	0.67	5.05	0.69	2.3
24	<i>1.15</i>	<i>2.65</i>	1.21	5.0	0.67	5.05	0.69	2.3
25	1.34	2.25	1.38	2.7	0.67	5.05	0.69	2.3
26	1.34	2.35	1.33	0.8	0.67	5.15	0.68	0.9
27	1.34	2.30	1.35	0.9	0.85	4.00	0.81	4.6
28	<i>1.72</i>	<i>1.70</i>	1.72	0.1	0.85	4.05	0.80	5.5
29	<i>1.72</i>	<i>1.70</i>	1.72	0.1	0.85	4.05	0.80	5.5
30	<i>1.72</i>	<i>1.70</i>	1.72	0.1	0.85	4.10	0.80	6.3
31	1.95	1.45	1.96	0.3	1.00	2.95	1.01	1.0
32	1.95	1.45	1.96	0.3	1.00	2.95	1.01	1.0
33	1.95	1.45	1.96	0.3	1.00	2.95	1.01	1.0
34	2.20	1.25	2.20	0.1	1.00	2.95	1.01	1.0
35	2.20	1.25	2.20	0.1	1.83	2.08	1.30	29.0
36	2.20	1.25	2.20	0.1	1.83	1.69	1.51	17.6
37					1.83	1.70	1.50	18.0
			AVERAGE	2.4				8.4

**Italicized font for NJGWS Model HFP-2293HFM*
Regular font for Princeton Geosciences, LLC Model HFP-2293 HFM

SHALLOW SUBSURFACE GEOPHYSICAL APPLICATIONS IN ENVIRONMENTAL GEOLOGY
GANJ XXXIII Annual Conference and Field Trip

Table A4: Intermediate flow, NJGWS custom diverter 1 in a 7.5-inch diameter pipe

ID	UPWARD		$y = 5.024x^{-0.866}$		DOWNWARD		$y = 3.361x^{-0.541}$	
	Rate gpm	Time (x) Seconds	Calculated (y) gpm	Error %	Rate gpm	Time (x) Seconds	Calculated (y) gpm	Error %
1	<i>0.26*</i>	<i>27.70</i>	<i>0.28</i>	<i>8.4</i>	<i>0.54</i>	<i>31.49</i>	<i>0.52</i>	<i>3.7</i>
2	<i>0.26</i>	<i>27.65</i>	<i>0.28</i>	<i>8.6</i>	<i>0.54</i>	<i>30.35</i>	<i>0.53</i>	<i>1.8</i>
3	<i>0.26</i>	<i>27.00</i>	<i>0.29</i>	<i>10.9</i>	<i>0.54</i>	<i>31.80</i>	<i>0.52</i>	<i>4.3</i>
4	<i>0.32</i>	<i>22.13</i>	<i>0.34</i>	<i>6.4</i>	<i>0.67</i>	<i>19.50</i>	<i>0.67</i>	<i>1.0</i>
5	<i>0.32</i>	<i>23.38</i>	<i>0.33</i>	<i>1.4</i>	<i>0.67</i>	<i>19.40</i>	<i>0.68</i>	<i>1.3</i>
6	<i>0.32</i>	<i>22.43</i>	<i>0.34</i>	<i>5.1</i>	<i>0.67</i>	<i>19.29</i>	<i>0.68</i>	<i>1.6</i>
7	<i>0.62</i>	<i>12.35</i>	<i>0.57</i>	<i>8.1</i>	<i>1.09</i>	<i>7.55</i>	<i>1.13</i>	<i>3.3</i>
8	<i>0.62</i>	<i>12.20</i>	<i>0.57</i>	<i>7.1</i>	<i>1.09</i>	<i>7.31</i>	<i>1.15</i>	<i>5.1</i>
9	<i>0.62</i>	<i>12.70</i>	<i>0.55</i>	<i>10.3</i>	<i>1.09</i>	<i>7.45</i>	<i>1.13</i>	<i>4.0</i>
10	<i>0.62</i>	<i>12.55</i>	<i>0.56</i>	<i>9.4</i>	<i>1.20</i>	<i>6.75</i>	<i>1.20</i>	<i>0.3</i>
11	<i>1.09</i>	<i>6.20</i>	<i>1.03</i>	<i>5.3</i>	<i>1.20</i>	<i>6.65</i>	<i>1.21</i>	<i>0.5</i>
12	<i>1.09</i>	<i>6.10</i>	<i>1.05</i>	<i>4.0</i>	<i>1.20</i>	<i>6.45</i>	<i>1.23</i>	<i>2.1</i>
13	<i>1.09</i>	<i>5.80</i>	<i>1.09</i>	<i>0.3</i>	<i>1.34</i>	<i>5.25</i>	<i>1.37</i>	<i>2.2</i>
14	<i>1.09</i>	<i>6.65</i>	<i>0.97</i>	<i>10.9</i>	<i>1.34</i>	<i>5.35</i>	<i>1.36</i>	<i>1.2</i>
15	<i>1.47</i>	<i>4.70</i>	<i>1.31</i>	<i>10.7</i>	<i>1.34</i>	<i>5.30</i>	<i>1.36</i>	<i>1.7</i>
16	<i>1.47</i>	<i>4.70</i>	<i>1.31</i>	<i>10.7</i>	<i>1.78</i>	<i>3.40</i>	<i>1.73</i>	<i>2.6</i>
17	<i>1.51</i>	<i>3.95</i>	<i>1.53</i>	<i>1.0</i>	<i>1.78</i>	<i>3.45</i>	<i>1.72</i>	<i>3.4</i>
18	<i>1.51</i>	<i>3.90</i>	<i>1.54</i>	<i>2.2</i>	<i>1.78</i>	<i>3.40</i>	<i>1.73</i>	<i>2.6</i>
19	<i>1.51</i>	<i>3.80</i>	<i>1.58</i>	<i>4.5</i>	<i>1.82</i>	<i>2.95</i>	<i>1.87</i>	<i>2.8</i>
20	<i>1.51</i>	<i>3.85</i>	<i>1.56</i>	<i>3.3</i>	<i>1.82</i>	<i>3.30</i>	<i>1.76</i>	<i>3.2</i>
21	<i>2.23</i>	<i>2.30</i>	<i>2.44</i>	<i>9.3</i>	<i>1.82</i>	<i>3.30</i>	<i>1.76</i>	<i>3.2</i>
22	<i>2.23</i>	<i>2.35</i>	<i>2.39</i>	<i>7.3</i>	<i>1.82</i>	<i>3.30</i>	<i>1.76</i>	<i>3.2</i>
23	<i>2.23</i>	<i>2.25</i>	<i>2.49</i>	<i>11.4</i>				
24	<i>2.34</i>	<i>2.45</i>	<i>2.31</i>	<i>1.4</i>				
25	<i>2.34</i>	<i>2.40</i>	<i>2.35</i>	<i>0.4</i>				
26	<i>2.34</i>	<i>2.55</i>	<i>2.23</i>	<i>4.7</i>				
27	<i>2.34</i>	<i>2.75</i>	<i>2.09</i>	<i>10.8</i>				
28	<i>2.34</i>	<i>2.65</i>	<i>2.16</i>	<i>7.8</i>				
29	<i>2.88</i>	<i>1.70</i>	<i>3.17</i>	<i>10.0</i>				
30	<i>2.88</i>	<i>1.75</i>	<i>3.09</i>	<i>7.3</i>				
31	<i>2.88</i>	<i>1.80</i>	<i>3.02</i>	<i>4.7</i>				
			AVERAGE	6.6				2.5

* *Italicized font for NJGWS sonde,*
Regular font for Princeton Geosciences, Inc. sonde

SHALLOW SUBSURFACE GEOPHYSICAL APPLICATIONS IN ENVIRONMENTAL GEOLOGY
GANJ XXXIII Annual Conference and Field Trip

Table A5: High flow, NJGWS custom diverter 2 in a 5.5-inch diameter pipe

ID	UPWARD		$y = 6.419x^{-0.640}$		DOWNWARD		$y = 5.899x^{-0.536}$	
	Rate gpm	Time (x) seconds	Calculated (y) gpm	Error %	Rate gpm	Time (x) seconds	Calculated (y) gpm	Error %
1	0.86	22.90	0.84	2.4	1.36	15.40	1.36	0.0
2	0.86	23.10	0.83	3.0	1.36	17.09	1.29	5.4
3	0.86	23.25	0.83	3.4	1.36	13.85	1.44	5.9
4	0.86	23.44	0.83	3.9	1.36	15.75	1.34	1.2
5	0.86	22.90	0.84	2.4	3.50	2.53	3.58	2.3
6	1.00	19.16	0.95	5.3	3.50	2.44	3.65	4.3
7	1.00	19.16	0.95	5.3	3.50	2.53	3.58	2.3
8	1.00	19.00	0.95	4.8	4.68	1.80	4.30	8.2
9	1.00	19.16	0.95	5.3				
10	1.54	8.35	1.66	7.8				
11	1.54	8.80	1.60	4.0				
12	1.54	9.10	1.57	1.7				
13	1.54	9.00	1.58	2.5				
14	2.50	4.15	2.66	6.5				
15	2.50	4.25	2.62	4.8				
16	2.50	4.25	2.62	4.8				
17	3.33	2.75	3.52	5.6				
18	3.33	2.70	3.56	7.0				
19	3.33	2.70	3.56	7.0				
20	4.70	1.80	4.68	0.3				
21	4.70	1.80	4.68	0.3				
22	4.70	1.80	4.68	0.3				
23	6.90	1.15	6.34	8.1				
24	6.90	1.15	6.34	8.1				
25	6.90	1.15	6.34	8.1				
			AVERAGE	4.5				3.7

SHALLOW SUBSURFACE GEOPHYSICAL APPLICATIONS IN ENVIRONMENTAL GEOLOGY
GANJ XXXIII Annual Conference and Field Trip

Table A6: High flow, NJGWS custom diverter 2 in a 7.5-inch diameter pipe

ID	UPWARD				DOWNWARD			
	Rate gpm	Time (x) seconds	Calculated (y) gpm	Error %	Rate gpm	Time (x) seconds	Calculated (y) gpm	Error %
1	1.72	16.80	1.95	13.6	1.50	40.10	1.45	3.2
2	1.72	17.75	1.87	8.8	1.50	38.73	1.48	1.4
3	1.72	18.70	1.80	4.4	1.50	32.60	1.63	8.6
4	1.72	20.70	1.66	3.6	1.50	35.14	1.56	4.1
5	1.72	23.95	1.48	14.0	1.87	31.25	1.67	10.8
6	1.72	16.65	1.97	14.4	1.87	31.49	1.66	11.2
7	2.50	14.08	2.25	10.2	1.87	31.17	1.67	10.7
8	2.50	13.56	2.31	7.5	2.30	14.70	2.54	10.2
9	2.50	13.25	2.36	5.8	2.30	17.05	2.33	1.5
10	3.40	7.70	3.61	6.1	2.30	16.30	2.39	4.1
11	3.40	7.80	3.57	5.1	2.30	17.85	2.28	1.0
12	5.80	3.83	6.25	7.7	2.30	17.55	2.30	0.1
13	5.80	4.20	5.81	0.2	2.88	11.01	2.98	3.4
14	5.80	3.75	6.35	9.5	2.88	11.10	2.96	2.9
15	5.80	4.30	5.70	1.7	2.88	10.50	3.06	6.2
16	5.80	4.00	6.04	4.1	3.26	8.25	3.50	7.2
17	6.70	4.25	5.76	14.1	3.26	7.80	3.61	10.6
18	6.70	3.95	6.10	9.0	3.26	8.13	3.52	8.1
19	6.70	3.56	6.62	1.2	3.26	8.20	3.51	7.6
20	6.70	3.40	6.86	2.4	5.35	4.30	5.02	6.1
21	6.70	3.65	6.49	3.2	5.35	4.15	5.12	4.3
22					5.35	3.35	5.77	7.9
23					5.35	4.50	4.90	8.5
24					5.35	4.00	5.23	2.3
25					6.25	2.60	6.64	6.3
26					6.25	2.80	6.38	2.0
27					6.25	3.15	5.97	4.5
28					6.25	2.90	6.25	0.0
29					6.52	3.00	6.14	5.9
30					6.52	3.10	6.02	7.6
31					6.52	2.75	6.44	1.2
32					6.52	3.05	6.08	6.8
			AVERAGE	7.0				5.5

Assessment of Electrical Resistivity Method to Map Groundwater Seepage Zones in Heterogeneous Sediments

Michael P. Gagliano, New Jersey Geological and Water Survey

Abstract

Underwater electrical-resistivity data were collected along the southwest shore of Mirror Lake, NH, as part of a multi-year assessment of the utility of geophysics for mapping groundwater seepage beneath lakes. We found that resistivity could locate shoreline sections where water is seeping out of the lake. A resistivity line along the lake bottom starting 27-m off shore and continuing 27-m on shore (1-m electrode spacing) showed the water table dipping away from the lake, the gradient indicative of lake discharge in this area. Resistivity could also broadly delineate high-seepage zones. An 80-m line run parallel to shore using a 0.5-m electrode spacing was compared with measurements collected the previous year using 1-m electrode spacing. Both data sets showed the transition from high-seepage glacial outwash, to low-seepage glacial till, demonstrating reproducibility. However, even the finer 0.5-m electrode spacing was insufficient to resolve the heterogeneity well enough to predict seepage variability within each zone. For example, over a 12.5-m stretch where seepage varied from 1-38 cm/day, resistivity varied horizontally from 700-3900 ohm-m and vertically in the top 2-m from 900-4000 ohm-m without apparent correlation with seepage. In two sections along this 80-m line, one over glacial outwash, the other over till, we collected 14 parallel lines of resistivity, 13.5 m long spaced 1 m apart to form a 13.5 x 13 m data grid. These lines were inverted individually using a 2-D inversion program and then interpolated to create a 3-D volume. Examination of resistivity slices through this volume highlights the heterogeneity of both these materials, suggesting groundwater flow takes sinuous flow paths. In such heterogeneous materials the goal of predicting the precise location of high-seepage points remains elusive.

Introduction

The interaction between groundwater and lakes has been the subject of considerable investigation (Schneider et al., 2005; Sophocleous, 2002; Winter, 2000; Cherkauer and Carlson, 1997). Common themes include watershed management (Winter et al., 2003), mapping contaminants (Sophocleous, 2002; Cherkauer, 1991), and connectivity between lakes and pumping wells on shore (Cherkauer and Carlson, 1997). Traditionally, both out-seepage (flow from the lake to the aquifer) and in-seepage (flow from the aquifer to the lake) zones have been mapped directly using seepage meters (Lee, 1977; Rosenberry, 2005), or indirectly using temperature measurements or flow analysis by dye tracing (Kalbus et al., 2006, Conant, 2004). These methods are tedious and time consuming, sometimes taking months to complete (Schneider et al., 2005). This explains the interest in using geophysical methods to optimize the locations of ground truth.

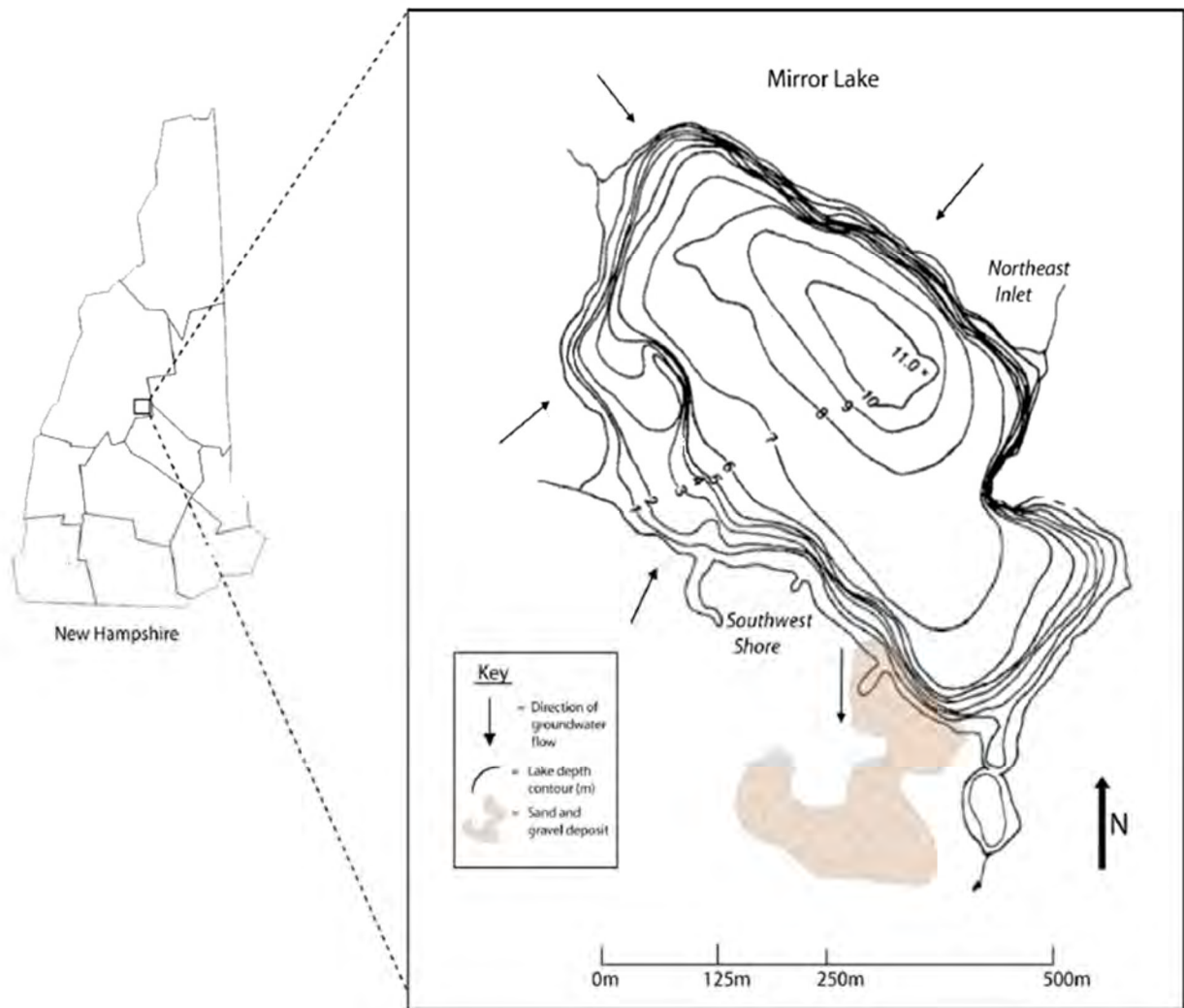


Figure 1: Mirror lake location and geology (from Mitchell et al., 2008, modified from Moeller, 1975).

Mitchell et al. (2008) reported the results of resistivity surveys and seepage measurements made at Mirror Lake, NH. In this paper we revisit some of that work, and extend our analysis to include pseudo-3D resistivity inversions made on new finer-resolution data collected at two locations along the southwest shore where the maximum seepage rate differed by a factor of 4.5.

Study Site

Mirror Lake (Figure 1) in the White Mountains of New Hampshire is a glacially formed lake of approximately 15 ha. It is a long-term study site for the USGS and is ideal for this project because of its small size and well described geology and hydrology (Ellefsen et al., 2002; Rosenberry and Winter, 1993). Rosenberry (2005) found seepage rates well in excess of 1 cm/day, which is large enough to be accurately measured, and reported considerable spatial heterogeneity in seepage rates, making this site an interesting target for testing geophysical methods.

Bedrock beneath Mirror Lake is crystalline and fractured, and fracture flow dominates the groundwater system (Winter et al., 2003; Ellefsen et al., 2002; Johnson, 1999). The glacial drift overlaying the bedrock varies in thickness from almost zero at the center of the lake to over 30 meters at the lake's edge. Composition ranges from silt to silty sand to sand and gravel with pockets of clay and a layer of organic matter covering the lakebed (Mitchell et al., 2008; Winter et al., 2003; Winter, 2000; Rosenberry and Winter, 1993). These variations in lithology affect seepage and were the target of our resistivity surveys.

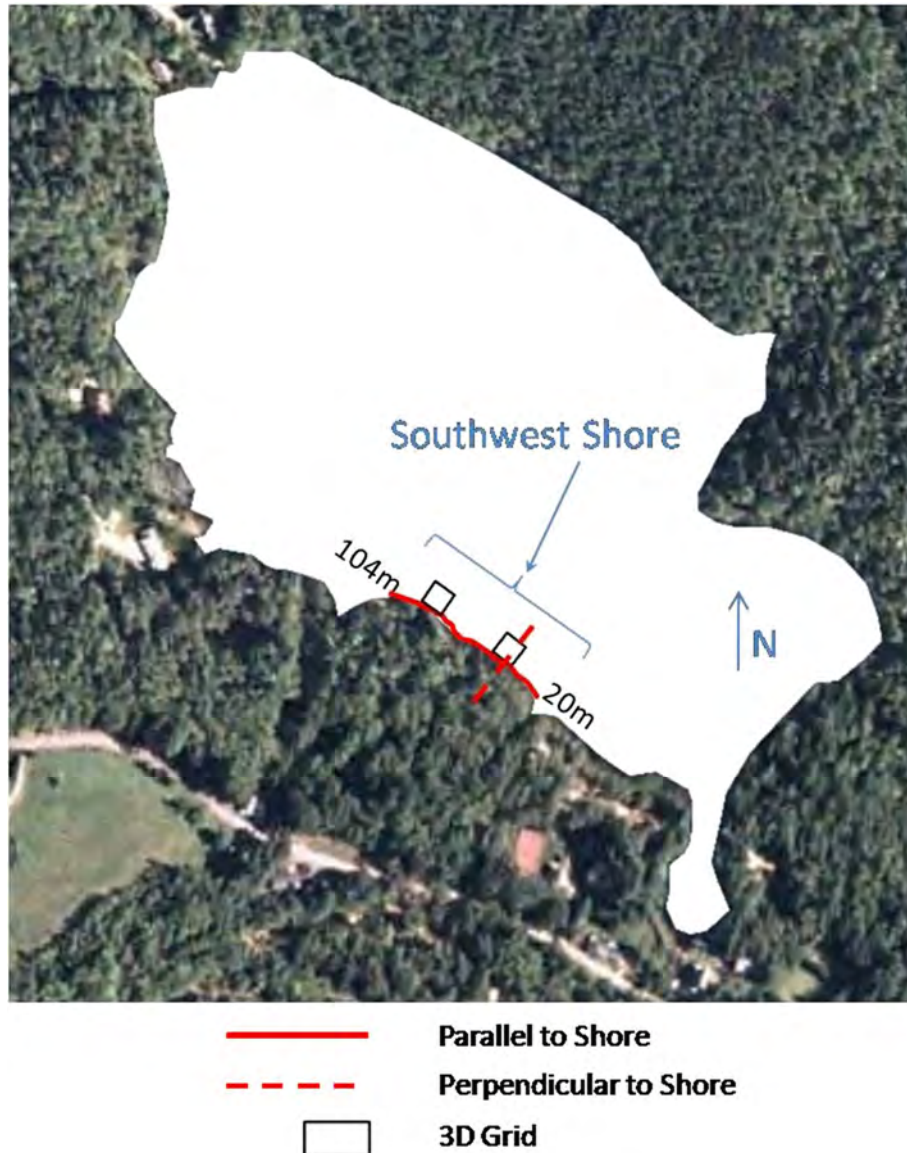


Figure 2: Location of the southwest shore resistivity surveys. The parallel-to-shore resistivity line starts at the 20 m mark and ends at the 104 m mark. The perpendicular-to-shore resistivity line crosses the 43 m mark. The 3D grids extend from 40-53.5 m and 84-97.7 m. The transition from outwash to till occurs at roughly the 70 m mark (see Figure 1).

Data presented in this paper were collected along the southwest shore of the lake (Figure 2). Most of this area is underlain by glacial till with the notable exception of an outwash deposit of sand and gravel (Figure

1). In the summer of 2007, electrical resistivity surveys and seepage measurements were made two meters from shore (Mitchell et al., 2008). Seepage rates were found to be highest in the sand and gravel with a high of -282 cm/day (negative indicates seepage from the lake to the groundwater, defined here as “out-seepage”), where resistivity values averaged approximately 1500 Ω -m. Seepage values were found to be low in the till with a high of -62 cm/day, where resistivity values were greater than 3000 Ω -m. Because there is no change in saturation or pore fluid resistivity, the changes in resistivity were attributed to changes in porosity, and at this site it appears increased porosity correlates with increased permeability and seepage. In both high and low seepage areas, however, the actual seepage values varied over distances of a few meters, indicating considerable heterogeneity.

Methods

Resistivity

We returned to this site in the summer of 2008 to check the reproducibility of the data collected the previous year, and to investigate the utility of 3D resistivity for characterizing small-scale heterogeneity. Four resistivity surveys were conducted using the SuperSting[®] electrical resistivity system. The first survey was an attempt to map the groundwater gradient by deploying a resistivity line perpendicular to shore, starting 27 m inland and extending 27 m into the lake, with the electrodes deployed along the lake bottom spaced 1 m apart. The second survey was an 80-m line parallel to shore replicating the line we reported in Mitchell et al. (2008), but collected using a 0.5 meter electrode spacing, rather than the 1-m spacing used in the 2007 survey. The data was also collected 2 m from shore.

The final two surveys were collected on 3D grids using a series of 2D lines (Yang, 2006). Each survey comprised 14 lines, each 13.5 m long, collected using a cable with 28 electrodes spaced 0.5 m apart. The lines were collected parallel to shore, beginning as close as practical to edge of the lake, with subsequent lines successively moved 1 m further from shore to encompass a total area of 13.5 x 13 m. In water too deep to stand, SCUBA diving was used to position the cable and to ensure that all electrodes were in direct contact with the bottom. One grid was centered in the sand and gravel deposit where seepage rates were found to be highest (maximum -282 cm/day); the second centered on the low-seepage section of the southeast shore, but encompassed one anomalously high value of -62 cm/day.

We used EarthImager2D[®] to invert the resistivity data for all surveys. Unlike the 2D module, the 3D module of EarthImager is not yet capable of processing a 3D data set where the electrodes are deployed underwater on an uneven bottom, so we created a pseudo-3D inversion by interpolating between the parallel 2D lines (Chambers et al., 2002). This method is less precise than a full 3D inversion, but still useful and less computationally demanding (Gharibi and Bentley, 2005; Chambers et al., 2002).

Seepage Meters

Seepage meters were constructed and deployed in the manner described by (Heaney et al., 2006;

Rosenberry, 2005). Plastic 55-gallon drums were cut in half to produce two seepage meters. The open end of the drum was then pushed slowly into the sediment so as to disturb natural seepage as little as possible, and then allowed to equilibrate. A plastic bag with a known volume of water was attached to the drum by a roughly 2-m section of garden hose. The bag was placed in a plastic box to protect it from waves and currents, and situated away from the seepage meter so that the operator could open and close the valve on the hose located next to the bag without stepping on the sediment close to the meter. After a set period of time, the bag was then weighed to determine the volume of water that seeped into or out of the bag.

Results and Discussion

2D Resistivity

Figure 3 shows the perpendicular-to-shore line in the area of high-seepage sand and gravel. The transect starts 27 m inland and continues 27 m off shore with a 1-m electrode spacing, crossing the shoreline at the 43 m mark on the resistivity line collected parallel to shore (Figure 2). Depth to water (DTW) was measured at two wells on shore located at a distance of 10 m (Well 1) and 24 m (Well 2) from the start of the line (Figure 3). Well 1 had a DTW of 1.5-m and Well 2 had a DTW of 1.0-m. The resistivity and DTW data show the water table dipping away from the lake, the unsaturated zone appearing as a region of high resistivity (red). The gradient (0.07) is consistent with out-seepage in this area. This suggests that resistivity can be used to determine whether there is out-seepage or in-seepage at a given shore location prior to any seepage measurements.

Resistivity could also be used to broadly delineate the high and low-seepage zones. Figure 4 shows two 80-m parallel-to-shore lines and the corresponding seepage data. Resistivity data collected using a 0.5-m electrode spacing were compared with data collected the previous year using 1-m electrode spacing. Of the three main factors controlling resistivity – porosity, saturation, and fluid conductivity – variations in resistivity for this line are best explained by heterogeneous porosity because the lake sediments are fully saturated and this is an out-seepage zone, so pore fluid conductivity should match that of the lake water.

Both data sets show the transition from high-seepage glacial outwash, to low-seepage glacial till, demonstrating reproducibility. However, even the finer 0.5-m electrode spacing was insufficient to resolve the heterogeneity well enough to predict seepage variability within each zone. This variability points to sinuous flow paths, and in such heterogeneous materials the goal of predicting the precise location of high-seepage is especially challenging. The next logical step was to employ 3D surveys once a broad zone of seepage had been identified to attempt to image these pathways.

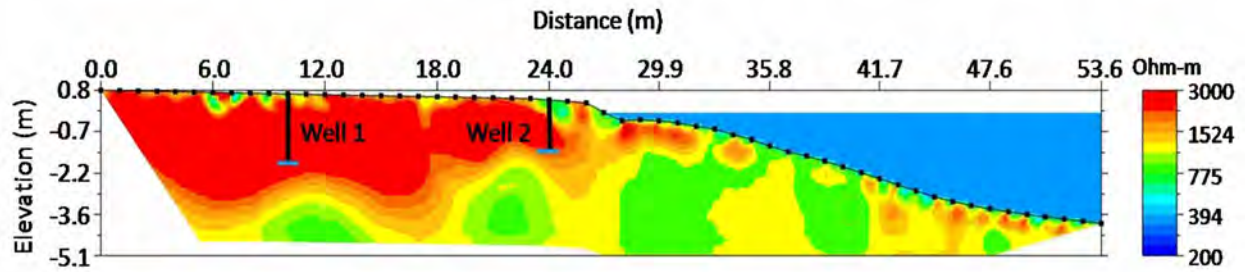


Figure 3: Resistivity data collected perpendicular to the SE shore. The vertical black lines are the locations of Well 1 (10-m mark) and Well 2 (24-m mark) and indicate depth to water. The black dots are the electrodes, spaced 1-m apart.

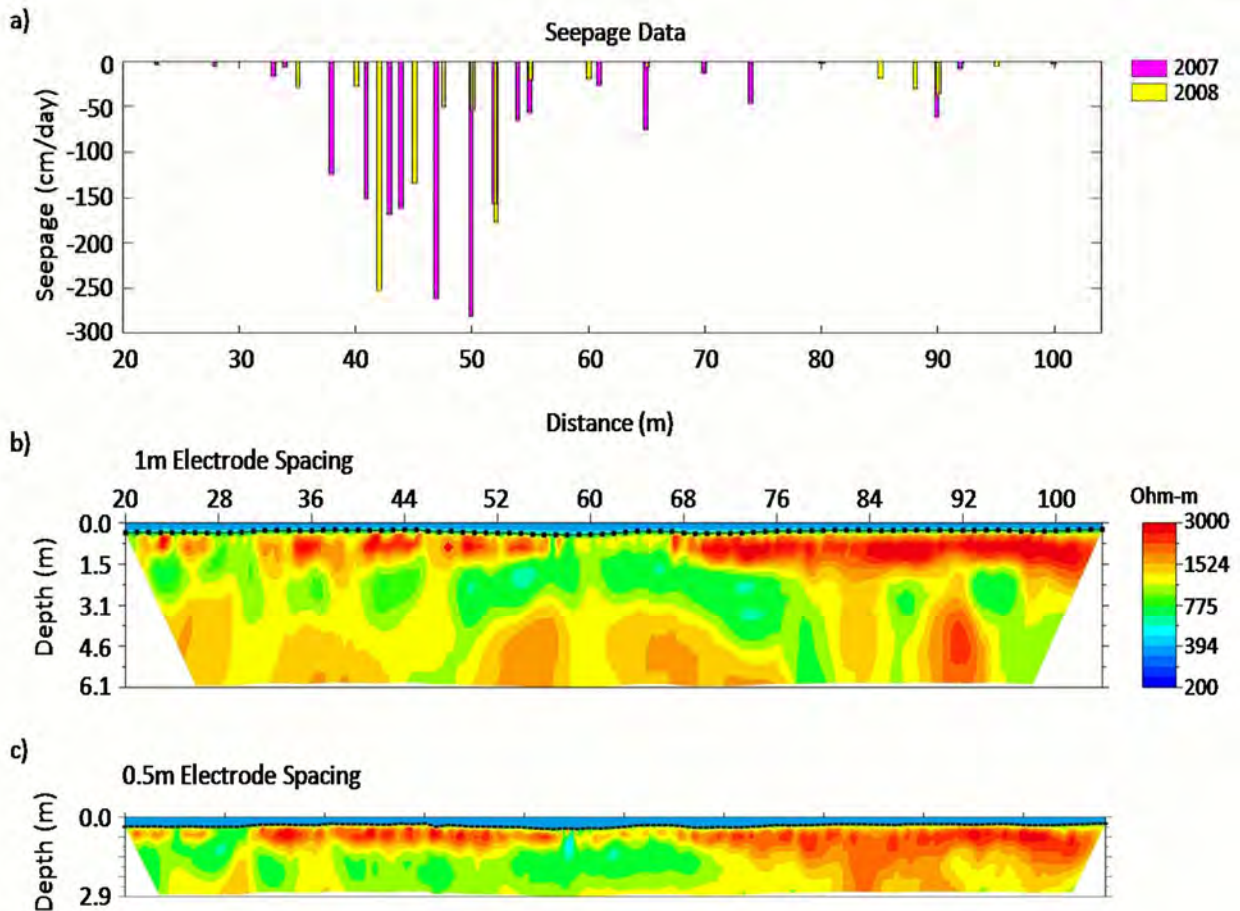


Figure 4: Parallel to shore lines: a) combined seepage data from 2007 and 2008. b) Resistivity data from 2007 with 1-m electrode spacing. c) Resistivity data from 2008 with 0.5-m electrode spacing.

Pseudo-3D Resistivity

Data from the 14 parallel, 2D inversions were interpolated to create a pseudo-3D inversion. At the time of this publication, 3D inversions involving a variable water layer cannot be processed in EarthImager®. Matlab® was used to interpolate data points between 2D inversions of the individual lines, which incorporate the water layer, to create a pseudo 3D volume. Slices could then be extracted allowing horizontal (plan) views of both the high and low-seepage areas. Two 3D surveys along with seepage measurements were completed at the southwest shore (Figure 2), one in the till (Figure 5) and one in the sand and gravel (Figure 6). Note the maximum seepage value in sand and gravel was -238 cm/d but only -36 cm/d in the till. The small zones of lower resistivity at 90-m (Figure 5) are coincident with the zones of seepage shown in the figure, and this low resistivity persisted throughout the different depths. This example indicates that it is possible to delineate finer scale heterogeneity if the background resistivity is relatively uniform and the zones are persistent with depth. This was the case in the till, where the intermediate resistivities corresponding to the seepage are more apparent.

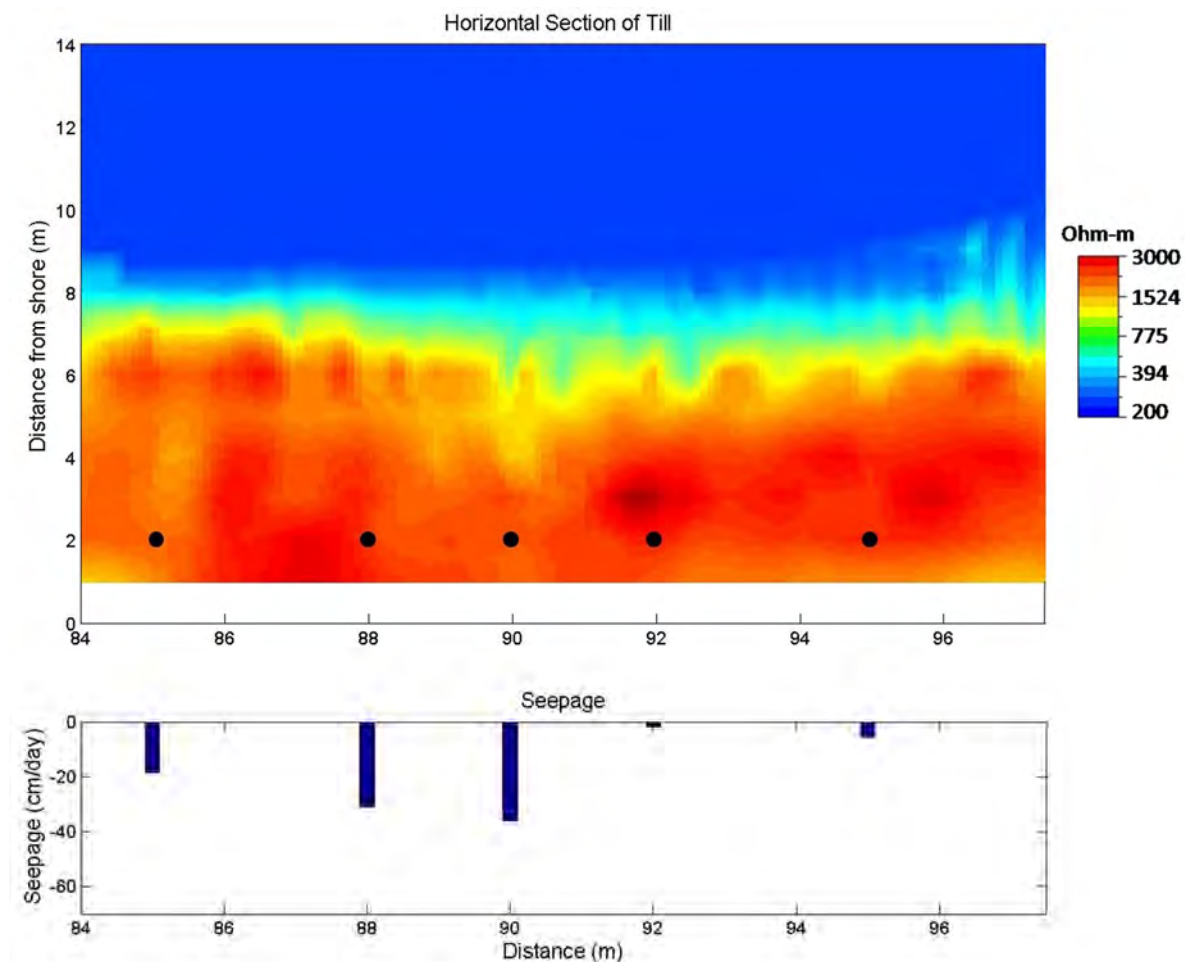


Figure 5: Horizontal resistivity slice in the till at a depth of 0.7-m with corresponding seepage values. The black dots are seepage meter locations.

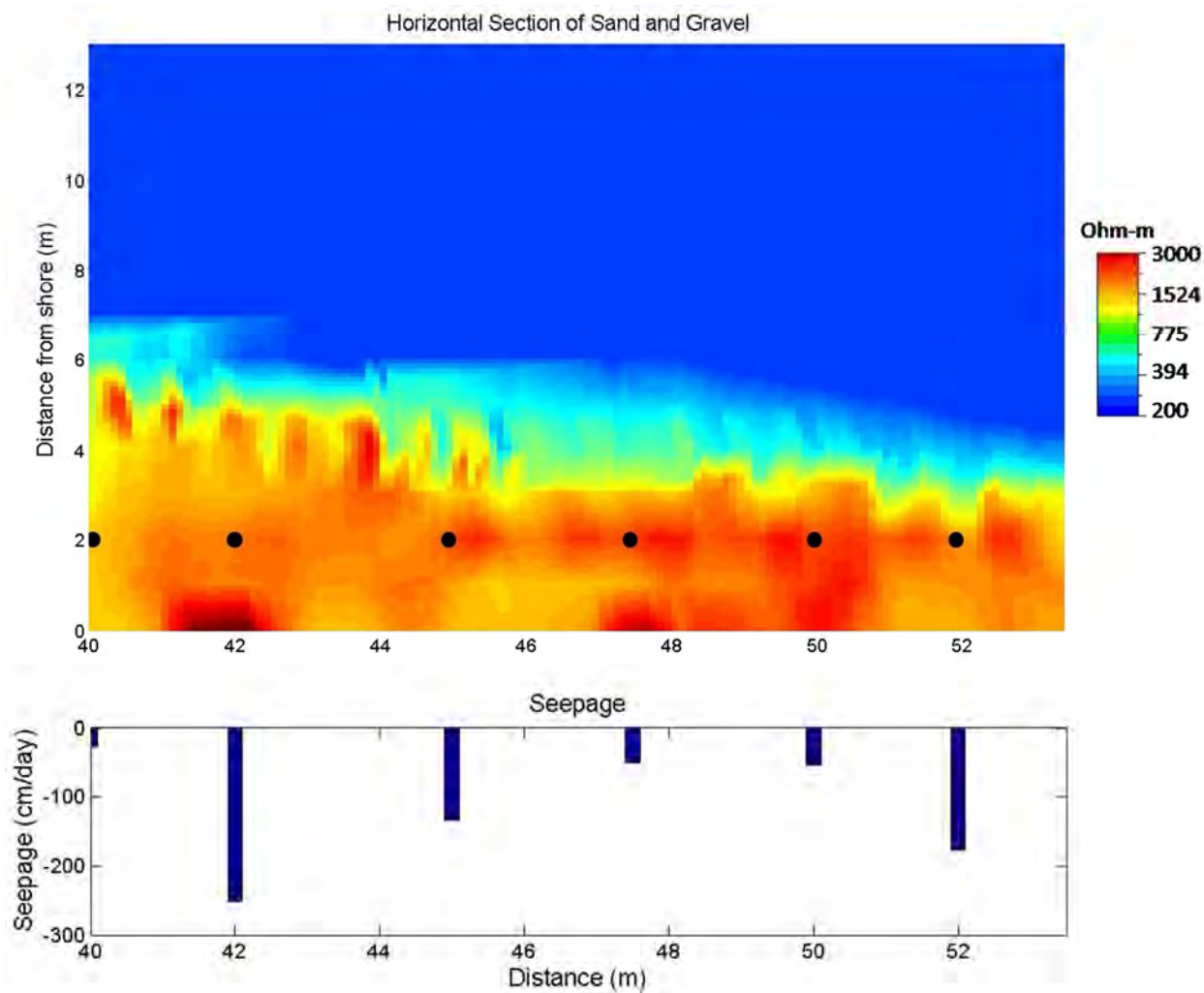


Figure 6: Horizontal resistivity slice in the sand and gravel at a depth of 0.7-m with corresponding seepage values. The black dots are seepage meter locations.

In the sand and gravel (Figure 6), the intermediate resistivity values are seen across the entire section, following the general trend of the long line (Figure 4) previously discussed. The variation in resistivities across the zone makes it difficult to pinpoint an exact seepage location where there are high seepage areas caused by a higher porosity/permeability material. These results show that even 3D resistivity may only be useful in pinpointing seepage in zones where there is a seepage spike associated with an isolated heterogeneity.

Our work at Mirror Lake showed that broad zones of seepage can be located using 2D resistivity and that the data are reproducible between years. Resistivity can also delineate the gradient of the water table, indicating the direction of seepage for various sections of the shoreline. The employment of 3D resistivity to delineate fine scale heterogeneity proved to be more useful in areas of more uniform resistivity where it is easier to pick out a seepage outlier by locating an unusually conductive path. However, only pseudo-3D sections based on interpolated 2D data inversions were examined here, so the full power of a true 3D

inversion for this application is yet to be determined.

Acknowledgements

This work was supported by the National Science Foundation Hydrologic Sciences Program under Award No. 0609827. Thanks to the Hubbard Brook Research Foundation for providing logistical support.

Authors' Note

Any use of trade, product, or firm names is for descriptive purposes only and does not imply endorsement by the U.S. government.

References

- Chambers, J.E., Ogilvy, R.D., Kuras, O., Cripps, J.C., and Meldrum, P.I., 2002, 3D electrical imaging of known targets at a controlled environmental test site, *Environmental Geology*, Vol. 41, pp. 690-704.
- Cherkauer, D.S., 1991, Geophysical mapping of pathways for entry of contaminated ground water to lakes and rivers: Application in the North American great lakes, *Hydrological Science and Technology American Institute of Hydrology*, Vol. 7, pp. 35-44.
- Cherkauer, D. S. and Carlson, D. A., 1997, Interaction of Lake Michigan with a Layered Aquifer Stressed by Drainage, *Ground Water*, Vol. 35, Issue 6, pp. 981-989.
- Conant Jr., B., 2004, Delineating and quantifying ground water discharge zones using streambed temperatures: *Ground Water*, Vol. 42, No. 2, pp. 243-257.
- Ellefsen, K.J., Hsieh, P. A., Shapiro, A.M., 2002, Crosswell seismic investigation of hydraulically conductive, fractured bedrock near Mirror Lake, New Hampshire, *Journal of Applied Geophysics*, Vol. 50, pp. 299-317.
- Gharibi, M. and Bentley, L.R., 2005, Resolution of 3-D electrical resistivity images from inversions of 2-D orthogonal lines, *Journal of Environmental and Engineering Geophysics*, Vol. 10, Issue 4, pp. 339-349.
- Heaney, M.J., Nyquist, J.E., Toran, L.E., 2006, Marine Resistivity as a Tool for Characterizing Zones of Seepage at Lake Lacawac, PA, *Symposium for the Application of Geophysics to Engineering and Environmental Problems (SAGEEP '07)*, pp. 704-711.
- Johnson, C.D., 1999, Effects of lithology and fracture characteristics on hydraulic properties in crystalline rocks; Mirror lake research site, Grafton County, New Hampshire, *Water Resource investigations*, U.S. Geol. Survey, pp. 795-802
- Kalbus, E., Reinstorf, K. F., and Schirmer, M., 2006, Measuring methods for groundwater-surface water interactions: a review, *Hydro. Earth Syst. Sci.*, Vol. 10, pp. 873-887.
- Lee, David Robert., 1977, A Device For Measuring Seepage Flux in lakes and Estuaries, *Limnology and Oceanography*, Vol. 22, No. 1, pp.140-147.
- Mitchell, N.M., Nyquist, J.E., Toran, L.E., Rosenberry, D.O., Mikochik, J.S., 2008, Electrical resistivity as a tool for identifying geologic heterogeneities which control seepage at Mirror Lake, NH, *Proceeding of the Symposium for the Application of Geophysics to Environmental and Engineering Problems (SAGEEP, 2008)*, pp. 749-759.
- Moeller, R. E., 1975, Hydrophyte biomass and community structure in a small oligotrophic New Hampshire lake, *Verhandlungen Internationale Vereinigung Limnologie*, Vol. 19, pp. 1004-1012.
- Rosenberry, D.O., 2005, Integrating seepage heterogeneity with the use of ganged seepage meters, *Limnology and Oceanography: Methods*, Vol. 3, pp. 131-142.

SHALLOW SUBSURFACE GEOPHYSICAL APPLICATIONS IN ENVIRONMENTAL GEOLOGY
GANJ XXXIII Annual Conference and Field Trip

- Rosenberry, D.O. and Winter, T.C., 1993, The significance of fracture flow to the water balance of a lake of fractured crystalline rock terrain, *Memoirs of the 24th congress of International Association of Hydrologists*, Oslo.
- Schneider, R.L., Negley, T.L., Wafer, C., 2005, Factors influencing groundwater seepage in a large mesotrophic lake in New York, *Journal of Hydrology*, Vol. 310, pp. 1-16.
- Sophocleous, Marios, 2002, Interactions between groundwater and surface water: the state of the science, *Hydrogeology Journal*, Vol. 10, pp. 52-67.
- Winter, T.C., 2000, Interaction of ground water and surface water, *Proceedings of the Ground-water/ Surface-Water Interactions Workshop*.
- Winter, T.C., Rosenberry, D.O., LaBaugh, J.W., 2003, Where does the water in a small watershed come from, *Ground Water*, Vol. 41, No. 7, pp. 989-1000.
- Yang, X. and Lagmanson, M., 2006, Comparison of 2D and 3D electrical resistivity imaging methods, *Proceeding of the Symposium for the Application of Geophysics to Environmental and Engineering Problems (SAGEEP, 2006)*, pp. 585-59.

Aquifer heterogeneity and the importance of calibrating ground-penetrating radar data in environmental investigations

Alex R. Fiore, U.S. Geological Survey

Introduction

Ground-penetrating radar (GPR) is a surface-geophysical tool with the ability to obtain continuous subsurface electromagnetic imaging quickly and economically over large areas, which frequents its use in hydrogeological and environmental applications. Owing to this convenience, GPR interpretations are sometimes advanced having not been calibrated, verified, or “ground-truthed” with additional subsurface testing methods, which can lead to false interpretations in aquifers with high heterogeneity.

The formations that comprise the Kirkwood-Cohansey aquifer system have heterogeneous hydrogeologies that vary from near-impermeable clays to highly permeable coarse sands and gravels. Although regionally regarded as an unconfined aquifer system, clay lenses will often create localized confined or semi-confined conditions within the system (Zapeczka, 1989). This will have a great impact to site-scale hydrogeology, especially for environmental investigations of smaller area sites. Localized heterogeneities may go unnoticed in a GPR profile collected in such an investigation, so performing additional tests is necessary for proper interpretation of the profile. Geophysical imaging should not be the sole method of determining subsurface properties, and instead be used in tandem with additional sources of data.

GPR Overview

In GPR, a transmitter antenna emits a radio-frequency electromagnetic pulse into the subsurface. When the pulse encounters an interface between earth materials with contrasting electromagnetic properties, some of the signal is reflected back to land surface and recorded by a receiver antenna, while the rest continues downward into deeper material. Wave velocity slows and signal attenuation increases in materials of high electrical conductivity and large dielectric permittivity, and less penetration depths occur as signal attenuation increases (Beres and Haeni, 1991). Strong wave reflections occur at interfaces where this electromagnetic contrast is greater, such as from unsaturated to saturated sediment and sand to clay.

The raw GPR data record only includes the two-way travel time for the emitted signal to enter the subsurface, encounter a reflector, and return to the antenna. The GPR analyst must convert travel times to depths below land surface by assuming a wave velocity:

$$d = tV/2$$

where d = depth to the reflector below land surface, t = two-way travel time, and V = wave velocity. This wave velocity is dependent on the earth material present, and numerous sources are available that provide

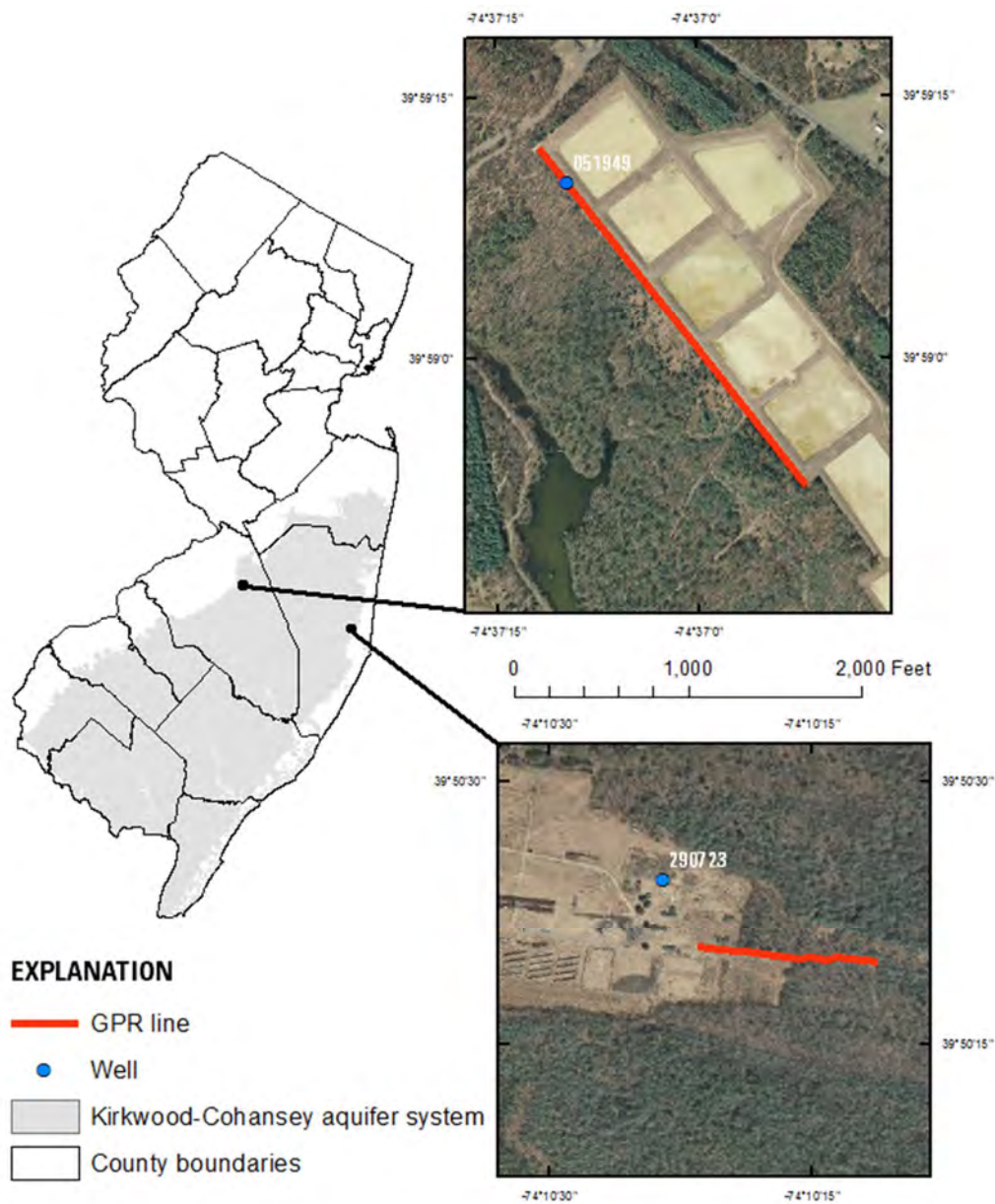


Figure 1: Locations of ground-penetrating radar sites and nearby wells in the Kirkwood-Cohansey aquifer system of New Jersey (top right, Cohansey Formation in Joint Base McGuire-Dix-Lakehurst, Burlington County; bottom right, Cape May Formation in Forked River, Ocean County).

ranges of velocities through various media, such as those in Table 1. Each component of the subsurface, including grain size, mineralogy, water levels/moisture content, and water quality, will have electromagnetic properties that will ultimately determine the resulting signal response. As such, each of these factors should be considered during analysis of the GPR profile.

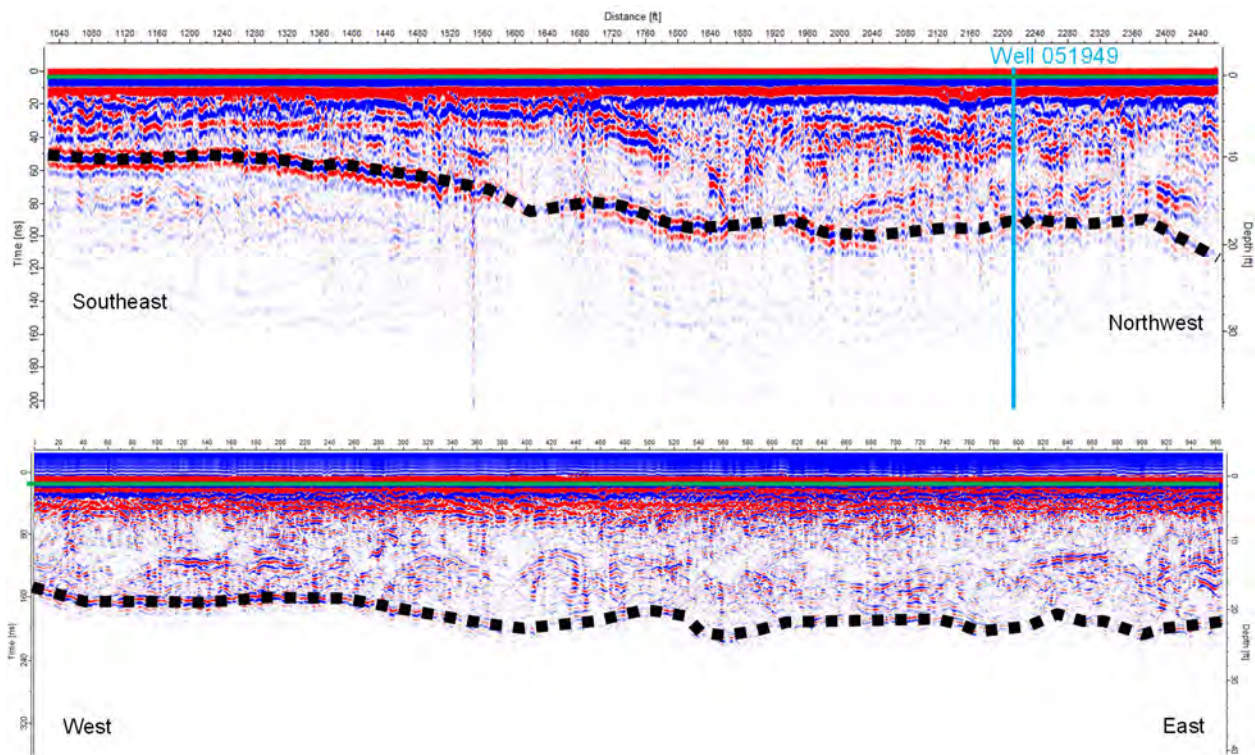


Figure 2: Ground penetrating radar profiles from sites in the Cohansey Formation (top) and Cape May Formation (bottom) using a 100 MHz and 80 MHz antenna, respectively, with applied time-varying gain filter. Depth scale is variable and only accurate to highlighted reflection.

Example 1: GPR from Cohansey Formation, Joint Base McGuire-Dix-Lakehurst, NJ

The following example is from a USGS study for a site at Joint Base McGuire-Dix-Lakehurst within the Kirkwood-Cohansey aquifer system (Fiore, 2016), where verification of GPR data from multiple subsurface testing methods evaded improper interpretations of reflection sources. This site overlies the Cohansey Formation near the outcrop of the finer-grained Lower Member of the Kirkwood Formation (Minard and Owens, 1963).

A GPR line exhibited a strong reflection occurring from 50 nanoseconds (ns) in the southeast to 100 ns in the northwest (Figure 2). The radar signal attenuates immediately after this reflection with few discernable later time reflections present, which indicates the radar has encountered an interface of strongly contrasting electromagnetic properties. Because this site is within the Kirkwood-Cohansey aquifer system, examples of likely interfaces that would cause such a reflection include unsaturated zone to water table or a contact between sandy and clayey sediment zones. This GPR line alone does not provide enough information to differentiate between which of these potential sources has caused the strong reflection; both explanations are plausible, and the subjectivity of the GPR analyst will come into play if attempting to make such a decision without further investigation.

The location of this GPR profile was designed to intersect pre-existing piezometer well 051949 (Figure 1,

2), where the reflection occurs at approximately 90 ns. The water level measured in well 051949 at the time of GPR collection was 16.99 feet below land surface. If the 90 ns reflection is interpreted as the water table, then the above equation would make the radar velocity through the unsaturated zone 0.38 ft/ns. This value is characteristic of unsaturated sand (Table 1), so the water table causing the reflection is a reasonable interpretation. However, the natural gamma log of this well indicates this reflection may potentially be caused by a clay contact based on increased gamma counts from about 9 to 12 feet depth (Figure 3). Using the above equation, the velocity of the radar wave to this depth would be about 0.200 ft/ns. This value is typical of either dry silty material (which is plausible based on the relatively higher gamma counts above 9 feet compared to the rest of the log) or saturated/high moisture sand.

On a subsequent site visit, a boring was hand-augered adjacent to well 051949 to create a well nest. The water table in the hand-augered hole was reached at 11 feet below land surface, and no fine-grained sediments were encountered through this depth, only sand and gravel. During this time, the water level in well 051949 was 11.27 feet depth, which is a negligible difference. This indicates the auger boring and the screened interval of the well are open to hydraulically connected aquifer material, and that the water level in the auger boring is not a perched water table on top of a clay lens between the bottom of the boring and the top of the well screen. As no clay was observed at 10 feet below land surface as the gamma log indicates, the GPR reflection at 90 nanoseconds near well 051949 is more likely caused by the water table than a sand-clay contact.

Multiple lines of evidence were required to narrow down the two possible interpretations, and the “ground truth” verification from the auger boring prevented an incorrect interpretation of the GPR data. Had these GPR profiles been collected for an environmental site evaluation, advancing a potentially inaccurate conclusion from unverified, uncalibrated data may prove consequential.

Example 2: GPR from Cape May Formation, Forked River, NJ

Given the heterogeneity of the Kirkwood-Cohansey aquifer system, conclusions from one site should not be extrapolated to others. This is evident in the GPR profile collected in Forked River, Ocean County, NJ. This profile is also in the Kirkwood-Cohansey aquifer system, and the shallow surficial geology is predominantly sand of the Cape May Formation (Stanford, 2013).

Visually, this profile appears very similar to the one collected in Example 1; a strong reflection runs from about 150 ns in the west to 200 ns in the east, and causes an almost immediate attenuation of the GPR signal indicating a contact with either the water table or a clay contact (Figure 2). Despite the visual similarities, the source of the reflections differed between these two profiles.

The water table in this area is generally less than 10 feet below land surface (Gordon, 2003). However, assuming a maximum of 10 feet depth for this reflector at 150 ns, the resulting velocity is a maximum of 0.133 ft/ns. This value is very low and indicates clay exists above the water table, which is an extremely unlikely interpretation.

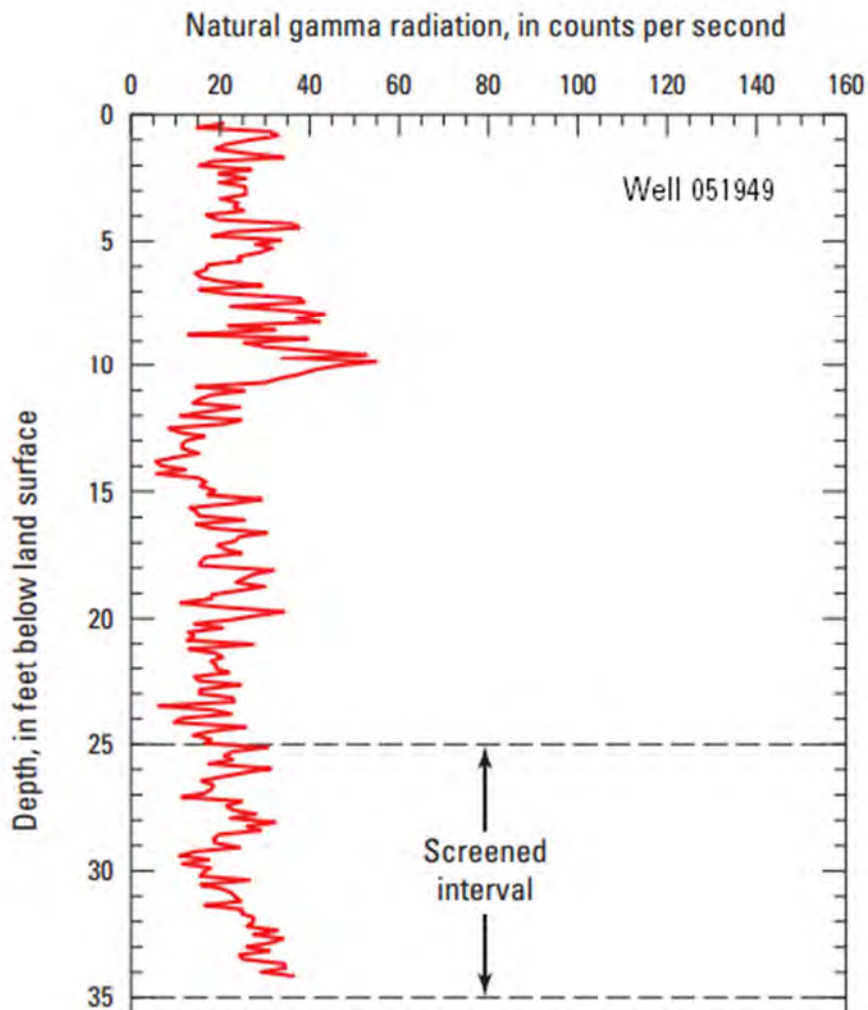


Figure 3: Natural gamma log of well 051949. Gamma intensity increases to right\

The natural gamma log of nearby well 290723 indicates a clay contact about 20 feet below land surface mapped as a fine-grained bay facies of the Cape May Formation (Stanford, 2013) (Figure 4). Well 290723 is screened in a deep confined aquifer, so its water level is not applicable to the shallow unconfined system. If the GPR reflection at 150 ns represents this clay contact at 20 feet depth, the wave velocity calculates to 0.266 ft/ns. Because the water table would fall above the contact, this 0.266 ft/ns velocity is an appropriate value for average velocity of the radar wave through both unsaturated then saturated sand (Table 1), which is the most plausible interpretation. A lower frequency GPR antenna was utilized in example 2, so the shallow water table had less effect on the emitted signal than the higher frequency pulse from example 1.

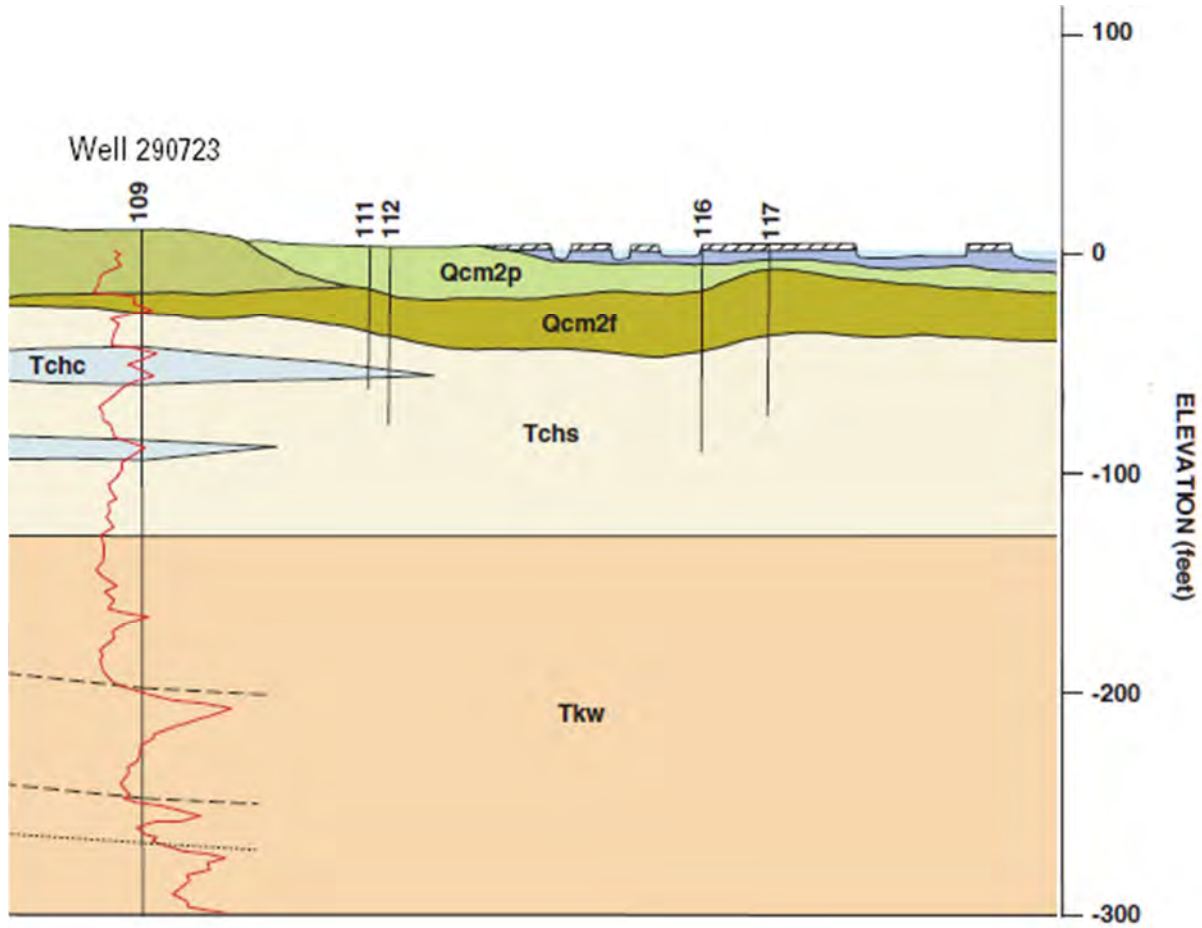


Figure 4: Geologic cross section modified from Stanford (2013) with natural gamma log of well 290723. Gamma intensity increases to right.

Table 1: Typical values of dielectric permittivity, electrical conductivity, and wave velocity for select earth materials.

Material	Dielectric permittivity	Electrical conductivity (mS/m)	Wave velocity (ft/ns)
Air	1	0	0.98
Fresh water	80	0.5	0.11
Sea water	80	3000	0.03
Ice	3-4	0.01	0.52
Dry sand	3-5	0.01	0.39-0.56
Wet sand	20-30	0.1-1	0.18-0.20
Limestone	4-9	0.5-2	0.33-0.37
Shale	5-15	1-100	0.30-0.37
Silt	5-30	1-100	0.23-0.31
Clay	5-40	2-1000	0.20-0.36
Granite	4-6	0.01-1	0.35-0.39

(mS/m, milliSiemens per meter; ft/ns, feet per nanosecond)

References

- Beres, Jr., M., and Haeni, F.P., 1991, Application of ground-penetrating radar methods in hydrogeologic studies: *Ground Water*, v. 29, no. 3, p. 375–386.
- Fiore, A.R., 2016, Hydrogeologic barriers to the infiltration of treated wastewater at the Joint Base McGuire-Dix-Lakehurst Land Application Site, Burlington County, New Jersey: U.S. Geological Survey Scientific Investigations Report 2016-5065, 83 p.
- Gordon, A.D., 2003, Hydrology of the unconfined Kirkwood-Cohansey aquifer system, Forked River and Cedar, Oyster, Mill, Westecunk, and Tuckerton Creek Basins and adjacent basins in the southern Ocean County area, New Jersey, 1998-99: U.S. Geological Survey Water-Resources Investigations Report 2003-4337, 5 pl.
- Minard, J.P., and Owens J.P., 1963, Pre-Quaternary geology of the Browns Mills quadrangle, New Jersey: U.S. Geological Survey Geologic Quadrangle Map GQ-264, scale 1:24,000.
- Stanford, S.D., 2013, Geology of the Forked River and Barnegat Light Quadrangles, Ocean County, New Jersey: New Jersey Geological Survey Geologic Map Series GMS 13-2, scale 1:24,000.
- Zapeczka, O.S., 1989, Hydrogeologic framework of the New Jersey Coastal Plain: U.S. Geological Survey Professional Paper 1404-B, 49 p., 24 pl.

Borehole Televiwer Synoptic and Hydrogeologic Framework of Adjacent RACER and NAWC Industrial Sites, West Trenton, Mercer County, New Jersey

Gregory C. Herman, Ph.D., New Jersey Geological and Water Survey (Retired)

Abstract

A detailed geological study was conducted for two adjacent industrial sites located in Trenton, New Jersey that are engaged in groundwater-pollution remedial activities. The study takes advantage of robust sets of borehole-geophysical data gathered at each site that were mostly evaluated independent of one another. The project was done because 1) these two industrial sites sit in close proximity to one another and both have a plethora of shallow subsurface information in the form of geophysical logs and cores collected over the past decade during efforts to characterize the conceptual groundwater flow models at each site, 2) because nearby Late Triassic strata are structurally inverted, which is anomalous with respect to other parts of the basin, and 3) because the Late Triassic section in this part of the Newark Basin is apparently metamorphosed to a slightly higher degree than elsewhere in the New Jersey parts of the basin. A thorough review and reinterpretation of these data sets compares and contrasts the hydrogeological framework of the fractured-bedrock aquifers at each site that happen to straddle the geological contact between sandstone-dominated clastics of the Stockton Formation and argillaceous mudstone of the superjacent Lockatong Formation. The borehole geophysical data sets include borehole televiwer (BTV) logs of both optical and acoustic types that provide good subsurface geological control for an area having a paucity of natural outcrops. For this study, 28 monitoring and test wells having BTV, natural gamma ray, and caliper (borehole diameter) logs were compiled, interpreted and structurally analyzed to determine the primary (stratigraphic) and secondary (structural) elements constituting the respective aquifer systems. The results show that stark contrasts occur between bedrock underlying each site that is reflected not only in the comparative stratigraphy but also in the structural responses to the multiple tectonic events having affected the Trenton area. This translates into having very different conceptual hydrogeological frameworks at each site. The Stockton Formation beneath the GM-RACER site displays more geological variability and is much more deeply weathered than the Lockatong Formation beneath the NAWC site. Although the average orientation of beds in both formations is similar, beds in the Stockton Formation show much greater dispersion that reflects its sedimentological origin as distributary channels in a fluvial system whereas the lacustrine beds of the Lockatong Formation are much more consistent in orientation and fracture style. The coarser, sandy nature of the Stockton Formation promotes deep bedrock weathering (~> 30m) because secondary authigenic minerals that otherwise fill tectonic fractures are commonly dissolved and removed. In contrast, the Lockatong Formation weathers to shallow depths (~<15 m) and probably behaves as a leaky-multi-unit aquifer system with a much higher degree of aquifer anisotropy.

Introduction

The results of a detailed hydrogeological study conducted during the past year in the Trenton, New Jersey area by the NJ Geological & Water Survey is summarized below using detailed subsurface geophysical logs obtained at two adjacent industrial sites having volatile-organic compound (VOC) pollution in groundwater. The site is located along the southeast edge of the central part of the Newark basin (Figures 1 to 3) The hydrogeological framework of these two sites is depicted in map and profile based on dozens of borehole televiewer (BTV) records and continuous cores obtained at the former General Motors manufacturing facility, now managed by RACER Development Corporation, and the adjacent Naval Air Warfare Center (NAWC) located immediately to the North (Figures 4 to 6). Subsurface data at each site (Table 1) were generated using multiple logging service companies on behalf a government agency and a commercial company over a two-decade time span but were previously analyzed separately with only cursory comparisons with respect to one another. The RACER site sits on Late Triassic, coarse-to-fine clastic sedimentary rocks of the Stockton Formation whereas the NAWC site is underlain by the overlying fine-grained clastic rocks and argillite of the Lockatong Formation. This study therefore straddles the stratigraphic contact between the Stockton and Lockatong Formations and provides a contrasting viewpoint of fractured-bedrock heterogeneity from both a geological and a geographic perspective. The purpose of this study is to use these robust data with modern analysis and visualizations methods to portray the geological complexities within the southeast-central part of the Newark Basin in the Trenton area where otherwise, outcrops are almost completely masked at land surface by deep weathering and anthropogenic landscapes. A primary goal is to compare and contrast the detailed stratigraphic and structural aspects constituting the respective hydrogeological models used to conceptualize groundwater flow in an industrial area having dissolved-phase groundwater contaminants. Data for RACER were shared with the NJGWS by Haley & Aldrich, Inc., the licensed environmental consulting firm conducting the groundwater investigation. Data for NAWC were obtained from personnel at the US Geological Survey New Jersey Water Science Center, Trenton, NJ Water Resources. The NAWC site has recently been a focus of their toxic substances hydrology program with hydrogeological research focused on mitigating groundwater pollution in complexly fractured bedrock. This work refines the geological complexities previously noted in this area using data generated during regulatory compliance work without addressing specific aspects of the latter. Stratigraphic and structural surface and subsurface details at each site are analyzed and summarized with respect to their relative positions in the Late Triassic stratigraphic sequence, and with respect to the geological heterogeneity of each formation at each site. This work therefore builds on previous hydrogeological reports while providing new insights into the local geological complexities. The data management and analysis methods employed in this study are the topic of this year's Teacher Workshop (Chapter 1).

Geological Setting and Prior Work

This study covers the southeast-central part of the Newark Basin (Figures 1 and 2). The area is underlain by an upward succession of Late Triassic fluvial sandstone to lacustrine shale filling the basin as detailed by Olsen and others (1992). The specific location of the study straddles the formation contact between the uppermost member of the Stockton Formation (sandstone to shale) and the lowermost member of the Lockatong Formation (siltstone to argillite). The siltstone and mudrock of the Lockatong are low-grade metamorphic rock resulting from deep burial, compaction, and regional heating from early Jurassic igneous activity of the Central Atlantic Magmatic Province (CAMP; Marzoli and others, 1999).

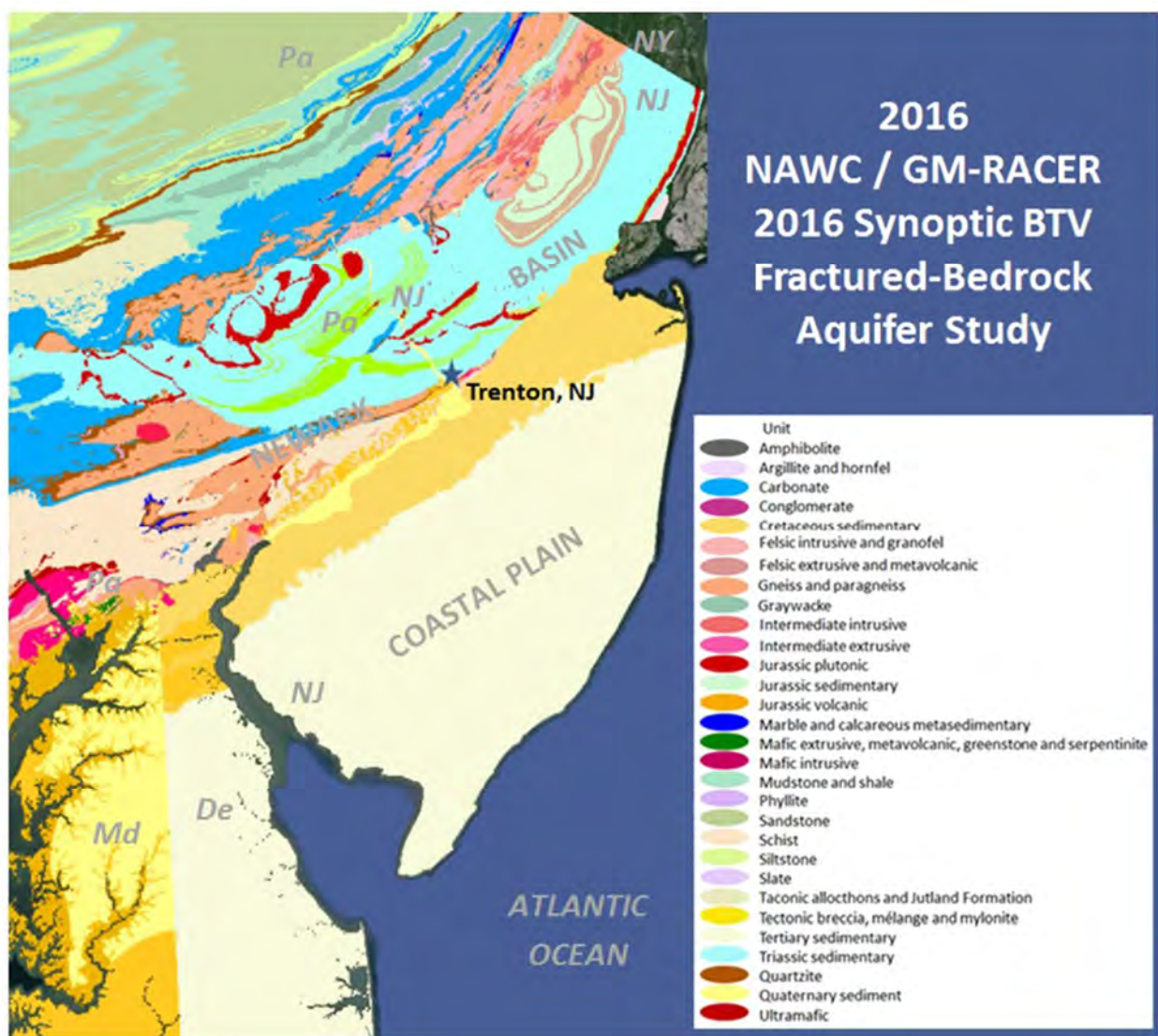


Figure 1: Regional geology map emphasizing the study location on the mid-central, southeastern border of the Newark Basin. Digital geology themes from the US Geological Survey were recompiled into a simplified regional theme for GANJ 32 (www.ganj.org/2015/Data.html).

SHALLOW SUBSURFACE GEOPHYSICAL APPLICATIONS IN ENVIRONMENTAL GEOLOGY
GANJ XXXIII Annual Conference and Field Trip

CAMP is the large-igneous province emplaced at the onset of supercontinent breakup and the birth of the Atlantic Ocean basin (Coffin and Eldhom, 1994). The contact between these two formations is defined as the first significant gray and black shale beds in the overall course- to fine-grained stratigraphic succession leading to predominately black shale in the middle of the Lockatong Formation. The formation

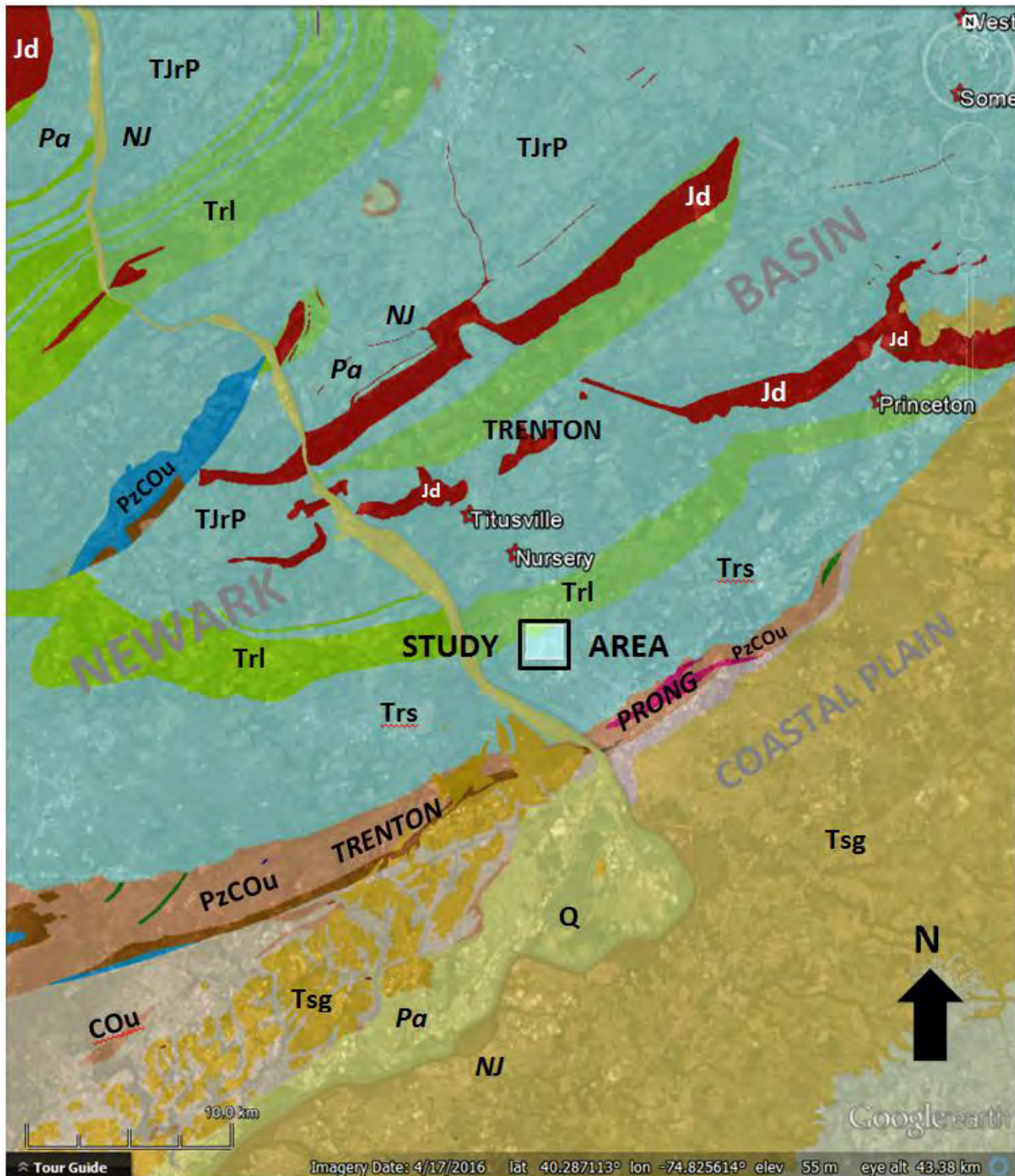


Figure 2: Geological map of the Trenton region in Google Earth showing locations of Newark Basin Coring Project cores discussed in the text (Olsen and others, 1997). Jd – Jurassic diabase, TJrP – Triassic Jurassic Passaic Formation, PzCOU – Paleozoic Cambrian-Ordovician undivided, Q Quaternary gravel, Tsg Tertiary sand and gravel, Trs – Stockton Formation, Trl – Lockatong Formation, CO- Cambrian-Ordovician undivided.

SHALLOW SUBSURFACE GEOPHYSICAL APPLICATIONS IN ENVIRONMENTAL GEOLOGY
GANJ XXXIII Annual Conference and Field Trip

contacts are mapped differently in the State geological maps of Pennsylvania (Berg and others, 1980) and New Jersey (Drake and others; Owens and others) and shown in a regional sense by a 1:250,000 scale compilation by Lyttle and Epstein (1980). In Pennsylvania, gray and black-dominated sections are mapped as Lockatong are interdigitated with red-dominated sections of both Stockton and Brunswick Formations. Olsen and others rectified these problems but they continue to persist in digital geological coverages available from the USGS for Pennsylvania. The section of focus here is detailed in Figure 7 with nearby NBCP core and geophysical logs helping to define the penetrated section covered by these

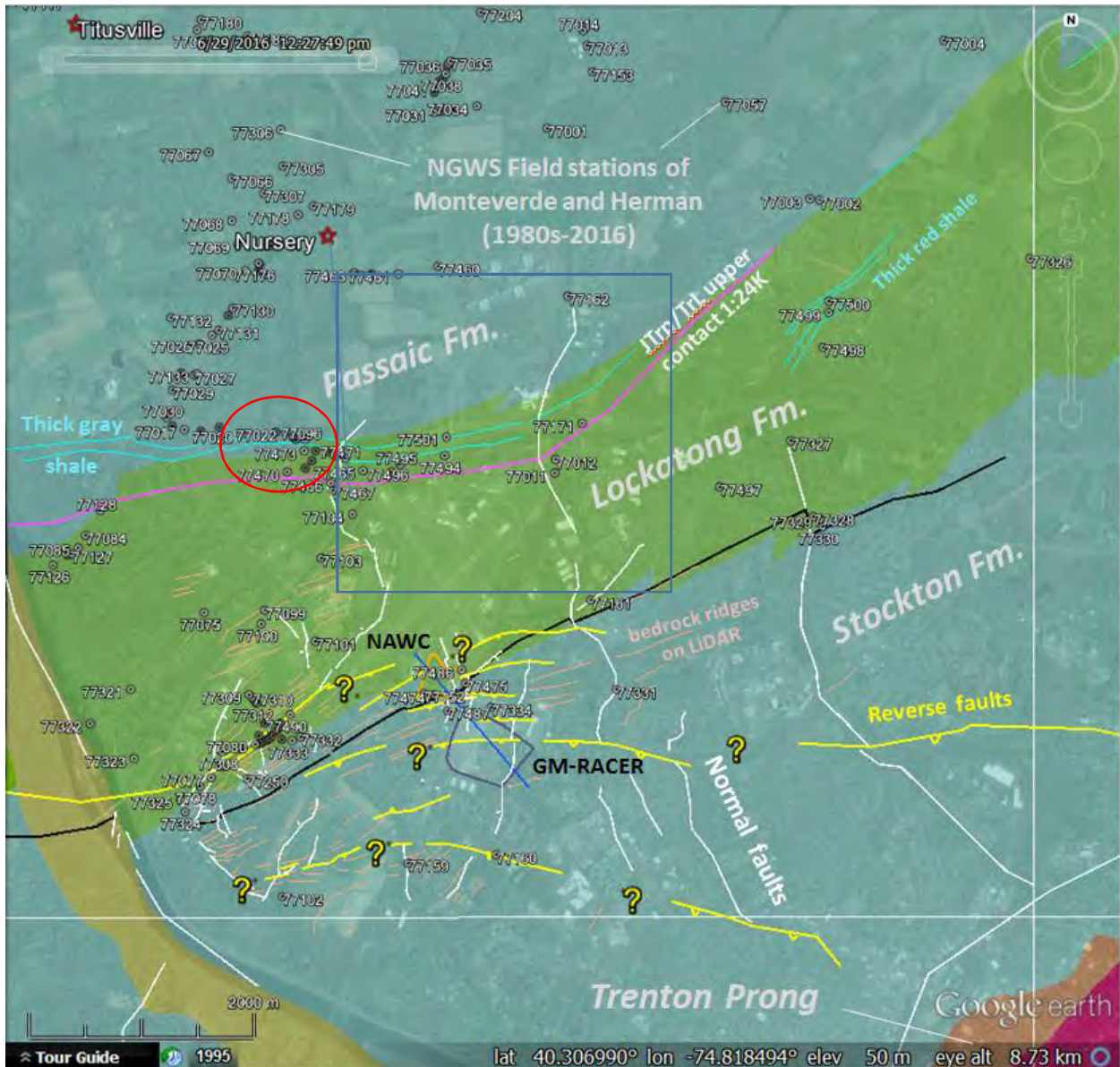


Figure 3: Geological map of the area around the NAWC/GM-RACER sites in Google Earth showing NJGWS field-station locations, bedrock ridges on LiDAR, and overlapping, inferred fault systems. The N-S trending faults are extensional faults with a major component of normal-slip and the E-W yellow faults are younger reverse faults. Red circle denotes the area of STOP 3 where structurally inverted Lockatong outcrops.

...In general, the Stockton Formation in the cores is lithologically very similar to the outcrops of the type section. The boundary between the upper Stockton and lower Lockatong formations is at the base of the lowest prominent black or gray shale sequence in the lower part of the Wilburtha Member. Comparison of the Princeton no. 1 core and the type section in outcrop suggests a correlation in which two different, but stratigraphically close, gray and black units mark the base of the Lockatong Formation, and thus the boundary between the two formations changes slightly laterally. The thickness of sedimentary cycles in the basal Lockatong Formation in its type area (as seen at Byram, New Jersey) is 177% of that in the

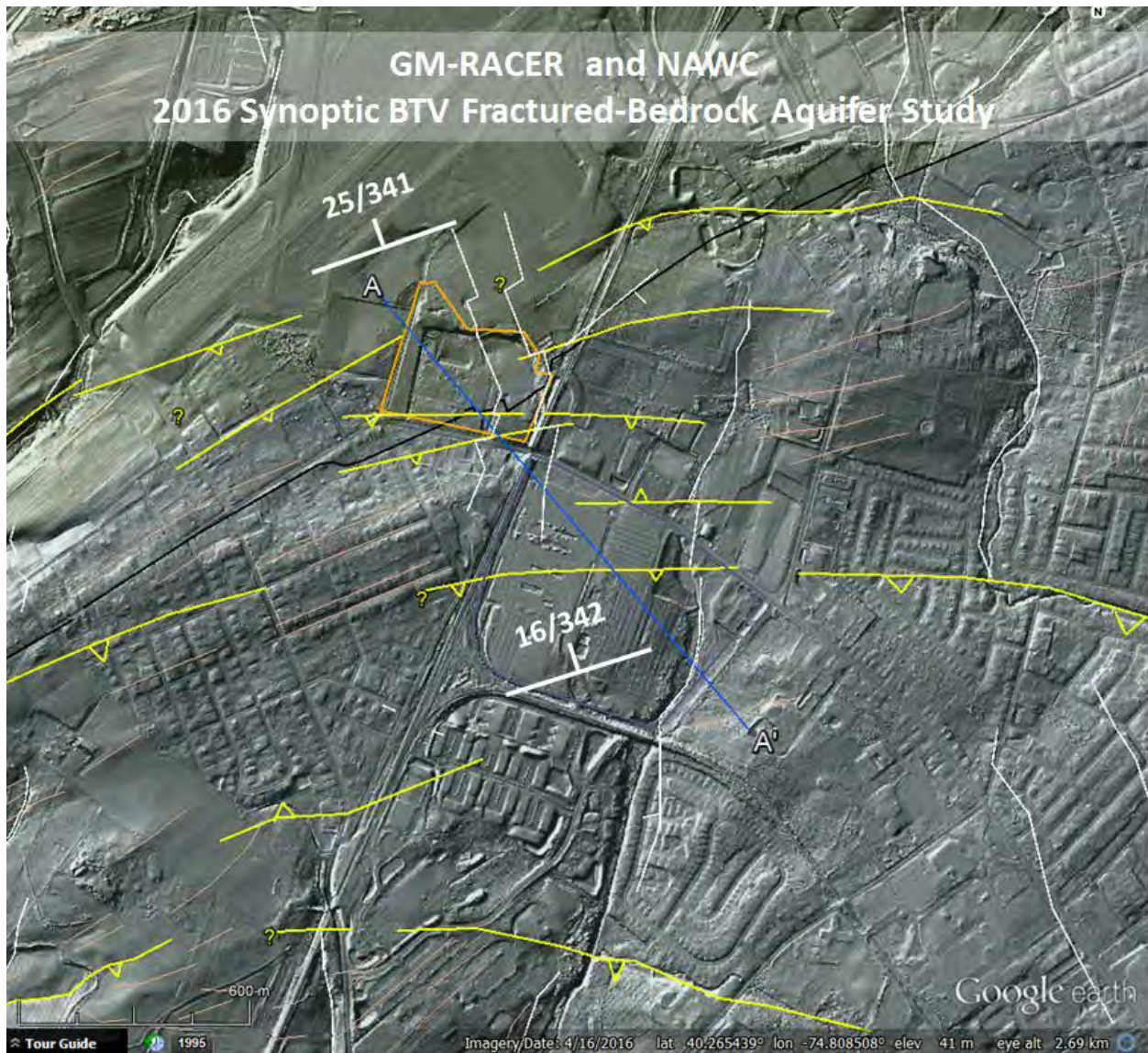


Figure 5: Tectonic elements of the area with respect to a gray, hill-shaded relief base from New Jersey LiDAR data. Note the correspondence of streams to interpreted, concealed normal faults and late-stage reverse faults (yellow) that are mostly queried because of uncertainty as to their continuity and density. The trace of cross-section traces A-A' is slightly skew with respect to average dip directions (~ 341 azimuths).

correlative portion of the Princeton no. 1 core. If the Stockton Formation in outcrop is similarly expanded relative to that in the Princeton no. 1 core, there would be a close match between the position of major sand and conglomerate-rich parts of the section. This proportional relationship between core and outcrop suggests that the members of the Stockton Formation identified by McLaughlin (1945) can be identified in the Princeton core. Overall, the Stockton Formation tends to fine upward, with the uppermost 102 m of Stockton Formation in the Princeton no. 1 core being dominated by red mudstone, as is true for the outcrop sections.

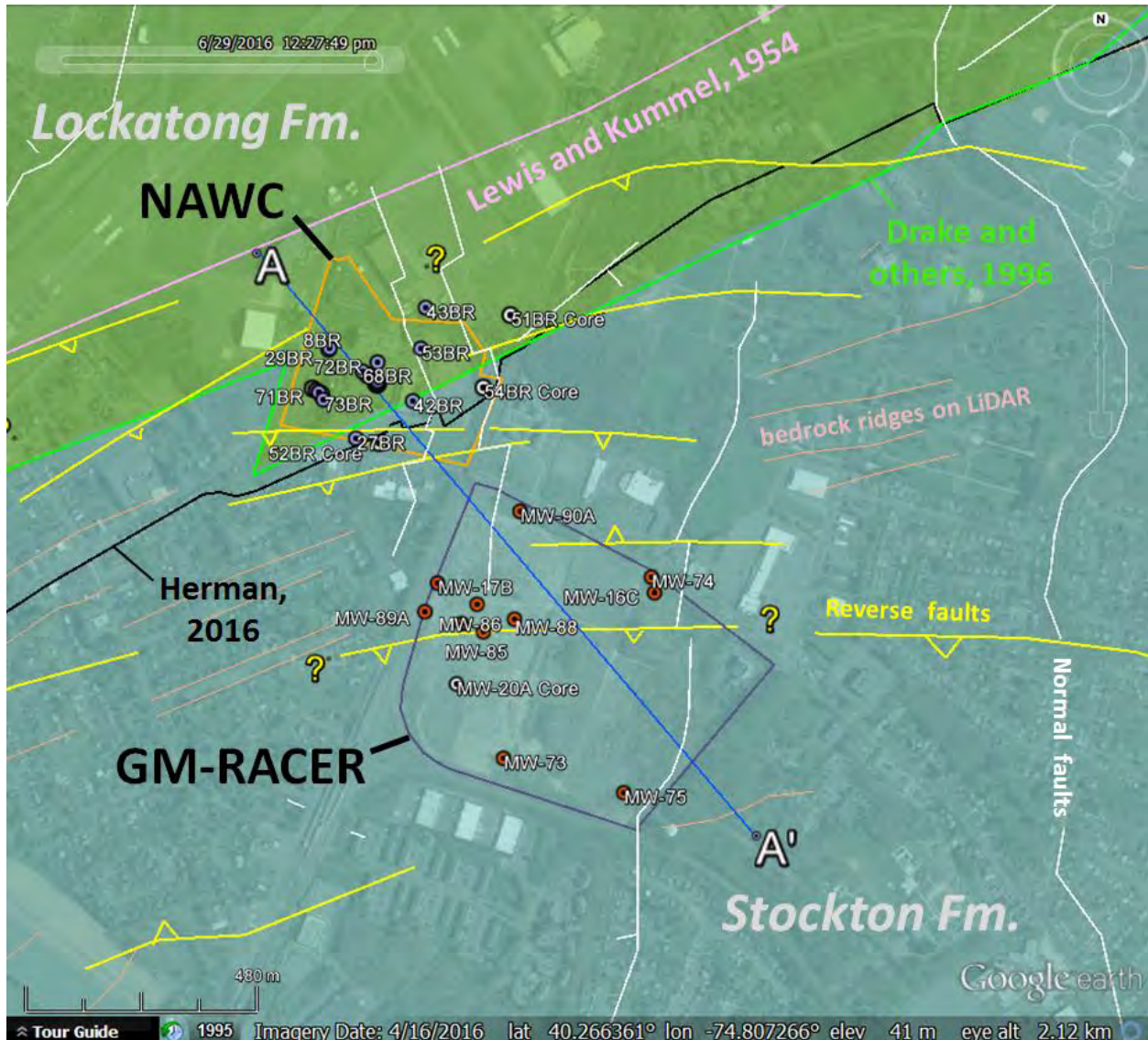


Figure 6: Bedrock geology map of the GM-RACER and NAWC sites showing the locations of wells with BTV records used in this project. Note the location of core MW-20A on the GM-RACER site.

SHALLOW SUBSURFACE GEOPHYSICAL APPLICATIONS IN ENVIRONMENTAL GEOLOGY
GANJ XXXIII Annual Conference and Field Trip

Table 1: List of locations, depths, BTV intervals and structural attributes of wells at each site. Tilt from BTV-telemetry data indicate that most boreholes vary by less than 2° from vertical. The red-accented records highlight aspects of the radial wellfield at NAWC. The average dip and dip direction (azimuth) is highlighted for each site.

Well	LON	LAT	GE DEM (m)	BTV diam (in)	Depth (m)	OBI Top (m)	OBI Bot (m)	OBI int (m)	Avg. Tilt (deg)	Bed	Dip	DipAzimuth	OBI comment
GM-RACER -270 m BTV including OBI Records													
1 MW-16C	-74.8053834	40.2650968	37.0	3.8	42.7	4.6	42.7	38.1	0.3	18/344	18	344	
2 MW-74	-74.8054573	40.2653924	38.0	3.8	41.5	5.2	41.5	36.3	0.7	17/344	17	344	
4 MW-86	-74.8097340	40.2648839	41.0	6.0	47.3	11.3	47.3	36.0	0.5	13/338	13	338	
3 MW-87	-74.8101113	40.2645228	41.0	6.0	47.3	12.5	47.3	34.8		17/342	17	342	
5 MW-88	-74.8088149	40.2646053	41.0	6.0	36.6	8.5	36.6	28.1		20/342	20	342	
6 MW-75	-74.8061350	40.2613490	35.0	3.8	34.1	6.4	34.1	27.7		19/350	19	350	
7 MW-85	-74.8095813	40.2643687	41.0	6.0	35.4	8.5	35.4	26.9		20/343	20	343	32' visibility
8 MW-90A	-74.8086797	40.2666205	41.0	3.8	32.3	12.5	32.3	19.8		13/339	13	339	
9 MW-17B	-74.8107013	40.2652822	41.0	3.8	30.8	12.2	30.8	18.6		10/340	10	340	
10 MW-89A	-74.8110100	40.2647480	41.0	3.8	19.5	12.5	27.7	15.2	0.7	8/321	8	321	21' visibility faulted?
11 MW-73	-74.8090890	40.2620030	35.0	3.8	11.6	7.0	11.6	4.6	0.8	17/360	17	360	
12 MW-20A CORE		40.2633950	41.0	3.8	242-270								200' fault Photos
Thin sections and radiometrics													
Avg. dip/dip azimuth 16 342													
NAWC -284 m BTV including OBI Records													
1 68BR	-74.8123950	40.2691550	45.7	4.0	52.1	3.7	52.1	48.4	-	26/350	26	350	Gray
2 70BR	-74.8135320	40.2688060	45.4	4.0	32.3	1.8	32.3	30.5	1.4	24/334	24	334	Gray
3 71BR	-74.8134400	40.2687790	45.1	4.0	34.8	6.1	34.8	28.7		21/351	21	351	Gray
4 73BR	-74.8133330	40.2686430	43.6	4.0	34.5	7.6	34.5	26.9		16/354	16	354	Gray
5 84BR	-74.8121500	40.2690360	45.7	4.0	35.7	16.8	35.7	18.9		19/334	19	334	Gray
6 89BR	-74.8122140	40.2690310	45.4	9.5	35.1	16.8	35.1	18.3		18/339	18	339	Gray
7 85BR	-74.8121220	40.2690060	45.7	4.0	35.1	17.1	35.1	18.0		10/347	10	347	Gray
8 87BR	-74.8121920	40.2689590	45.7	4.0	29.9	12.5	29.9	17.4		21/343	21	343	Gray
9 88BR	-74.8122280	40.2689890	45.4	4.0	32.0	14.9	32.0	17.1		19/355	19	355	Gray
10 83BR	-74.8121760	40.2689970	45.7	4.0	33.2	17.1	33.2	16.1		21/344	21	344	Gray
11 86BR	-74.8122140	40.2690300	45.4	4.0	27.4	13.1	27.4	14.3	1.5	10/347	10	347	Gray
12 8BR	-74.8131810	40.2695800	45.7	4.0	16.5	9.8	16.5	6.7		25/327	25	327	Red w kinematics
13 42BR	-74.8111970	40.2686170	45.4	4.0	42.1	36.3	42.1	5.8		52/298	52	298	Gray and reverse sheared
14 53BR	-74.8110060	40.2695720	45.1	4.0	36.0	29.0	36.0	7.0		45/327	45	327	Gray
15 43BR	-74.8108900	40.2703150	51.5	4.0	124.7	116.8	124.7	7.9		20/332	20	332	Gray
16 29BR	-74.8132110	40.2695530	45.7	4.0	30.5	25.9	30.5	4.6		47/351	47	351	Red
17 27BR	-74.8125550	40.2679390	45.1	4.0	24.4	20.1	24.4	4.3		46/357	31	357	Red
Avg. dip/dip azimuth 25 341													

Locketong Formation - Kummel (1897) named the Locketong Formation for the mostly gray and black massive and fissile mudstones that crop out in Locketong Creek in the western fault block. The base of the Locketong Formation is defined as the base of the lowest prominent black or gray shale unit, and its top is defined where red beds predominate over gray. The reference section for the type area is the New Jersey Route 29 exposures along the Delaware River. In his description of the type area of the Locketong Formation, McLaughlin (1945) divided the upper part of the formation into a series of gray and black informal units (B, A2, A1) and gave informal names to the distinctive intervening red mudstone sequences. These red gray couplets were subsequently given the informal member names of Walls Island, Tumble Falls, and Smith Corner, and the underlying four units of equal rank were named in descending order the Prahl's Island, Tohickon, Skunk Hollow, and Byram members (Olsen, 1986). Below we formalize these members and provide type sections for each. The remaining lower part of the Locketong Formation is very poorly exposed in the type area, and 5 members (Ewing Creek, Nursery, Princeton, Scudders Falls, and Wilburtha) are proposed, based on the NBCP cores. In total there are 12 members in the Locketong Formation; the proposed new members of the Locketong Formation, the origin of their names, their earlier informal synonyms, and locality data for the type sections are summarized in Table 2 and in data in the GSA Data Repository.²

² Geological Society of America Data Repository item 9601, P.O. Box 9140, Boulder, CO 80301.

Ms Excel Compilation of NBCCP data including unpublished magnetostratigraphy
 (Kent and Olsen written communication 2016-02-17)

Only section having gamma repeatedly peaking beyond 1000 cps is the Scudder's Fall member

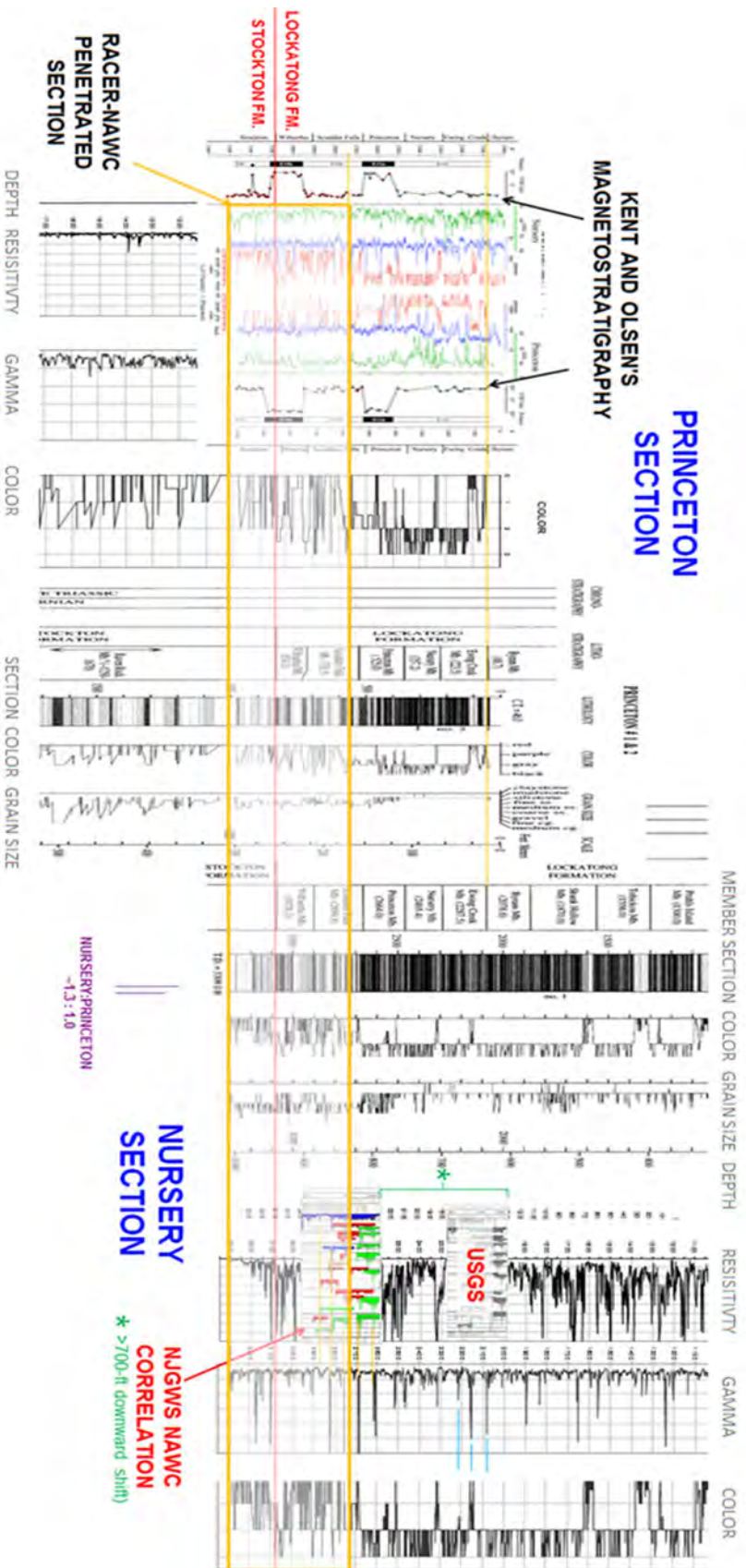


Figure 7: Stratigraphic details of the Late Triassic stratigraphic succession in the study area based on the NBCCP Nursery and Princeton cores that overlap the section of interest. Note that the NJGWS correlation of the penetrated section is shifted down three members relative to the former correlation by the USGS. Also note that Kent and Olsen's magnetostratigraphy is positioned in the figure relative to the Princeton core (left) and that the only section having gamma log readings repeatedly peaking over 1000 counts per second (cps) is the Scudder's Fall member near the base of the Lockatong Formation. Correlative sections of the two NBCCP cores also show about 30% thickening of the section in going from the Princeton to the Nursery core.

Princeton and Nursery Core Overlap Zone - The transition from Stockton to Lockatong Formation is represented in the Princeton and Nursery cores by the Wilburtha, Scudders, Falls, and Princeton Members, and the lateral changes seen between these two cores are the largest seen in any of the NBCP core overlap zones. There is a general irregularity of the pattern of the cyclicity, so regular in the overlying section, associated with high sandstone content. However, there is still an overall correspondence in lithostratigraphy. The correlation is tested by the overall correspondence between the relative position of the E10n polarity zone, which in both cores encompasses the lowest black shales in the Lockatong Formation and corresponds to the Lockatong-Stockton formational boundary). The basal black shale of the Lockatong Formation in the Nursery No. 1 core are replaced by sandstone of the Stockton Formation in the Princeton no. 1 core. The change between these cores is best seen in the basal Princeton Member, which has several black shales in the E11n polarity zone in the Nursery no. 1 core but only one black shale in the corresponding portion of the Princeton no. 1 core. Lithological correlation between the cores markedly improves from the middle of the Princeton Member upward, and the upper boundary of polarity zone E11n occurs in both cores in excellent agreement with a matching sequence of Van Houten cycles. The details of lithology and cyclicity in the overlying Nursery and Ewing Creek members match very well between core holes.

Outcrop and near-surface data

The first New Jersey geological map (Lewis and Kummel, 1912) placed the Stockton-Lockatong contact just north of NAWC (Figures 4 and 6). The recently revised NJ geological map (Owens and others, (1998) locates the contact a little more southeastward as does the most recent, unpublished mapping by Don Monteverde for STATEMAP compilation of the Pennington, NJ 7-1/2' quadrangle, and from NJGWS research on the distribution and nature of fractured-bedrock aquifers (Herman, 1997; Herman and others, 2010). The 1998 state map also maps this contact as offset in multiple places by a system of poorly constrained, steeply dipping, normal faults that branch and splay northward from the Trenton area. These faults are left off maps shown here but their residual traces are seen where the formation contact is sharply offset along a ~N10E trend (Figures 4 and 6). Local geological details were also provided by Lacombe (2000), Lacombe and Burton (2010), and Goode and others (2014) that include a significant reverse fault along the mapped contact between the Stockton and Lockatong that contracts the section and locally omits some of the lowest members of the Lockatong section near land surface. This work shows the fault striking SW-NE and cutting the SE corner of the NAWC site (Figures 3 to 6). This USGS work also produced many unpublished photographic glimpses of the local tectonic style where small reverse faults were uncovered in excavation and rock core (Figures 8 to 10).

One particularly interesting core retrieved by Haley-Aldrich at GM-RACER has a section of massive fault breccia (Figure 9) that was generously shipped to the NJGWS for slabbing and thin sectioning (Figures 9 and 10). This autoclastic breccia in the Stockton Formation is cemented with calcite and shows significant tectonic compaction from intense mechanical twinning of the spar cement (Figure 9A). This breccia was

SHALLOW SUBSURFACE GEOPHYSICAL APPLICATIONS IN ENVIRONMENTAL GEOLOGY
 GANJ XXXIII Annual Conference and Field Trip

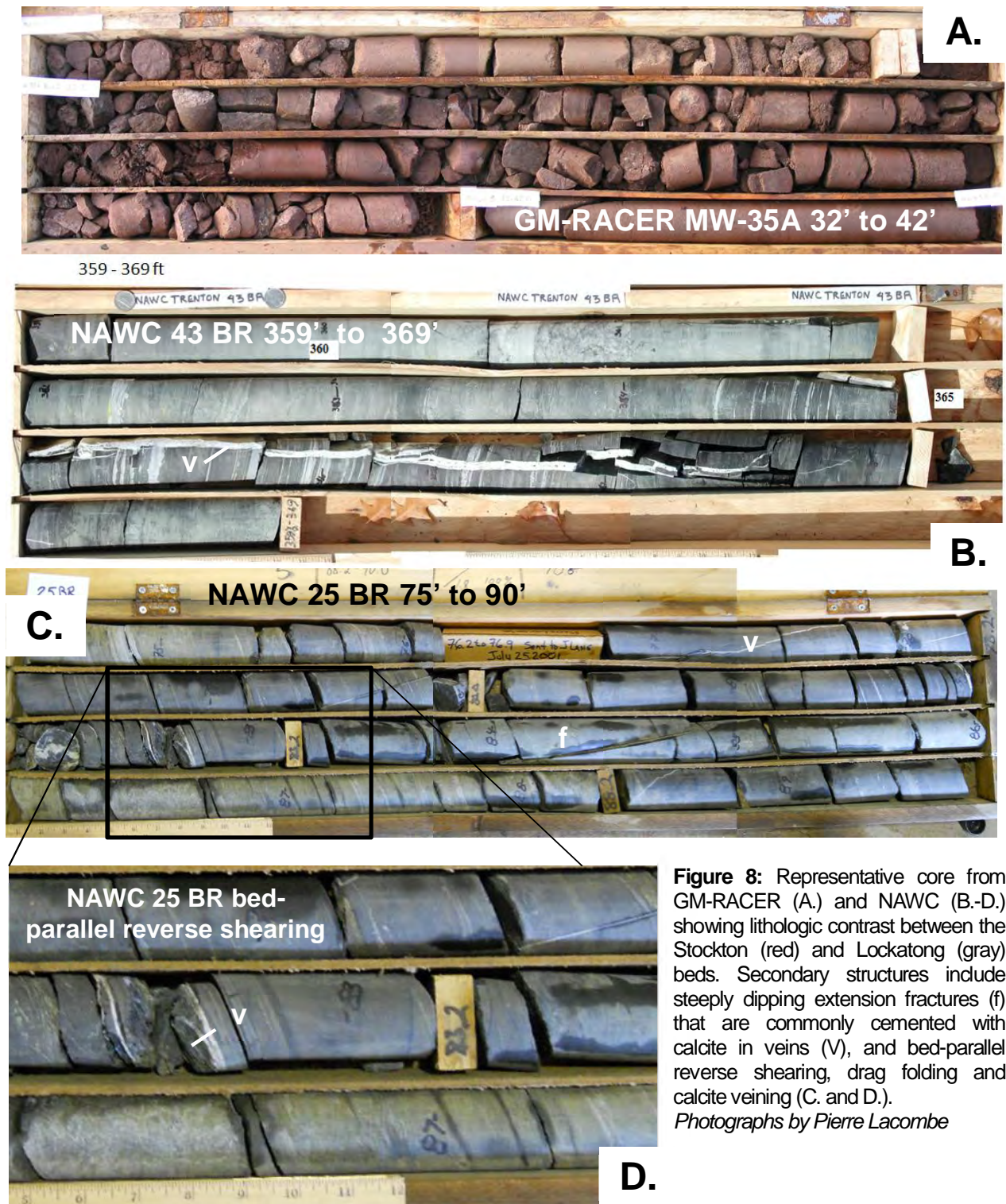


Figure 8: Representative core from GM-RACER (A.) and NAWC (B.-D.) showing lithologic contrast between the Stockton (red) and Lockatong (gray) beds. Secondary structures include steeply dipping extension fractures (f) that are commonly cemented with calcite in veins (V), and bed-parallel reverse shearing, drag folding and calcite veining (C. and D.).
 Photographs by Pierre Lacombe

probably consolidated after extensional faulting of tensile origin and then overprinted by a compressive tectonic event that horizontally contracted but thickened the section with reverse shear faulting as portrayed here. Lomando and Engelder (1984) found similar compaction in rocks of the northern part of the Newark basin that aligns with other calcite-strain gauge data for bedrock of the Paleozoic foreland of Pennsylvania

and New York (Engelder, 1979; Herman, 2015). We will visit overturned panels of Lockatong strata dipping ~80° SE that are mapped nearby in Villa Victoria Brook (Figure 3) at STOP 3 of this year's field excursion. These steeply dipping beds also likely arose from this compressional event and are the only Early Mesozoic structurally inverted strata found so far in the New Jersey part of the basin (Figure 1). The extensional and compressional structures seen in core and excavations are also seen in the BTV records.

Geological analysis of borehole televiewer (BTV), caliper and gamma logs

This project had access to a wide variety of geophysical logs collected at both sites, but mostly uses BTV records with natural-gamma-ray and caliper (borehole diameter) logs (Figures 11 and 12). Gamma logging has proven useful for correlating strata between wells in the basin using dark gray to black, organic-rich shale marker beds having noticeably elevated natural gamma ray emissions (Figure 7). Caliper logs are also critical for structural analysis and are used to derive accurate orientation measurements of geological planes in BTV records that are dependent on borehole diameter (Figure 13). BTV records include both optical (OBI – optical borehole image) and acoustic (ATV) types (Figures 10-, with the OBI being digital photographic image and the ATV including records of both acoustic-signal amplitude (AMP) and travel time (TT) responses (Figure 11) . The BTV records shown here are shown as flattened, 'unrolled' images of the borehole walls that intersect primary (stratigraphic bedding or layering) and secondary fractures and fault planes penetrated by the borehole (Figure 12). The records are interpreted in this flattened layout using WellCAD structural-analysis software module and the set of geologic and hydraulic parameters outlined in Figure 12. Sedimentological bedding and any secondary planar features such as structural discontinuities are traced and thereby measured using the amplitude and trough of each sinusoidal traced feature to determine the dip and dip direction (dip azimuth) of each plane. The mathematical details of this process are beyond the scope of this paper, but basically, gently dipping planes have low-amplitude traces that increase with increasing dip (Figure 12A).

In order to estimate the total penetrated section at each site (Figures 14 to 16) a set of logs were charted and analyzed for each well (examples given in Figures 11 and 12) and then visually compared to one another in geospatial arrangement after projection into a profile trace (Figure 15B). This process was used to assess subsurface stratigraphic continuity and the geological nature of the various fractures, shear planes, and fault zones that otherwise disrupt the section. As seen in Figures 11 through 16, the red and white beds of the Stockton Formation contrast vividly with the gray-and-black beds of the Lockatong although the boundary between these Formations is gradational and shows lateral sedimentological variation in the NBCP cores (Figure 7). The GM-RACER section covered by BTV records is estimated to span a thickness of about 60 meters whereas the NAWC section has about 130 meters coverage from gamma-log coverage and about 100 meters from BTV (Figure 17).

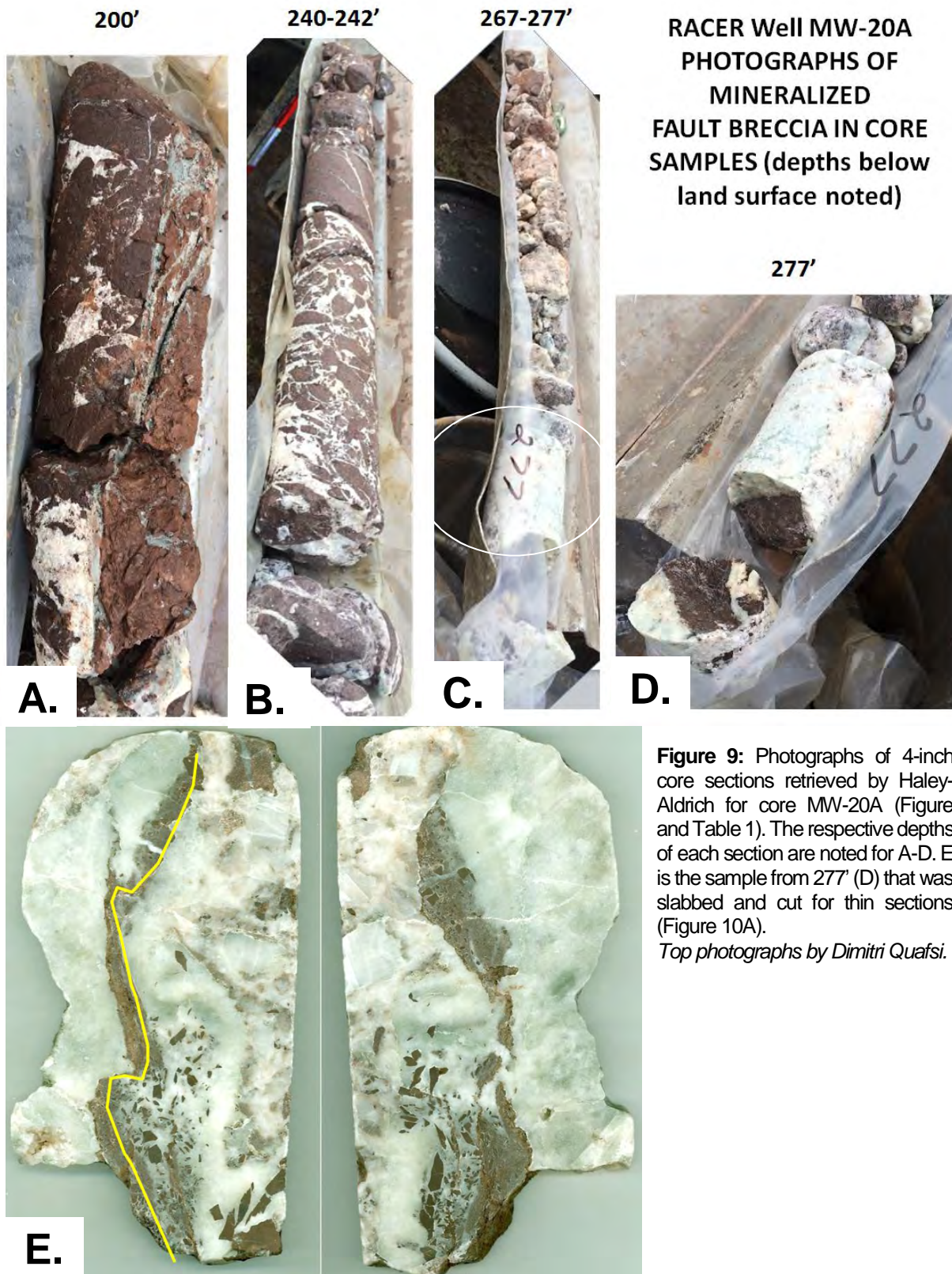
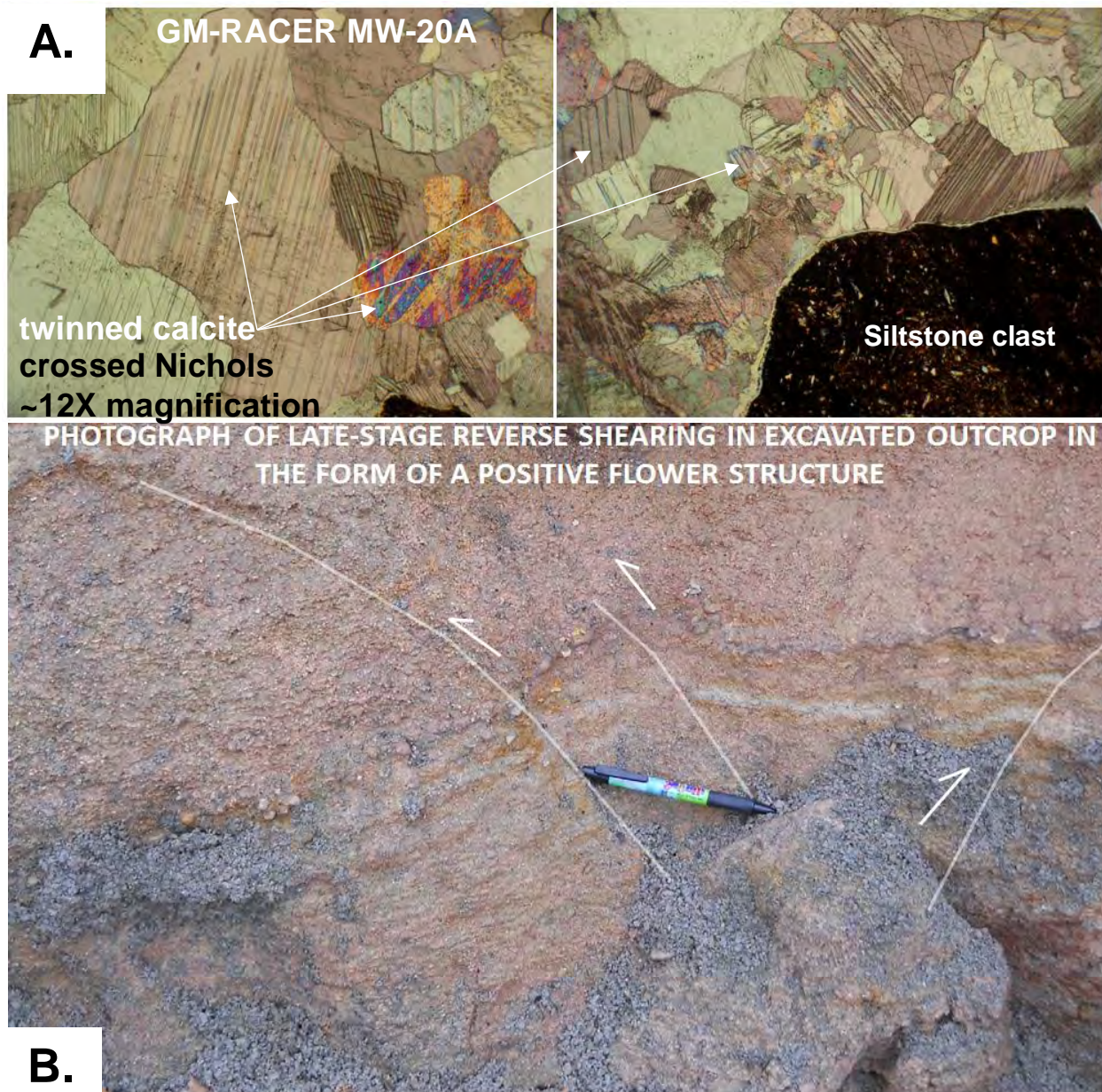


Figure 9: Photographs of 4-inch core sections retrieved by Haley-Aldrich for core MW-20A (Figure and Table 1). The respective depths of each section are noted for A-D. E is the sample from 277' (D) that was slabbed and cut for thin sections (Figure 10A).
Top photographs by Dimitri Quafsi.




Photograph from Gold's Run 2011-11-28 by Pierre Lacombe, US Geological Survey

Figure 10: Photographs of tectonic faults in GM-RACER core (**A**) and a nearby excavation. **A.** Photomicrographs of thin sections from the slabbed core of autoclastic breccia (Figure 9E) that is calcite cemented and later tectonically compacted as seen in the extreme calcite twinning. Photo **B.** is that rare excavation that belies the structural style in the area by revealing a positive flower structure with reverse dip slip offsetting layering in Stockton Formation bedrock residuum.

SHALLOW SUBSURFACE GEOPHYSICAL APPLICATIONS IN ENVIRONMENTAL GEOLOGY

GANJ XXXIII Annual Conference and Field Trip

	State of New Jersey Department of Environmental Protection New Jersey Geological & Water Survey Bureau of Water Resources & Geoscience Geological Research and Support Section	
PROJECT: GM-RACER WELL ID: MW-86 COORDINATES: STATE: COUNTY: TOWNSHIP: USGS 7-1/2' QUADRANGLE: OPEN-HOLE DIAMETER: ~ 5 in. STATIC WATER DEPTH:	LOG TITLE: 2016-03 GCH GM-RACER MWMW-86 BTV.WCL DATE PROCESSED: March 3 and 22, 2016 PROCESSED BY: G.C. Herman TOP LOGGED INTERVAL: 37.3 BOTTOM LOGGED INTERVAL: 154.8 NOTES: Rotated all BTV images 12.5 degree CC to ~True North.	
HAGER-RICHTER GEOSCIENCE, INC. 840 Main Street Fords, NJ 08803 Phone: 732-661-0555 Fax: 732-661-0122	MW-86 - BOREHOLE GEOPHYSICAL LOGS DATE LOGGED: February 11, 2014	
CLIENT: Haley & Aldrich, Inc. PROJECT: GM-RACER LOCATION: 1445 Parkway Avenue, Ewing, New Jersey LOGGING GEOPHYSICIST(S): Nick DeCristofaro PROJECT REP ON-SITE: Jeremy Miller & Kevin Corcoran	HAGER-RICHTER FILE: 14RG04 LOG DATUM: Ground Surface ORIENTATION REFERENCE: Magnetic North WATER LEVEL DEPTH: 15.0 Feet LOGS PROCESSED BY: Robert Garfield	
<div style="display: flex; justify-content: space-between;"> <div style="width: 30%;"> <p>Depth</p> <p>1in:2ft</p> <p>0' 90° 180° 270° 0'</p> <p>Acoustic Caliper (Inches)</p> <p>4 8 170</p> <p>Natural Gamma Ray (cps)</p> <p>0 150</p> </div> <div style="width: 30%;"> <p>Fluid Temperature (Deg C)</p> <p>10 15</p> <p>Fluid Conductivity (uS/cm)</p> <p>290 0</p> <p>ATV Amplitude TN</p> <p>0' 90° 180° 270° 0'</p> <p>5 1000</p> <p>Single Point Resistance (Ohms)</p> <p>100 1000</p> <p>NJGWS Structures</p> <p>0' 90° 180° 270° 0'</p> </div> <div style="width: 30%;"> <p>ATV Travel Time TN</p> <p>0' 90° 180° 270° 0'</p> <p>800 0.1us 1250</p> <p>Heat Pulse Flow Meter (gpm)</p> <p>-1.2</p> </div> </div> <p style="text-align: center; font-weight: bold; font-size: 1.2em;">N E S W</p>		

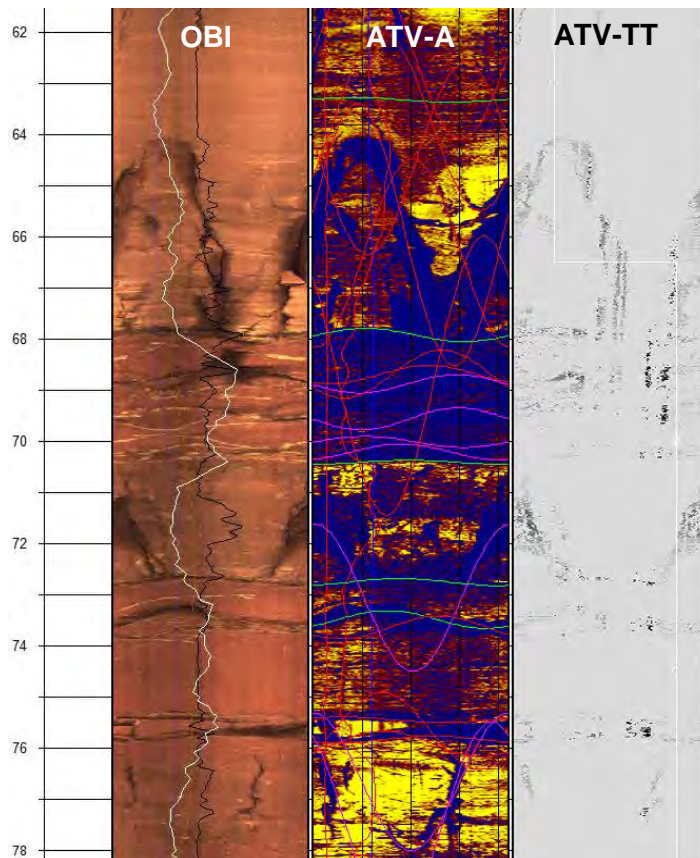
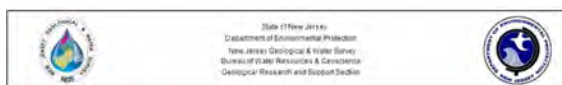


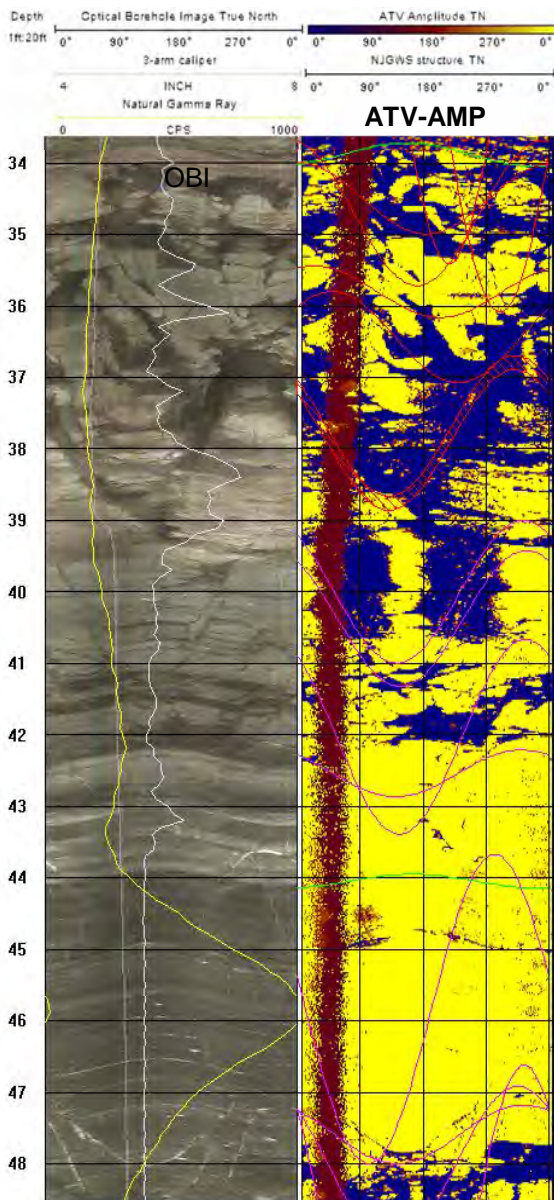
Figure 11: Example BTV logs for GM-RACER well MW-86 including the NJGWS structural interpretation overlain on the ATV-Amplitude log (middle). The OBI log is overlain with acoustic caliper (borehole width) as black-line trace and a natural gamma ray log (white line trace). Interpreted structures include bedding (green line trace and Type 1 of Figure 10), fractures (red line traces and Type 6), and veins (or mineralized fractures – purple line traces and Type 7).

SHALLOW SUBSURFACE GEOPHYSICAL APPLICATIONS IN ENVIRONMENTAL GEOLOGY

GANJ XXXIII Annual Conference and Field Trip



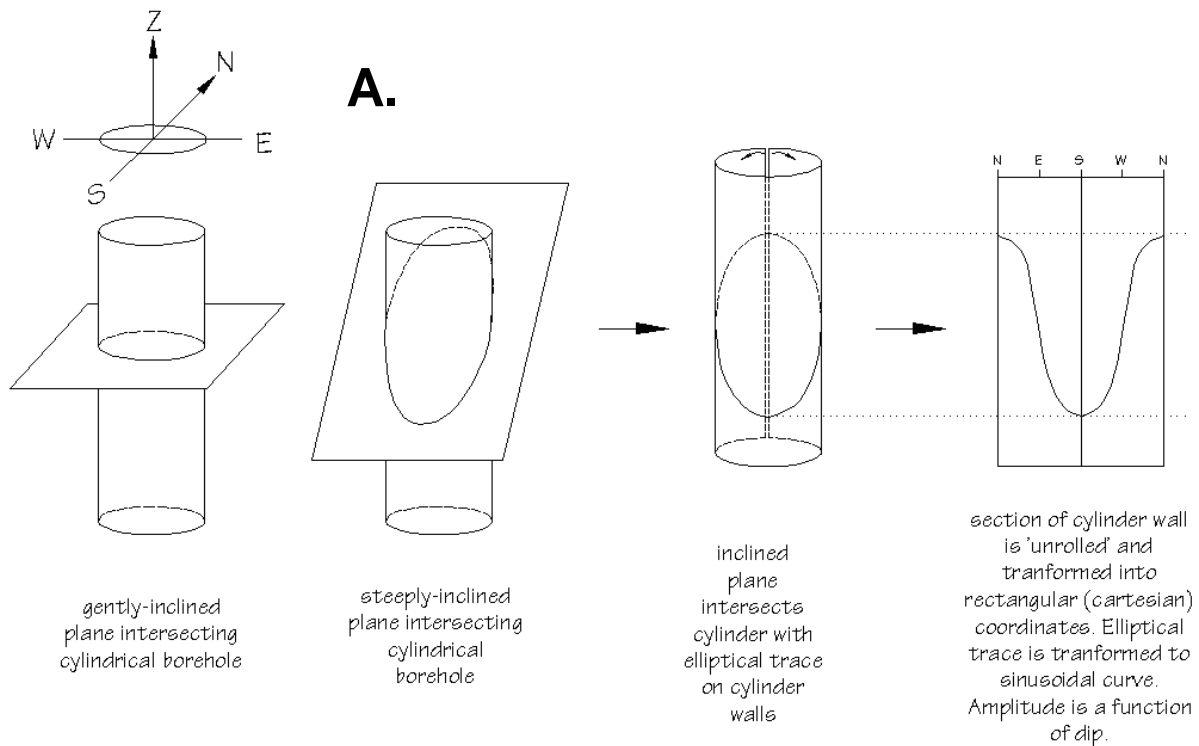
Company	USGS	Site ID		Station name	
Other ID	BR-68	Date of log		Start time of log	
County/State	Mercer/N.J.	Office/logging unit	TROY		
Logging operator	BSC	Observer	JHW		
Description of log-measuring point(LMP)	LS				
Height of LMP above/below LSD	0.0	Altitude of LMP			
Log orientation	MN	Mag declination		Logging direction	
Logging speed		Depth error after logging			
Logging probe manufacturer	MOUNT SOPRIS/CENTURY				



The beds at NAWC dip at a slightly steeper angle (~ 25°) than those at GM-RACER (~16°, Table 1) so even though the site spans are similar, NAWC has more stratigraphic coverage. The stratigraphic details at NAWC match the NBCP records closely when correlated with the upper part of the Wilburtha and lower part of the Scudder's Fall members of the Lockatong Formation (Figure 7). In particular, the multiple gamma-log responses exceeding 1000 counts per second (cps) for this interval are not only among the highest responses seen in the Lockatong Formation, but the entire > 6km-thick section of Early Mesozoic strata in the NJ part of the basin (Olsen and others, 1997; Herman, 2010).

A detailed structural analysis was completed for each well record using both OBI and ATV imagery (Figures 11 and 12). Feature planes were categorized using the geological criteria listed in Figure 13B and Table 2. Upon completion, feature orientations and annotations were exported from WellCAD into ASCII text files that were used for data sorting and structural analyses. Bed, fracture, shear plane, and fault orientations were analyzed first for individual wells (Figures 17 and 18) and then grouped for each site to compare structures in contrasting lithologies (Figures 19 and 20). Circular histogram and stereonet structural analyses used GEOrient ver. 9.5 software. Care was taken to

Figure 12: Interpreted section of NAWC well BR-68. The NAWC records acquired from the USGS include an optical borehole image (left) that is overlain with line traces of the borehole caliper (borehole thickness - white line) and natural gamma ray (yellow) logs. This OBI record shows an upward succession of dark- to light-gray sequence capped by a pink layer before returning to gray. This section also includes the gray bed with a gamma-response exceeding 1000 cps that facilitates stratigraphic correlation (Figures 7 and 15A). The middle gamma-log trace in the Scudder's Falls Member is the most pronounced of three high-gamma kicks in this section (Figure 7).



TYPE → KIND → SENSE → PERMEABLE → ALTERED

0 - Broken Zone / Undifferentiated

1 - Bedding

2 - Metamorphic layering

3 - Metamorphic foliation

4 - Igneous layering

5 - Igneous foliation

6 - Fracture

7 - Vein

8 - Cleavage

10 - Shear plane

9 - Fault zone

1 - Fracture

2 - Interval

3 - Shear

4 - Extension

5 - Sealed

6 - Open

7 - Zone

1 - Reverse

2 - Normal

3 - Oblique

4 - Left lateral

5 - Right lateral

6 - Crosses

7 - Cuts

0 -

1 - Permeable

1 - Staining

2 - Alteration

3 - Mineralized

B.

Note: TYPE is the primary criteria. Fracture is repeated in TYPE and KIND categories so that fracturing subparallel to bedding ($\pm 5^\circ$ strike and dip) can be noted (bed, fracture) and treated separately from non-bed-parallel fractures. All secondary criteria are optional.

Figure 13: A. Schematic diagram illustrating how cylindrical BTV records are processed by 'unwrapping', flattening, and transforming borehole data. The trough of the trace (or the bottom of the 'V') gives the structure dip azimuth. Higher dips correlate with sharper Vs. **B.** The systematic ranking criteria used at the NJGWS for interpreting BTV records (ca. 2000-2016).

Table 2: Geological variables used to catalogue measured structural features for this study.

- 1 - bed or layer
- 2 - fracture (un-cemented)
- 3 - vein (cemented)
- 4 - shear plane
- 5 - fault zone

Please note: Structural planes coded as 1 - 5 can have secondary variables denoting additional mineralization, alteration, staining, and permeability. Shear planes and faults can also include normal or reverse secondary notation. Beds were measured along sedimentological traces in OBI records and can include a secondary fracture variable used to spatially discriminate sections having little to abundant bed-parallel fracturing.

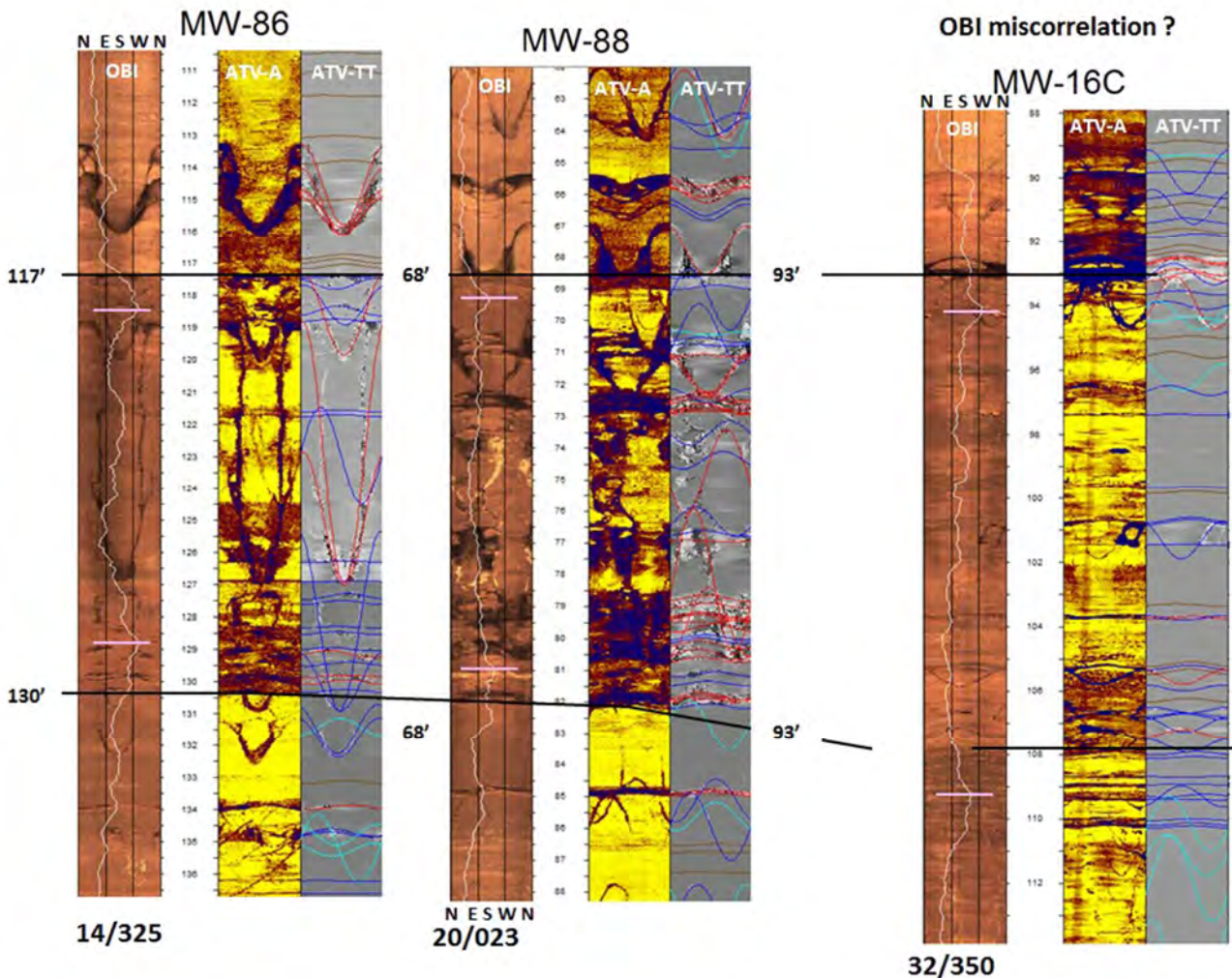


Figure 14: Example BTV sections for three wells at GM-RACER having both optical (OBI) and acoustic (ATV- Yellow Amplitude and Gray Travel Time). White gamma-log traces are overlain on the OBI records and Hager Richter's structural interpretation are overlain on ATV Travel Time (TT) logs. The left two logs show a definite stratigraphic correlation whereas the other is similar but not the same.

PROFILE SUMMARY OF OPTICAL BTV SECTIONS SHOWING HETEROGENEITY OF SANDSTONE AND SILTSTONE BEDS IN THE RAVEN ROCK MEMBER OF THE STOCKTON FORMATION

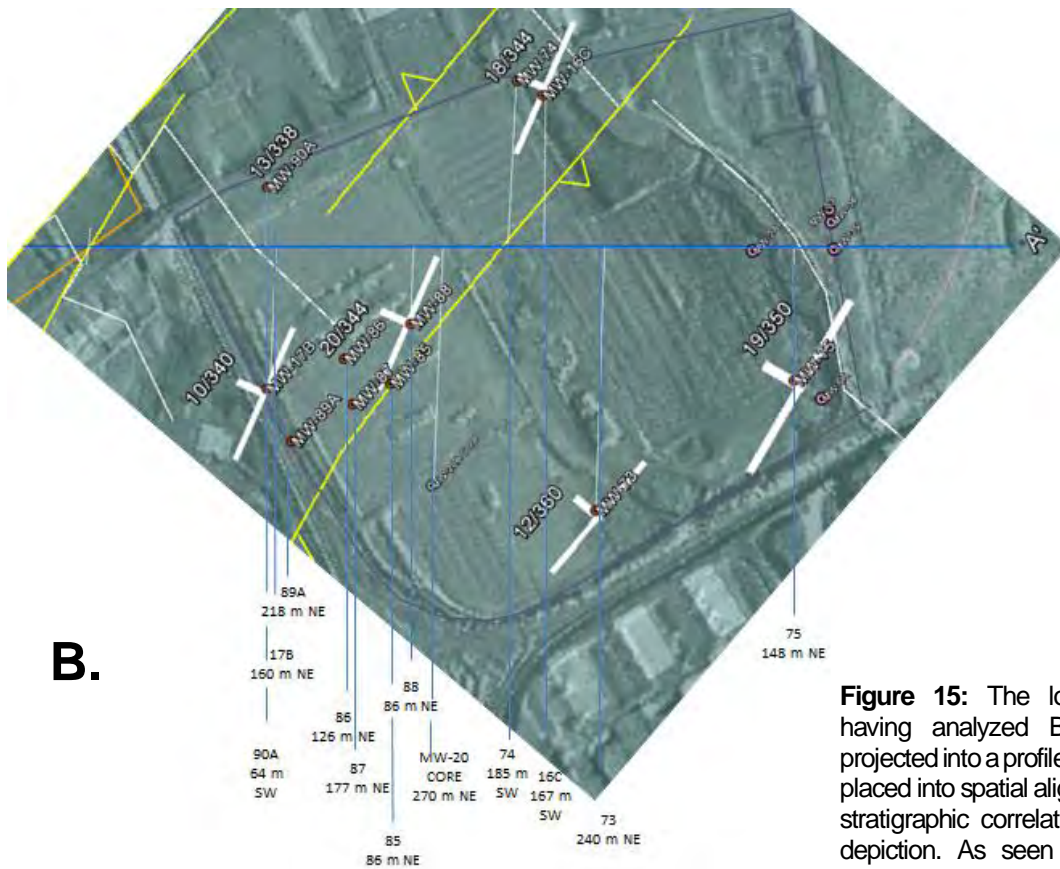
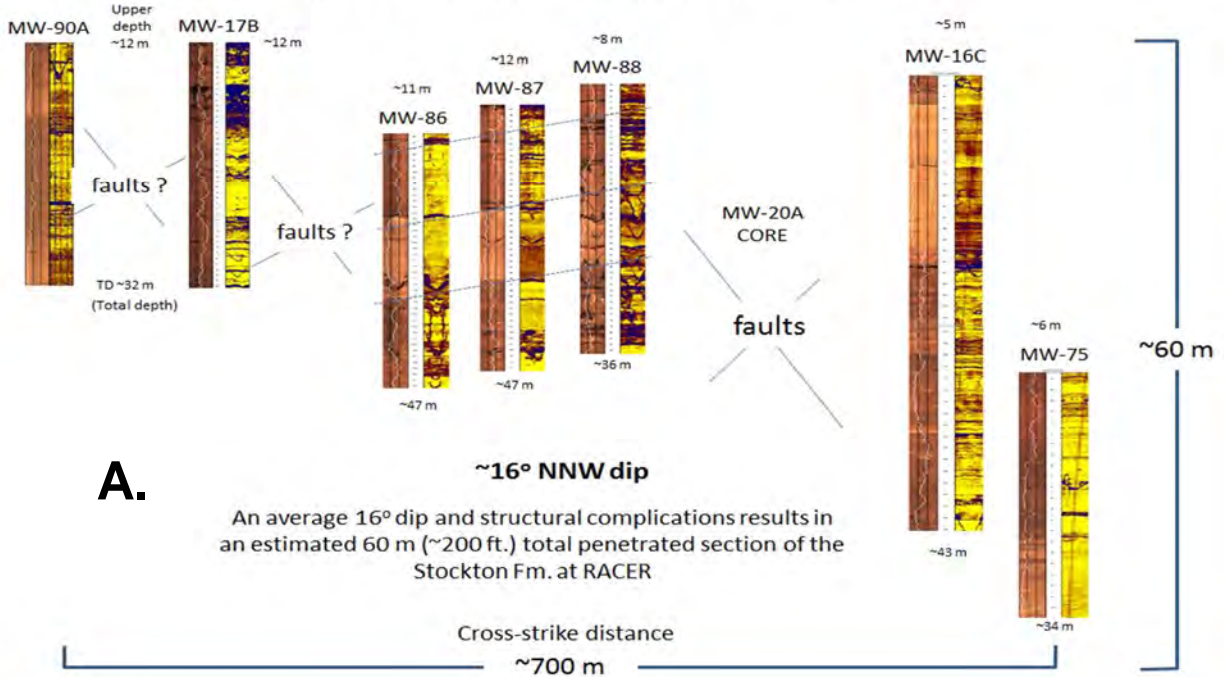


Figure 15: The locations of wells having analyzed BTV records are projected into a profile trace and thereby placed into spatial alignment to facilitate stratigraphic correlation and structural depiction. As seen in A., there are uniformly dipping panels that are structurally offset along fault zones.

differentiate mineralized fractures (veins) from unhealed ones. Bed orientations are based on traces of sedimentological features rather than bed-parallel fractures that were noted separately to spatially account for sections having little or abundant bed-parallel fracturing, presumably stemming from erosional unroofing or glacial loading and unloading processes. For this project, the main classes of feature that were noted and cataloged as part of the NJGWS geophysical log library are specified in Table 2.

The NJGWS method of BTV analysis differs slightly from most commercial contractors that focus on fractures that are potentially permeable in order to cover potential pathways constituting the hydrogeological framework. Some cemented fractures are not seen in ATV records because their acoustic properties vary little from the host rock. ATV records therefore are useful for imaging structures through turbid water that can obscure optical records, but they cannot be solely relied upon to provide a thorough structural and tectonic analysis. The best approach is to use both OBI and ATV records to interpret structural features. More details about NJGWS methods of interpreting BTV records are provided in this year's teacher's workshop (Chapter 1).

Shear planes and fault zones are mapped based on visual indicators of structural discontinuity and offset of strain markers like bed forms and early fractures cut and offset by later ones (figure 21). Observed shear in BTV records was modeled using Trimble Navigation, Inc.'s SketchUp 2015 computer-aided drafting software. Borehole models were manually constructed using intersecting planes of known orientations and shear slip, manually offsetting cut structures, and then unrolling them to see how they look in the 'flattened' perspective that BTV-processing software relies upon. To date, models have only been constructed of small dip-slip shears as visual references to help resolve the nature of apparent offsets observed in BTV records (Figures 21 and 22). It is usually time and cost prohibitive to resolve kinematic solutions to a higher degree when using BTV records for groundwater evaluations, but the methods exist for subsurface mineral exploration at a price (for example see <http://vektore.com/>).

Cross-section analysis including structural profiling of fractures using stereonet statistics and apparent dips

The profile depiction of the hydrogeological framework (Figures 24 and 25) was built using Google Earth (GE) and Microsoft (MS) PowerPoint software. GE was used to extract a screen-captured image of the topographic profile that was pasted into PowerPoint for tracing as a freeform polyline (Figure 23). After many years of representing digital geological form in profile, I have come to rely on MS PowerPoint software for communicating this type of information as it provides a multipurpose, widely used, and multifunctional platform for graphics production that includes options for specifying object rotation angles and line length by accessing object-property dialog boxes. For example, the profile boundaries are augmented with depth and length graticules of specific length. MS PowerPoint therefore provides the necessary functions to easily represent geological structures to be depicted in profile at their apparent dip angles. This is done by calculating apparent-dips for each structure and simply rotating lines into position at known locations using built-in software functions. Examples of this process are demonstrated in Chapter 1.

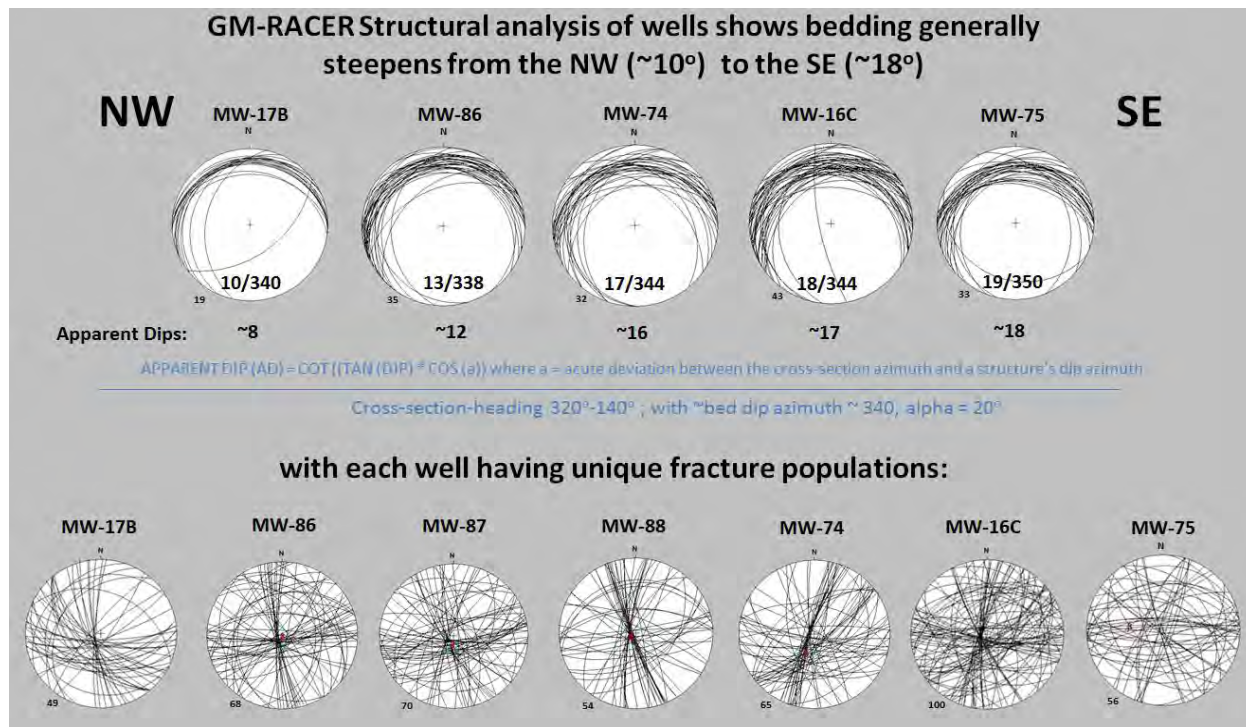


Figure 17: Stereonet structural analysis of the GM-RACER wells showing bed dip steepens across the site from NW to SE. Note that the apparent dips of bedding used in the cross section are close to true dips and each well has a unique fracture population (bottom).

BTV data were projected into cross-section A-A' as the primary control for constructing a profile interpretation of the conceptual hydrogeological framework (Figures 23 to 25). Some well records overlapped in places when projected into profile and were culled from the depiction to help preserve graphic clarity. In those instances, the most pertinent record was represented, usually predicated by having the thickest imaged section or deepest penetration. The process of constructing the profile depicted in Figures 24 and 26 involved the steps outlined below.

- a) Generate the topographic profile using GE (Figure 24) and develop section boundaries from the section trace.
- b) Project each well location into profile (Figure 15B) and represent their sub-vertical trace with simple lines scaled to the appropriate size depicting cased and open sections (Table 1).
- c) Project mapped stratigraphic contacts and fault traces onto the surface trace along with any
- d) Project primary and secondary geological structures gained from BTV analysis of each well, or group of wells, into profile using apparent-dip values of structural features determined from stereonet analysis. This requires knowing the deviation angle between the dip azimuth of each representative structure and the azimuth of the cross-section trace (Figure 23). For a simple

graphic depiction of apparent versus true dip, please see www.impacttectonics.org/GEO310/Labs/3A-Apparent_Dip.pdf.

- e) Stylize the section components to reflect the observed geometry of primary and secondary structures identified in the BTV structural analyses. For example, offset primary and secondary structures by younger ones as observed from kinematic analyses (Figure 21).

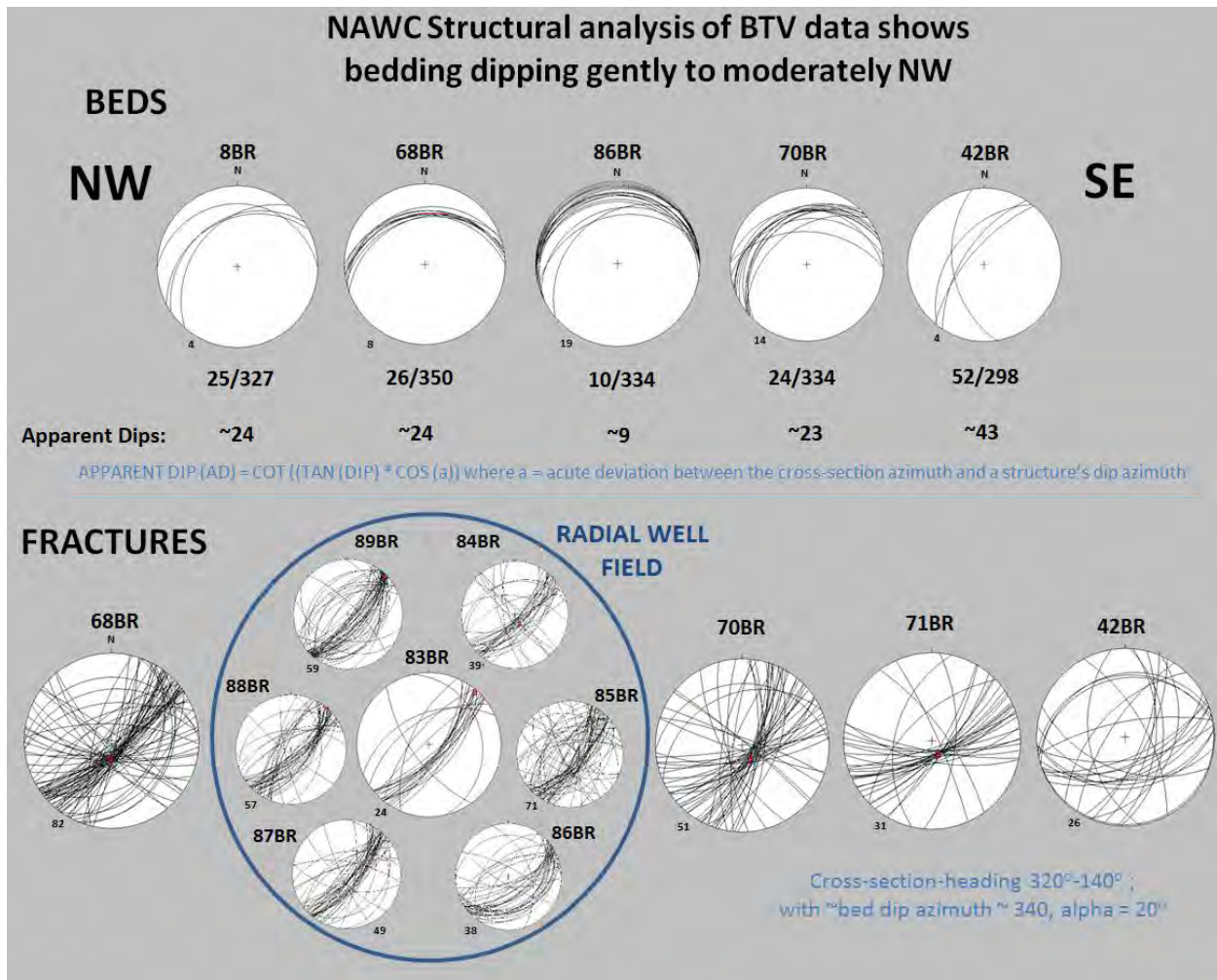


Figure 18: Stereonet structural analyses of BTV data from NAWC. Beds dip gently to moderately NW across the site (top diagrams). Rock fractures are more uniform in orientation (bottom diagram) than for the Stockton Formation at GM-RACER (Figure 17). Note the consistent orientation of rock fractures in the 80BR-series radial wellfield.

As seen in Figure 24, overall BTV coverage is good but a significant data gap occurs in the middle of the section between the sites where the major reverse fault is mapped by Lacombe and Burton (2010). Nevertheless, these BTV data provide geological coverage for thick sections of the upper member of the Stockton Formation and lower members of the Lockatong Formation (Figure 7). The comparative structural heterogeneity observed for these two sites (Figures 19 and 20) may simply reflect the stratigraphic heterogeneity, with bed and fracture sets in the Stockton Formation displaying much more variability those for those measured in the Lockatong Formation (Figures 15 to 18). Beds and fractures in the Lockatong Formation mostly cluster about the regional strike axis of the basin (S1 of Herman 2007 and Figure 20) and account for almost 1/3 of the total number of fractures measured in this unit. In comparison, S1 fractures in the Stockton Formation are subordinate in abundance to other, more prevalent ones (Figure 19 - S2, S3, SC3 8% trends) that likely reflect later extensional and compressional strains (Herman, 2009)

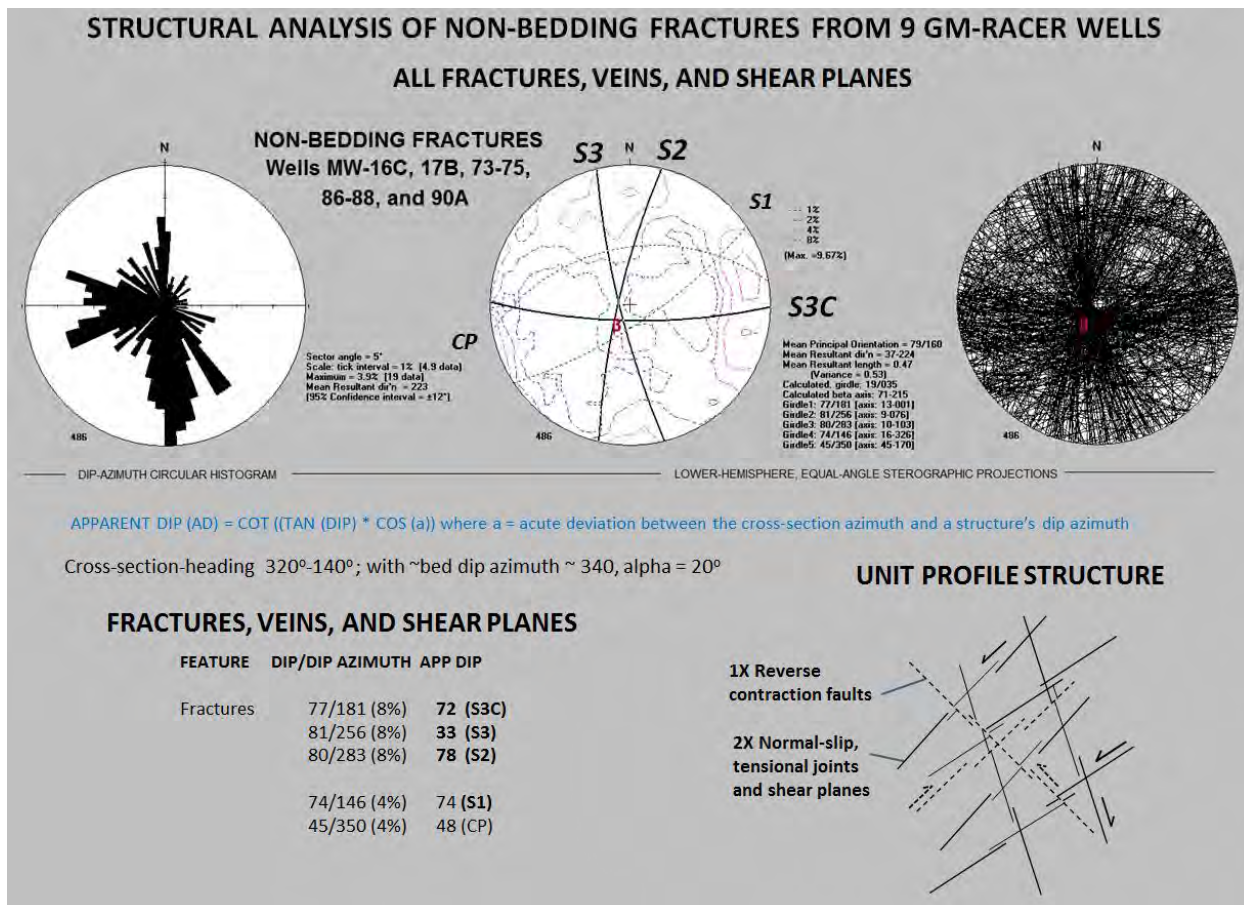


Figure 19: Structural analysis of non-bedding fractures from 9 GM-RACER wells (Table 1). Five principle fracture planes are identified and diagrammed using their apparent dips and relative percentages of the overall fracture population. The three most abundant, representative planes account for only 24% of the fractures measured. These three and two subordinate fracture sets (4%) are represented in profile using their relative abundances to create a unit profile structure (lower right) that is repeated in profile for the cross-section interpretation (Figures 24 and 25).

But these contrasts may simply reflect variable strain responses to the stark sedimentological differences between alluvial beds laid down in the distributary channels of a braided-stream deposit (Stockton) versus those deposited in shallow-to deep lakes and their margins (Lockatong). Consequently, these two sites have very different conceptual hydrogeological frameworks despite being located in such proximity. A structural-interpretive process termed ‘structural-feature density profiling’ was used to illustrate these conceptual differences by developing unit-profile structures for each site that are depicted in Figures 19 and 20. This structural technique was developed over many years while working at the NJGWS and is covered more thoroughly this year’s teacher’s workshop (Chapter 1).

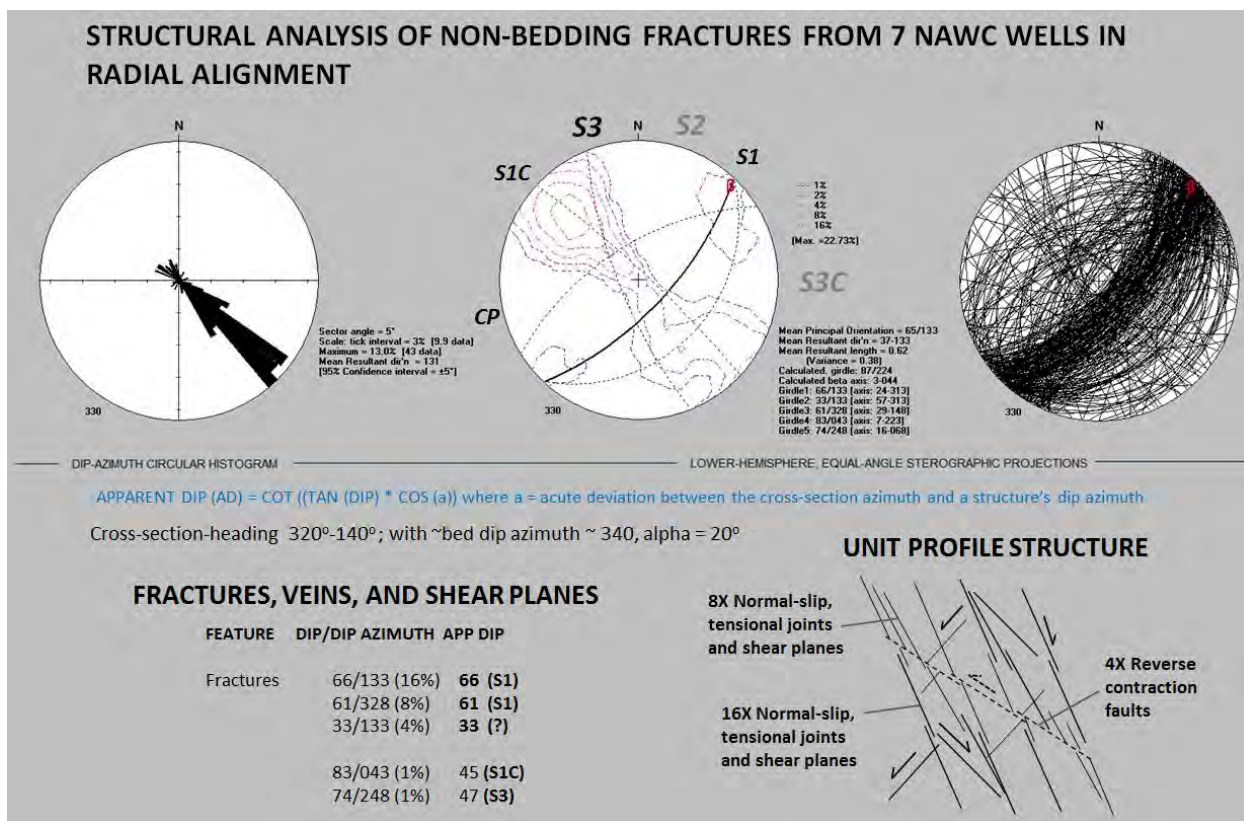
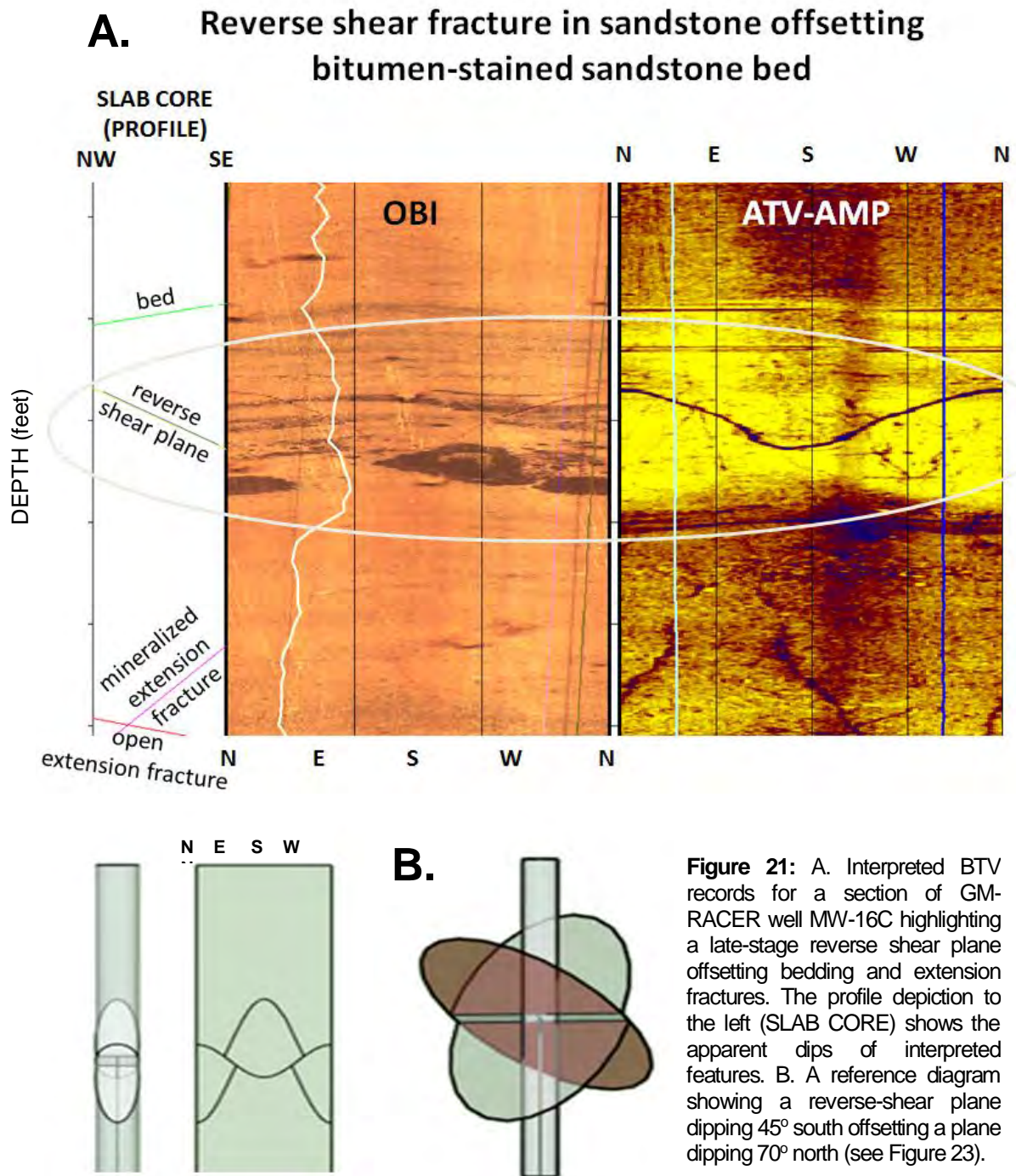


Figure 20: Structural analysis of non-bedding fractures from 7 NAWC wells in radial alignment (Table 1, Figures 6 and 19). Fracture sets measured in this well field were used to construct the representative fracture model for the Lockatong Formation at NAWC. The three most prevalent fractures planes account for 28% of the total number of fractures measured. These three and two subordinate trends (S1C) are combined in relative proportion to create the unit profile structure that is repeated in profile for the cross-section interpretation (Figures 24 and 25)

Discussion

The reverse faults depicted in map (Figures 3 to 6) and in profile (Figures 24 and 25) are stylized depictions of a penetrative, regional strain field where the Late Triassic section has been contracted and thickened by concealed reverse faults. I initially thought that the autoclastic breccia recovered in the MW-20A core at GM-RACER was an expression of this compressional event and reflected reverse faulting during late-stage basin inversion. The calcite spar from this breccia was sent to Ryan Mathur



at Juniata College, Pa. for radiometric dating with the hope that it contained ample uranium and lead isotopes that could define a reliable isochron. But these efforts proved futile as no isotopic traces were found in the submitted samples, and as seen in thin section, this fault breccia was cemented and hardened prior to structural compression. The reverse fault depicted as running southward of the MW-20A core was mapped based on this initial, erroneous assumption, and so revision is already in order. The only well-constrained reverse faults that occur near the surface are those associated with the nearby,

overtured beds of Lockatong in Villa Victoria Brook (Field Trip, STOP 3). Representation of the concealed reverse faults for this project therefore relied upon the geometry of local stream corridors where they correspond to abrupt changes in surface-water drainage patterns, for instance where streams take E-W jogs, perhaps coinciding with late-stage fracture swarms or reverse faults of the type that we see glimpses of in excavation and cores but otherwise concealed and therefore inferred on maps owing to the lack of telltale outcrops in the area. The tectonic setting of the Trenton area appears to be unique because I have measured fibrous-quartz-cemented fractures in Lockatong Formations outcrop near

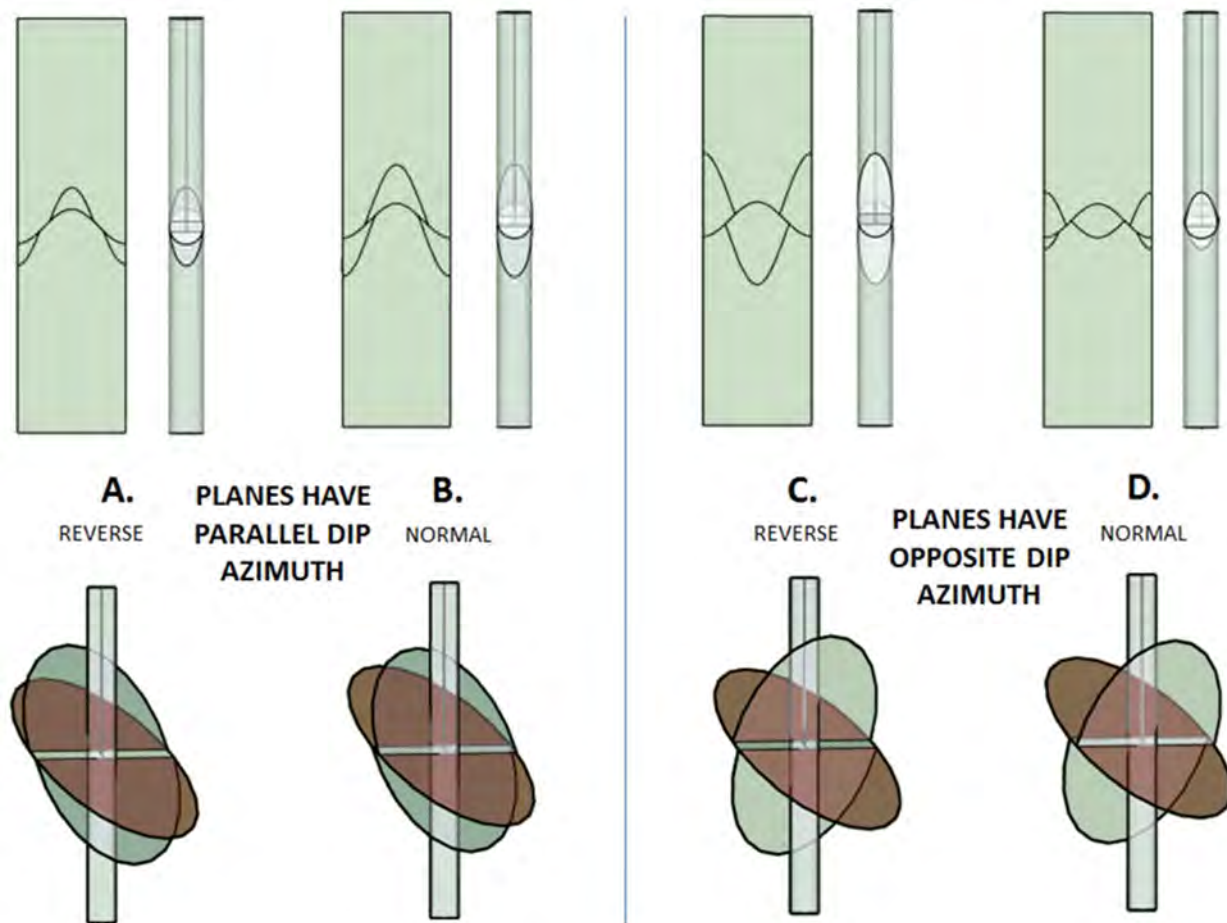


Figure 22: Trimble Navigation, Inc.'s SketchUp 2015 software was used to generate a series of borehole models with shear planes dipping 45° that offset extension fractures dipping 70° and in different directions to serve as a visual aid when interpreting kinematic indicators in BTV records. Each borehole segment was modelled using a 6-inch diameter borehole section that intersects two sorts of cross-cutting planes. The dip separation on each shear plane is 2 inches. After modelling each offset (bottom), the excess area of each plane was trimmed, leaving only the geometric patterns occurring on the borehole walls (top) that were next unrolled and flattened into rectangles using a custom Ruby script by Alexander Schreyer downloaded from the SketchUp Extension Warehouse. The unrolled fracture patterns reveal similar patterns to those seen in BTV records (Figure 21). The four models cover end-member structural scenarios where cross-cutting planes dip in the same (A. and B.) and opposing (C. and D.) directions and have either reverse or normal dip separation.

Villa Victoria Brook, and have held a hand sample of a quartz-cemented fault breccia, also apparently from the Lockatong Formation that Pierre Lacombe found at land surface near the GM-RACER site. This points

SHALLOW SUBSURFACE GEOPHYSICAL APPLICATIONS IN ENVIRONMENTAL GEOLOGY
GANJ XXXIII Annual Conference and Field Trip

to a slightly higher metamorphic grade of Late Triassic rocks in this area with respect to other parts of the basin in New Jersey, but Lucas and others (1988) also report fibrous quartz infilling tectonic veins in the western part of the basin near Jacksonwald, Pennsylvania. It thus seems that the Newark Basin was buried deeply before being 'inverted', or structurally elevated into its current position, with tectonic inversion increasing along the Appalachian grain to the southwest. It's likely that the tectonic episode or episodes that structurally inverted this section, perhaps by as much as a few kilometers, also overturned



APPARENT DIP (AD) = $COT ((TAN (DIP) * COS (alpha)))$ where alpha = acute deviation between the cross-section azimuth and a structure's dip azimuth



Figure 23: Google Earth (GE) was used to develop cross-section elements including a topographic profile (bottom graphic) that was auto-generated along the section trace (top A-A'). The profile topography requires further manipulation to place it into the project with the proper aspect because it is not captured with equal horizontal and vertical scales (1:1 scale). The deviation between dip azimuth and the section trace is highlighted in A. simply screen captured, pasted into MS PowerPoint (B.) and then traced using a freeform polyline. Note that when using GE to generate a topographic profile, that the resulting image is a scale other than 1:1

Combined GM-RACER and NAWC Hydrogeological Framework
 West Trenton Township, Mercer County, New Jersey

Profile view of stratigraphic intervals penetrated by BTV records

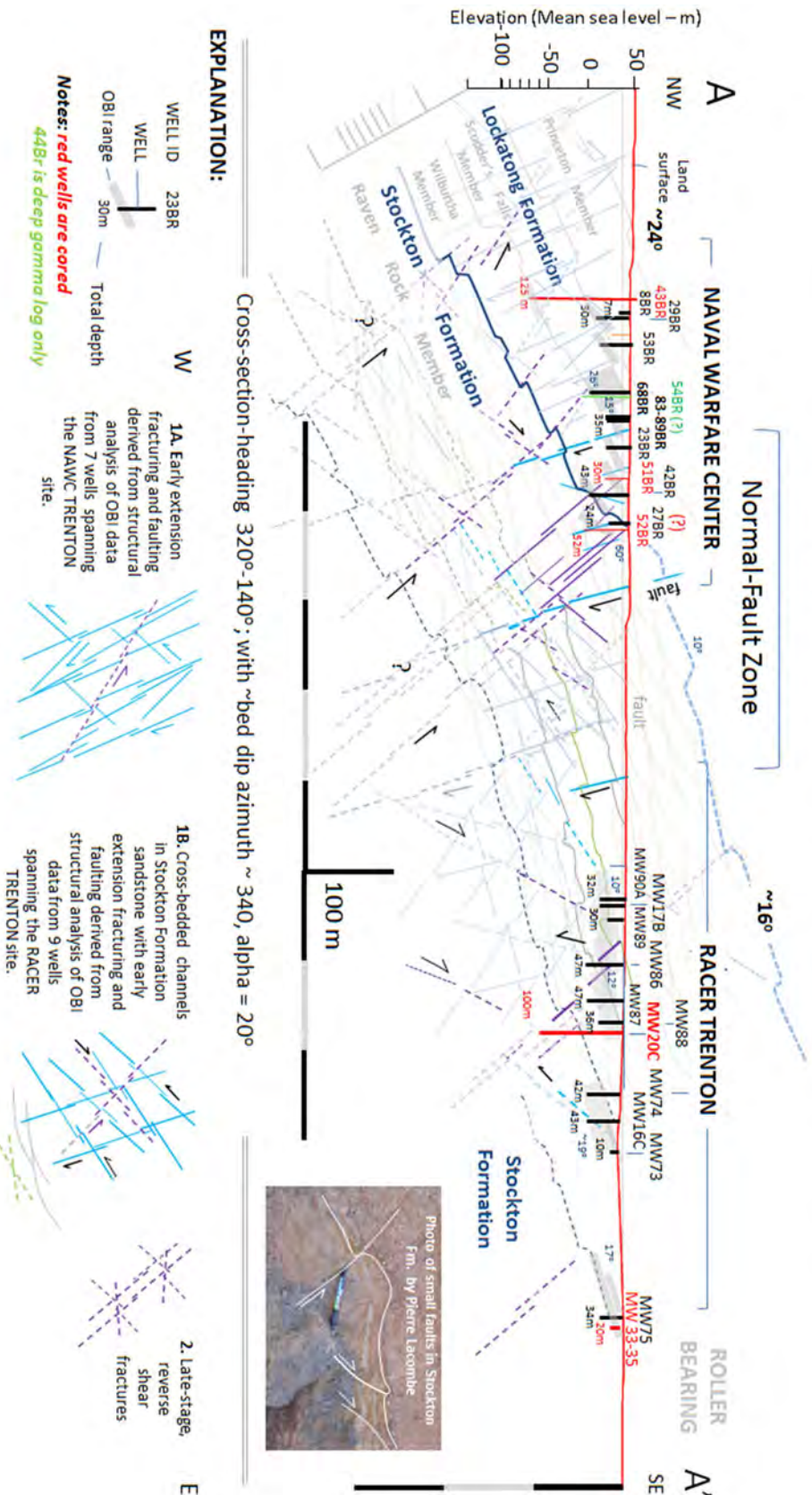


Figure 24: Schematic geological profile detailing the structural style of the area. Please note that not all wells and core are represented owing to graphic cluttering. The 'unit profile structures' (1A. - 1B.) derived in Figures 19 and 20 are repeated as fracture ornamentation in the cross section. Note the similarity between structures seen in the embedded photo (Figure 10B) and the interpreted structural style.

SHALLOW SUBSURFACE GEOPHYSICAL APPLICATIONS IN ENVIRONMENTAL GEOLOGY

GANJ XXXIII Annual Conference and Field Trip

The nearby Lockatong beds and imparted mechanical twins to the calcite-spar-cemented autoclastic fault breccia (Figures 9 and 10A) during late-stage tectonic compression after a prolonged, extension-dominated phase of continental rifting (Herman, 2015). The lack of such overturned beds north and east of Trenton and quartz-grade hydrothermal annealing of rock pores lends support to an argument that the compressional strain field increases in intensity southwestward towards Chesapeake Bay (Herman, 2015).

With respect to this conceptual hydrogeological framework, it is important to stress that the contrasting lithologies beneath these two adjacent sites results in very different hydrogeological conditions. The stratigraphic, structural, and hydrogeological contrasts seen between the Stockton and Lockatong Formations has been observed before (Herman, 2010; Herman and Curran, 2010) and result in the former having a much deeper, weathered section than the latter. It is common to see fracture interstices in the Lockatong Formation healed with secondary minerals at depths of only a few meters, whereas fracture interstices and macropores in the Stockton are mostly unhealed or partially open to depths of tens of meters below land surface because any secondary minerals that once filled pores were removed by chemical weathering. This is important to consider when defining the local hydrogeological framework for the conceptual flow model because groundwater flow at significant depths in the Stockton Formation will be less anisotropic than for the Lockatong Formation that behaves as a leaky-multiunit aquifer system like the Passaic Formation (Michalski and Britton, 1997). The difference in primary fracture direction between these two formations is also interesting to note. The Lockatong fractures are predominantly

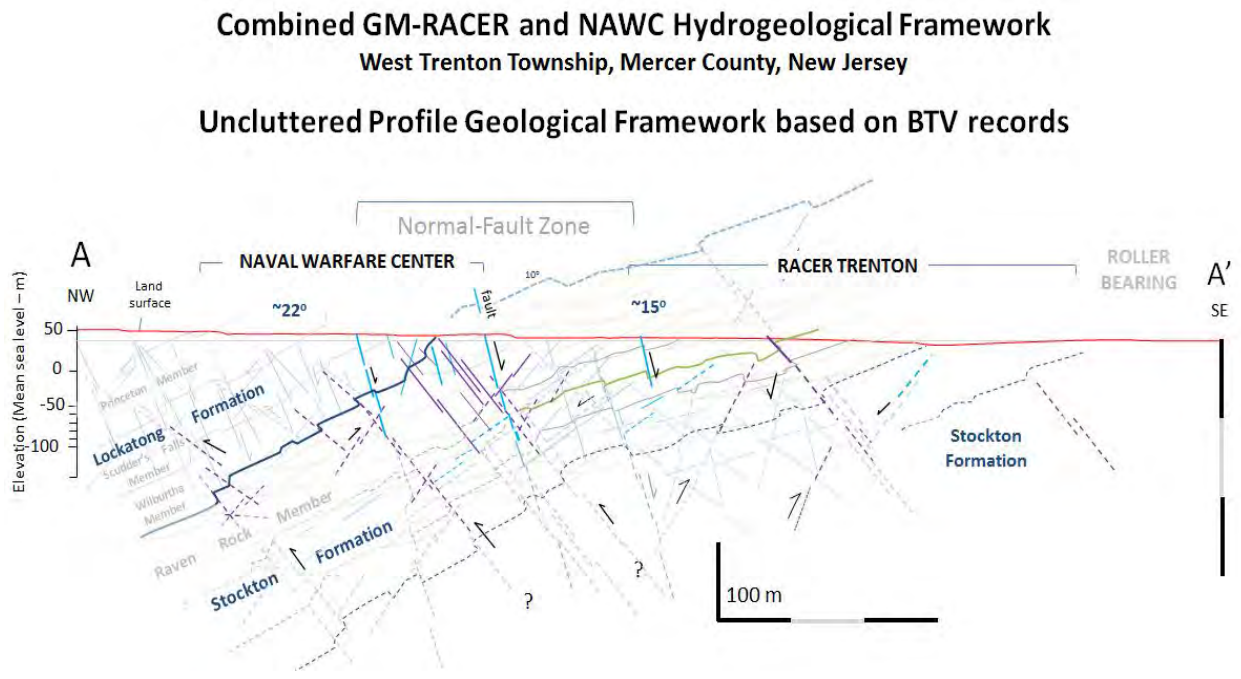


Figure 25: The cross section resulting from this work is clarified by removing all of the well elements and notes thereby emphasizing the conceptual framework for further evaluating the site hydrogeology.

Sub-parallel to the basin-bounding border faults to the northwest (S1 strike group of Herman, 2009). In contrast, the Stockton Formation displays strong N-S and E-W fracture trends, more in line with the strain axes indicated by the regional calcite-strain-gauge data (Herman, 2015). It therefore seems as if the Stockton sandstone behaved rheologically with a relatively higher level of structural competency than the Lockatong Formation, and simply reflects compressional overprinting differently than the argillaceous mudstone and siltstone of the Lockatong.

To conclude, this is the final project that I worked on as a research geoscientist on behalf of the State of New Jersey. There are many remaining geological mysteries to solve in this region, not to mention those that have yet to be unearthed. But the nature of tectonics in the Trenton area has been variously interpreted and depicted in modern times, and it is important to pay attention to new excavations and opportunities like this to acquire the kind of shallow subsurface information that can advance our understanding of complex geological systems in a realistic manner. After decades of mapping geology in New Jersey I have come to greatly admire the ancient practitioners that reported only what they saw and inferred little. But science is speculative by nature and as we continue to push boundaries, a cautious approach is warranted that employs established scientific methods because of the complex, deeply weathered and concealed nature of the bedrock in this region. The system of normal faults cutting through this region as depicted by Owens and others (1998) is stylistic and flawed, and in need of more 1:24,000-scale refinement. Surface-water drainages follow inherent weaknesses in bedrock corresponding to intervals, or zones of relatively dense fracturing and faulting (Ackerman and others, 1997). The steeply dipping rock joints that we see at the surface impart bulk shear in competent rock during extension and collapse of this thick pile of rift-basin fill (Herman, 2009), and so it becomes a matter of degree to where fault zones versus dense fracture zones are mapped. But this work has laid the groundwork for further investigations that should examine the depth of fracture healing in more detail with respect to observed groundwater flow at each site. The geological nature and extent of this area has historically been elusive, but it is further elucidated here using BTV and core records in an integrated, synoptic approach. Many such complex groundwater-pollution cases occur in this region, and as we deploy better tools in an effort to gain a firmer foothold on the hydraulic nature of complex aquifers, this type of approach may prove valuable elsewhere in deciphering just how fractured-bedrock holds and transports groundwater and its contaminants.

References

- Ackermann, R. V., Seidl, M. A., Schlische, R. W., 1997, First-order structural controls on modern drainage networks within the Newark rift basin, New Jersey: Geological Society of America Abstracts with Programs, v. 29, n. 1, p. 25
- Berg, T. M., Edmunds, W. E., Geyer, A. R., and others, compilers, 1980, Geologic map of Pennsylvania: Pennsylvania Geological Survey, 4th ser., Map 1, 2nd ed., 3 sheets, scale 1:250,000.
- Coffin M. F., and Eldholm, O., 1994. Large igneous provinces: crustal structure, dimensions, and external consequences: Reviews of Geophysics, vol. 32, p. 1-36.
- Engelder, T., 1979, The nature of deformation within the outer limits of the central Appalachian foreland fold and thrust belt in New York State, Tectonophysics, 55, 289-310.

SHALLOW SUBSURFACE GEOPHYSICAL APPLICATIONS IN ENVIRONMENTAL GEOLOGY
GANJ XXXIII Annual Conference and Field Trip

- Goode, D. J., Imbrigiotta, T. E., and Lacombe, P. J., 2014, High-resolution delineation of chlorinated volatile organic compounds in a dipping, fractured mudstone: Depth- and strata-dependent spatial variability from rock-core sampling: *Journal of Contaminant Hydrology*, v. 171, p. 1-11.
- Herman, G. C., 2015, [Neotectonics of the New York Recess](#), in Herman, G. C., and Macaoay Ferguson, S., eds., *Neotectonics of the New York Recess: 32nd Annual proceedings and field guide of the Geological Association of New Jersey*, Lafayette College, Easton, Pa., p. 80-151 (16.0 MB)
- Herman, G. C., 2010, [Hydrogeology and borehole geophysics of fractured-bedrock aquifers](#) (5 MB PDF), in Herman, G. C., and Serfes, M. E., eds., *Contributions to the geology and hydrogeology of the Newark basin: N.J. Geological Survey Bulletin 77*, Chapter F., p. F1-F45.
- Herman, G. C. and Curran, J. F., 2010, [Borehole geophysics and hydrogeology studies in the Newark basin, New Jersey](#) (38 MB PDF), in Herman, G. C., and Serfes, M. E., eds., *Contributions to the geology and hydrogeology of the Newark basin: N.J. Geological Survey Bulletin 77*, Appendixes 1-4, 245 p.
- Herman, G. C., 2009, [Steeply-dipping extension fractures in the Newark basin](#) (5 MB PDF), *Journal of Structural Geology*, V. 31, p. 996-1011.
- Herman, G. C., 1997, Digital mapping of fractures in the Mesozoic Newark basin, New Jersey: Developing a geological framework for interpreting movement of groundwater contaminants: *Environmental Geosciences*, v. 4, no. 2, p. 68-84.
- Herman, G.C., Dooley, J.H., and Mueller, L.F., 2010, *Geology of the Pennington Trap Rock (Diabase) Quarry, Mercer County* (6 MB PDF), in Lacombe, Pierre, ed., *Geology of Trenton and its impact on the Capitol City: 27th Annual Meeting of the Geological Association of New Jersey*, Trenton, NJ, p. 92-119.
- Lewis-Brown J. C., and Rice, D. E., 2002, *Simulated ground-water flow, Naval Air Warfare Center, West Trenton, New Jersey: U.S. Geological Survey Water-Resources Investigations Report 02-4019*, 44 p.
- Lacombe, P.J., 2000, *Hydrogeologic framework, water levels, and trichloroethylene contamination, Naval Air Warfare Center, West Trenton, New Jersey, 1993-97: U.S. Geological Survey Water-Resources Investigations Report 98-4167*, 139 p.
- Lacombe, P.J., 2001, *Water levels and potentiometric surfaces, Naval Air Warfare Center, Trenton, New Jersey, 2000: U.S. Geological Survey Water-Resources Investigations Report 01-4197*, 46 p.
- Lacombe, P.J., and Burton, W., 2010, *Hydrogeologic framework of fractured sedimentary rock, Newark Basin, New Jersey. Groundwater Monitoring & Remediation V. 30, no. 2, p. 35-45.*
- Lomando, A. J. and Engelder, Terry, 1984, *Strain indicated by calcite twinning: Implications for deformation of the Early Mesozoic Northern Newark Basin, New York: Northeastern Geology*, vol. 6, no. 4, p. 192-195.
- Marzoli, A., Renne, P., Piccirillo, E., Ernesto, M., Bellieni, G., and De Min, A, 1999. *Extensive 200-million-yearold continental flood basalts of the Central Atlantic Magmatic Province: Science v. 284, p. 616-618.*
- Michalski, Andrew, and Britton, Richard, 1997, *The role of sedimentary bedding in the hydrogeology of sedimentary bedrock - Evidence from the Newark Basin, New Jersey: Ground Water, Vol. 35, No. 2, p. 318-327.*
- Robinson, J., Slater, L., Johnson, T., Shapiro, A., Tiedeman, C., Ntarlagiannis, D., Johnson, C., Day-Lewis, F., Lacombe, P., Imbrigiotta, T., and Lane, J., 2015, *Imaging pathways in fractured rock using three-dimensional electrical resistivity tomography: Groundwater, v. 54, Issue 2, p. 186-20.*
- Owens, J. P., Sugarman, P. J., Sohl, N. F., Parker, R. A., Houghton, H. F., Volkert, R. A., Drake, A. A., Jr., and Orndorff, R.C., 1998, *Bedrock Geologic Map of Central and Southern New Jersey, U. S. Geological Survey Miscellaneous Investigation Series Map I-2540-B, scale 1:100,000, 4 sheets.*

Acknowledgements

This study was facilitated by the cooperative efforts of the USGS Water Science Center in Trenton, NJ, by Haley-Aldrich, Inc. from their Cleveland, OH and Parsippany, NJ offices, and by Hager-Richter, Inc. out of their Fords, NJ office. Accordingly, I am sincerely grateful to Pierre Lacombe, Emmanuel Charles, and Alex Fiore of the US Geological Survey, to Dimitri Quafsi of Haley-Aldrich and Rob Garfield of Hager-Richter for providing the BTV data records, reports, maps, photographs, and core samples for inspection and interpretation. This project could not have happened without their contributions.

Mapping Bedrock Fractures and Other Subsurface Conditions in Urbanized Environments Using the Multi-Channel Analysis of Surface Waves (MASW) Geophysical Method

Richard Lee, P.G., R.GP, President and Principal Geophysicist, Quantum Geophysics

Those working on contaminated sites often need to identify subsurface conditions that control the movement of contaminants. Subsurface conditions include bedrock fractures, faults, geologic contacts, localized depressions in the top of rock, "breaks" in confining layers, and voids (karst). These conditions tend to be small and unpredictable, which makes them difficult to find via traditional exploratory drilling. Many sites are located in urban environments where site conditions (e.g., buried piping, fill, paved surfaces) impact the effectiveness of some geophysical methods, especially those more familiar to geologists and environmental scientists (GPR, EM, electrical resistivity). There is now a growing awareness that some "non-traditional" geophysical methods can be very effective in mapping subsurface conditions in urbanized settings, especially the multi-channel analysis of surface waves (MASW) method.

This session will describe how MASW works (e.g., equipment, data acquisition, data processing, and analysis), and look at several case histories. We will also discuss what conditions can impact MASW (some can be mitigated, some can't), and why GPR, EM, and electrical resistivity are generally not effective in urbanized settings.

About the Speaker

Mr. Lee received a B.S. degree in geology from Colgate University, and an M.S. degree in geology from the University of Pittsburgh. He is a registered geophysicist (CA) and a professional geologist (PA). In over 35 years as a practicing geophysicist, Mr. Lee has worked closely with engineers and geologists on a variety of projects throughout the lower 48 states, Alaska, Hawaii, and Puerto Rico. Mr. Lee specializes in applying geophysics to the evaluation of karst terrain, the characterization of hazardous waste sites, identifying seepage, locating water supply (sand and gravel, and fractured aquifers), and evaluating infrastructure (pipelines, roads, dams, levees, tunnels, railroads, wind and solar farms, airports, maritime harbors).

FIELD GUIDE

Stop 1– New Jersey Geological and Water Survey, Ewing, NJ

Fern Beetle-Moorcroft and Michael Gagliano, New Jersey Geological & Water Survey

At Stop 1 we will view and discuss a variety of equipment utilized in conducting shallow subsurface geophysical investigations at the NJGWS garage and workshop.

Staff at NJGWS makes use of a plethora of geophysical tools to image the subsurface. These tools provide support evidence for pollution studies, historical research, determining the location of buried tank, just to name a few. Some of these tools are used for near surface data collection, whereas, others are down hole tools:

Near Surface Tools

Ground Penetrating Radar (GPR)



Figure 1: GSSI SIR-4000 GPR unit with 400 mHz antenna

Ground Penetrating Radar (GPR) is a geophysical technique for imaging the subsurface that sends electric radar pulses into the ground. These pulses are produced by the control unit, amplified by the antenna, and sent into the ground at a particular frequency. The GPR unit records the strength and the time of return of these electrical signals. It compiles a series of these measurements into a scan. Notable reflections are produced when the energy pulse enters a material with a different dielectric permittivity. Water content is greatly changes the dielectric content of a material and can make distinguishing different lithologies difficult (GSSI Website). Thus, we typically use GPR to find metal objects such as buried tanks as

the dielectric content between any unconsolidated sediments and metal can be easily noted (Figure 1).

Electrical Resistivity

Electrical Resistivity is a measurement of how much a material resists carrying an electrical current. Electrical Resistivity Tomography is a geophysical method that determines the resistivity distribution of the subsurface by making measurements on the ground surface. Measurements are made using an automated multi-electrode resistivity meter, which sends AC or DC current into the ground, and records the resistivity

at different electrodes. The pattern of sending and receiving current is controlled by the chosen array, which is set up beforehand and dependent upon the size of the area being measured and the desired depth of penetration. Electrical resistivity is typically used to pick out particularly resistive or conductive materials. Most recently, we have used electrical resistivity to quantify salt contamination, as saline water is much more conductive than pure, uncontaminated water (Figure 2).



Figure 2: AGI Supersting Resistivity unit with 84 electrode switchbox.

Electromagnetic Induction (EM)



Figure 3: GSSI EMP-400 Profiler

Electromagnetic Induction (EM) is a measurement of conductivity in the subsurface. EM instruments are made up of two coils, which are electrically connected and spaced at a fixed distance. One coil, the transmitter coil, generates an electromagnetic field, the primary field, at a specific frequency. This causes electrical currents to flow in conductive materials in the subsurface. The flow of currents in the subsurface generates a secondary magnetic field that is picked up by the receiver coil (Figure 3).

Magnetometer



Figure 4: Geometrics G-858 cesium magnetometer

Magnetometer surveys pick up slight, localized variations in Earth's magnetic field. Magnetometers utilize proton rich fluids surrounded by an electric coil. When a current is applied, the protons temporarily become polarized; when the current is removed, the protons realign according to Earth's magnetic field at that point. Magnetometers are used to detect magnetic ore bodies, igneous rocks, or buried steel objects (Figure 4).

Seismic Reflection/ Refraction

Seismic Reflection/Refraction surveys send shots, sound waves, into the subsurface, which reflect and refract at each acoustic impedance change. These changes are measured by geophones (on land) or hydrophones (in water), which track the two-way travel times of the sound waves. Seismic Reflection/Refraction surveys are useful for identifying the location of bedrock, offshore sand resources, or the subsurface geology of an area (Figure 5).



Figure 5: (Top) Applied Acoustics S-Boom marine seismic reflection unit and Edgetech 216 Chirp. (Bottom) Geometrics Geode Seismic refraction system.

Down Hole Tools

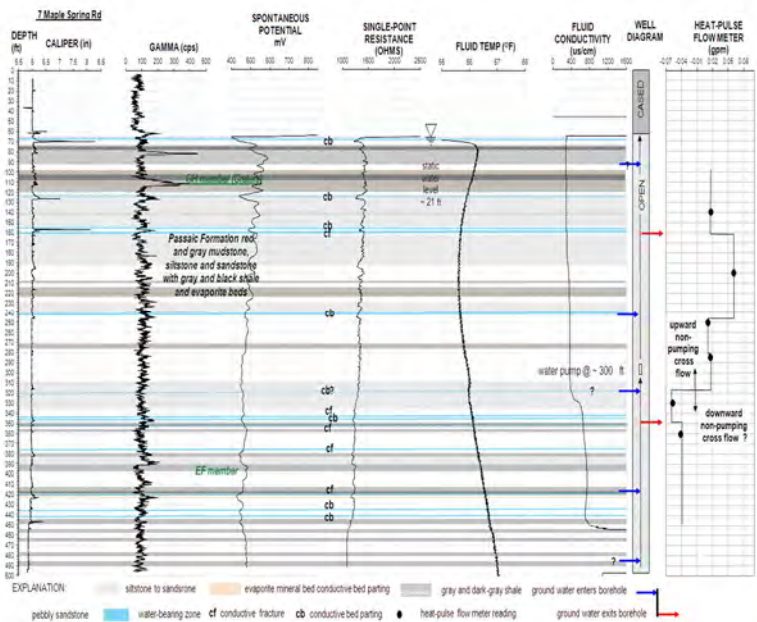


Figure 6: (Left) Mount Sopris Matrix data logger and winch. (Right) Full suite of downhole logs.

Gamma

Gamma logging is a method of measuring naturally occurring gamma radiation to characterize and differentiate between lithologies in a borehole. This tool is different from most of the others in that it is passive (e.g. caliper) in that it does not emit a signal but measures the already present radiation. Shales and clays tend to have a higher gamma signal due to the higher percentage of radioactive elements. Thus, gamma logs are often used to differentiate between shales and non-shales.

Acoustic Televiwer (ATV)

The acoustic televiwer (ATV) is a borehole geophysical probe that relies on propagating acoustic waves using compression and decompression and measuring acoustic wave reflections. Waves are reflected at interfaces, which represent a change in acoustic impedance. These acoustic impedance changes can be caused by structural and lithological differences. The travel time and amplitude are collected by the ATV and used to generate high-resolution images of the borehole wall. AT NJGWS, we have recently acquired the ATV. We are excited about having the ATV because it still produces good data in muddy water and it can help differentiate between open and sealed fractures (Figure 7).



Figure 7: Mount Sopris QL40-ABI-2G Acoustic Televiwer

Optical Televiewer (OPTV)

The Optical Televiewer (OPTV) is a geophysical logging tool that provides a continuous, orientated, detailed, color image of the borehole substrate. The OPTV captures 360° stacked photographic rings in geographic alignment collected at 1mm depth intervals. The OPTV is particularly useful for identifying changing lithologies, permeable zones, fractures, veins, and other structural features. The main drawback of the OPTV is that the water needs to be clear for the data to be usable. If the water is muddy, it can be almost impossible to see the borehole walls.



Electrical Resistivity Tool

Electrical Resistivity logging is a measurement of how much a formation resists carrying an electrical current. This aids in differentiating between formations filled with saline water (very conductive and non-saline water (very resistive). This tool varies in penetration from a few centimeters to meters. It can be useful to combine downhole resistivity with data from an electrical resistivity array to get more data points.



Caliper

The Caliper tool is three-pronged tool that measures the size and shape of the borehole down depth. Specifically, it measures variation in the diameter of the borehole and is useful for identifying dissolved layers, large fractures, and borehole breakout. This tool is especially helpful when utilized with the OPTV and ATV to assist with characterizing features. The caliper tool is a staple in well logging projects at NJGWS.

Fluid Tool

Provides temperature and fluid conductivity measurements in the borehole. Logs can be used for salt-water intrusion studies, the identification of fluid flow in the hole, for geothermal gradient logging and water table location identification (Figure 8).



Figure 8: H Mount Sopris QL40-FTC Fluid Temperature and Conductivity

Heat Pulse Flowmeter



The Heat Pulse Flowmeter is a unique flowmeter tool designed to measure low flow rates in the borehole environment. It will also give the direction of the flow of fluid vertically. To detect these low flow rates, measurements must be made while the probe is stationary at different depths within the borehole.

Stop 2 – Stockton Formation, Stockton, NJ

Francesca Rea and Don Monteverde, New Jersey Geological & Water Survey

At Stop 2 we will visit a former Quarry in the Triassic Stockton Formation, near Stockton, NJ.

Prallsville Mills

The field stop is located NW from the Prallsville Mills parking lot approximately 0.25 miles down the Delaware and Raritan Canal State Park Trail (Figure 1). Prallsville Mills has been around for hundreds of years and is historically significant to the Borough of Stockton. In the early 1790s, John Prall, Jr. purchased this tract of land acquiring a grist and saw mill. Being the business man that he was, he wanted to turn

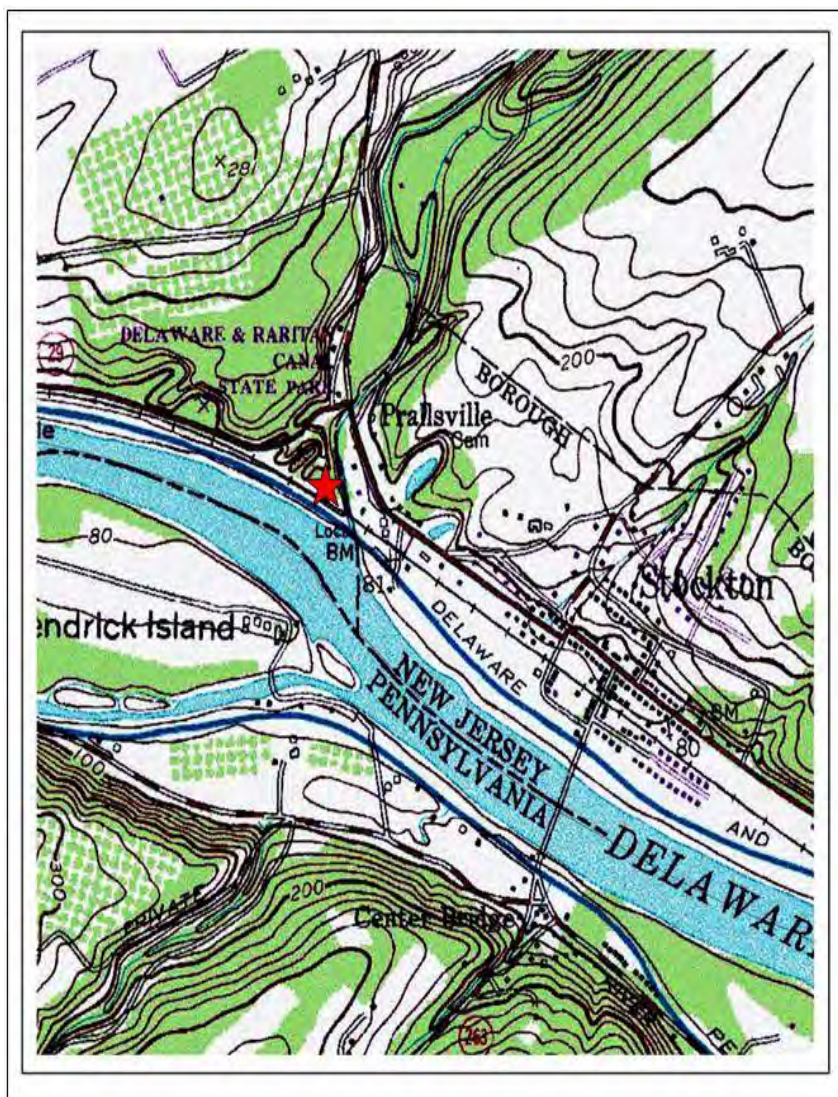


Figure 1: A topographic map of the region of study indicating where Field Stop 2 is located.

Prallsville into a principal industrial center focusing on the milling of linseed oil and lumber. Industry and infrastructure were growing and there was a need for building stone, so Prall opened and ran a quarry with prime access to the Delaware and Raritan Canal (Figure 2). The canal offered a direct route for the shipment of building stone between Philadelphia and New York City. Although all operations at Prallsville Mills ceased in 1969, preservation of this historic site remains today. It is representative of the 19th and early 20th century structural design, commerce, business, and culture, which is why its land is protected as part of the Delaware and Raritan Canal State Park and preserved by the Delaware River Mill Society for the public's enjoyment (Delaware and Raritan Canal Commission).



Figure 2: The Prallsville Quarry in 1906 (Strunk, 2008).

Quarrying of the Stockton stone

During the late 1800s and early 1900s, quarrying was a key component to the success of the Stockton area. With the Borough of Stockton located along the Delaware River, a large majority of quarries were in operation for the production of brownstone, a reddish- to chocolate-brown sandstone used as building material during the nineteenth century (Pallis, 2012).

The quarryman profession was rigorous and physically challenging. Many immigrants traveled to the United States and worked in the quarries. They would oftentimes work from sunup to sundown six days a week from April through November (Saja, 2012). According to the 1880 census, the mean salary of a quarryman was just \$566.00/year (Zdepski, 2002). The physical and mechanical labor was also very taxing on the workers to the point that severe injuries were not uncommon. Accidents frequently occurred leaving quarrymen's extremities, especially hands and feet vulnerable to being crushed (Saja, 2012).



Figure 3: Plug and feather tools used to harvest building stone (Gage and Gage, 2005).



Figure 4: Quarrymen relying on mechanical equipment to harvest building stone (Pallis, 2012).

The Stockton Formation was the ideal building material of the time due to its natural perpendicular jointing and outcrop location along the river. Before a quarry operation could commence, all of the trees, vegetation, soil, and debris must be removed from the site in order to reach the sandstone. Upon successful inspection of the stone, by a geologist or quarry boss, quarrymen could start production (Saja, 2012). In the early stages of quarrying, the plug and feather method was the popular technique used to harvest building stone (Figure 3). First, a succession of holes would be drilled while a plug was placed into each hole. Then two wedge-like feathers would be placed into the channel along both sides of the plug. A quarryman would then hit the plug with a sledgehammer in order to split the rock. The unfinished block was then cut to the desired building size using steel blades that were cooled with water to ensure clean cuts. The blocks were moved from the quarry floor using animal-powered wagons and sleds, or, later on, mechanically transported by a series of derricks and cables. The next step in the process happened in the scrambling area where the stone was made resilient to weathering. Since sandstone is porous, the moisture had to be removed in a process called seasoning. During this process, the block would be buried in soil for about four months until it could be retrieved and considered ready for construction (Saja, 2012). Eventually, mechanical equipment replaced manpower in the latter part of the nineteenth century (Figure 4) (Pallis, 2012).

Geologic Setting

The Stockton Formation is a sedimentary unit deposited in the Newark Basin. Henry Kümmel, a future State Geologist, named the formation in 1896 from investigations of the exposures in and around the Stockton area (Kümmel, 1897). Although the Stockton Formation is native along the Delaware River, as per

SHALLOW SUBSURFACE GEOPHYSICAL APPLICATIONS IN ENVIRONMENTAL GEOLOGY
GANJ XXXIII Annual Conference and Field Trip

Kümmel's notes, it can also be observed at the Palisades Interstate Park along the trail leading up to the George Washington Bridge.

The Newark Series is a group of geological formations that make up the Newark Basin with the Stockton Formation being the oldest unit. Deposition of the Newark Basin started during the late Triassic period roughly 220 million years ago with the breakup of Pangea. The basin extends across northern New Jersey into eastern Pennsylvania and part of the southern region of New York State (Figure 5). Due to the half-graben structure of the basin, source sediment came from multiple directions including from the northeast down the length of the basin as well as down the rider blocks, from the southeast along the length of the basin and a second axial transport from the southwest (USGS, 2015). Subsequently, as the Newark Basin widened sediment continually filled the newly available space (Smoot, 2010).

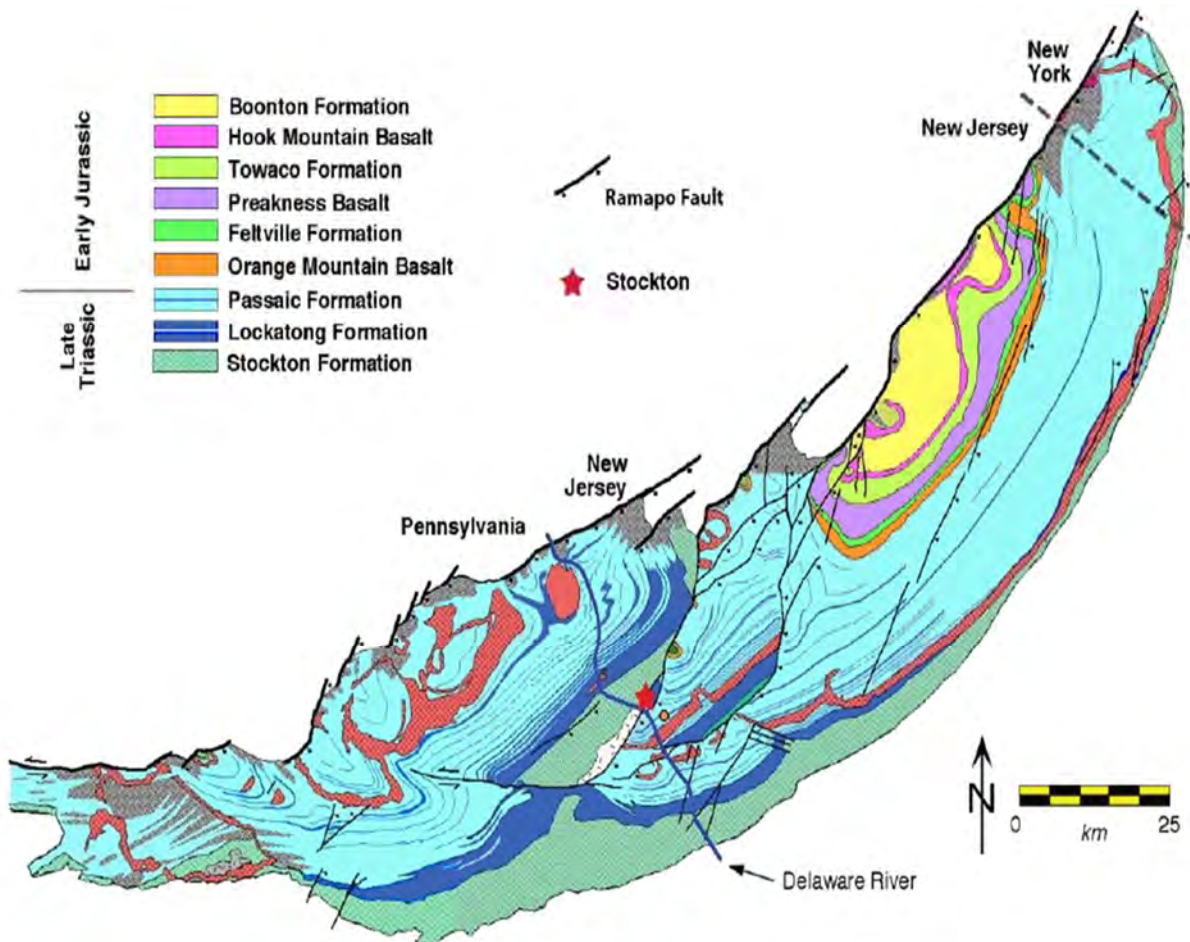


Figure 5: Map of the Newark Basin and Ramapo Fault (Rea, in press).

Smoot (2010) separates the Stockton Formation into three facies based on sediment grain size and sedimentary structures: conglomerate and conglomeratic sandstone, arkosic sandstone, and micaceous sandstone, siltstone, and mudstone (Figure 6). The conglomeratic facies is light yellow-brown colored sandstone encompassing pebbles and cobbles. The arkosic facies can be observed as alternating layers of purplish-tan sandstone with red sandstone, mudstone, and siltstone. The last facies is often interbedded between the previous two units as a reddish-purple very fine grained unit (Smoot, 2010).

It can be inferred based on the sedimentology that the Stockton Formation was deposited in a fluvial setting. Additional understanding of the development of the Newark Basin can further support the depositional environment. Initially, the basin was narrow with steep borders supporting random drainage outlets. Water naturally travels the path of least resistant, so a system of braided rivers carved its way into the basin depositing cobbles and pebbles. Sometimes the influx of water would be so great that the banks would flood creating periods of standing water depositing fine grained sediment.

As the Newark Basin continued to fill, a gentler stream gradient developed. The previous coarser material could not be transported past the outer margins of the basin and rivers started to meander to cope with the changing state of the basin. Ultimately, the Newark Basin became too extensive to tolerate the number of network and drainage passages it had previously carried and the development of a

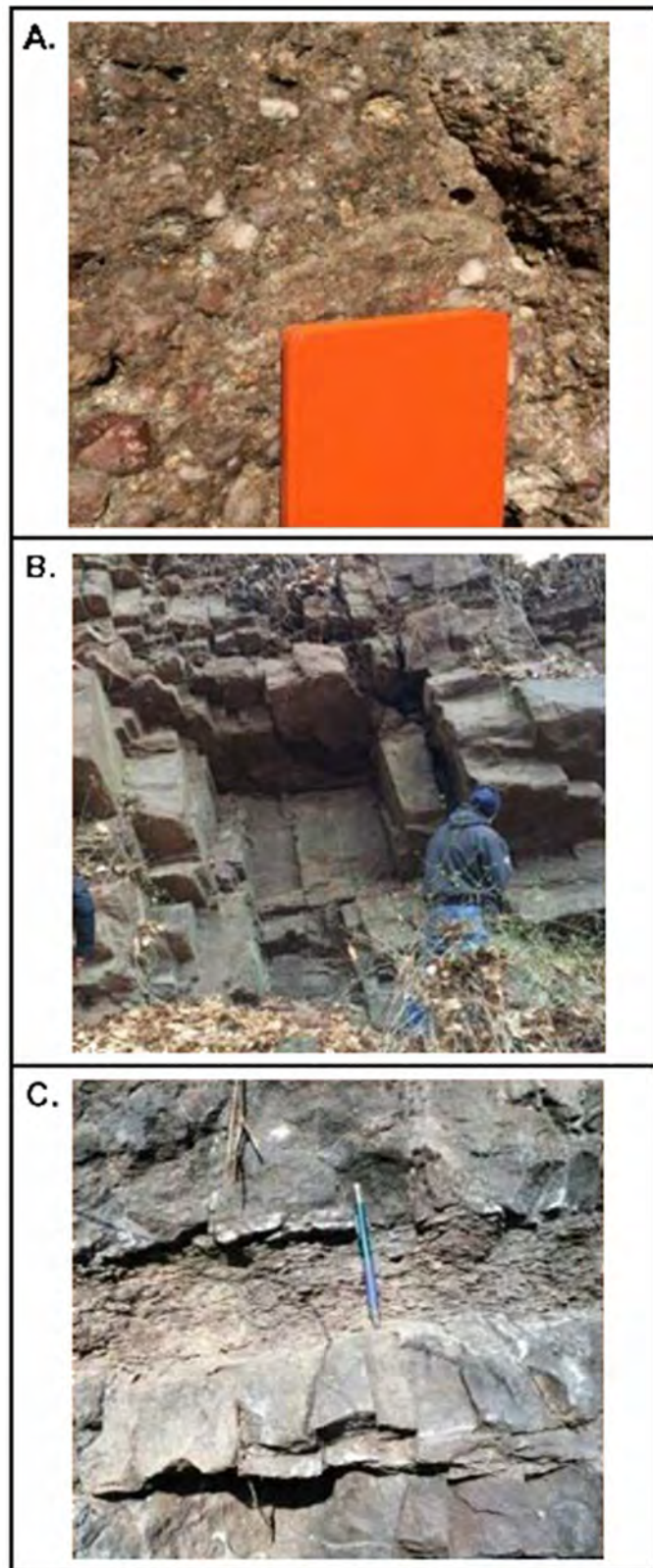


Figure 6: A) Conglomerate and Conglomeratic Facies, B) Arkosic Sandstone, C) Micaceous Sandstone, Siltstone, Mudstone (modified from Rea, in press).

lacustrine-type settings prevailed. This ended the deposition of the Stockton Formation paving way for the subsequent series (Smoot, 2010).



Figure 7: The original Linseed Mill building stone showing similar fracture patterns in the building stone with hammer for scale (Photo by F. Rea).

Stop A:

The first part of the stop discusses the Stockton Formation in a historical way. Surrounding the parking lot where the buses parked, there are several buildings of Prallsville Mills still standing. Many have been renovated to ensure the historical preservation of the site, but much of the exposed building stone is assumed to be the original. The original Linseed Mill from 1794, located diagonally across from the Delaware and Raritan Canal Commission building, is built of stones more suggestive of the quarrying process. It

can be observed that the edges of the stone appear to fracture along a common surface (Figure 7), which is why the Stockton Formation was so desirable for quarrying. This is suggestive of a natural joint set in which the stone could be separated along during the process of plug and feathering. Across the parking lot, the Delaware River Mill Society building appears to have a more rugged looking brick, perhaps taken from the banks of the Delaware River which can be seen in the Wickecheoke Creek when walking to Stop B.



Figure 8: Brick at Prallsville Mills showing coarse pebbles down-cutting a sandy unit with pencil as scale (photo taken by

Although this building stone has been removed from its original depositional location, evidence of sedimentology can still be observed in the stone. For example, erosional processes such as down-cutting can be seen (Figure 8). However, the actual orientation of the structure is unknown but, it appears that coarse pebbles have eroded away at the sands through river processes. In addition, cross-bedding is a predominant feature of the Stockton Formation and can also be seen here at Prallsville (Fig. 9). Other features visible at this stop are small borrows within the reddish-brown bricks, as well as, rip-up clasts. What traces of geology do you see?



Figure 9: Brick at Prallsville Mills showing cross-bedding with pencil as scale (photo taken by F. Rea).

Stop B

Please migrate to the canal tow path to your west. Continue northwestward on the path and across Wickechoke Creek to a rock exposure on the northeast side of the path. As you walk, please be careful of the foliage as poison ivy appears to dominate the landscape. For those who have forgotten poison ivy has three almond-shaped leaves that are usually shiny dark green in the summer and turn red to orange in the fall. It's a climbing vine commonly with red "hairs" on the main stem. Recent studies (Ziska et al., 2007, Mohan et al., 2006) have shown that poison ivy will become more abundant with increased toxicity due to the increasing CO₂ levels predicted by climate change, oh joy. This exposure forms the western edge of an old quarry. Currently this location resides on private land so authorization must be obtained before entering to investigate the rocks. We will just look at the very western edge of the quarry. Also please restrict hammer usage here. Spend some time looking at the southwest facing exposure before taking a look at the southeast face of the outcrop. Both of these are described in more detail below.

Despite the overabundance of foliage inhibiting a complete view of the outcrop, this is a very interesting exposure of the Stockton Formation. After climbing up the short incline through the poison ivy please look at the southwest facing slope. Low down, there appears some old metal ties and rings attached at the two places along the base of the outcrop in both the blocky sandstone bed and the underlying finer grained layer (Figure 10). I am really not sure what their function was but, this is a field trip stop so let's hypothesize. My best guess is that the rings were part of the quarrying process as opposed to being part of the equipment for the towpath work.



Figure 10: Weathered large metallic rings embedded in rock face that parallels the canal towpath.

At first glance, the rocks on this face portray a relatively uniform bedding relationship between more resistant red and arkosic sandstone and the thin, finer-grained interbeds. The large blocky bed just above the southern metal ring is an arkosic sandstone varying from fine- to coarse-grained with subrounded and moderately sorted grains. Upon closer inspection it shows not to be a single layer but contains various interbedded sandstone layers displaying various sedimentary structures including cross bedding, burrows and overall fining upwards sequences.



Figure 11: Southeast facing exposure of Stockton Formation. Note blocky layers of arkosic and red, medium- to coarse-grained sandstone with finer grained sandstone, siltstone and mudstone interbeds. Red lines mark bottoms of sand beds and outline the lensing nature of these units. Fractures are well developed in the blocky coarser sandstone beds that do not transect the finer interbeds. Hammer for scale.



Figure 12: Example of circular burrows identified by black arrows. Photo of loose block south of main outcrop

Move around to the right to east-southeast face for a better look at the sedimentology of the Stockton here. Resistant medium to coarse grained sandstone beds display variable bed thickness that thins and thickens across the outcrop leaving an appearance of slight channels. Finer grained interbeds generally separate these sand layers but locally the finer interbeds pinch out leaving sand on sand. Sand beds present the morphology of fluvial channels (Figure 11). The thick basal bed is an example of the arkosic sandstone facies of the Stockton. A fining upwards sequence marked by a basal quartz pebbly sand layer with pebbles up to 3 cm across occurs within the upper part of this blocky arkosic unit. The loose block lying slightly away from the outcrop show some nice vertical burrow structures (Figure 12).

Structural trends

BTV has become an effective tool in cataloging and understanding fracture development and trends. Together with the heat pulse flow meter important water-bearing trends can be identified. This is especially true in regions of limited outcrop. Bedding and lithologic data from BTV records can also aid in regional mapping by projecting contact information to the surface. This has been done on numerous geologic bedrock maps of the Newark Basin, where outcrop data is sparse (Monteverde and others, 2014, 2015, Monteverde and Herman, 2015). This stop offers an opportunity to compare various fracture and bedding data collected as BTV and both small and large outcrop data.

Note the degree of jointing in this outcrop. Joints appear to be strata bound and restricted to the coarser-grained beds. They are not found in the thinner grained interbeds (**fig**). Fractures in a detached block of medium to coarse grained sandstone below the outcrop show the discontinuous nature of one trend of fairly closely spaced parallel fractures (**fig**). Two trends dominate this outcrop; one trend is best exposed on either of the two rock faces seen here. A small sampling (10 readings) of the joint trends was collected to compare with both the regional data (Monteverde and others, 2015) as well as a single well BTV data collected on Pine Street to the northeast (Herman and Curran, 2010) (**figure n**). Data from this stop clearly outlines two dominant fracture trends here. A more comprehensive collection of fractures throughout this quarry would have been better for the analysis but was put off to a future time due to access. Pine Street BTV data from both the Lockatong and Stockton (Herman and Curran, 2010) were reanalyzed using Stereonet version 9.8.3 (Allmendinger and others, 2013; Cardozo, and Allmendinger, 2013). Results here are slightly different than those of Herman and Curran (2010) as only two dominant trends were selected for comparison. Again comparing these two sites is not the best due to both their separation distance and that one samples both Lockatong and Stockton lithologies and the other is only within the Stockton and at a lower stratigraphic horizon. The dominant trend on both is separated by only 13 degrees along strike but with similar dips and dip directions. The secondary fracture from this stop was not recorded in the BTV data. Part of this discrepancy could be due to the lithologies as the Stockton is more commonly composed of micaceous sandstone, siltstone and mudstone near the Lockatong contact while medium to coarse grained sandstone dominates here.

A third more complete and regional database consisting of all data recorded in Lockatong and Stockton lithologies during regional field mapping (Monteverde and others, 2015) was used for comparison between the two smaller sampled and restricted locational data. Dominant trends between this stop and regional data correlate very well which again is close to the BTV trend. The secondary BTV trend compares fairly well with the regional trend. Finally, the strike of tertiary regional trend matches well with that of the secondary trend at the stop but dip in opposite directions. In the end the trends from the two restricted samples combined to match fairly well some of the regional trends. Lithologic variations can account for the absence of some of the regional trends in the BTV and this stop data. Also at play is the proximity to major structural features such as the Flemington fault of some regional data points.

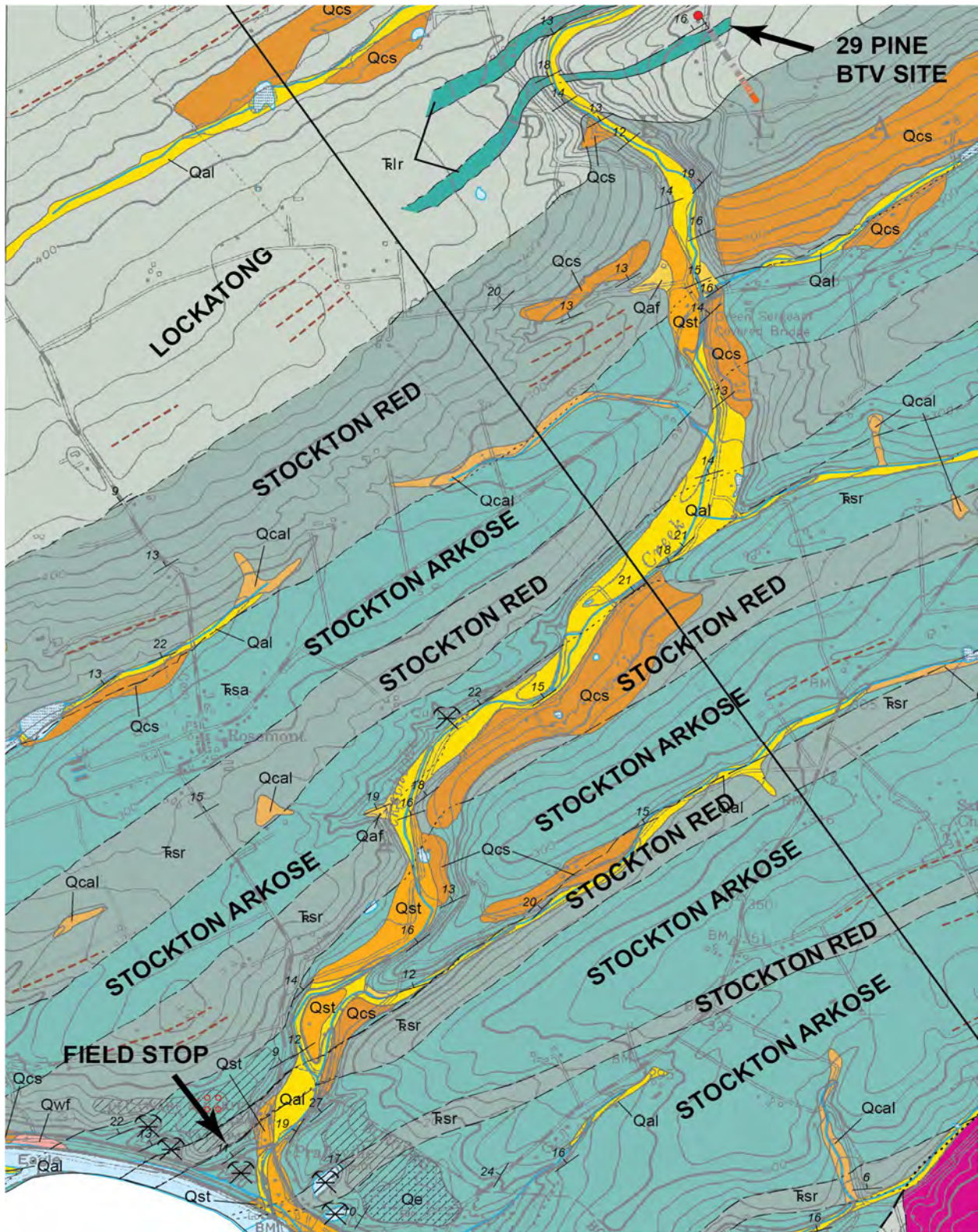


Figure 13: Geological map showing the location of this stop and the 29 Pine BTV. Note the 29 Pine HTV data has been projected to the surface to aid in delineating the Stockton-Lockatong contact. Map altered from Monteverde and others (2015).

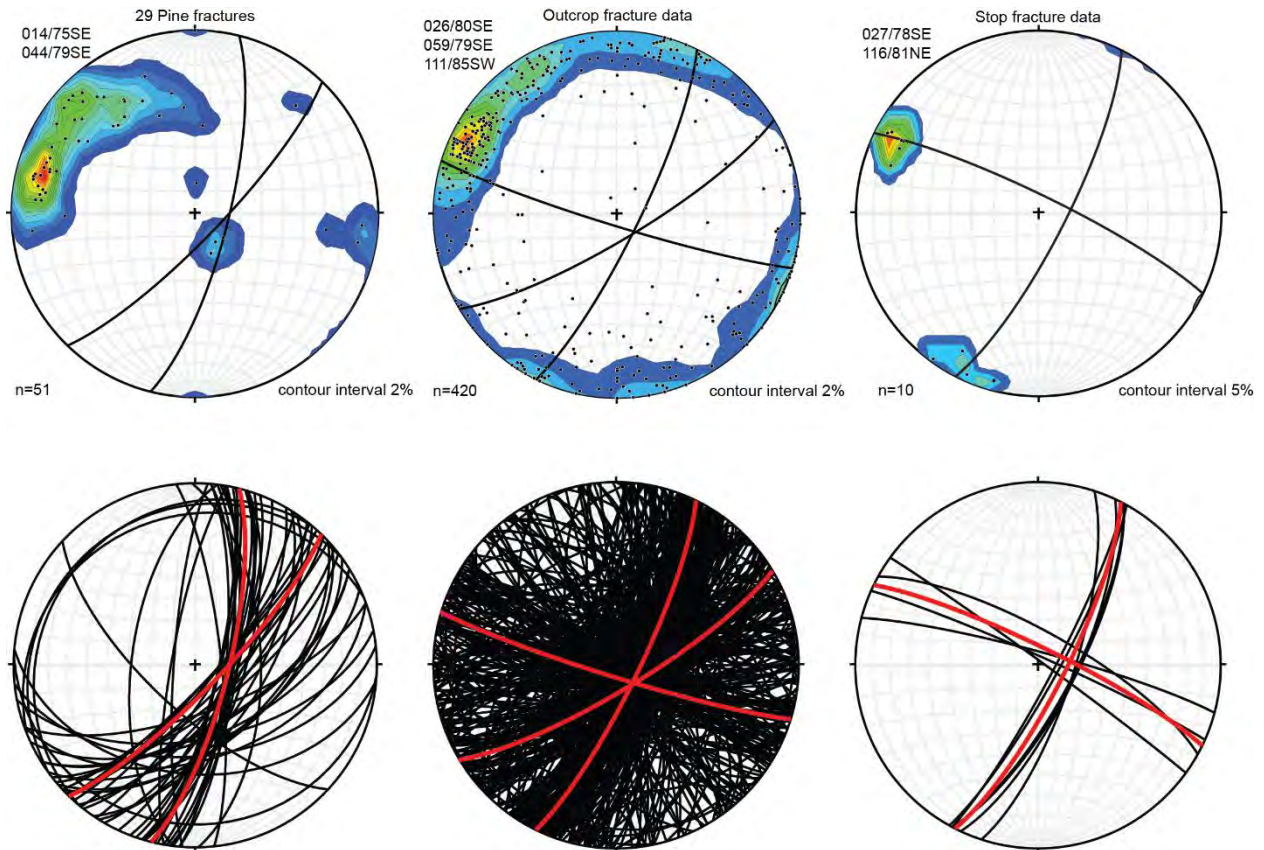


Figure 14: Fracture data from three different databases depicted at pole to planes (upper three plots), as well as, showing all planes (lower plots). Data is from three different sources including BTV logs of Lockatong and Stockton lithologies on the left labeled “29 Pine fractures” (Herman and Curran, 2010), regional data from both Lockatong and Stockton Formations recorded during regional mapping labeled “Outcrop fracture data” (Monteverde and others, 2015), and limited data collected from the Stockton here labeled as “Stop fracture data”. All data are plotted on lower hemisphere equal area stereonet diagrams using the Stereonet program version 9.8.3 (Allmendinger 2013; Cardoza and Allmendinger, 2013). Contour intervals of poles vary per plot and represent pole %/per 1% area. Black planes on upper stereonets represent maximum values as defined by contoured data. Values of planes are shown at top left of each plot. Maximum planes are reproduced on lower plot in red. Number of planes sampled on each stereonet is shown by n=number.

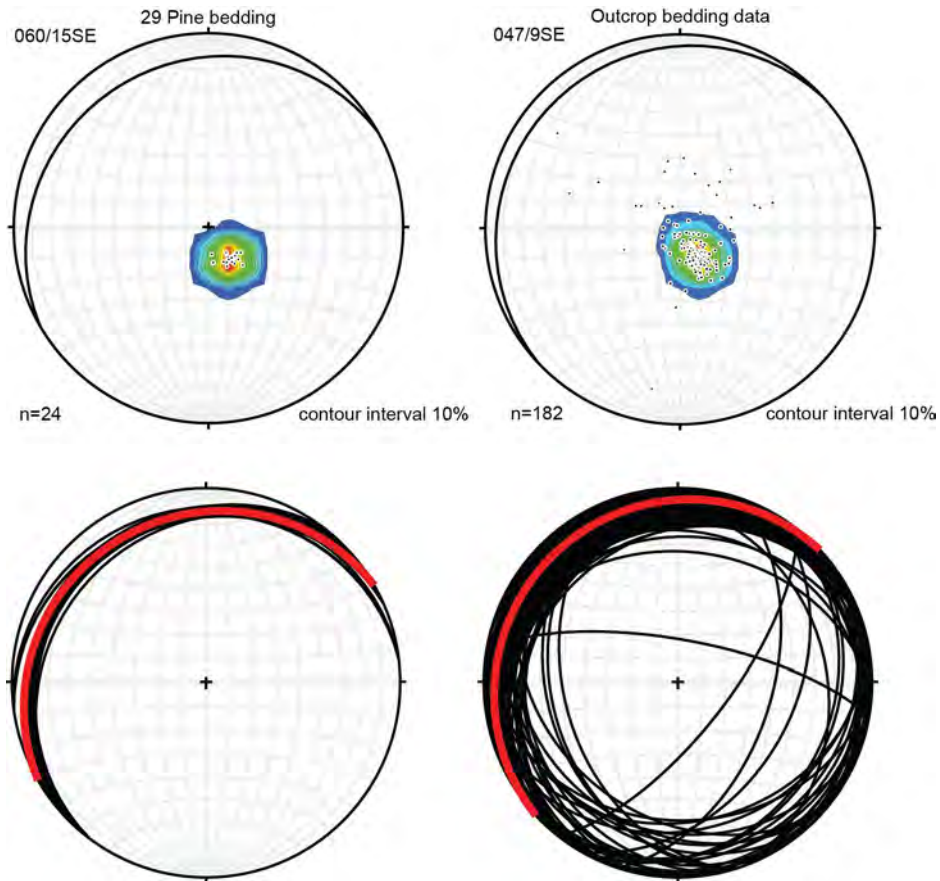


Figure 15: Bedding trends are only compared between BTV data and regional mapping data as this outcrop shows a considerable amount of channels. As can be seen both databases show a tight clustering of bedding orientations. Strike orientations are only 13 degrees.

References

- Allmendinger, R. W., Cardozo, N. C., and Fisher, D., 2013, *Structural Geology Algorithms: Vectors & Tensors*: Cambridge, England, Cambridge University Press, 289 pp.
- Cardozo, N., and Allmendinger, R. W., 2013, Spherical projections with OSXStereonet: *Computers & Geosciences*, v. 51, no. 0, p. 193 - 205, doi: 10.1016/j.cageo.2012.07.021
- Delaware and Raritan Canal Commission, Prallsville Mills: Delaware and Raritan Canal State Park, <http://www.dandrcanal.com/prallsville.html>, website accessed August, 2016.
- Gage, M., and Gage, J., 2005, *The Art of Splitting Stone: Early Rock Quarrying Methods in Pre-Industrial New England 1630-1825 (2nd Edition)*: Powwow River Books, 88p.
- Herman, G.C., and Curran, J.F., 2010, Borehole geophysics and hydrogeology studies in the Newark basin, New Jersey, Appendix 4, in, Herman, G.C., and Serfes, M.E., eds, *Contributions to the Geology and Hydrogeology of the Newark basin*, N.J. Geological Survey Bulletin 77, p. 4C1-4C4.
- Kümmel, H.B., 1897, The Newark System – Report of Progress: in *Geological Survey of New Jersey Annual Report of the State Geologist for 1896*, p. 25-88.
- Mohan, J.E., Ziska, L.H., Schlesinger, W.H., Thomas, R.B., Sicher, R.C., George, K., and Clark, J.S., 2006, Biomass and toxicity responses of poison ivy (*Toxicodendron radicans*) to elevated atmospheric CO₂, *Proceedings of the National Academy of Science*, v.03, n.24, p.9086-9089.
- Monteverde, D.H., and Herman, 2015, *Bedrock geologic map of the Elizabeth quadrangle, Essex, Hudson and Union Counties, New Jersey*, N.J. Geological and Water Survey, Geological Map Series, GMS 15-4, scale 1:24,000.
- Monteverde, D.H., Herman, G.C., and Stanford, S.D., 2014, *Geologic map of the Hopewell quadrangle Hunterdon, Mercer, and Somerset Counties, New Jersey*, N.J. Geological and Water Survey, Geological Map Series, GMS 14-1, scale 1:24,000.
- Monteverde, D.H., Herman, G.C., Stanford, S.D., and Spayd, S., 2015, *Geologic map of the Stockton quadrangle Hunterdon County, New Jersey*, N.J. Geological and Water Survey, Geological Map Series, GMS 15-1, scale 1:24,000.
- Pallis, T. 2012, *New Jersey Brownstone*. New Jersey Geological and Water Survey, Information Circular.
- Rea, F. R. in press. *Stockton, New Jersey and the Stockton Formation*. New Jersey Geological and Water Survey, Information Circular.
- Saja, B., 2012, *Quarrying in Raven Rock: in Stories from Raven Rock, New Jersey*, p. 132-135.
- Smoot, J., 2010, *Triassic Depositional Facies in the Newark Basin: in Contributions to the Geology and Hydrogeology of the Newark Basin*, v. 77, p. A4-A104.
- Strunk, K., 2008, *The Mills Complex: in Prallsville Mills and Stockton*, image.
- U.S. Geological Survey, 2015, *Mesozoic Basins: Geology of National Parks, 3D and Photographic Tours*, <http://3dparks.wr.usgs.gov/nyc/mesozoic/mesozoicbasins.htm>, website accessed August, 2016.
- Zdepski, M.J., 2002, *The Brownstone Quarrying Industry in New Jersey*, presented to the Society for Industrial Archaeology, Roebing Chapter, 22nd Annual Drew Symposium, Drew University.
- Ziska, L.H., Sicher, R.C., George, K., and Mohan, J.E., 2007, *Rising Atmospheric Carbon Dioxide and Potential Impacts on the Growth and Toxicity of Poison Ivy (Toxicodendron Radicans)*. *Weed Science*, Vol. 55, No. 4, pp.288-292.

Stop 3 – Lockatong Formation, Villa Victoria Brook, Ewing, NJ

Gregory Herman, Princeton Geoscience, Inc.

A 0.44-mile hike along a stream bank to see vertical, to slightly overturned beds in the Lockatong Formation.



Figure 1: Google Map overview (A) and Google Earth captured view (B) of STOP 3 in relation to the Delaware River and the GM-RACER/NAWC sites in North Trenton, NJ (see Chapter 5). There are very few places in the Newark Basin where sub-vertical beds are found, especially with slight overturning. I have only seen instances along the Flemington fault at Mine Brook Park in Flemington, NJ and here. The nature of the folding and shearing of these beds is questionable owing to the weathered and only fair exposure state of these natural outcrops. STOP 3 is located along the dark red line on the left side of (B) near the DRBC Parking Lot where the buses park.

Background

The NJ Geological & Water Survey (NJGWS) mapped the part of North Trenton where the GM-RACER and NAWC sites are located in the Pennington topographic quadrangle during COGEMAP (Owens and others, ref). Subsequent mapping was done during 1999 to 2001 at the NJGWS and as part of my dissertation at Rutgers where I studied the joints systems (extension fractures) that are so prevalent throughout the region (Herman, 1997, 2005). During that work, a series of vertical to slightly overturned

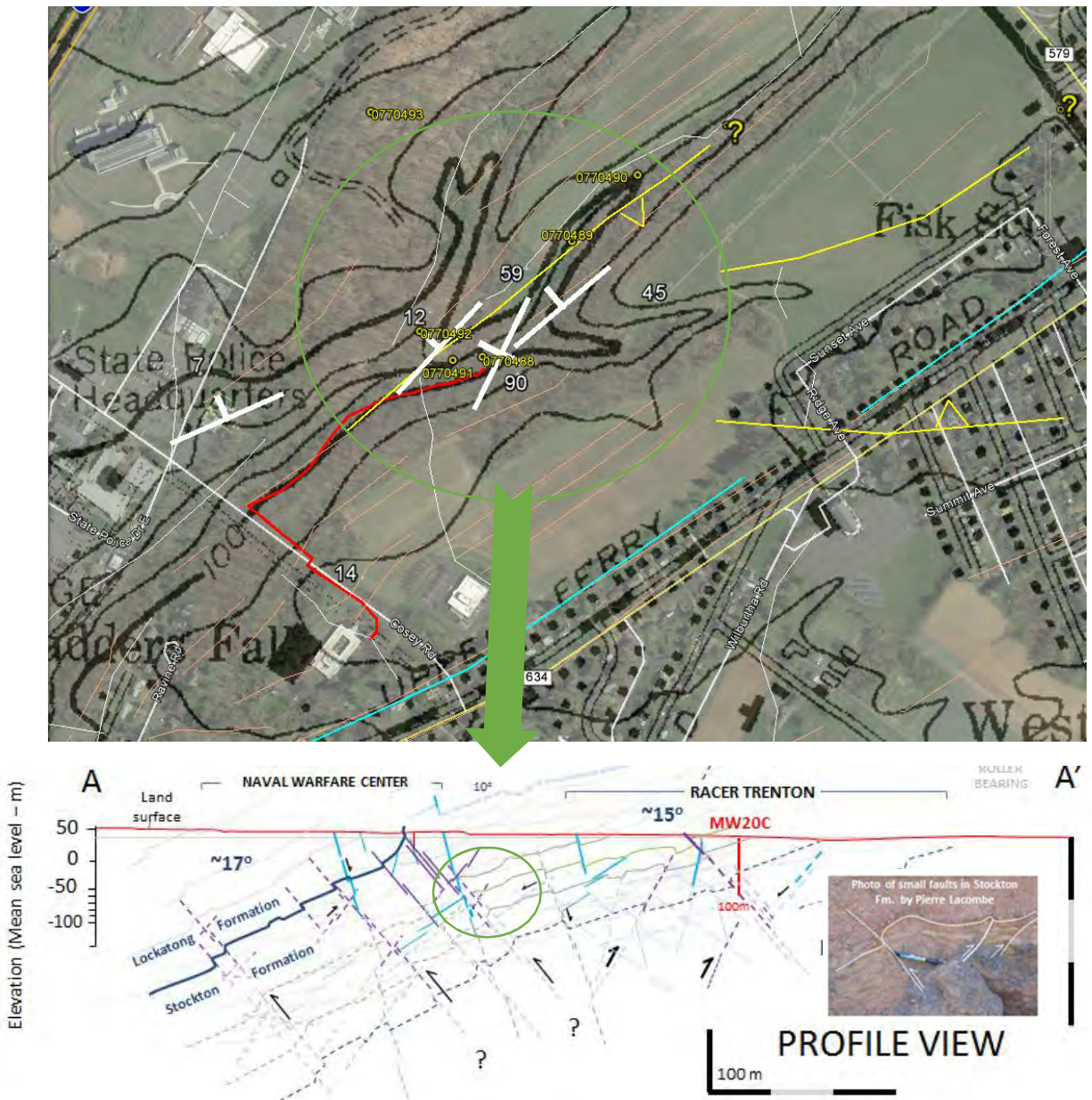


Figure 2: Top map shows bedding readings taken in outcrop along Villa Victoria Brook at STOP 3. The profile diagram at the bottom is taken from the nearby GM-RACER and NAWC studies (Chapter 5). Narrowly focused, vertical-dipping panels of rock seen here probably form along late-stage reverse faults.

SHALLOW SUBSURFACE GEOPHYSICAL APPLICATIONS IN ENVIRONMENTAL GEOLOGY GANJ XXXIII Annual Conference and Field Trip

shale beds were measured in the Brook running just east of the Delaware River as pictured in Figures 1 and 2. We will walk along the brook heading NE from the road for a distance of about 0.4 miles to where the vertically dipping beds of argillite occur as a series of weathered beds cutting across the drainage and locally forming the channel base where the stream bends and splits. This is not a particularly spectacular field stop. However, the woods are mature and there are some large, old, orange and yellow shelf fungus growing just off the beaten path along stream banks. There are a few poor exposures of bedrock close to the bridge, but we are going to walk upstream for about one-half mile without getting sidetracked in the lower reaches of the stream.

TO PROCEED TO STOP 3, get off the buses and wait for instruction on when and where to cross the road leading to the bridge crossing the brook. We descend from the road into the woods along the brook and trek upstream 0.44 miles in from the road where a series of yellowish-brown, grayish green and red silty argillite beds crop out in the stream beds. Very intense tectonism occurs here including slickensided shear planes and beds of varying orientations resulting from folding of Lockatong beds. Joints striking



Figure 3: STOP 3 is a series of natural outcrops in the stream beds of a tributary to the Delaware River that is informally referred to as Villa Victoria Brook in reference to the academy located near its mouth. Pictured from left to right is Pierre Lacombe (US Geological Survey) and NJ Geological & Water Survey personnel Michelle Kuhn, Mike Gagliano (GANJ President this year) and Katy Diaz. The rocks are in place just under the bank and waterline to the right where they're standing. My experience has been that fair exposures like these can result in exciting discussions because of the lack of certainty.

SHALLOW SUBSURFACE GEOPHYSICAL APPLICATIONS IN ENVIRONMENTAL GEOLOGY
GANJ XXXIII Annual Conference and Field Trip

060°, and 090° are most abundant with most sets having 2 to 3-meter trace lengths. The 090° set is weaker and curved between the other two sets. Otherwise gently NW-dipping beds are vertical here and perhaps slightly overturned. Bed readings taken in 1999 include ones dipping 70° southeast as tabulated below. The following data were collected on a day's traverse on October 5th, 1999 with Joe Smoot and Pierre Lacombe of the US Geological Survey. The data below are catalogued in the NJGWS field-data management system (Kaeding and Herman, 1985).

Table 1: Structural geological data collected at six stations around STOP 3.

STATION	FEATURE	DIP/DIP AZIMUTH	STATION	FEATURE	DIP/DIP AZIMUTH
0770488	Bed of yellow-brown silty argillite	56/317	0770492	Thin bed of gray argillite	7/313
	Healed joint spaced 5-25 /m	70/094		Open joint spaced 5-25 /m	70/320
	Healed joint spaced 5-25 /m	64/258		Healed joint spaced 1-2 /m	55/054
	Healed joint spaced 2-5 /m	35/174		Healed joint spaced 1-2 /m	50/214
	Shear plane	26/113		Healed joint spaced 2-5 /m	75/075
0770489	Bed of yellow-brown silty argillite	10/178	0770493	Beds of medium gray to greenish-gray silty and muddy argillite	25/000
	Bed of yellow-brown silty argillite	6/154			27/336
	Bed of red siltstone	31/308		Healed joint spaced 2-5 /m	72/155
	Healed joint spaced 5-25 /m	88/358		Healed joint spaced 5-25 /m	80/130
	Healed joint spaced 5-25 /m	73/094		Healed joint spaced 5-25 /m	80/310
	Healed joint spaced 5-25 /m	29/316		Healed joint spaced 5-25 /m	90/279
	Healed joint spaced 5-25 /m	48/343		Healed joint spaced 5-25 /m	90/314
	Healed joint spaced 25-50 /m	80/334		Healed joint spaced 2-5 /m	65/288
	Healed joint spaced 25-50 /m and 2-3 m trace lengths	80/154		Slickensided shear plane with normal slip lineation	16/142
0770490	Beds of very-thick laminated to thin- bedded red silty and muddy argillite.	32/327		Slickensided shear plane with slip lineation	10/143
		61/324		26/163	
	Healed joint spaced 5-25 /m	49/149	23/146		
	Healed joint spaced 2-5 /m	51/102			
0770491	Healed joint spaced 5-25 /m	60/358			
	Bed of gray silty argillite	20/292			
	Bed of gray silty argillite	70/140			
	Bed of gray silty argillite (OT)	7/313			
	Mineralized joint spaced 2-5/m	20/296			
	Healed joint spaced 5-25 /m	53/155			
	Healed joint spaced 1-2 /m	72/238			
Healed joint spaced 25-50 /m	87/240				
Healed joint spaced 5-25 /m	66/104				

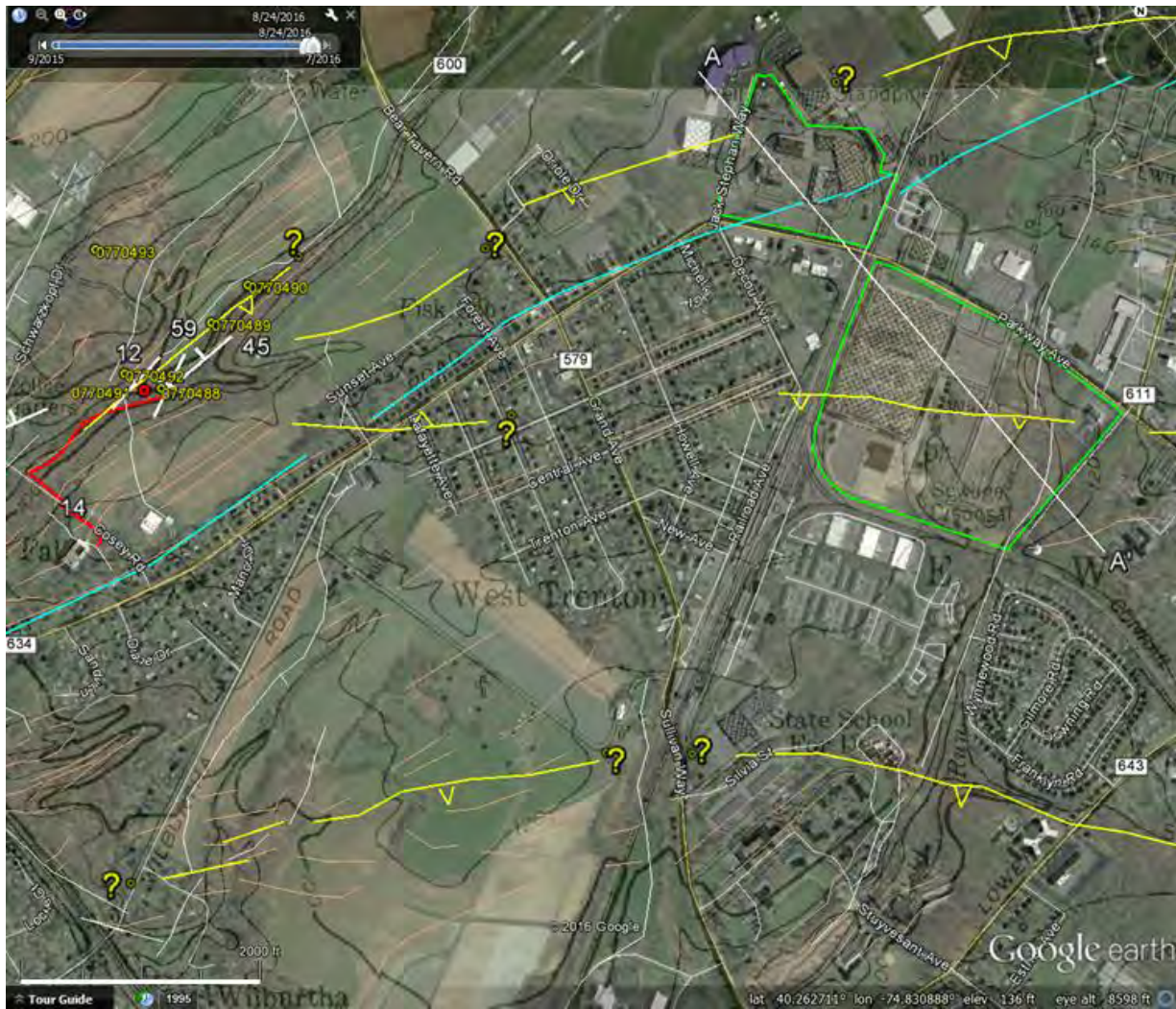


Figure 4: Google Earth captured view of STOP 3 in relation to cross section A-A' including the Pennington 7-1/2' topographic images as a transparent overlay. The lower left white line is 2000' long. The straight distance between the western NA WC boundary and STOP 3 is 0.8 miles.

References

- Herman, G. C., 1997, [Digital mapping of fractures in the Mesozoic Newark basin, New Jersey: Developing a geological framework for interpreting movement of groundwater contaminants:](#) Environmental Geosciences, v. 4, no. 2, p. 68-84.
- Kaeding, Margaret, and Herman, G. C., 1988, Field data management system (FMS); A computer software program for organization and analysis of geologic data: New Jersey Geological Survey Technical Memorandum 88-4, 48 p., 1 floppy disk.
- Owens, J. P., Sugarman, P. J., Sohl, N. F., Parker, R. A., Houghton, H. F., Volkert, R. A., Drake, A. A., Jr., and Orndorff, R.C., 1998, Bedrock Geologic Map of Central and Southern New Jersey, U. S. Geological Survey Miscellaneous Investigation Series Map I-2540-B, scale 1:100,000, 4 sheets.

Stop 4 – Naval Air Warfare Center, Ewing, NJ

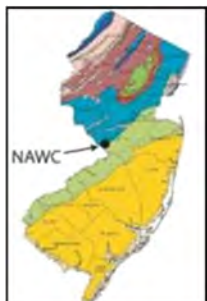
Pierre Lacombe, Thomas Imbrigiotta, Dan Goode, Alex Fiore, Claire Tiedeman
U.S. Geological Survey, Trenton, NJ and Menlo Park California

Stop 4 will be at Naval Air Warfare Center (NAWC), an active environmental investigation and remediation site, located in Ewing, NJ. The NAWC is also a U.S. Geological Survey Toxic Substances Hydrology Program contaminated fractured bedrock aquifer research site. This stop will provide an opportunity to see and discuss experimental approaches to contaminated site investigation and remediation. Cores of the underlying geology will be available for viewing and discussion.

The US EPA, State Departments of Environmental Protection, and industrial scientist in the environmental field consider contamination in fractured bedrock as one of the greater challenges for remediation. The US Geological Survey addressed this challenge with the development of the USGS Toxics Substances Hydrology Program to investigate remediation issues in fractured bedrock. The Naval Air Warfare Center (NAWC), near Trenton NJ, is a former military base where 1000s of gallons of trichloroethylene (TCE) leaked or were disposed during 1953-1990. The research site overlies fractured mudstones of the Newark Basin.

Research addressing contaminated fractured bedrock by governmental, academic, and industrial scientist has been conducted at the NAWC since 1992. Investigations include the geology, hydrogeology, hydrology, water chemistry, rock chemistry, biotic and abiotic degradation, biostimulation, surface and borehole geophysics, fate and transport issues, adsorption to minerals, volatilization, groundwater discharge, pump and treat, monitored natural attenuation, dig and haul, aquifer modeling, thermal conductive heating, diffusion sampler's, passive flux meters, electrical tomography, and many other methods, techniques, and tools.

The common theme for all research is the need for a well-defined natural laboratory with an extensive data base focusing on the hydrogeologic framework and long term water-level and water-quality. The focus of this presentation is the development of the hydrogeologic framework and the use of the framework in the multifaceted research and the applicability of framework development in other gently dipping fractured sedimentary bedrock settings.



Geologic map of New Jersey showing the location of the Naval Air Warfare Center about 3 miles north of Trenton NJ.

Stop 1: Road cut of Lockatong Formation, red mudstone of upper Prahls Island Member. Indurated road cut reveals many local hydrogeologic features. Intercalated massive mudstone and fissile mudstone are the gross features to be discussed. Indurated strata form the cap of small hill. Indurated strata here will be contrasted with fissile strata found at the former Naval Air Warfare Center located ½ mile away in adjacent lowlands near a small stream. Van Houten cycles will be identified and explained with respect to groundwater flow and hydrogeology. Hydrogeologic, biogeologic, mudcracks, desiccation breccia, orthorhombic micro fractures showing weathering rinds, strata-bound joint patterns, and punctuated flow paths in water- bearing strata as well as other hydrologic and geochemical features will be noted.



Figure 1: Road cut exposure of upper part of Prahls Island Member of Lockatong formation showing: (A) chemically altered micro fractures, (B) differentially weathered strata of Van Houten cycles (C) Strata bound joints and fissile and indurated strata, and (D) punctuated flow in a water bearing fissile strata.

Station A: History of the NAWC

During the late 1930's and prior to WWII, an auto parts manufacturing plant was located across the street from the Navy site. The auto plant closed down, retooled, and open 6 months later manufacturing Navy Avengers, a torpedo bomber prop plane. About 16,000 planes were built and flown from the Mercer County Airport to staging areas for the European and Asian Theater. At the end of WWII, the US captured German jet engine and rocket scientists and their research papers. The US used this new information along with British and American research data to construct the Navy's Jet Propulsion Laboratory. Jet engine tests at simulated high altitude, high latitude, and in cold weather required a heat transfer agent to chill intake air and fuel. TCE (trichloroethylene) was initially used as the heat transfer agent. TCE leaked onto land surface during 1953-93.



Figure 2: Air photograph of the former Naval Air Warfare Center.

Station B: Hydrogeologic Framework

The hydrogeologic framework was created from regional and local geologic maps, hydrogeologic concepts, Newark Basin Coring Project framework results (Olsen and Kent), rock cores, drillers, geologists, and geophysical logs, water-level and water-quality data. Lacombe wrote reports on the framework. See below

<http://pubs.er.usgs.gov/publication/wri984167>

<http://dx.doi.org/10.1111/j.1745-6592.2010.01275.x>

Basic framework: Byram and Nursery Road Members of the Lockatong Formation; cyclically deposited mudstones; strike- N60°E, dip- 27°NW (Figures 3 and 4).

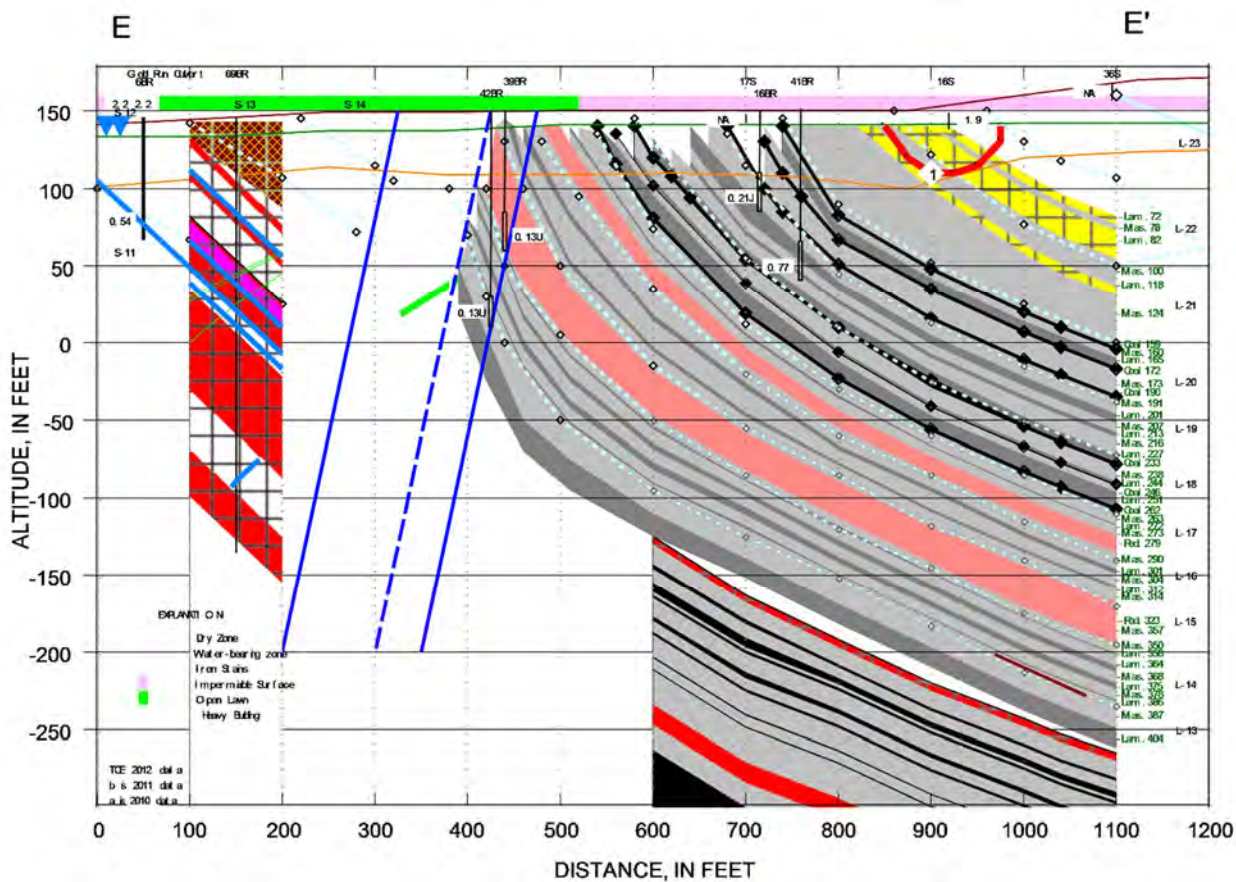


Figure 3: Section E-E' showing lithostratigraphy and gamma stratigraphy at the NAWC research site.

SHALLOW SUBSURFACE GEOPHYSICAL APPLICATIONS IN ENVIRONMENTAL GEOLOGY
 GANJ XXXIII Annual Conference and Field Trip

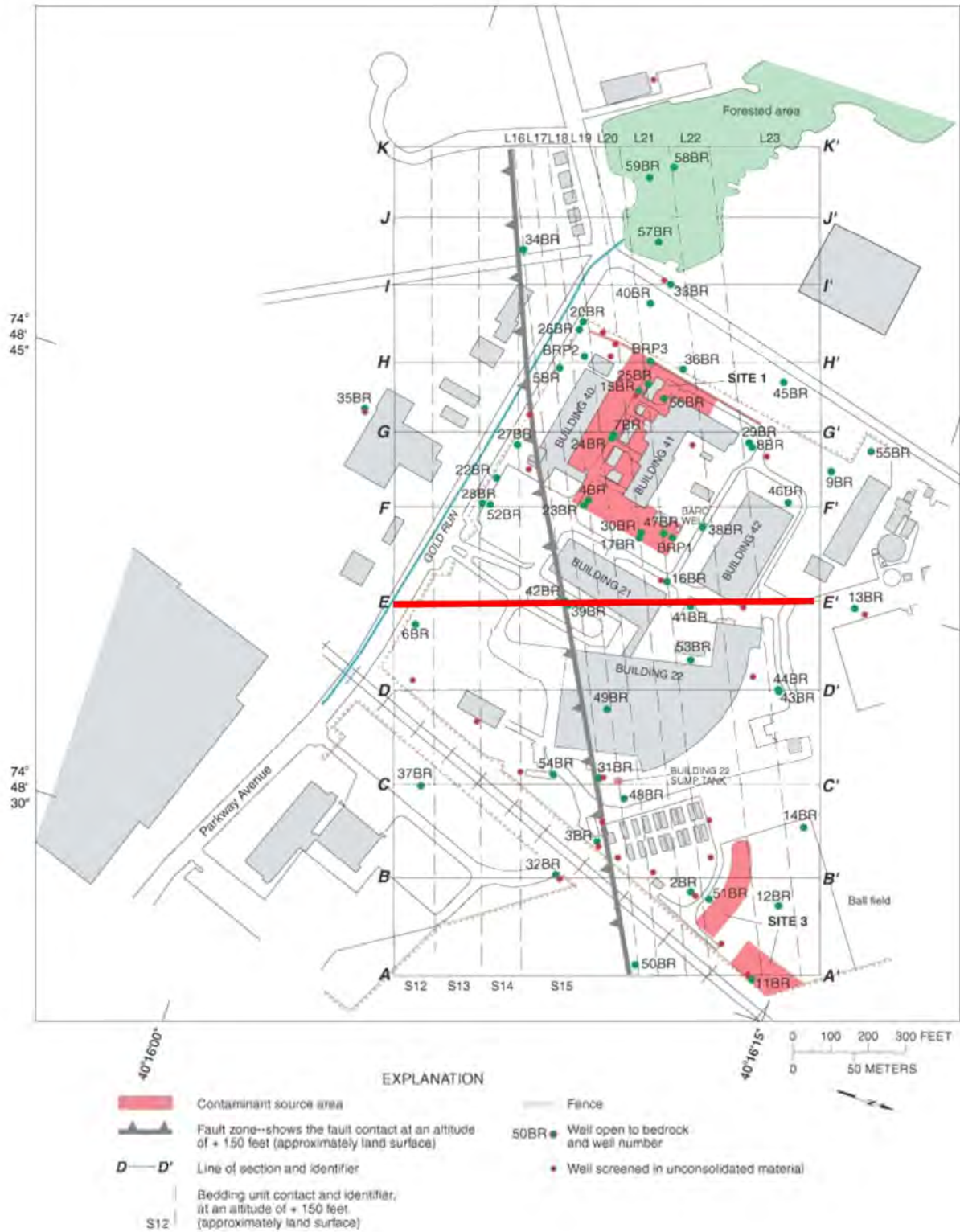


Figure 4: Map showing gamma stratigraphy of the NAWC fractured bedrock research site.

Station C. Pump and Treat System, Contaminant Containment

The P&T system began operations in 1995 with one recovery well. It expanded in 1998 to 14 potential recovery wells. Generally, 7 to 8 recovery wells are pumped to contain the CVOC plumes. System used air stripping and incineration during 1995-2007, and granulated activated carbon (GAC) stripping during 2007-2014 (Figures 5 and 6).

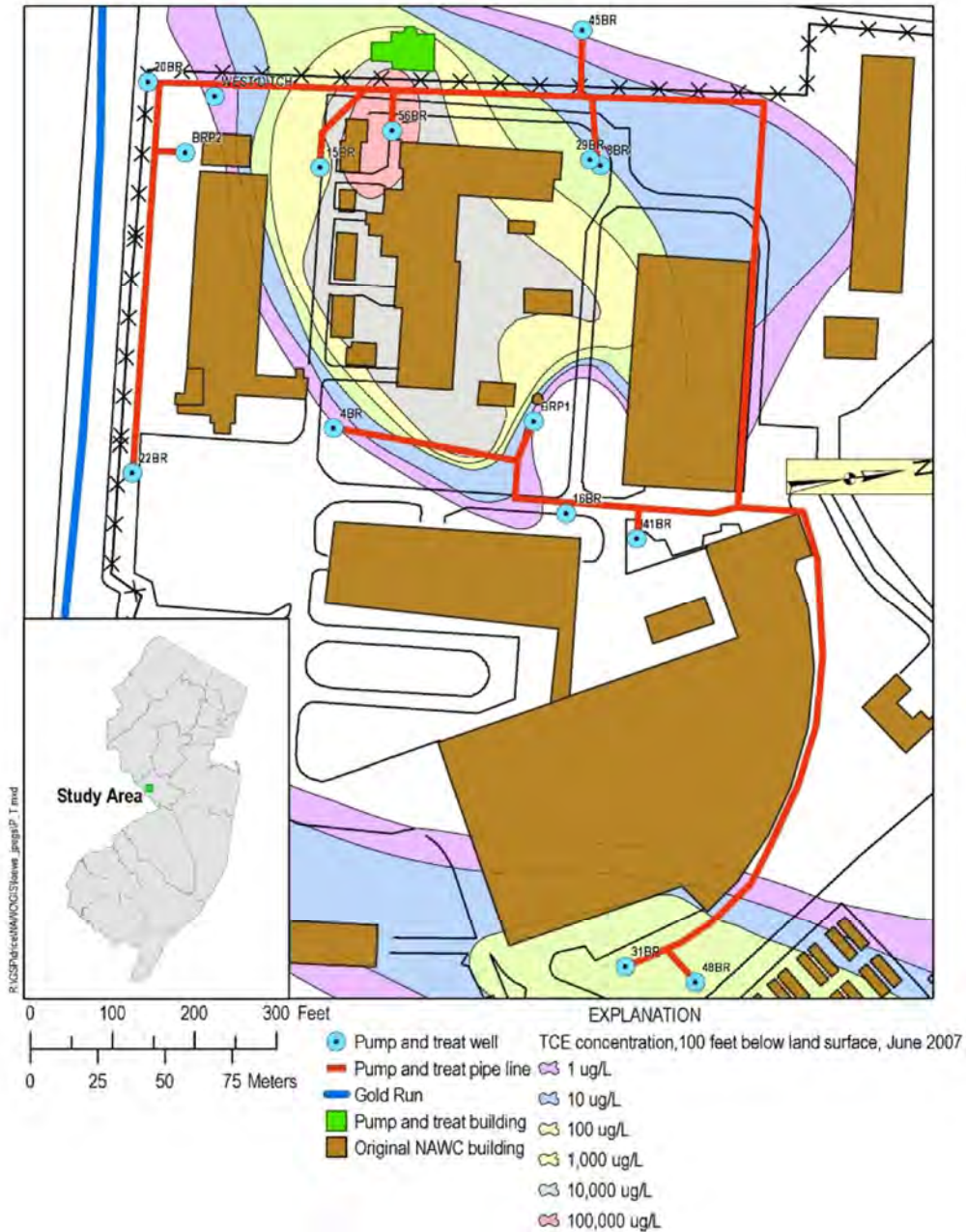


Figure 5: Maps showing the location of the P&T contamination containment system and major TCE plume at site.

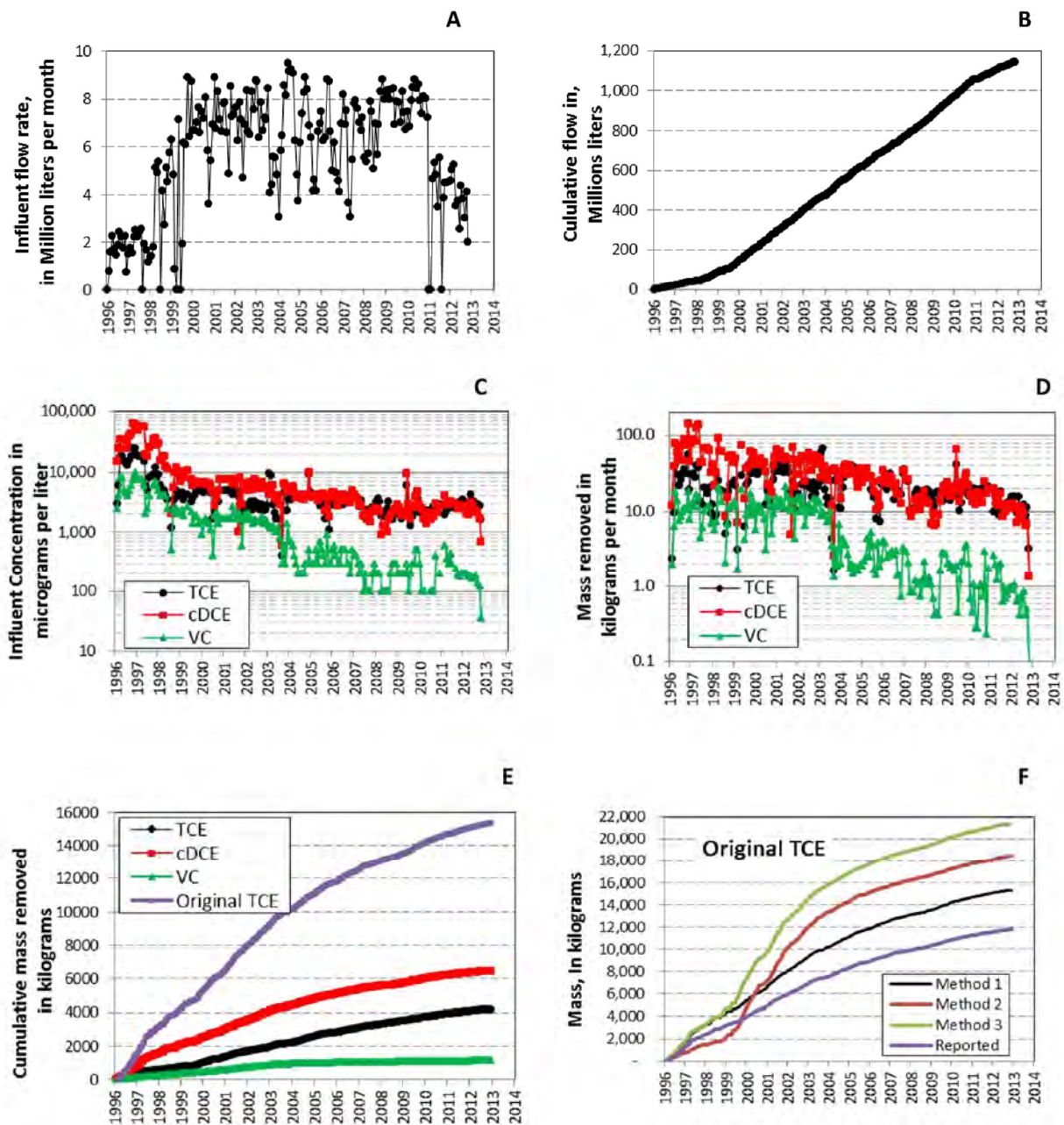


Figure 6: Figures for P&T plant (A) monthly influent flow rate, (B) Cumulative influent flow, (C) Monthly influent CVOC concentration, (D) Monthly CVOC removal rate, (E) Cumulative CVOC removal. Similar data were collected for each recovery well. (F) Analysis shows that as much as 21,500 kg of TCE has been removed.³

³ See <http://pubs.usgs.gov/sir/2011/5003/>

Station D: Rock Core Library

The NAWC toxics Rock Core Library consists of more than 2,000 ft of core from 20 wells. The core library also holds core from two nearby contamination sites. Core is used for strata identification, biotic and abiotic degradation rates, porosity measurement, mineral and chemical research.



Figure 7: Rock core used to research and teach about NAWC site geology and hydrogeology. Professor Lampousis and students from City College of NYC.

Station E Weathering of Rock Core



Figure 8: Rock core exposed to climate which induced physical, chemical, and biological degradation of core. Franklin Van Houten described chemical/detrital cycles in durated and fissile strata. Paul Olsen described Van Houten Cycles results of deposition changes as a result of water depth changes. Both researchers attribute changes to Milankovitch cycles.

Station F: Push-Push Technology site

Dr. Charles Schaefer and team, from CB&I (formerly Shaw Environmental) is in the initial phase of research entitled 'Rapid Assessment of Remedial Effectiveness and Rebound in Fractured Bedrock'. *The overall objective is to evaluate the use of "Push-Push" remedial assessment technique, coupled with compound specific isotope analysis (CSIA), for use as a rapid and cost-effective means to assess the limits of in situ remediation on long-term groundwater quality.* This evaluation will be most relevant to evaluating the extent to which biological and chemical amendment delivery (e.g., biostimulation, chemical oxidation) can reduce groundwater concentrations for a given contact time and/or dosage. By carefully evaluating amendment distribution, rebound (in chlorinated solvent and isotopic signature), and isotopic analysis in both transmissive and low permeability zones, limits to remedial success will be identified early in the process, and the potential for contaminant rebound will be assessed without the need for long term and costly testing.

Coring began in 2014. For full information please visit: [http://www.serdp-estcp.org/Program-Areas/Environmental-Restoration/Contaminated-Groundwater/Persistent-Contamination/ER-201330/ER-201330/\(language\)/eng-US](http://www.serdp-estcp.org/Program-Areas/Environmental-Restoration/Contaminated-Groundwater/Persistent-Contamination/ER-201330/ER-201330/(language)/eng-US)

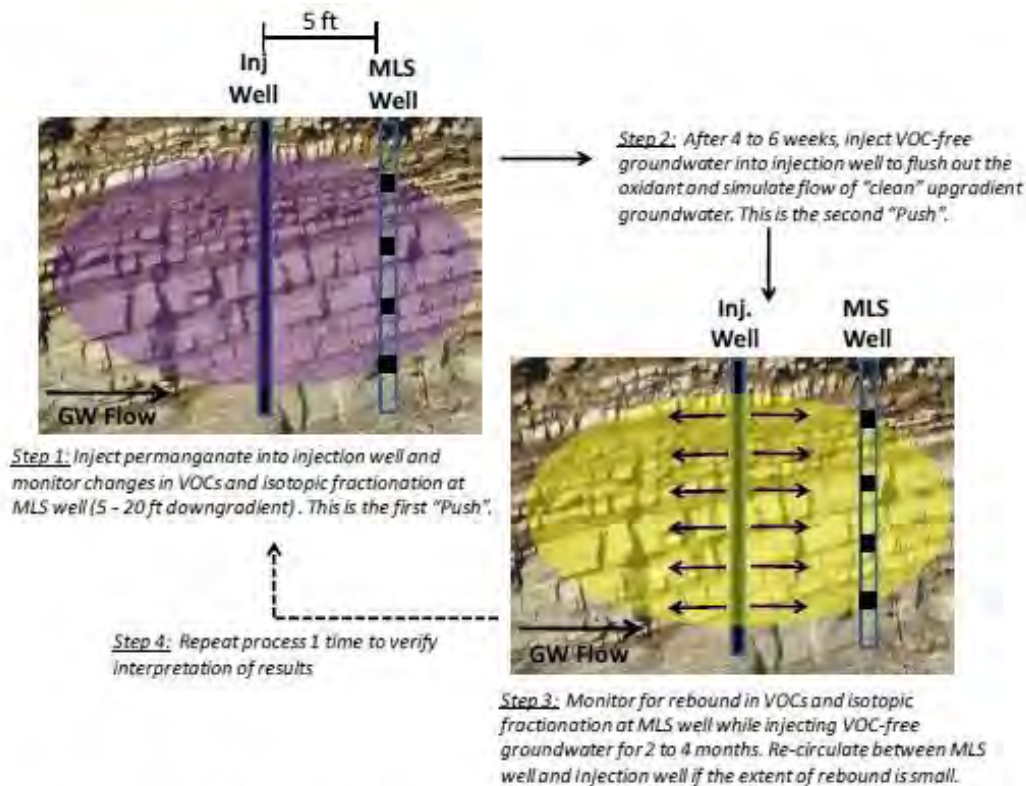


Figure 2. Conceptual methodology for the proposed Push-Push testing. For simplicity of illustration, flow that is limited to conductive fractures is not shown, but rather a simplified homogeneous flow regime. The distance between the injection and MLS well may be increased depending upon the groundwater velocity and fracture porosity.

Figure 9: Figure from Charles Schaefer showing the method of Push-Push Technology

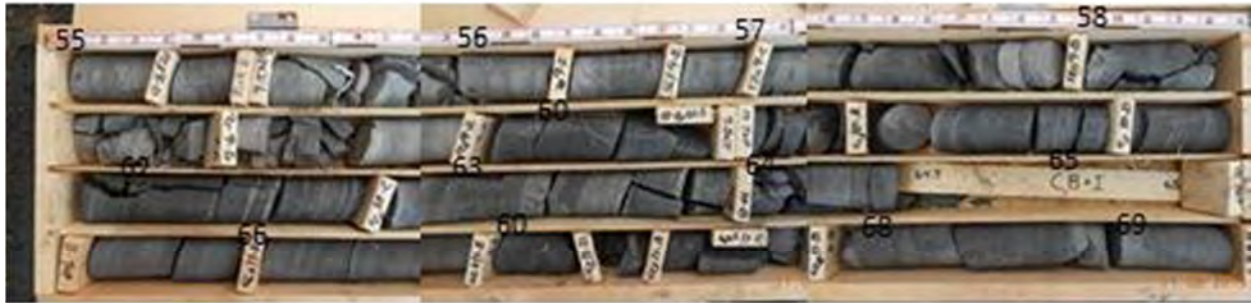
Station G: Coupled Diffusion and Abiotic Reaction of Trichloroethylene in Minimally Disturbed Rock Matrices

Dr. Charles Schaefer and team from CB&I (formerly Shaw Environmental) assessed abiotic degradation of chlorinated solvents near ferrous minerals. TCE abiotically degrades to acetylene. Rock core samples were collected during coring 90BR. Pyrite and marcasite rich rock core were selected, hermetically sealed, and then analyzed for acetylene.

For this significant work, *Dr. Schaefer received the 2013 SERDP Project-of-the-Year Award for Environmental Restoration.*

For more information see: <http://dx.doi.org/10.1021/es400457s>

90BR 55.0 to 69.4 ft



90BR cored for Charles Schaefer

90BR 69.4 to 83 ft



Figure 10: Rock core containing massive and disseminated sulfide minerals where abiotic TCE degradation occurs.

Station H: Comparison of Pump-and-Treat, Natural Attenuation, and Enhanced Biodegradation to Remediate Chlorinated Ethene-Contaminated Fractured Rock Aquifers

Dr. Allen Shapiro and team from the USGS.

The objective of this project is to evaluate and compare CVOC removal and destruction from the well-characterized NAWC site by three remediation technologies—P&T, MNA, and EB—and to better understand the hydrogeologic and biogeochemical mechanisms that control contaminant removal by P&T and destruction by MNA and EB in fractured rock.

For more information, see:

[http://www.serdp-estcp.org/Program-Areas/Environmental-Restoration/Contaminated-Groundwater/Persistent-Contamination/ER-1555/ER-1555/\(language\)/eng-US](http://www.serdp-estcp.org/Program-Areas/Environmental-Restoration/Contaminated-Groundwater/Persistent-Contamination/ER-1555/ER-1555/(language)/eng-US)

SHALLOW SUBSURFACE GEOPHYSICAL APPLICATIONS IN ENVIRONMENTAL GEOLOGY
 GANJ XXXIII Annual Conference and Field Trip

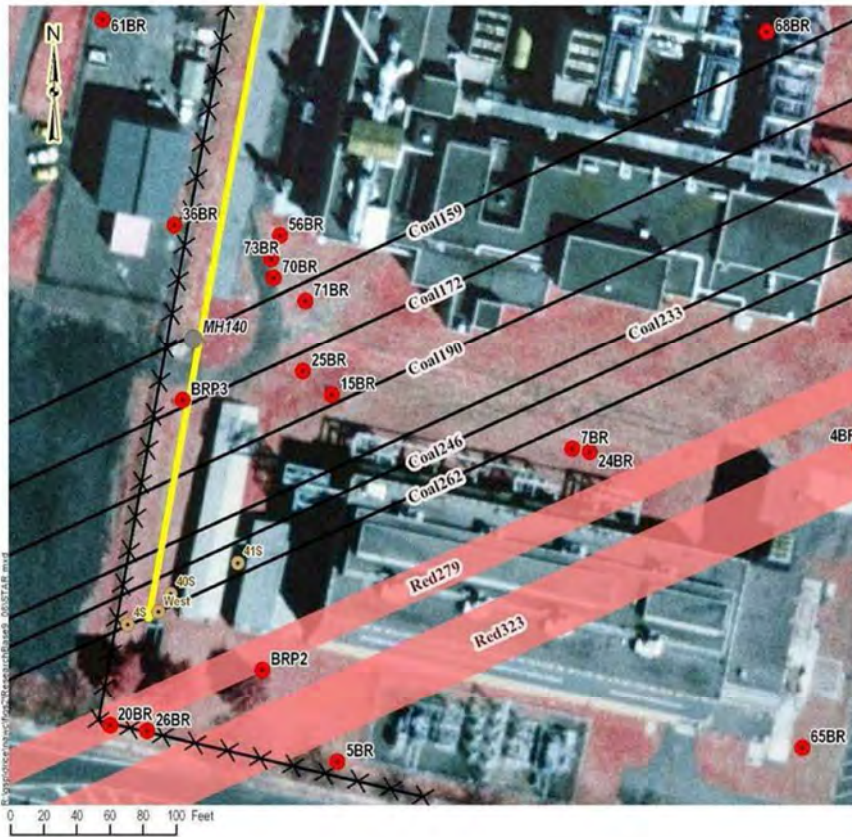


Figure 11: Map and section showing P&T, MNA, and EB research site with subcrops zones of black, carbon-rich fissile and red siliceous indurated mudstones. Well 15BR is recovery well, well 36BR is injection well, and other wells are observation wells.

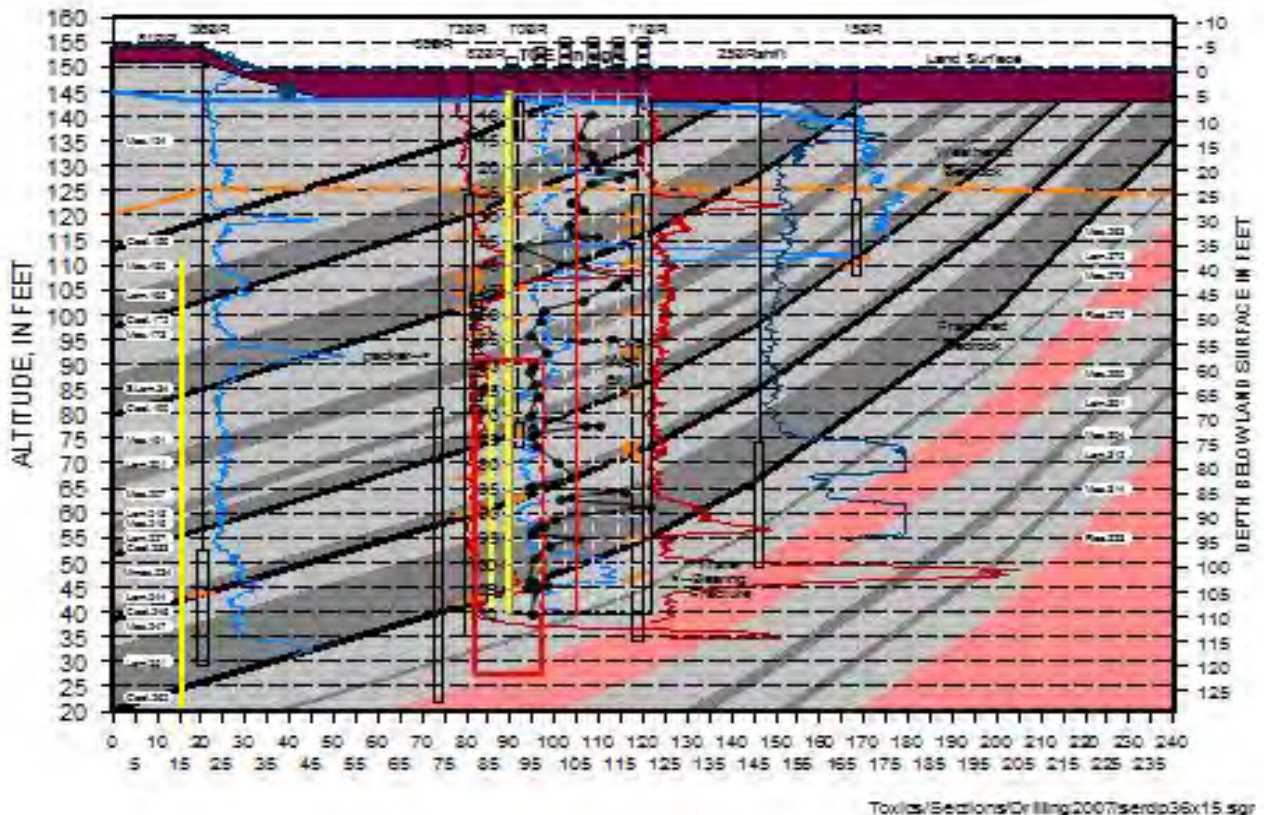




Figure 12: **A)** Photo of Shapiro/USGS P&T, MNA, and EB research Site, **B)** Photo of bags filled with EOS to be injected into research well 36BR

To date the research involves coring strategically located wells between a highly contaminated deep well and a shallow P&T recovery well. Researchers conducted multiple well shutdown tests and site scale flow simulation in fractured rocks. See report by Claire Tiedeman <http://dx.doi.org/10.1111/j.1745-6584.2009.00651.x>

Researchers evaluated MNA rates and many other aspects of bioactivity at the NAWC. See reports by Chapelle and by Bradley at the NAWC bibliography web site <http://toxics.usgs.gov/bib/bib-NAWC.html>

Pump and Treat component of research has been discussed above. EB research involved a bromide injection test that was followed by an EOS and dehalococoides (DHC) injection and observations of response to the injection (Figure 12).

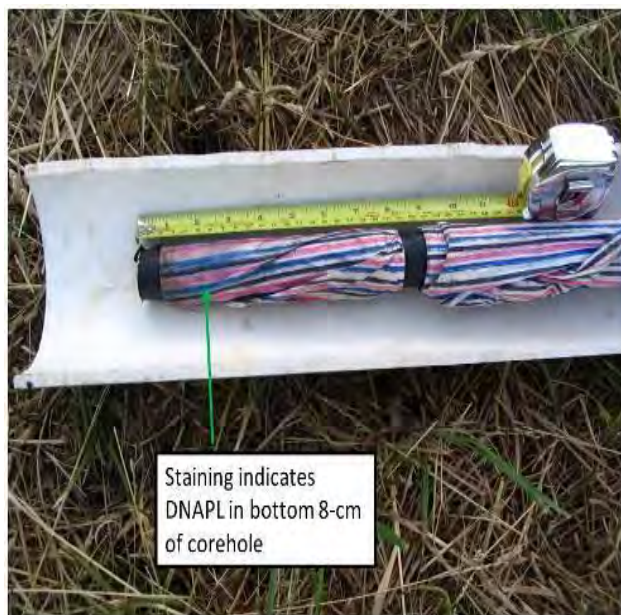


Figure 13: DNAPL TCE which caused bleeding of cloth

During coring for this research activity, DNAPL CVOC sensitive cloth was placed in the core hole each night. DNAPL TCE was detected via the bleeding of special dyes on the cloth (Figure 13) and via a shake kit.

Rock core sections were analyzed for adsorbed and adsorbed CVOC. Dan Goode, Thomas Imbrigiotta, and Pierre Lacombe will present findings of this effort at the GSA Northeast Region conference this week. CVOC concentrations in core from hole 70BR are color coded (Figure 1) and shown on the rock core (Figures 14a, b and, c).

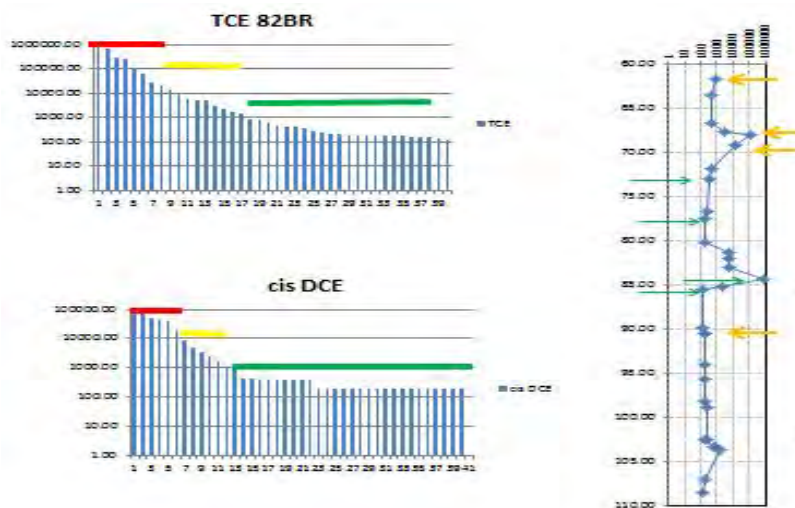
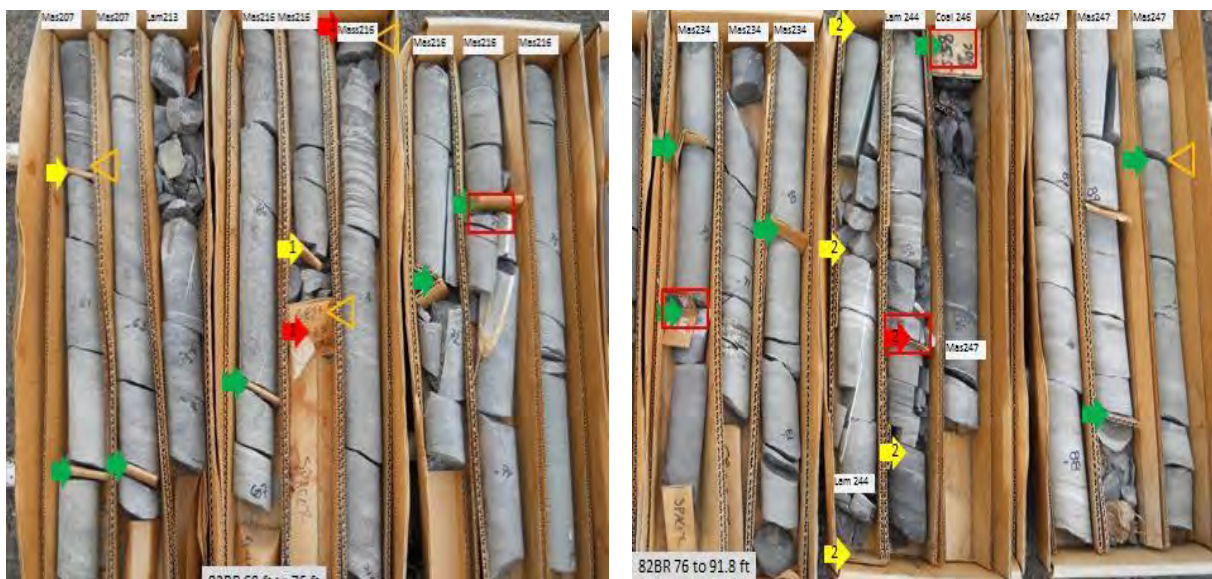


Figure 14a: TCE and cDCE concentrations ranked from most to least contaminated and color coded in corehole 82BR

Figure 14b: TCE concentration vs depth in corehole 82BR

Figure 14c: Rock core and rock type showing color coded concentrations



Station I: Thermal Conductive Heating Research Site

Carmen LeBron (US Navy) and TerraTherm Inc., a thermal remediation and research firm, conducted this investigation. The objective of this research was to demonstrate and validate Thermal Conductive Heating (TCH) performance in fractured bedrock and develop guidelines for practitioners on how to apply TCH. Specific objectives for the on-site TCH demonstration included: 15 heating/recovery wells and 8 research wells were installed in 30 ft diameter area to a depth of 55 ft BLS. Strata were heated to +100oC and kept at that temperature for about 60 days.

Results of the survey are published in: <http://www.serdp.org/content/download/18746/206355/file/ER-200715-FR.pdf>

SHALLOW SUBSURFACE GEOPHYSICAL APPLICATIONS IN ENVIRONMENTAL GEOLOGY
 GANJ XXXIII Annual Conference and Field Trip

Results of this thermal research indicated that 65 to 70% of the CVOC adsorbed and absorbed to the rock minerals and primary porosity was removed. Drilling and coring methods that reduce fracture generation would improve mass removed.

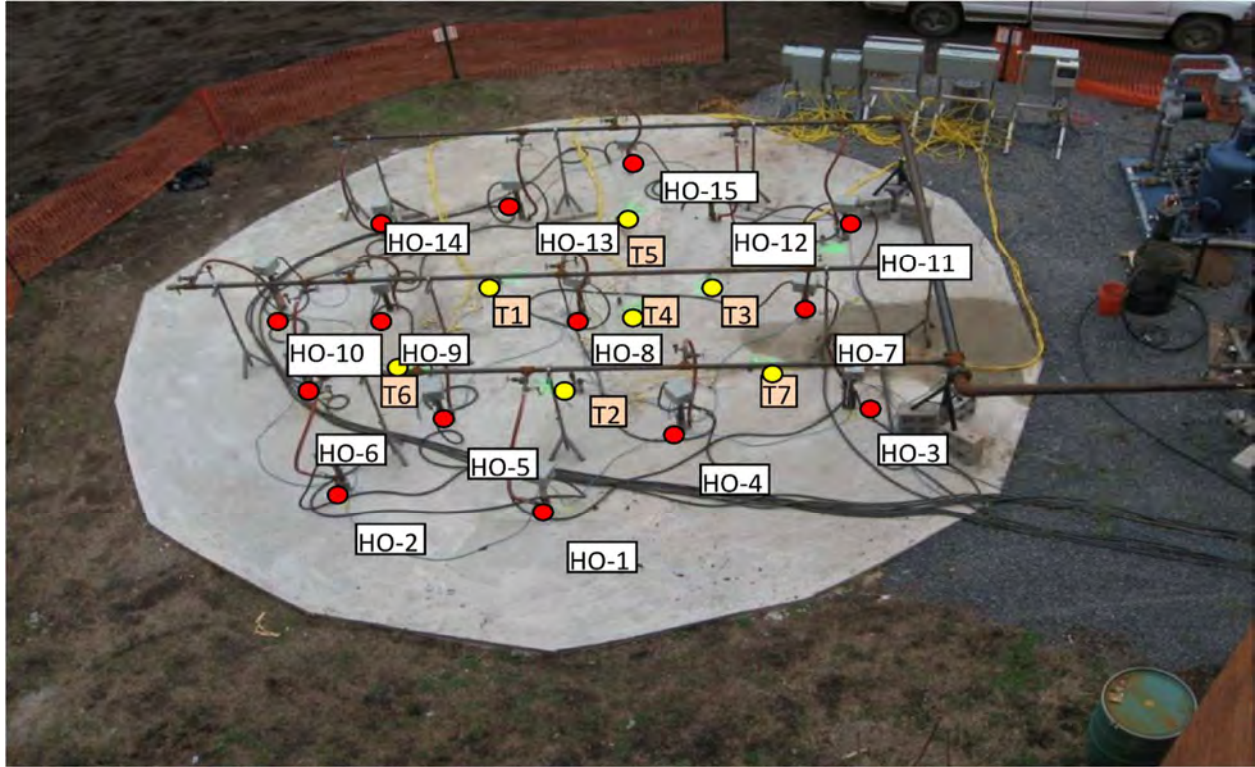
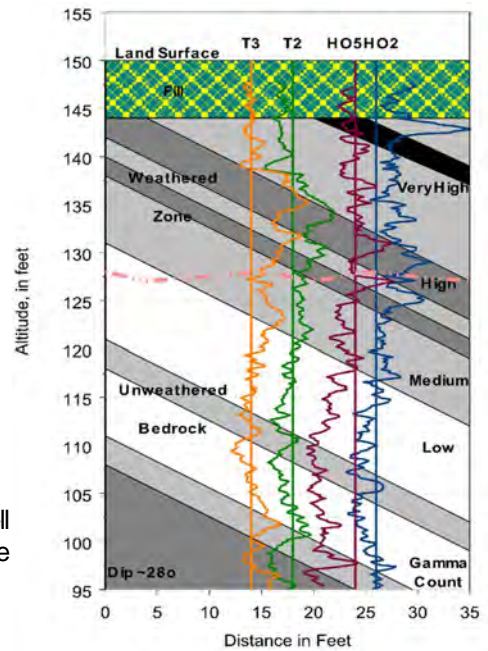


Figure 15: Thermal conductive research site with 15 heating wells (HO) and 8 observation wells (T).



Figure 16: A) Infrared photograph of Thermal Conductive Heating well array. Photo at night showing hot recovery and cold recovery pipe sections.



B) Preliminary gamma stratigraphy map of TCH site.

Station J: First recognition that contamination was following strata down dip.

Section F-F': Well Pair 4BR--23BR - shallow well contaminated, deep well uncontaminated.

Well Pair 30BR--17BR - shallow well uncontaminated, deep well contaminated.

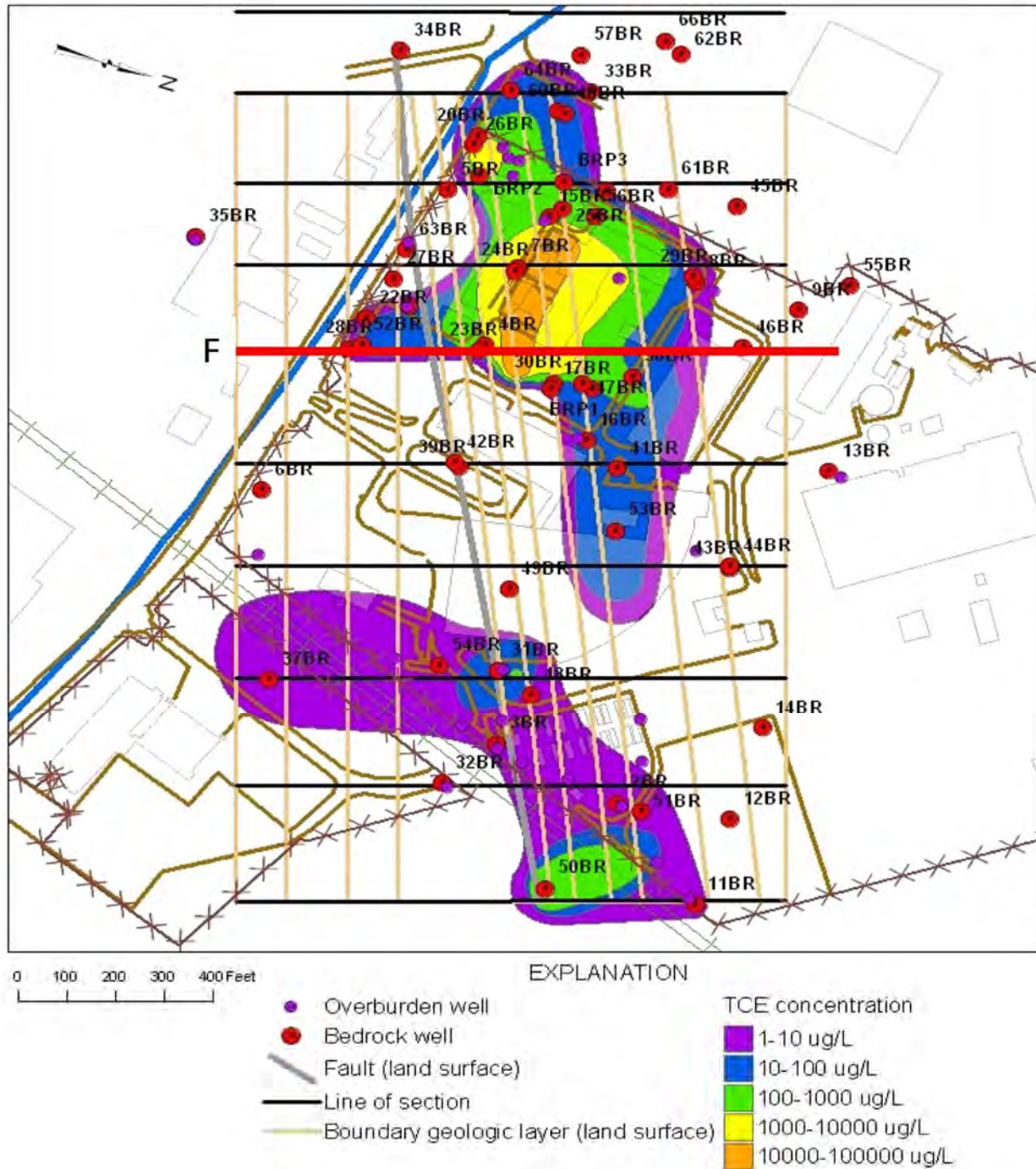


Figure 17: Map showing section F-F' TCE contamination plume near land surface and location

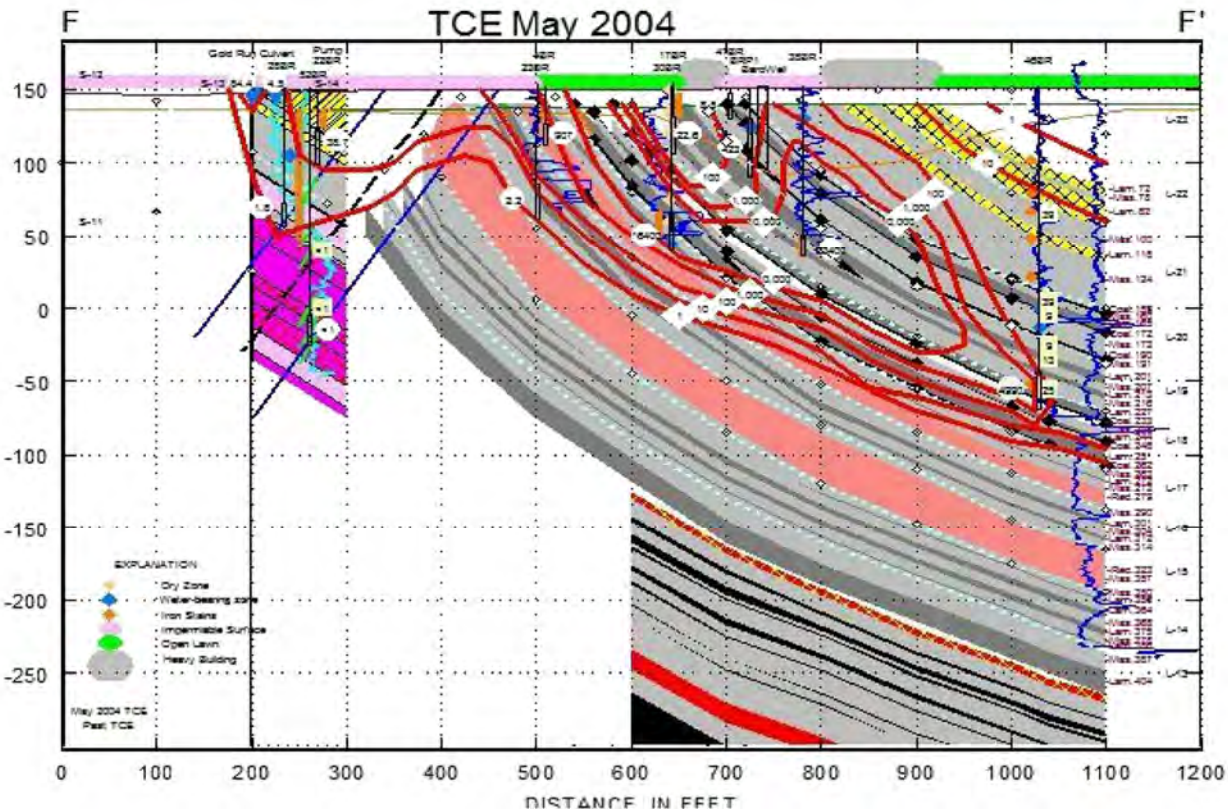


Figure 18: Section showing section F-F' TCE contamination plume near land surface and location

Station K: Groundwater level recorder

A network of 5 to 20 continuous groundwater level recorders is located at the NAWC. The Navy conducts an annual water level synoptic of the 110 wells at the NAWC each year. Data are contoured in section and Map views to show potentiometric surface in the high k Fractures.

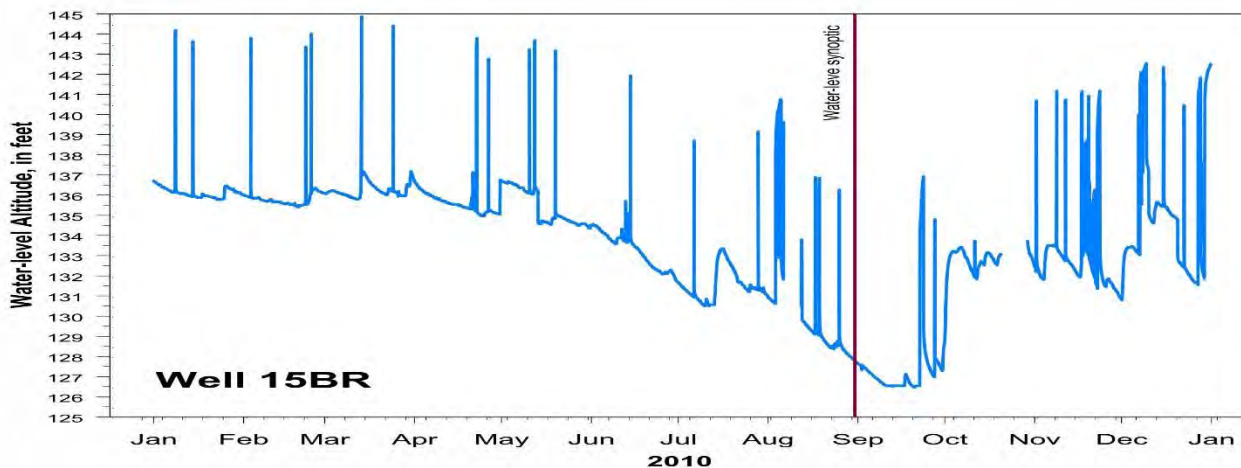


Figure 19: Water-level hydrograph for recovery well 15BR showing stress and unstressed water levels

Station L: Demonstration of a Fractured Rock Geophysical Toolbox for Characterization and Monitoring of DNAPL Biodegradation in Fractured Rock Aquifers

Dr. Lee Slater and PhD candidate Judy Robinson of Rutgers University Newark. The overall objective of this project is to demonstrate a method for characterization and monitoring of dense non-aqueous phase liquid (DNAPL) biodegradation (including free and dissolved phase) in fractured rock aquifers based on a fractured rock geophysical toolbox (FRGT).

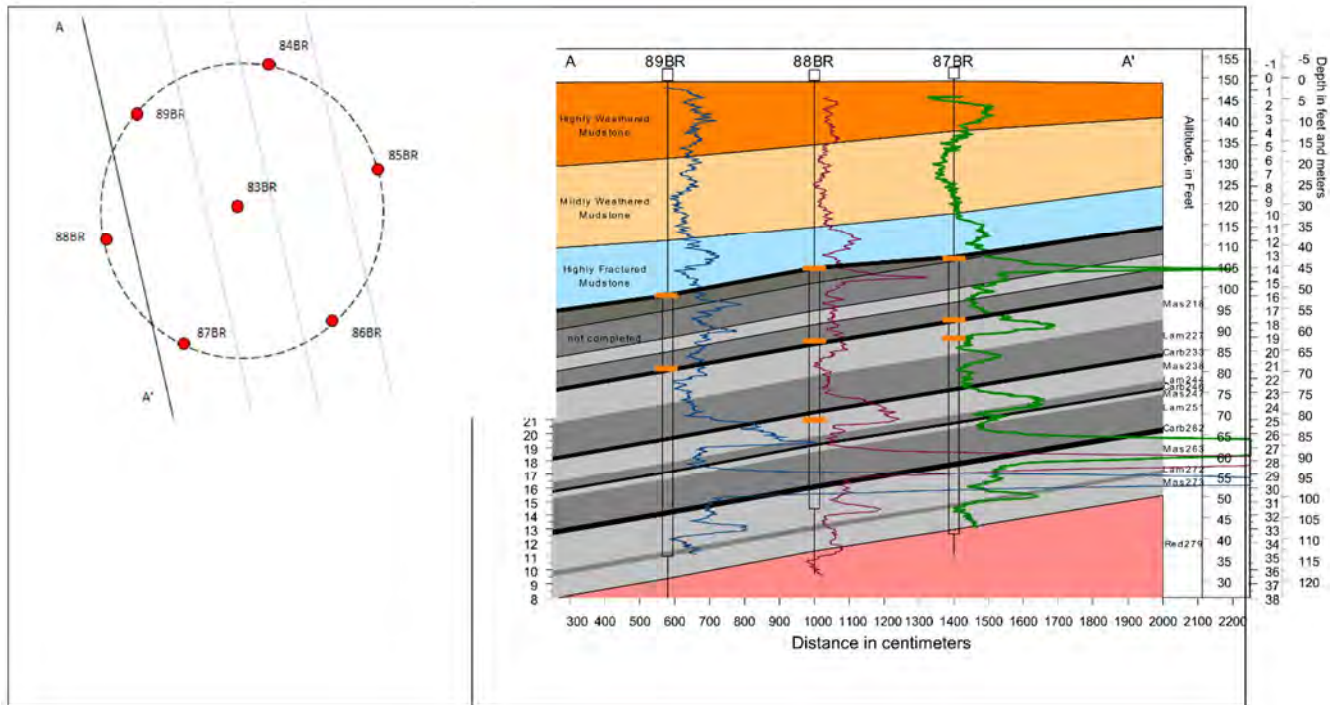


Figure 20: A) Map and B) section of wells used for Geophysical Toolbox research, C) Electrode array, below.



SHALLOW SUBSURFACE GEOPHYSICAL APPLICATIONS IN ENVIRONMENTAL GEOLOGY

GANJ XXXIII Annual Conference and Field Trip

Rock core samples were collected from 7 core holes to determine the mass of sorbed CVOC.

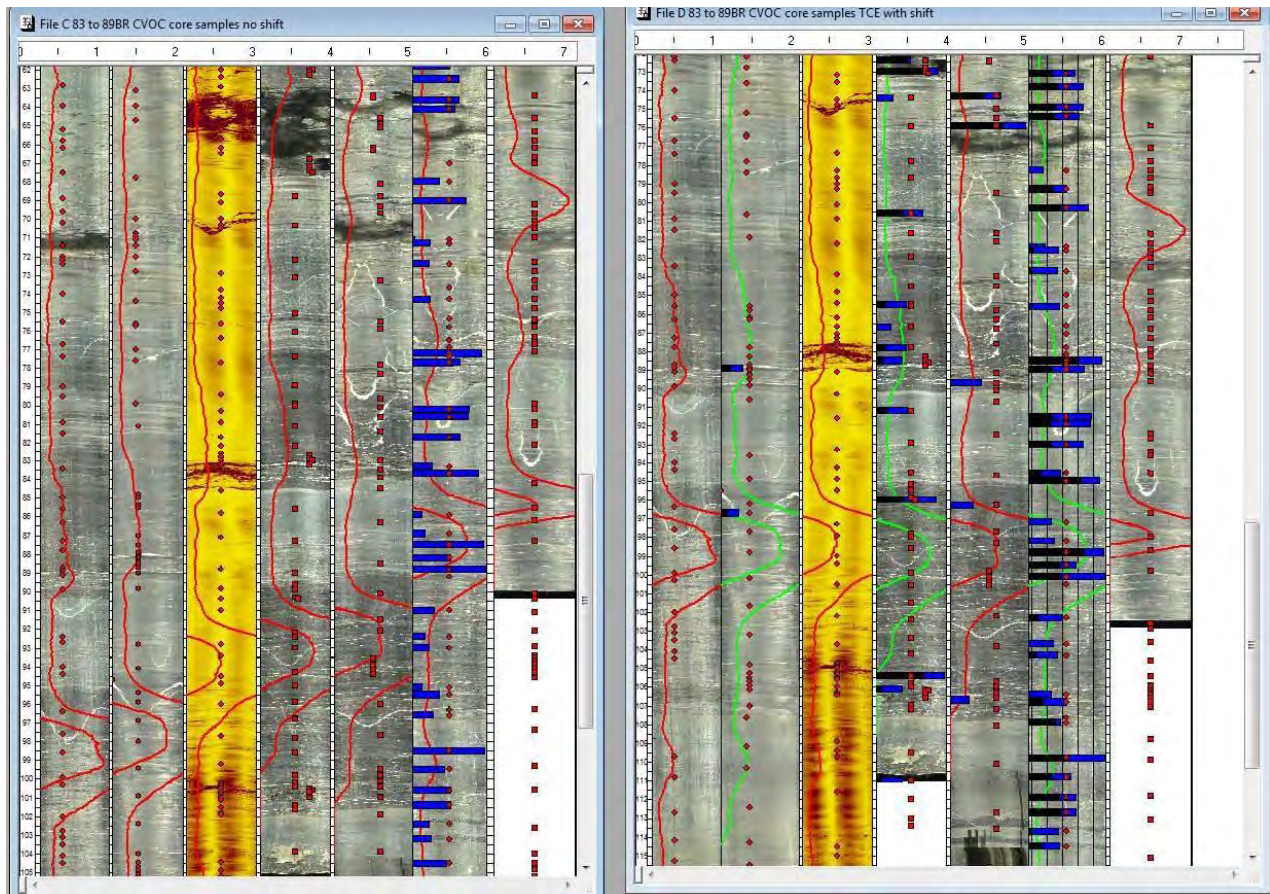


Figure 21: OBI logs with core sample locations (red dots) in depth below land surface, blue bars are CVO concentration available to date. B) Same logs but strata correlated.

Station M: Framework concepts

Integration of three strata. Dipping bedding strata, horizontal weathering strata, horizontal lithostatic pressure strata; when combined the three strata create concepts for fractured bedrock stratigraphy.

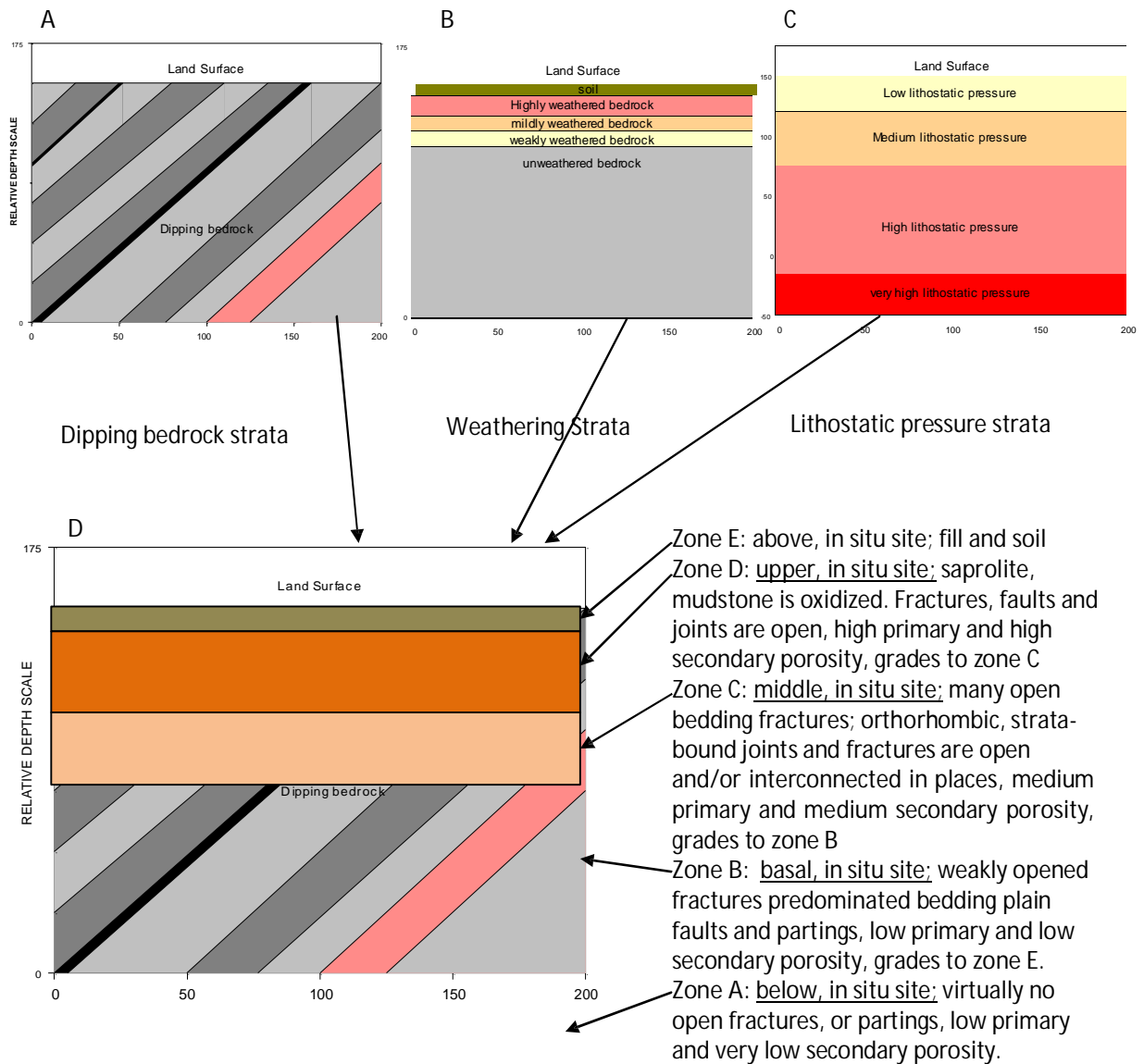
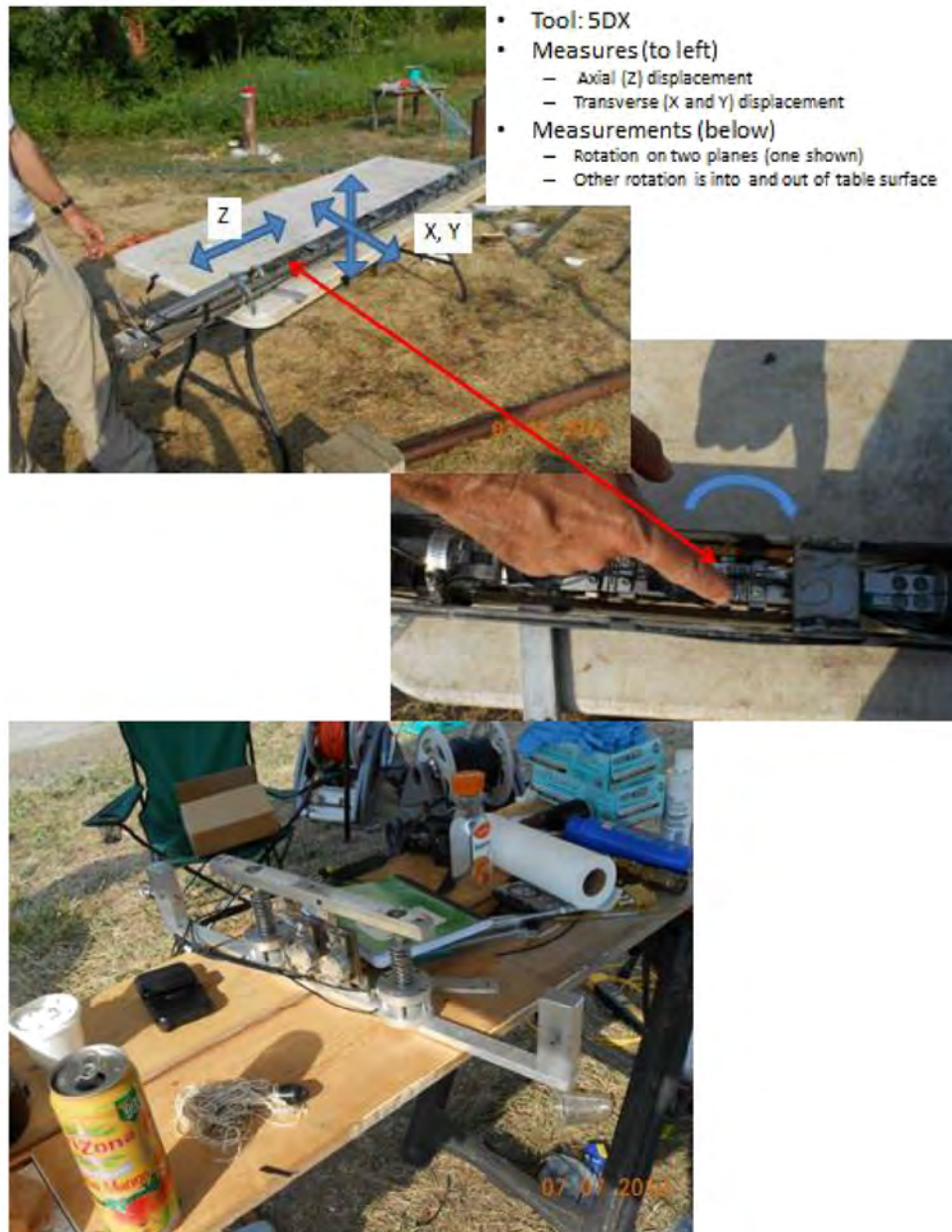


Figure 22: Diagram showing concept of joining various strata to create a simple hydrostratigraphic framework.

Station N: Fracture dilation research for Carbon Sequestering: Dr. Larry Murdoch, Clemson University Research

Carbon sequestering requires injection of fluid carbon compounds in deep fractured bedrock. Such injections will cause borehole and fracture dilation. This research is preliminary and conducted in a shallow bedrock environment.



- Tool: 5DX
- Measures (to left)
 - Axial (Z) displacement
 - Transverse (X and Y) displacement
- Measurements (below)
 - Rotation on two planes (one shown)
 - Other rotation is into and out of table surface

- Tool: Rad X
- Measures dilation and compression of borehole diameter

Figure 23: Three borehole dilation measurement tools.

Station O: Demonstration and Validation of a Fractured Rock Passive Flux Meter; Dr. Mark Newman and Dr. Kirk Hatfield University of Florida.

The project objectives are to: 1) Demonstrate and validate an innovative technology for the direct in situ measurement of cumulative water and contaminant fluxes in fractured media; 2) Formulate and demonstrate methodologies for interpreting contaminant discharge from point wise measurements of cumulative contaminant flux in fractured rock; and 3) Enable the technology to receive regulatory and end user acceptance.

For more information, see:

[http://www.serdp-estcp.org/Program-Areas/Environmental-Restoration/Contaminated-Groundwater/Persistent-Contamination/ER-200831/ER-200831/\(language\)/eng-US](http://www.serdp-estcp.org/Program-Areas/Environmental-Restoration/Contaminated-Groundwater/Persistent-Contamination/ER-200831/ER-200831/(language)/eng-US)

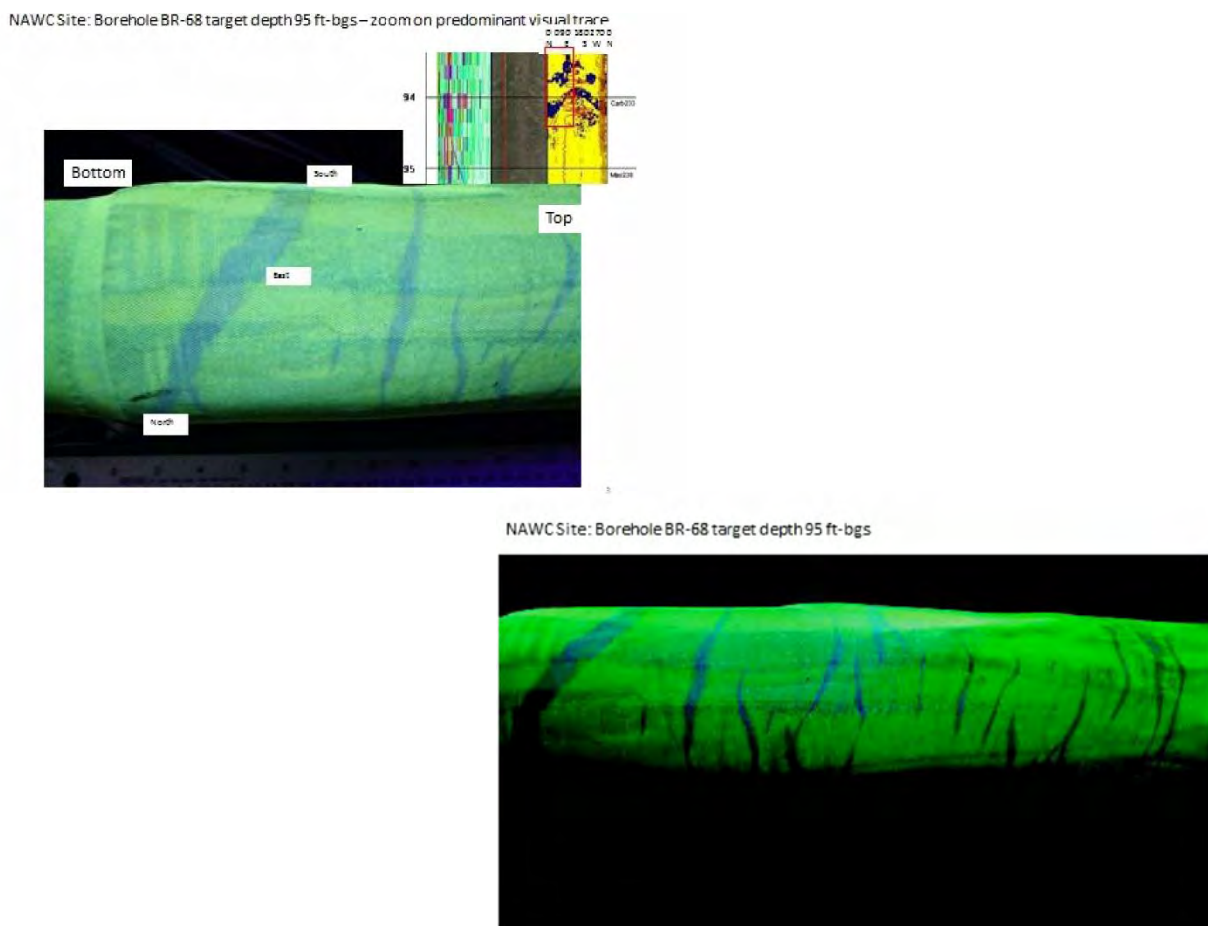


Figure 24: Photograph under black light. False color. Outer shroud show water-bearing fractures that appear as blue zone, non-water bearing rock zone remain green. Inner fabric (not seen) is carbon impregnated and adsorbs TCE for concentration values.

SHALLOW SUBSURFACE GEOPHYSICAL APPLICATIONS IN ENVIRONMENTAL GEOLOGY
GANJ XXXIII Annual Conference and Field Trip

Preliminary research include FLUTe Liner installation, and high resolution temperature logging



FLUTe liner hydraulic conductivity test of 68BR NAWC



Ben Divens



Dave Frederick



Ryan Kroeker, University of Guelph

Acoustic Borehole Image log
Full wave sonic log
Temperature log
Inside of FLUTe liner
After FLUTe liner was removed



Figure 25: FLUTe liner installation and measurement of fracture conductivity.

SHALLOW SUBSURFACE GEOPHYSICAL APPLICATIONS IN ENVIRONMENTAL GEOLOGY

GANJ XXXIII Annual Conference and Field Trip

Station P: Navy BioAug BioStim research site of 2005

Four wells in a trapezoid array were injected with EOS and DHC via the push-pull method. CVOC reduction expected to last 6 weeks to 6 months. CVOC reduction lasted about 3 years.

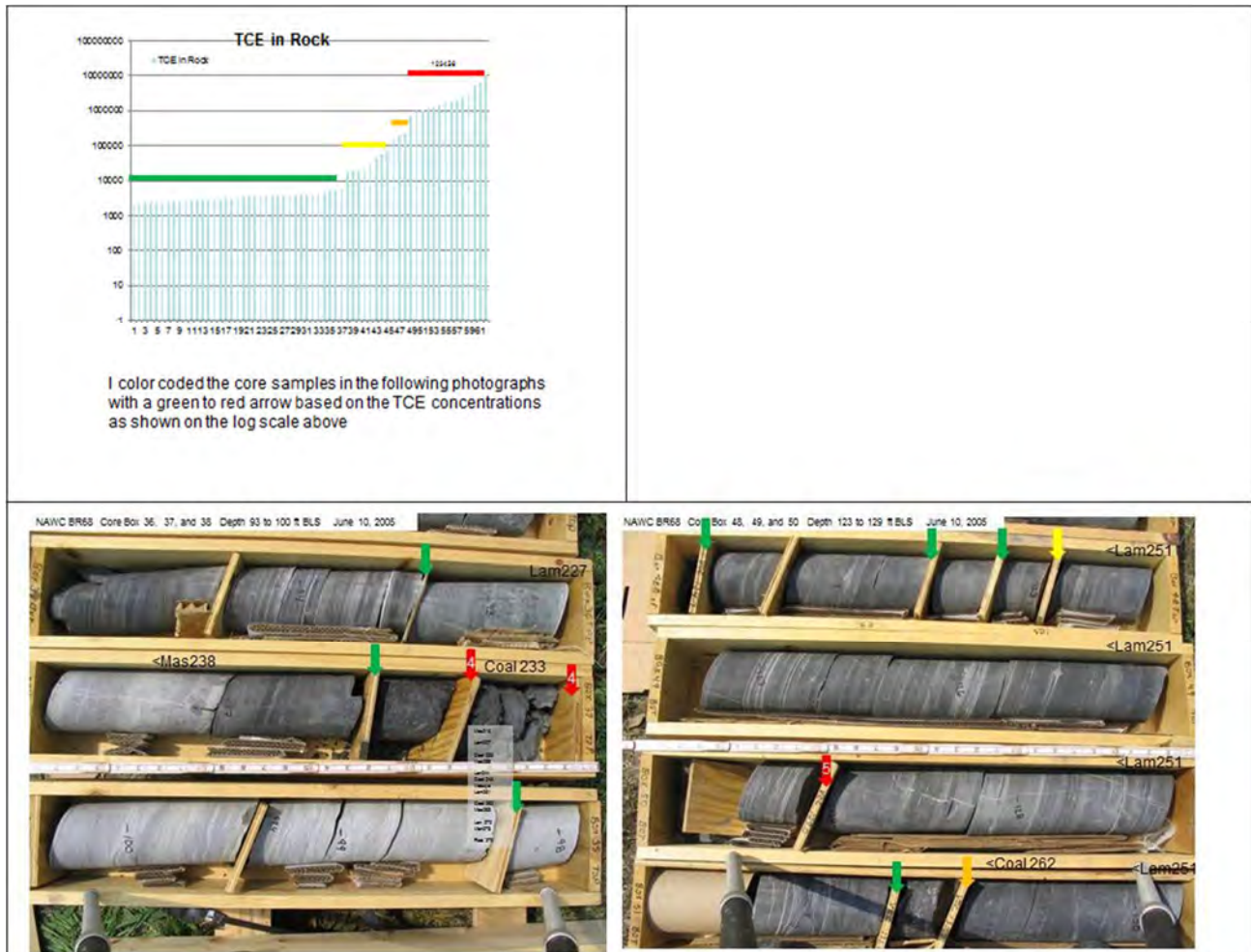


Figure 26: CVOC concentration are high in black mudstone and low in gray mudstone 2 inches away. Preliminary concept is the black mudstone has a high sorption and chemical reaction rate.

Station R: Springs, stream discharge, and surface water contamination

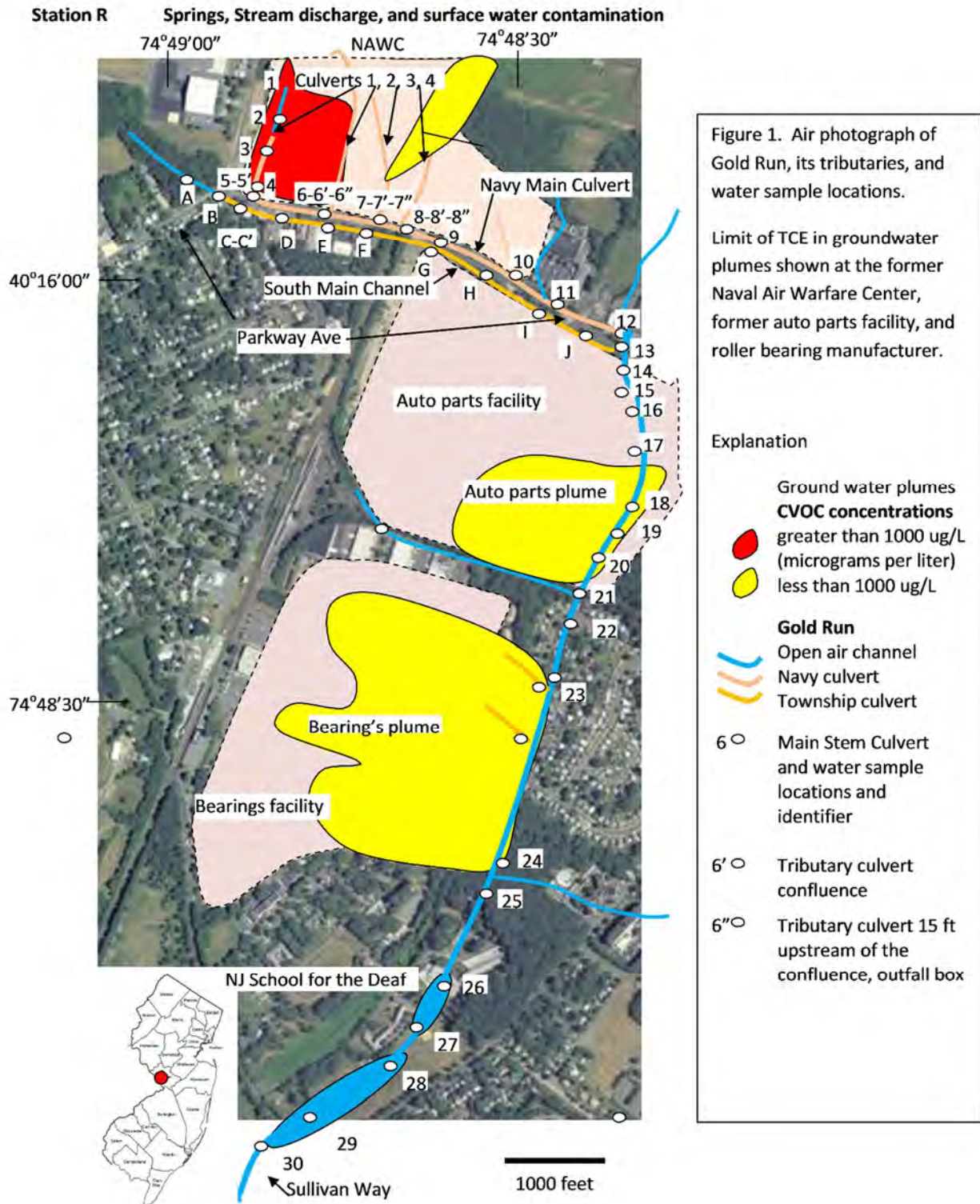


Figure 27: Groundwater discharge at the NAWC contaminates Gold Run, a local stream. Similarly, GW discharge from two downstream industrial contamination sites but with much lower contamination concentrations. USGS research determined the rate and mass of CVOC that discharges to Gold Run.

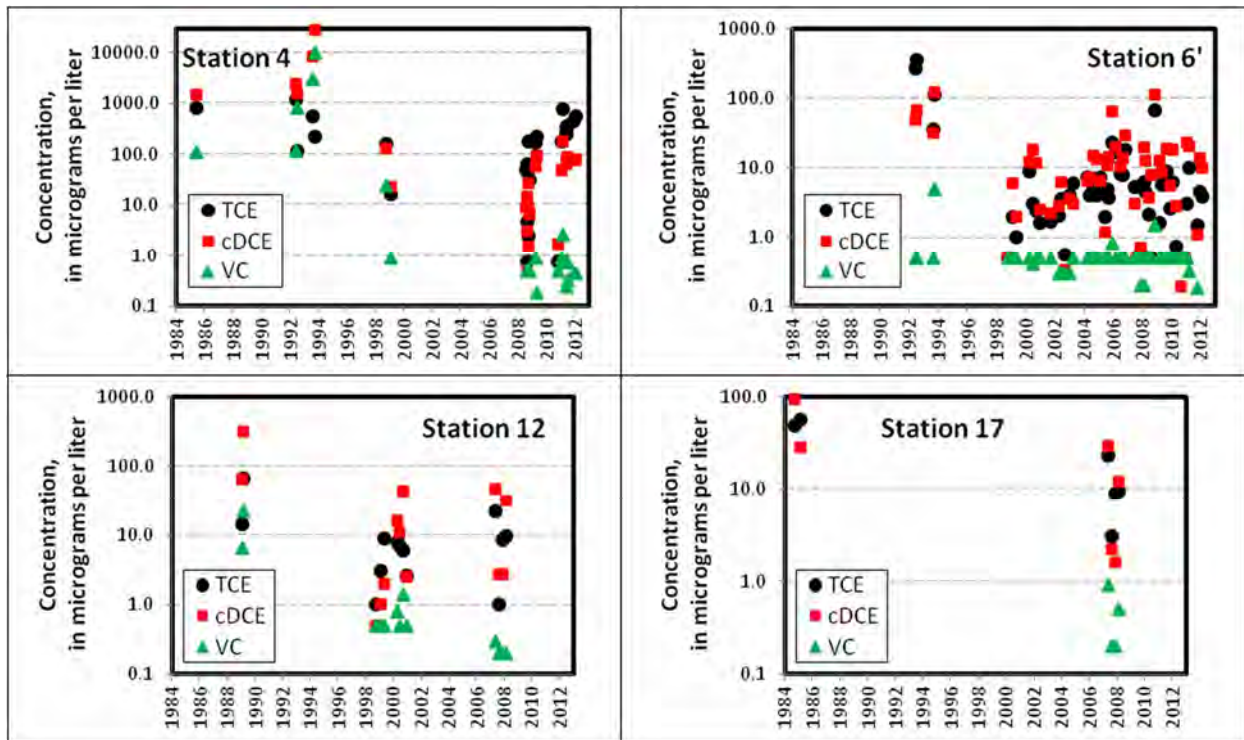


Figure 28: CVOC concentration at 4 of 48 stations in Gold Run 1984 -2012

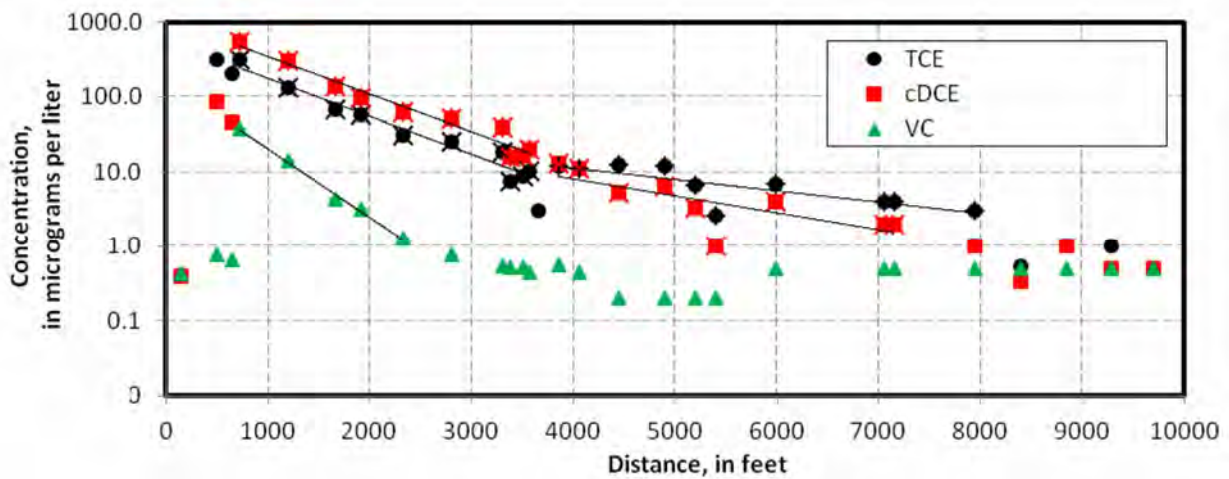


Figure 29: Mean CVOC concentration at station along the full reach of Gold Run.

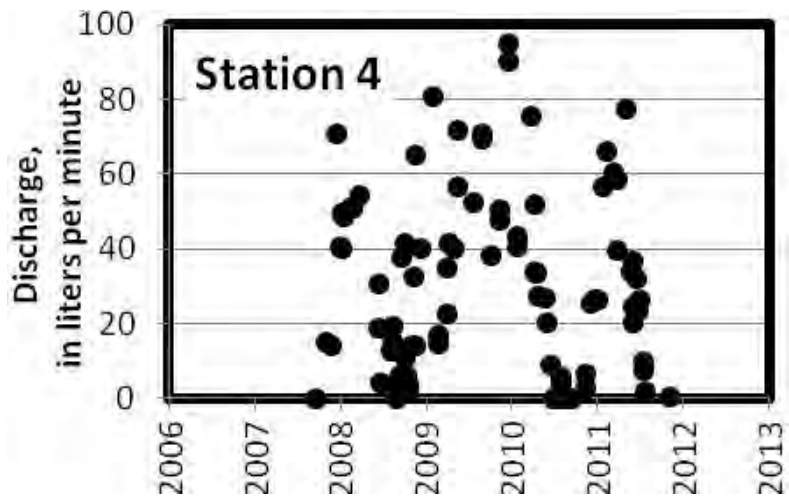


Figure 30: Flow rates at one station rates collected at 13 stations

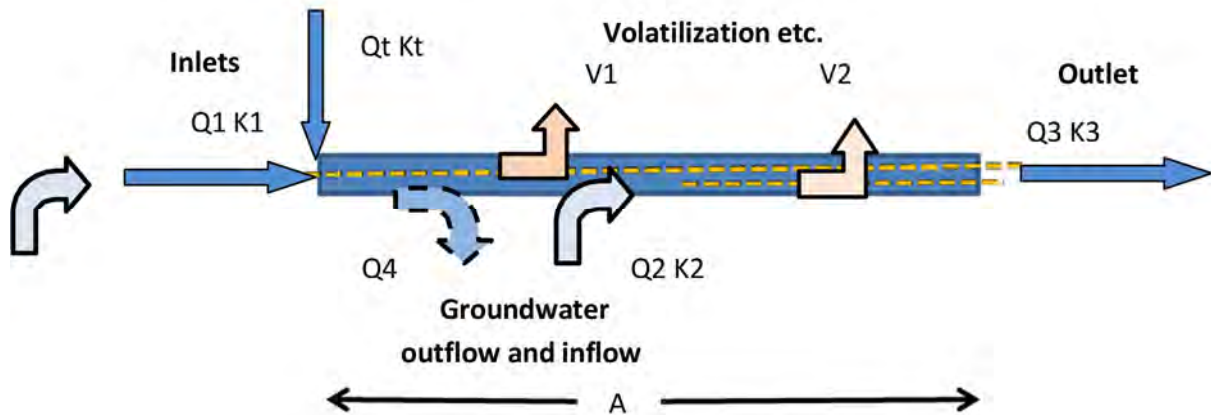


Figure 31: Diagram showing inputs and output needed to calculate CVOC discharge for each reach of Gold Run between data collection stations.

Station S: Navy's stream restoration proposal

Station T: Rutgers University arsenic mobilization research

Station U: Information transfer

Colleges and professional groups visit the NAWC each year



List of recent visitors:

City College of NYC Rider College
Rutgers University, Newark
SUNY New Paltz
Geological Association of New Jersey (GANJ)
Geological Society of America (GSA)
Association of Environmental and Engineering Geologist (AEG) NY and Philadelphia Chapter
US EPA
American Institute of Professional Geologists (AIPG)

